



HAL
open science

Geometric lattice models and irrational conformal field theories

Romain Couvreur

► **To cite this version:**

Romain Couvreur. Geometric lattice models and irrational conformal field theories. Mathematical Physics [math-ph]. Sorbonne Université, 2019. English. NNT : 2019SORUS062 . tel-02569051v2

HAL Id: tel-02569051

<https://hal.science/tel-02569051v2>

Submitted on 21 Oct 2020

HAL is a multi-disciplinary open access archive for the deposit and dissemination of scientific research documents, whether they are published or not. The documents may come from teaching and research institutions in France or abroad, or from public or private research centers.

L'archive ouverte pluridisciplinaire **HAL**, est destinée au dépôt et à la diffusion de documents scientifiques de niveau recherche, publiés ou non, émanant des établissements d'enseignement et de recherche français ou étrangers, des laboratoires publics ou privés.

**THÈSE DE DOCTORAT
DE L'UNIVERSITÉ PIERRE ET MARIE CURIE**

Spécialité : Physique

École doctorale n°564: Physique en Île-de-France

réalisée

au Laboratoire de Physique Théorique - ENS

et

à l'Institut de Physique Théorique - CEA

sous la direction de Jesper Jacobsen et Hubert Saleur

présentée par

Romain Couvreur

pour obtenir le grade de :

DOCTEUR DE L'UNIVERSITÉ PIERRE ET MARIE CURIE

Sujet de la thèse :

**Geometric lattice models and irrational
conformal field theories**

soutenue le 25 juin 2019

devant le jury composé de :

M.	Paul Fendley	Rapporteur
M.	Ilya Gruzberg	Rapporteur
M.	Jean-Bernard Zuber	Examineur
M ^{me}	Olalla Castro-Alvaredo	Examinatrice
M.	Benoit Estienne	Examineur
M.	Jesper Lykke Jacobsen	Directeur de thèse
M.	Hubert Saleur	Membre invité (co-directeur)

Geometric lattice models and irrational conformal field theories

Abstract:

In this thesis we study several aspects of two-dimensional lattice models of statistical physics with non-unitary features. This bottom-up approach, starting from discrete lattice models, is helpful to understand the features of the associated conformal field theories. They are non-unitary and often irrational, logarithmic or even non-compact. First, we study the problem of the entanglement entropy in non-unitary spin chains and its interpretation in loop models. We discuss the role of the effective central charge, a relevant quantity to study the next problems in this thesis. We then address two problems related to the Chalker-Coddington model, an infinite-dimensional supersymmetric chain important for the study of the plateau transition in the integer quantum Hall effect. Since the model has an infinite number of degrees of freedom, it has been proposed to study it with a series of truncations. We present new results based on this approach and extend this methodology to the case of Brownian motion in its supersymmetric formulation. Next, a new model is proposed to interpolate between class A and class C. The Chalker-Coddington model is a particular realisation of class A whereas class C, describing the physics of the spin quantum Hall effect, can be related to a model of percolation. This interpolating model provides an example of a RG-flow between a non-compact CFT and compact one. The last part of this thesis deals with the problem of classifying observables in lattice models with discrete symmetries. The process is illustrated on the Potts model and its symmetry under the group of permutations and previous results are extended for non-scalar operators. This approach is important to study indecomposability of non-unitary models and can be used to study models such as percolation in higher dimensions.

Modèles géométriques sur réseau et théories conformes irrationnelles

Résumé :

Dans cette thèse nous étudions différents aspects des modèles critiques non-unitaires de physique statistique en deux dimensions. Notre approche, partant de modèles discrets sur le réseau, permet d'en apprendre plus sur les théories conformes associées. Celles-ci sont non-unitaires et souvent irrationnelles, logarithmiques ou encore non-compactes. Pour commencer, le problème de l'entropie d'intrication dans des chaînes de spin non-unitaires et son interprétation dans les modèles de boucles sont considérés. Le rôle de la charge centrale effective, une quantité pertinente pour étudier aussi d'autres problèmes de ce manuscrit, y est discuté. Ensuite, nous regardons deux problèmes liés au modèle de Chalker-Coddington, une chaîne de spin supersymétrique de dimension infinie, importante pour l'étude de la transition entre plateaux dans l'effet Hall quantique entier. Puisque ce modèle a un nombre infini de degrés de liberté, il a été proposé de considérer une série de troncations. Nous présentons de nouveaux résultats basés sur cette approche et développons cette méthode dans le cadre du mouvement Brownien dans sa formulation supersymétrique. Ensuite, un nouveau modèle est proposé pour interpoler la classe A et la classe C de l'effet Hall quantique. Le modèle de Chalker-Coddington est une réalisation particulière de la classe A tandis que la classe C, qui décrit la physique de l'effet Hall quantique de spin, est relié à un modèle de percolation. Ce modèle donne un exemple de flot sous l'action du groupe de renormalisation entre une théorie conforme compacte et non-compacte. La dernière partie de cette thèse discute la classification des observables sur réseau avec une symétrie discrète. Le processus est illustré sur le modèle de Potts avec sa symétrie sous l'action du groupe des permutations et des résultats déjà connus sont étendus au cas des opérateurs non-scalaires. Cette approche est importante dans l'étude de l'indécomposabilité des modèles non-unitaires et peut être utilisée pour étudier la percolation en dimension supérieure.

Remerciements

Je voudrais commencer par remercier les deux rapporteurs, Ilya Gruzberg et Paul Fendley, d'avoir accepté la pénible tâche de relire mon manuscrit ainsi que les examinateurs, Jean-Bernard Zuber, Olalla Castro-Alvaredo et Benoit Estienne. Je vous suis très reconnaissant d'avoir accepté d'être dans le comité de thèse et d'avoir fait le déplacement, parfois de loin, pour ma soutenance.

Je tiens ensuite à remercier mes deux directeurs de thèse, Jesper et Hubert, qui m'ont apporté leur soutien indéfectible tout au long de ces années. Vos conseils et réflexions ont été inestimables. Jesper, je garderai un excellent souvenir de nos longues discussions sur des sujets très variés. Hubert, merci beaucoup pour ta grande aide lors de la recherche de postdoc et tes encouragements.

Je voudrais remercier toutes les autres personnes qui ont croisé mon chemin scientifique ces dernières années. J'ai eu la chance de discuter et travailler avec les anciens thésards de Jesper et Hubert, en particulier Romain Vasseur, Éric Vernier, Yacine Ikhlef et Roberto Bondesan. Je profite de ce paragraphe pour remercier de nouveau Ilya Gruzberg pour son accueil lors de ma visite à Columbus, pour ce qu'il m'a enseigné lors de nos discussions scientifiques et pour nos discussions musicales. J'en profite pour remercier mes deux collaborateurs chinois, Youjin Deng et Xiaojun Tan ainsi que tous les chercheurs du LPT et de l'IPhT avec qui j'ai pu discuter. Je remercie les différents organisateurs des écoles de physique théorique auxquelles j'ai participé à Florence, Cargèse et Gand mais aussi les organisateurs de l'école Ecoclim à Orsay. Lors de mes voyages pour ma recherche de postdoc, j'ai eu la chance d'être accueilli dans différents laboratoires, merci en particulier à Frank Verstraete, Pasquale Calabrese, Ignacio Cirac et Norbert Schuch.

Merci aux membres du personnel administratif de l'ENS et de l'IPhT, en particulier Viviane Sébille, Sandrine Patacchini, Laure Sauboy, Sylvie Zaffanella, Loïc Bervas et Emmanuelle de Laborderie. Enfin merci à tous les thésards et postdocs que j'ai croisé, tout particulièrement à Niall, Etienne, Jonathan, Jerome, Thibault, Kemal, Benoit, Anna, Thomas, Séverin, Pierre, Santiago, Miguel, Michal, Thiago, Yifei et Linnéa.

Merci ensuite à ma famille, qui n'a jamais douté de l'intérêt de mon travail malgré mon manque de pédagogie pour leur expliquer mon sujet de thèse. La soutenance n'aurait pas pu être la même sans l'aide précieuse de ma mère pour la préparation du pot en plus de son soutien constant. Il ne serait pas correct d'oublier de remercier Jean-Christophe, qui a eu depuis le début l'honnêteté de ne pas faire semblant de s'intéresser à mon sujet de thèse mais sans qui ces quatre années n'auraient pas été aussi drôles. J'ai eu le grand privilège d'habiter près de ma soeur Stéphanie. Nos discussions durant cette période ont suscité de nombreuses interrogations et m'ont certainement changé définitivement. Merci à Claude également pour nos discussions très variées, ses réponses à mes questions d'informatique un peu futiles et ses quelques relectures de dernières minutes.

J'ai eu le plaisir de vivre, la première année, au A6 de Montrouge, merci à Salim, Quentin, Paul, Jean, Charles, Benjamin, Simon, Axel et Chloé. Ces années à Paris n'auraient pas non plus été les mêmes sans Les Concerts d'Athalie, j'ai eu le privilège d'avoir été dirigé par Léonard qui m'a fait confiance pour jouer La Traviata jusqu'en Chine. Merci également à mes amis physiciens de l'ENS, Frédéric, Louis et Florence. Je remercie également Wei et Raphaël pour leurs "informations sûres" sans oublier Marine et nos parties de Gloomhaven. Merci enfin à mes camarades de prépa Tarik, Quentin, Adrien ainsi qu'à Bill et Emmanuel.

Mes derniers remerciements vont à Oriane, qui a eu le courage de lire l'intégralité du manuscrit et pour son soutien sans faille au quotidien.

Je termine par une digression sur l'empreinte carbone due à mes différents voyages dans le cadre de cette thèse. J'ai cumulé un total de presque 20000 kilomètres effectués en avion, ce qui correspond à environ 6 tonnes d'émissions de CO₂ (d'autres gaz à effet de serre sont à prendre en compte). A titre de comparaison, limiter l'augmentation de température à 1.5-2 degrés demande de ne pas dépasser un total d'environ 2 tonnes de CO₂ par habitant et par an. Mes déplacements professionnels correspondent donc déjà à environ 70 – 80% de mon capital carbone.

Contents

1	Introduction to non-unitary critical phenomena	9
1.1	Universality and CFT	9
1.2	The quantum Hall effect	10
1.3	Geometric systems and polymers	13
1.4	Non-unitary features	15
1.4.1	General considerations	15
1.4.2	Non-unitary representations of the Virasoro algebra and negative conformal dimensions	15
1.4.3	Indecomposability and logarithmic correlators	16
1.4.4	Irrationality and non-compactness	17
1.4.5	PT symmetry and RG-flow	19
1.5	The plan of this manuscript	20
2	Entanglement in non-unitary critical systems	22
2.1	Entanglement entropy	23
2.1.1	Definitions	23
2.1.2	Conformal field theory interpretation	24
2.1.3	The non-unitary case: first observations	27
2.2	The XXZ spin chain	28
2.2.1	Potts model	28
2.2.2	Loop model formulation	29
2.2.3	The six-vertex model and the XXZ Hamiltonian.	30
2.2.4	Quantum group	32
2.3	Quantum group entanglement entropy	33
2.3.1	Pedagogical example on 2 sites	33
2.3.2	Entanglement in the loop model and Markov Trace	35
2.3.3	Definition of the quantum group entanglement entropy and motivations	37
2.3.4	A more complex example: $2M = 4$ sites	39
2.3.5	Properties of the entropy	41
2.4	The scaling relation of the quantum group entanglement entropy	43
2.4.1	A brief introduction to Coulomb Gas	44
2.4.2	The replica trick and the modified scaling relation	44
2.4.3	Numerical analysis	46
2.5	Extensions	47
2.5.1	Restricted Solid-on-Solid models	47
2.5.2	A supersymmetric example	51
2.5.3	Entanglement entropy in the non-compact case	52
2.6	Comparisons and conclusion	54
2.6.1	Entanglement in non-unitary minimal models	54
2.6.2	The null-vector conditions in the cyclic orbifold	54

3	Truncations of non-compact loop models	56
3.1	The Chalker-Coddington model	56
3.1.1	Definition as a one-particle model	56
3.1.2	Supersymmetric formulation	59
3.1.3	The supersymmetric $gl(2 2)$ spin chain	61
3.1.4	Exact results and critical exponents	62
3.2	The first truncation as a loop model	63
3.2.1	Truncations as a loop model: the case $M = 1$	64
3.2.2	An integrable deformation	66
3.2.3	Symmetries	67
3.2.4	Comparison	72
3.2.5	A word on the dense phase	76
3.2.6	Lattice observables in the network model	79
3.3	Higher truncations	81
3.3.1	The second truncation	81
3.3.2	Generalisation	84
3.3.3	Preliminary numerical results	84
3.4	Truncations of the Brownian motion	86
3.4.1	Brownian motion as a supersymmetric spin chain	88
3.4.2	Equivalence between oriented/unoriented lattice	89
3.4.3	The first truncation: self-avoiding walks	92
3.4.4	Hamiltonian limit	93
3.4.5	Symmetries in the continuum limit	95
3.4.6	Higher truncation of the Brownian motion	98
3.4.7	The multicritical point of the second truncation	99
4	A flow between class A and class C	102
4.1	Lattice model interpolating between class A and class C	102
4.1.1	The Spin Quantum Hall Effect as a network model	103
4.1.2	Second quantisation and the Hamiltonian limit	105
4.1.3	Choosing an interpolation	106
4.1.4	Loop formulation of the model	109
4.1.5	Percolation as a two-colours loop model	111
4.2	The untruncated model	115
4.2.1	Symmetries	115
4.2.2	Lyapunov exponents	117
4.3	Truncations	122
4.3.1	The phase diagram	122
4.3.2	Symmetries	124
4.3.3	The dense phase	125
4.3.4	Critical exponents of the critical dilute phase	126

5	Operators in the Potts model	130
5.1	Observables in the Q -state Potts model	130
5.1.1	Potts model and Fortuin-Kasteleyn clusters	131
5.1.2	Definitions and representation theory of \mathcal{S}_Q	131
5.1.3	Observables of one spin	133
5.1.4	Observables of two spins	136
5.1.5	Procedure for general representations	141
5.1.6	Internal structure and LCFT	144
5.2	Correlation functions	145
5.2.1	Symmetric observables of two spins	147
5.2.2	Anti-symmetric observables of two spins	147
5.2.3	Observables with mixed symmetry: $[Q - 3, 2, 1]$	149
5.2.4	Generic case	150
5.3	Physical interpretation	151
5.3.1	Primal and secondary operators	151
5.3.2	Critical exponents on a cylinder	151
5.3.3	Numerics	154
5.3.4	Spin	156
5.4	Logarithmic correlations in 3D percolation	158
	Conclusion	160

1 Introduction to non-unitary critical phenomena

1.1 Universality and CFT

Many interesting problems in physics involve a large number of degrees of freedom and are effectively described by a quantum field theory. The continuum limit of a generic system is described by a massive field theory, where correlation functions decay exponentially with a characteristic correlation length ξ . However, at some particular values of the physical parameters, a model can become critical and its correlation functions decay algebraically. The field theory description becomes massless and scale invariant. The two-point function of a local observable $\mathcal{O}(\vec{x})$ has the following behaviour

$$\langle \mathcal{O}(\vec{x})\mathcal{O}(\vec{y}) \rangle \sim \frac{A}{|\vec{x} - \vec{y}|^{2\Delta_{\mathcal{O}}}}, \quad (1.1)$$

where \vec{x} and \vec{y} are positions such that $|\vec{x} - \vec{y}|$ is much larger than any microscopic scale, A is an amplitude and $\Delta_{\mathcal{O}}$ is the conformal dimension associated with \mathcal{O} . The set of conformal dimensions, or critical exponents, is universal. In other words, the physical properties of the system at large scale do not depend on the microscopic details but rather on qualitative properties such as symmetries or the dimension. The form of the correlation function (1.1) comes from the underlying global symmetry that all critical systems share: scale invariance. In two dimensions, the classification of scale invariant quantum field theory is strongly constrained since, in most cases, systems are even invariant under local conformal transformations. These transformations are functions preserving scale invariance locally such as translations, rotations or dilatations. The general framework to describe critical systems is called Conformal Field Theory (CFT) and was very successful after the pioneering work of Belavin, Polyakov and Zamolodchikov [1]. In two dimensions, the conformal symmetry is infinite-dimensional and encoded in the celebrated Virasoro algebra

$$[L_n, L_m] = (n - m)L_{n+m} + \frac{c}{12}n(n^2 - 1)\delta_{n+m,0} \quad (1.2)$$

where $c \in \mathbb{R}$ is the central charge, an universal parameter. Classifying conformal field theories is reduced to the study of representations of this algebra. This led to the very famous minimal models [2, 3], among them can be found very important universality class such as the Ising model, the tricritical Ising model and the 3-state Potts model.

The origin of universality can be understood with the Renormalisation Group (RG), formulated by Wilson [4, 5]. Let us take a simple example and consider a square lattice where each vertex is a small magnet (a spin). The RG procedure aims at describing the system at a scale larger than the microscopic one. This is illustrated by the decimation process. The large distance behaviour or correlation functions can be obtained by summing over the interactions at small distance to obtain an effective description, only describing the physics at a larger scale. In the square lattice of magnets, this is obtained by grouping together spins in the same vicinity and averaging over the local magnetisation. The process is iterative and at each step a new Hamiltonian is obtained. It defines a flow in the space

of coupling constants called renormalisation group flow. A critical theory is a scale invariant fixed point of the RG-flow. Conformal field theory's main goal is to provide a description of fixed points under the action of the RG. It is thus not always useful to study two different models if they, in the end, flow toward the same fixed point. The aim of the RG procedure is to map the space of Hamiltonian and classify the different universality classes.

Despite many breakthroughs in statistical physics, condensed matter or string theory that came from conformal field theory, the description of many complex systems remains mysterious. In this thesis, we are interested in irrational non-unitary conformal field theories and their lattice discretisations. Contrary to the unitarity case, many new properties make this task intricate. Since this thesis is primarily concerned with non-unitary models, we start by describing two examples of such models: the plateau transition in the quantum Hall effect in section 1.2 and polymer models in section 1.3. Several specific properties of non-unitary models, relevant for this thesis, are then presented section 1.4.

1.2 The quantum Hall effect

The integer quantum Hall effect is a phenomenon observed in a two-dimensional gas of electrons subject to a strong magnetic field perpendicular to the sample (see figure 1.1a). In the classical Hall effect the electrons, driven by the current, are deviated by the magnetic field, thus creating a transverse current.

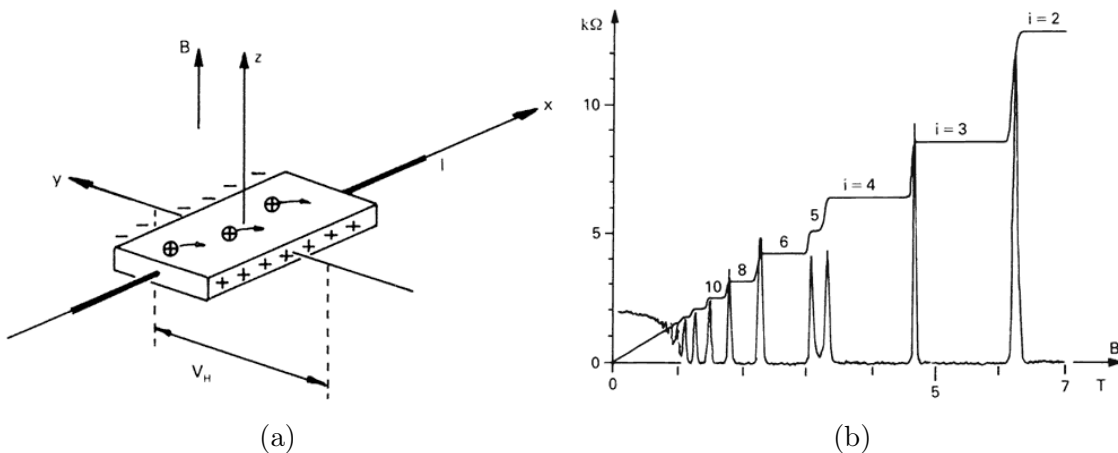


Figure 1.1 – On the left: Experimental setup to measure the Hall effect. A current goes through a piece of metal subject to a perpendicular magnetic field B . A resulting voltage V_H is measured in the transverse direction. On the right: resistance of a piece of metal as a function of the amplitude of the magnetic field B . We observe a quantised resistance with plateaux. The figures are taken from [6]

The transverse resistance ρ_{xy} reads

$$\rho_{xy} = \frac{B}{en}, \quad (1.3)$$

where B is the amplitude of the magnetic field, e is the electric charge and n the density of the cloud of electrons. In 1980, Von Klitzing discovered experimentally the (integer) quantum Hall effect [7]. In a regime of very strong magnetic field and low temperature, the transverse resistance develops plateaux at the particular values

$$\rho_{xy} = \frac{1}{n} \frac{h}{e^2}, \quad (1.4)$$

where n is an integer called filling factor and h the Planck constant. Under a change of the magnetic field B , the resistance forms plateaux as illustrated in figure 1.1b. The existence of the plateau can be understood by considering the Hamiltonian H_L of a single electron in a two-dimensional space with a perpendicular magnetic field

$$H_L = \frac{1}{2m} \left(\vec{p} + e\vec{A} \right)^2, \quad (1.5)$$

where the vector potential \vec{A} is chosen in the Landau gauge $\vec{A} = (0, Bx, 0)$ and \vec{p} is the momentum. The energies of eigenfunctions are called Landau levels and labelled by an integer n

$$E_n = \hbar\omega_B \left(n + \frac{1}{2} \right), \quad (1.6)$$

where $\omega_B = |e|B/m$ is the cyclotron frequency. Each electron in a Landau band is delocalised. The Landau levels have an enormous degeneracy N , identical for each level,

$$N = \frac{S}{2\pi l_B^2}, \quad (1.7)$$

proportional to the area S of the sample. Surprisingly the quantisation (1.4), one of the most accurately measured universal phenomena, needs an other key component to be explained: disorder. In practice the Hamiltonian reads

$$H = H_L + V(\vec{x}) \quad (1.8)$$

where V is a random potential created by the disorder. As a consequence, in a sample of metal with impurities, the Landau levels widen and can even overlap (see figure 1.2a).

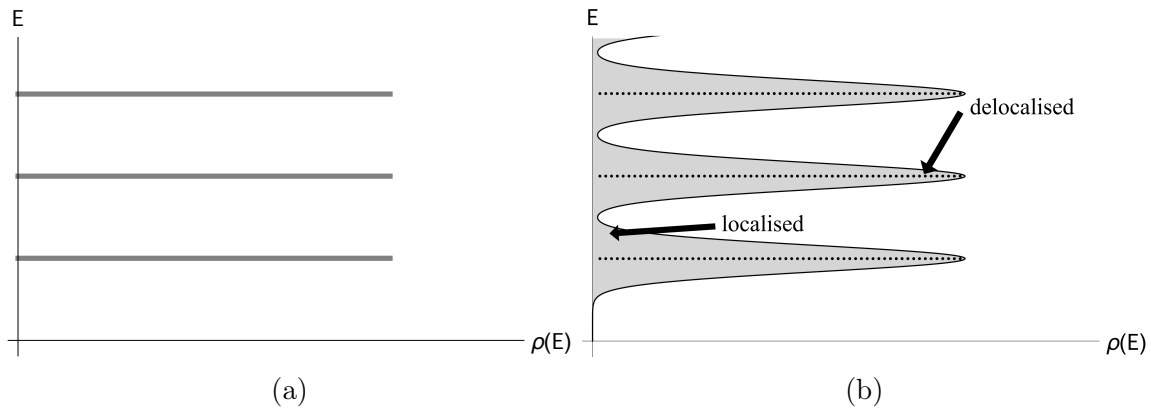


Figure 1.2 – Spectrum of the system with E the energy and $\rho(E)$ the density. On the left: In a pure system the (non-interacting) electrons fill the Landau bands that have a huge degeneracy. All states are delocalised. On the right: in the presence of disorder the bands widen and states are localised except near the original Landau levels.

The electrons fill the vacant eigenstates up to a certain level called Fermi level. States between two Landau levels are localised around extrema of V , hence they do not contribute to the conductivity. However, eigenstates with the energy of a Landau level are delocalised and provide a current. Notice that the degeneracy, and so the density of the bands, can be changed by varying the magnetic field. This affects the Fermi level. As a consequence, jumps are observed whenever the Fermi level crosses the middle of a Landau band, creating a sudden change in the conductivity. This simplistic explanation gives a picture of what happens but does not explain why the jumps are exactly multiples of h/e^2 . We refer to good reviews such as [8] for more details.

The presence of plateaux, and the amplitude of the jumps are perfectly understood. However, the physics at the transition [9] remains mysterious. This plateau transition is believed to be described by a second order phase transition where the localisation length ξ of a wave function at the Fermi energy E diverges as it comes close to a Landau energy E_n

$$\xi \propto \frac{1}{|E - E_n|^\nu}. \quad (1.9)$$

The critical exponent ν , called the localisation length exponent, is independent of the Landau band index n . Its value has been the subject of many investigations over the years. Experimental works report a value close to $\nu = 2.38$, using a heterostructure GaAs-AlGaAs [10, 11]. A lattice model was proposed by Chalker and Coddington in 1988 [12] to study the critical properties of the transition. Recent numerical simulations report an exponent ν in the range $2.55 - 2.6$ [13–17]. Many exact approaches were proposed such as: conformal restriction [18], non-linear σ model description [19].

There exists a second kind of plateau transition called spin quantum Hall effect (SQHE) [20, 21]. It is the analog of the IQHE but charge transport is replaced by spin transport. The spin Hall conductance measures the spin current created in the system by a spatially varying

Zeeman magnetic field. The spin conductivity σ_{xy} is defined by

$$j_x^z = \sigma_{xy} \left(-\frac{dB^z(y)}{dy} \right) \quad (1.10)$$

with j_x the spin current in the direction x and B^z the Zeeman field perpendicular to the sample in the direction z . The role of the electric field in the IQHE is played by the derivative of the Zeeman field.

The IQHE and SQHE plateau transitions are quantum systems in a two dimensional space. Therefore the field theory describing the system can naturally be expected to be a $2+1$ D quantum or a 3D Euclidean field theory. However it is possible to take advantage that electrons are not interacting to reduce the problem to a $1+1$ D quantum or 2D Euclidean field theory. This is explained in an example later in this manuscript. Therefore all the machinery of conformal field theory in two dimensions can be applied to this phase transition. From the point of view of quantum mechanics the system is perfectly unitary. However we are left with one difficulty to overcome, the presence of disorder. Conformal field theory describes long range features and correlation functions averaged over the random potential. The two possibilities to deal with this complication are the replica trick and the supersymmetric method [22–25]. Later in this thesis, the second one is explored. However using those methods to deal with the disorder breaks the unitarity of the model. The conformal field theory obtained is a textbook case exhibiting many non-unitary features. A lattice regularisation of this universality class, known as the Chalker-Coddington model, gives a description in terms of a network model. The main difficulty comes from its supersymmetric formulation, where each site (in a 1D quantum chain) has an infinite dimensional representation of the superalgebra $gl(2|2)$. The model is said to be non-compact since, even in finite-size, there is an infinite number of degrees of freedom. It is thus a rich laboratory to develop the formalism of non-unitary conformal field theory.

1.3 Geometric systems and polymers

Many geometrical models in two dimensional statistical physics are described by a non-unitary conformal field theory. In many cases, it can be traced back to the non-local nature of the objects of interest. For example, a typical observable in percolation [26, 27], a system of uncorrelated bonds, is the probability of having two given sites in the same cluster (see figure 1.3a). This probability defines a correlation function that cannot be described in a unitary conformal field theory. In many cases, the apparent non-locality of the model can be replaced with a perfectly local description where some Boltzmann weights are negative or complex [28]. One of the most famous example is the relation between the Potts model described in terms of Fortuin-Kasteleyn clusters [29], the 6-vertex model and loop models. Many other geometrical models have a loop representation [30, 31]

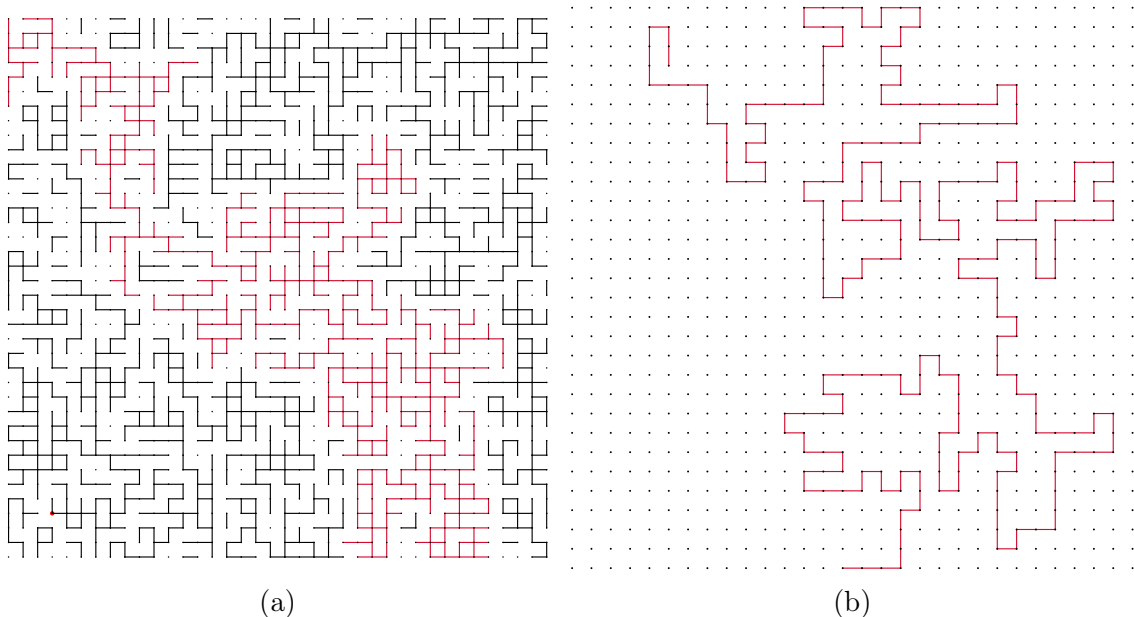


Figure 1.3 – On the left: typical configuration of percolation on a two-dimensional square lattice. At criticality, the objects considered are clusters that propagate on long distances. A single cluster is drawn in red. On the right: a typical path of a self-avoiding walk.

Polymers models are also an interesting class with rich and diverse behaviours. They describe very long chains made of monomers that interact with each other. This family of systems has many connections with quantum systems, especially supersymmetric spin chains [32]. Geometrically, a polymer does not close on itself and can be seen as the Feynman path of bosons and fermions [33]. The connections between loop models and quantum mechanical models are not restricted to polymers models, see for instance [34] for an application to topological phases and quasiparticles in $2 + 1$ dimensions. A famous example of a polymer model is the self-avoiding walks (SAWs) (see figure 1.3b) where two monomers cannot be on the same edge, corresponding to the $O(n)$ model [35] in the limit $n \rightarrow 0$ [36]. Its study is very closely related to the problem of the plateau transition in the quantum Hall effect. We will observe that the geometric description of the plateau transitions are in fact close to a polymer system. In particular, an interesting problem is to study two interacting oriented self-avoiding walks on a square lattice [37].

An additional aspect of polymer models is particularly intriguing. The phase diagram of the $O(n = 0)$ model has been studied for a while [38, 39]. There exists an interesting tri-critical line where two points are exactly solvable. The first, found by Blöte and Nienhuis and called point θ_{BN} , is an interesting non-compact conformal field theory. On the other hand, the point θ_{DS} was studied by Duplantier and Saleur [40] and found to correspond to percolation, a compact conformal field theory. The behaviour of the $O(n)$ models between those two points is still not understood. It remains an important point to study the RG-flow between those two universality classes. It would provide an interesting example of a non-unitary RG-flow between two $c = 0$ theories.

1.4 Non-unitary features

In this subsection, several features of non-unitary models are presented. We will focus on interesting properties, relevant to the models studied in the context of this thesis.

1.4.1 General considerations

Let us first start with general considerations. A non-unitary model is described by a transfer matrix T in its two-dimensional description or by a one-dimensional quantum Hamiltonian H . Both are, in general, related by what is called the anisotropic limit, where the continuum limit in the 2d system is taken only in one spatial direction labelled as time. In a classical model, non-unitarity can usually be detected if the local Boltzmann weights of some configurations are negative or complex. Indeed the Osterwalder-Schrader reconstruction theorem [41] states that if the Euclidean correlators satisfy the condition of reflection positivity then the quantum field theory is unitary. In general it is not satisfied if Boltzmann weights are not positive or if correlators involve non-local objects. For many systems, there exists a way to trade the apparent non-locality for the non-positivity of the local weights. An example is provided in the second chapter where the identification between the loop model based on the Temperley-Lieb algebra [42, 43] and the 6-vertex model is detailed. For the quantum system, the Hamiltonian is non-Hermitian

$$H^\dagger \neq H. \quad (1.11)$$

In practice, having negative or complex weights leads to some difficulties in a numerical approach. Moreover, even though a non-Hermitian Hamiltonian can be disconcerting or even considered non physical, it is a very natural object in statistical physics.

1.4.2 Non-unitary representations of the Virasoro algebra and negative conformal dimensions

One of the most unnerving property of non-unitary systems is the possibility of having negative conformal weights. Naively, a two-point correlator (1.1) with $h_{\mathcal{O}} < 0$ diverges as the distance between the points grows. Of course this is very strange and, *a priori*, non physical. The resolution of this apparent issue comes from the precise relation between a lattice model, where a real correlation is measured, and the conformal field theory. Indeed, the conformal vacuum $|0\rangle$ is assumed to exist and to satisfy the following constraints

$$L_n|0\rangle = 0, \quad n > -1, \quad (1.12)$$

exactly as for a harmonic oscillator. In fact, the conformal vacuum is not the actual ground state of the system since there is a state with a lower energy. Eigenvalues of the dilatation operator L_0 correspond to the energies and, in the radial quantization, L_0 satisfies

$$L_0|0\rangle = 0, \quad L_0|h_{\min}\rangle = h_{\min}|h_{\min}\rangle. \quad (1.13)$$

for $h_{\min} < 0$. As a consequence, a two-point function in the quantized language reads

$$\langle h_{\min} | \phi(0) \phi(r) | h_{\min} \rangle \quad (1.14)$$

where the expectation value of the operators is computed in the actual ground state and not the conformal vacuum. It leads to correlation functions that decay effectively with the distance. Nevertheless, the inner structure of CFT is profoundly modified by the non-unitary representation of the Virasoro algebra. Note that the free energy of the system and its finite-size corrections do not provide anymore a measure of the central charge as expected by the usual formula [44]

$$f_0^L = L f_\infty - \frac{\pi c}{6L} + o(L^{-1}), \quad (1.15)$$

but instead

$$f_0^L = L f_\infty - \frac{\pi c_{\text{eff}}}{6L} + o(L^{-1}) \quad (1.16)$$

where f_∞ is the bulk free energy and c_{eff} is called the effective central charge and in many cases is explicitly $c_{\text{eff}} = c - 24h_{\min}$ [45].

1.4.3 Indecomposability and logarithmic correlators

The loss of unitarity permits a CFT to be indecomposable. Logarithmic conformal field theories have a non-diagonalisable dilatation operator L_0 [46]. As an example, if it contains a Jordan cell of rank 2

$$L_0 = \begin{pmatrix} \Delta & 1 \\ 0 & \Delta \end{pmatrix}. \quad (1.17)$$

then there exists two fields ϕ and ψ , with the correlation functions

$$\langle \psi(0) \psi(r) \rangle = 0, \quad (1.18)$$

$$\langle \psi(0) \phi(r) \rangle = \frac{b}{z^{2\Delta}}, \quad (1.19)$$

$$\langle \phi(0) \phi(r) \rangle = -\frac{2b \log r}{z^{2\Delta}}. \quad (1.20)$$

The quantity b is universal and called indecomposability parameter. Note that the normalisation in (1.18) is already fixed and it is impossible to simply renormalise ϕ to change b . Since the pioneering work of Gurarie [47], LCFT has become a very active subject [48] and much progress has been made thanks to the study of indecomposable algebras [49, 50]. The structure of the logarithmic correlation functions can involve higher ranks of Jordan cells, making the study of the conformal field theory much more challenging. The representation is, in the bulk case, believed to be *wild* [51], meaning that a given theory can contain arbitrary large Jordan cells. Of course, an indecomposable representation of the Virasoro algebra is

also non-unitary. Logarithmic conformal field theories are not simple curiosities with a few scarce examples. Many non-unitary models are indecomposable and it is believed that not being a LCFT is the exception rather than the rule. In particular, all non-trivial theories at $c = 0$ must be logarithmic, this is known as the $c \rightarrow 0$ catastrophe [52]. Singularities appear in the operator product expansions due to the collision of k (k being the rank of the resulting Jordan cell) conformal dimensions in certain limits. These divergences can be fixed by introducing logarithmic partners that mix in a Jordan cell as in (1.17). In the case of $c = 0$ theories, a vanishing central charge implies that the stress energy tensor must have a logarithmic partner. The set of correlations (1.18) is satisfied with ψ replaced by the energy momentum tensor T and ϕ by its logarithmic partner t . The indecomposability parameter is believed to be universal and its value is known in many cases. For example $b = -5/8$ for dilute critical polymers and $b = 5/6$ for percolation. The logarithmic structure and the value of b can be extracted even in finite size by using the Hamiltonian or the transfer matrix [53, 54]. It is, however, hard to extract them directly because it requires large sizes and is subject to a slow convergence even for the most simple cases. In many cases, the logarithmic structure of LCFT can be studied as a limit of ordinary (non-unitary but not indecomposable) CFTs. This was realised first by Cardy [55, 56] when he proposed a mechanism to explain the appearance of logarithmic terms. Whenever, in a certain limit, two conformal fields collide (have the same conformal dimension), a resonance phenomenon happens and a log is produced in a correlation function. Those ideas, particularly powerful in the presence of additional symmetries, were applied successfully to the Potts model (in its formulation in terms of percolating clusters) [57, 58] and to the plateau transition in the integer quantum Hall effect [59].

1.4.4 Irrationality and non-compactness

The systematic characterisation of many CFTs is often made possible thanks to the rationality of the theories [60, Chapter 3]. A 2D conformal field theory is rational if it possesses a finite number of primary fields of some extended algebra thus simplifying drastically the analysis. The most famous examples of rational conformal field theories are the minimal models [1]. Conversely, irrational conformal field theories have an infinite number of primary fields and, because of their complexity, many aspects are not perfectly understood. On the lattice, many geometrical models are discrete regularisations of non-rational CFTs and are used to study them. For instance, most well-known logarithmic conformal field theories are non-rational (see [61] for an exception). Some irrational CFTs are called *quasi-rational* [62] if they are described by an infinite number of fusion rules but any fusion of two representations decomposes on a finite sum of representations. Particular extreme cases of irrational models are the non-compact CFTs (see below) for which the set of primary fields is not even countable.

Many interesting systems have an infinite number of degrees of freedom and are called non-compact. A very simple example is the Brownian motion where each edge can be visited an arbitrary number of times. It is also the case for the supersymmetric formulation of the Chalker-Coddington model describing the plateau transition in the IQHE. In the continuum,

a theory is said to be non-compact if described by a field living in a non-compact space. As an example, the Brownian motion is described [63], by a bosonic field ϕ with free Euclidean action

$$S = \int d^2x (\nabla\phi)^2. \quad (1.21)$$

The field ϕ lives on the real axis, which is non-compact. In practice, these theories have a continuum of critical exponents, whereas in usual CFT, the set of conformal dimensions is discrete. The consequence on the lattice are very important. Given a lattice observable \mathcal{O} , it can usually be written as a sum over primary operators and their descendants. In the case of a continuum of fields this sum becomes naturally an integral. As a consequence, a two-point function has the form

$$\langle \mathcal{O}(0)\mathcal{O}(r) \rangle_{\text{lattice}} = \int_{x=0}^{\infty} dx \rho(x) r^{-2\Delta_0+x^2} \quad (1.22)$$

where ρ plays the role of a non-universal density and Δ_0 is the smallest conformal dimension appearing in the decomposition of \mathcal{O} on conformal fields. This is very different to what is observed for compact theories where the largest contribution dominates all the subleading terms. Here, for large distances r , the correlation functions have logarithmic corrections

$$\langle \mathcal{O}(0)\mathcal{O}(r) \rangle_{\text{lattice}} \sim r^{-2\Delta_0} (\log r)^{\alpha_\rho} \quad (1.23)$$

where α_ρ depends on the precise behaviour of ρ in the vicinity of $x = 0$. Let us emphasize that the logarithmic part in the correlation function has a quite different origin than the one encountered in logarithmic conformal field theory. It comes from the lattice discretisation whereas, for LCFTs, the logarithm correlation functions are intrinsic properties of the continuum.

A few years ago, it was realised that a non-compact continuum limit can be obtained from the thermodynamic limit of a compact lattice model. It is far from obvious that a model with a finite number of degrees of freedom can flow toward a non-compact fixed point. The first instance of this observation was in a paper [64] of Jacobsen, Read and Saleur where, in the supersymmetric formulation of self-avoiding walks, they introduced the possibility of having loop crossing. The critical point involves non compact bosonic fields despite the apparent compactness of the model on the lattice. The same situation was later found in many models such as the antiferromagnetic Potts model (and the staggered six-vertex model) [65], a pair of coupled Potts models [66] or $a_{N-1}^{(2)}$ spin chains [67, 68]. Non-compact continuum limits are maybe more common than what was previously thought and not constrained to curious non-unitary and non-physical models. An additional example is the θ_{BN} point of polymers related to the black hole theory $SL(2, \mathbb{R})/U(1)$ [69].

As mentioned earlier, many systems of great interest are already non-compact (infinite-dimensional) on the lattice. It is natural to hope that they can be studied using truncations [37] where maybe the perturbation introduced is not relevant in the RG picture. Indeed, compact lattice models are much more convenient from the point of view of numerics and

exact methods (integrability). In general, the truncation changes of course the universality class but the untruncated model could still be approached by a series of successive truncations. In the case of the Brownian motion, this procedure is very easy to understand. Let us take a Brownian path with the additional constraint that an edge can be visited at most k times. All configurations of the usual Brownian motion are recovered in the limit $k \rightarrow \infty$ but the nature of the model at finite k is far from being obvious. Note that the case of $k = 1$ is actually well known since it corresponds to self-avoiding walks, a particular point of the $O(n)$ model discussed previously. The case of the Brownian motion is interesting since the untruncated model is already known.

The situation is extremely different in the case of the plateau transition in the Integer quantum Hall effect. Very few exact results were found for its CFT and critical exponents remain unknown. This program of truncations was partially proposed by Marston and Tsai [70]. They considered hard on-site truncations and approached the IQHE transition with a series of non-critical truncations. This idea was pushed further in the recent work of Ikhlef, Fendley and Cardy [37] where they proposed to define a series of critical truncations. The first one was studied and found to be in a different universality class than the full theory. Nevertheless, some aspects are related to the real plateau transition and, in particular, it is non-compact in the continuum. We would like to push this program further and understand the relation between a full non-compact model and its compact (in terms of the lattice degrees of freedom) truncations.

1.4.5 PT symmetry and RG-flow

The Hermiticity of a Hamiltonian is not a necessary condition to have a valid quantum system. However, it is required that the spectrum is real [71]. The class of quasi-Hermitian Hamiltonians are non-Hermitian operators such that an invertible operator η exists and satisfies

$$\eta H = H^* \eta. \quad (1.24)$$

This property ensures that H is Hermitian with respect to the inner product

$$\langle u|v \rangle_\eta \equiv \langle u|\eta|v \rangle. \quad (1.25)$$

The Hamiltonian can be transformed to a Hermitian operator $\eta^{1/2} H \eta^{-1/2}$. Note that such maps are usually hard to find. The quasi-Hermiticity property ensures that the spectrum of H is real. An important criterion to determine if a Hamiltonian is quasi-Hermitian is the PT -symmetry. Let us first give some definitions and consider a spin chain of length L with an on-site basis $|i\rangle$, $i = 1, \dots, d$. The space reversal operator P is linear and acts on the Hilbert space $\mathcal{H} = V^{\otimes L}$ as

$$P|i_1, \dots, i_L\rangle = |i_L, \dots, i_1\rangle. \quad (1.26)$$

The time reversal operator T acts as the identity

$$T|i_1, \dots, i_L\rangle = |i_1, \dots, i_L\rangle \quad (1.27)$$

but is an antilinear operator. It means that any matrix operator M is transformed under the action of T as

$$TMT = M^*, \quad (1.28)$$

with M^* the conjugate operator of M . A Hamiltonian H is said to be PT -symmetric if

$$[PT, H] = 0. \quad (1.29)$$

This criterion is not exactly sufficient to obtain real spectra, the eigenstates of the Hamiltonian also need to be PT -invariant. This criterion is very useful in the context of the XXZ spin chain and its loop representation [72,73] and many non-Hermitian systems are described by a PT -symmetric Hamiltonian.

This extra symmetry permits the extension of several results obtained in unitary conformal field theory. In particular, a version of the celebrated c -theorem, found in 1986 by Zamolodchikov [74], exists for PT -invariant Hamiltonian [75]. We first recall the classical result in unitary CFT. The c -theorem states that, along an RG-flow, there exists a scaling function $c(s)$ that decreases monotonically. At a fixed point, $c(s)$ corresponds to the central charge of the universality class. In other words, an RG flow between two universality classes always goes towards the theory with the smallest central charge. This very famous result is true only in the unitary case. Different versions of this theorem exist and the function $c(s)$ is interpreted as a measurement of the number of degrees of freedom at a given scale s . Note that equivalent results exist in higher dimension where the irreversibility of the flow is not measured by c . Whether a similar theorem exists in the non-unitary case is an important question. The breaking of unitarity allows a flow with increasing $c(s)$.

A version of this theorem was recently proposed by Castro-Alvaredo, Doyon and Ravanini in [75]. The generalisation of the c -theorem [75] to this class of models shows that the irreversibility of the flow is measured by the effective central charge, mentioned earlier in 1.4.2. This important result shows that this quantity is important from a physical point of view and a proper way to quantify the number of degrees of freedom.

1.5 The plan of this manuscript

In the second chapter, based on [76], the concept of entanglement entropy in non-unitary CFTs is discussed. Ideas coming from quantum information have radically changed our understanding of quantum systems. The entanglement entropy has many applications in condensed matter and statistical physics. However, most of results are derived for unitary systems where probabilities and norms are well-defined and the non-unitary case remained unexplored until the last few years. After discussing the relation between conformal field theory and quantum information theory we propose a new approach. The concept of quantum group entanglement entropy is discussed and motivated by symmetries and geometrical considerations. A link with loop models is established and a geometric way of computing entanglement directly within this formalism is given. Our main toy model is the Potts model in its vertex representation related to the $U_qsl(2)$ invariant XXZ chain. The quantum group

entanglement entropy distinguishes the role of the central charge and the effective central charge. The proposed approach is then applied to different systems such as the Restricted Solid-on-Solid models or the supersymmetric spin chain $sl(2|1)$.

The third chapter, based on [77], discusses the truncations of the Chalker-Coddington model. The beginning presents the network model and the first truncation introduced and studied by Ikhlef, Fendley and Cardy. They considered in their paper an integrable deformation of this model in order to use usual techniques of integrability. The equivalence between the integrable deformation and the first truncation is not obvious. We study their similarities and differences. A generalisation of the procedure to higher levels of truncation is then given. In parallel, a similar work is done for the Brownian motion to gain some insight about the phenomenology of this approach.

In the fourth chapter, we propose to study a flow between class A and class C in the plateau transition of the Hall effect. Even though they describe different physical quantities, the two classes are formally very close in terms of their lattice description. Despite their similarities, class C is solvable and found to be related to percolation. We take advantage of the network formalism to propose a model with a RG-flow between the two universality classes. The direction of the flow is studied numerically and the symmetries discussed. The advantage of our approach is to be easily generalised to describe the flow between class C and all the truncations of the Chalker-Coddington model. In particular, it is a good playground to understand flows in non-unitary models and extension of the c -theorem of Zamolodchikov.

In the fifth and last chapter, following the articles [78, 79], we use the Fortuin-Kasteleyn formulation of the Q -state Potts model, a generalisation of the concept of percolation clusters, to study non-local observables. This approach, following the original work of Cardy, uses the underlying discrete symmetry S_Q to classify the operator content of the theory. This is in particular very interesting from the point of view of indecomposability and provides very practical examples of logarithmic correlation functions in a model. Moreover, the nature of the observables is related to the irrationality of the theory, a common feature of non-unitary minimal models. Our contribution to this topic is the extension of the previous analysis to a large new class of observables. Previous works were focused on operators transforming purely symmetrically under the action of the symmetric group. The classification is extended to any representation of the group of permutations and provides lattice definition of non-scalar operators. In two dimensions, a connection is made with conformal field theory and the representation of the Jones-Temperley-Lieb algebra. In particular, the conformal dimensions and the spins of many observables are identified exactly. This is satisfied numerically using Monte-Carlo simulations for percolation and transfer matrix diagonalisation. The present approach is however not limited to two dimensions. The same analysis holds in three dimensions where the same classification is relevant. Of course, obtaining exactly the conformal dimensions is out of reach. Nevertheless, it is possible to predict the presence of Jordan cells in any dimension. This formalism is very promising to study Logarithmic Conformal Field theory in $d > 2$.

2 Entanglement in non-unitary critical systems

Ideas coming from both quantum information theory and field theory have profoundly affected our understanding of quantum systems at criticality. Let us consider a partition of a quantum system into two parts A and B . The quantity called *entanglement entropy* S_A (or equivalently S_B) is a measurement of the entanglement between A and B . It has many physical implications and, in particular, important consequences in numerical simulations. Methods such as DMRG or more generally tensor networks [80,81] were developed thanks to the improving understanding of entanglement. They are now applied to strongly correlated systems with great success.

For non-critical (gapped) systems, the entanglement entropy satisfies the so called *area law* [82–85]

$$S_A \sim k \text{Area}(\partial A) \tag{2.1}$$

where k is non-universal. In other words, the entanglement entropy grows as the size of the boundary between A and B . Indeed, in a gapped system, correlation functions decay exponentially. As a consequence, on a lattice, a site in A and a site in B are entangled only if they are close to each other. Globally, the entanglement between A and B is located near their boundary and thus S_A grows with the size of ∂A . Of course, in the case of critical (gapless) systems, this simple argument breaks down. Critical systems have long-range correlation functions that decay only algebraically. Therefore, the area law is not satisfied anymore. It was found [86,87], in the case of $1 + 1D$ critical systems where A is an interval of length L in an infinite system, that

$$S_A \sim \frac{c}{3} \log \frac{L}{a}, \quad L \gg a \tag{2.2}$$

where a is a lattice cutoff and c the central charge of the associated CFT. This scaling relation involves a universal quantity and opens many possible connections between quantum information and conformal field theory [88,89]. It is a very natural question to ask whether this result holds for non-unitary systems. Different approaches [90] have been investigated in order to derive (2.2). In several cases [91,92], it is expected for non-unitary systems to have a modified scaling relation of the form

$$S_A \sim \frac{c_{\text{eff}}}{3} \log \frac{L}{a} \tag{2.3}$$

where c_{eff} is the effective central charge.

In this chapter, this result is revisited in practical examples. The focus of the discussion is on systems with quantum group invariance or supergroup symmetry. In particular, the XXZ spin chain with open boundary condition is considered with its quantum group $U_qsl(2)$ invariance [93]. The first section introduces basic concepts and recalls the definition of entanglement entropy as well as its interpretation in conformal field theory. The XXZ spin chain is then briefly presented in 2.2. Its physical relevance as a description of the Potts model is

discussed and its correspondence with a loop model is detailed. The third section 2.3 introduces a new quantity, called *quantum group entanglement entropy*. This concept, motivated by the loop model, is shown to have interesting properties and simple illustrations are given. The derivation of the scaling law within our framework is then presented using Coulomb gas techniques. Other problems can be addressed using this approach, in particular, results for RSOS models, supersymmetric spin chains or non-compact models are all derived. Lastly, the similarities and differences between this work and other approaches are discussed.

2.1 Entanglement entropy

2.1.1 Definitions

Consider a quantum system described by a density matrix ρ . In this chapter, only pure quantum states (associated to a normalised ket $|\psi\rangle$) are considered hence the density matrix is simply

$$\rho = |\psi\rangle\langle\psi|. \quad (2.4)$$

The state $|\psi\rangle$ lives in a Hilbert space \mathcal{H} . Let us assume \mathcal{H} to be a direct product of two subspaces \mathcal{H}_A and \mathcal{H}_B

$$\mathcal{H} = \mathcal{H}_A \otimes \mathcal{H}_B. \quad (2.5)$$

The reduced density matrix ρ_A is defined as the partial trace of ρ , over the degrees of freedom in B,

$$\rho_A = \text{Tr}_B \rho. \quad (2.6)$$

The entanglement entropy, or von Neumann entropy, is defined by

$$S_A = -\text{Tr}_A (\rho_A \log \rho_A). \quad (2.7)$$

This quantity measures effectively *how much* the subsystem A is entangled with the subsystem B. In particular, when the ket is a product of a state $|\psi_A\rangle \in \mathcal{H}_A$ and a state $|\psi_B\rangle \in \mathcal{H}_B$ then

$$S_A = S_B = 0 \quad \text{if} \quad |\psi\rangle = |\psi_A\rangle \otimes |\psi_B\rangle. \quad (2.8)$$

Other measures of entanglement are possible. In particular, the Rényi entropies

$$S_A^{(N)} = \frac{1}{1-N} \log \text{Tr}_A (\rho_A^N) \quad (2.9)$$

are a generalisation of the von Neumann entropy. Indeed the definition (2.7) is recovered in the limit $N \rightarrow 1$. Note that the entanglement entropy (or more generally the Rényi entropies) is not a good measurement of the entanglement in the case of mixed states. For instance, when ρ is not the density matrix of a pure state, $S_A^{(N)} = S_B^{(N)}$ is not satisfied. Other

measurements of the entanglement, such as the entanglement negativity, are also interesting. It provides, for instance, a measure of the entanglement between two disjoint parts of a system. This chapter focuses on the von Neumann entropy (and more generally the Rényi entropies) and extensions to other measurements of the entanglement are not considered in this work.

2.1.2 Conformal field theory interpretation

Let us first give a brief presentation of some connections between the entanglement entropy and conformal field theory, following the ideas of Calabrese and Cardy [94]. In order to provide a connection between the entanglement entropy and conformal field theory, let us consider a 1 + 1D quantum system at finite inverse temperature $\beta = 1/T$ described by a Hamiltonian H . Its density matrix reads

$$\rho = \frac{1}{Z} e^{-\beta H} \quad (2.10)$$

with $Z = \text{Tr} (e^{-\beta H})$ the partition function, appearing here to ensure the right normalisation $\text{Tr} \rho = 1$. Given two states $|\phi\rangle, |\phi'\rangle$, the matrix element $\rho(\phi, \phi') = \langle \phi | \rho | \phi' \rangle$ is the overlap between ϕ and ϕ' after a propagation, in imaginary time evolution, at a time $\tau = \beta$. It can be represented by the picture 2.1a.

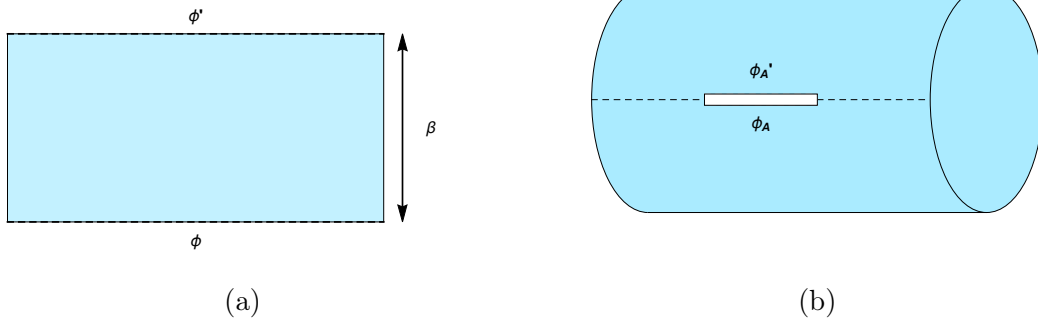


Figure 2.1 – The left figure shows the diagrammatic representation of an element of matrix $\rho(\phi, \phi')$. The horizontal (resp. vertical) direction corresponds to the spatial (resp. time) space. At finite temperature, the density matrix ρ connects two states by a slice of the quantum system of height β . The right figure (b) shows a picture representing the reduced density matrix when the subsystem A is a single interval. The two dashed line of left picture are stitched together except along A .

The trace operation corresponds, in this picture, to sewing the two dashed edges in figure 2.1a. Thus the partition function is indeed a cylinder of circumference β . The picture for the partial trace is very similar. A partial trace over the subsystem B is diagrammatically obtained by only stitching together the part of the dashed lines of figure 2.1a in B . In the

case where A is an interval, there is a cut in the middle of the cylinder 2.1b. The resulting operator, ρ_A , connects quantum states of \mathcal{H}_A . At zero temperature for a cylinder of infinite length, the circumference becomes infinite and we obtain a full plane with a cut in the middle. Note that, in the case of a non-Hermitian Hamiltonian, the mapping between the density matrix and its path integral picture is of course still valid for the density matrix (2.10). However the limit at zero temperature is not simply $\rho = |0\rangle\langle 0|$, with $|0\rangle$ the ground state, but

$$\rho = |0_R\rangle\langle 0_L| \quad (2.11)$$

where we distinguish right and left ground states. Let us disregard this issue for now and consider the case of a Hermitian Hamiltonian with $|0\rangle \equiv |0_R\rangle = |0_L\rangle$. It is now possible to give a path integral formulation of the entanglement entropy. The idea, known as the replica trick, is to consider the Rényi entropy for integer N . The object $\text{Tr} \rho_A^N$ can be computed by considering N copies of the system where each copy is connected to an other on one side of the cut. A picture is given in the case $N = 2$ figure 2.2.

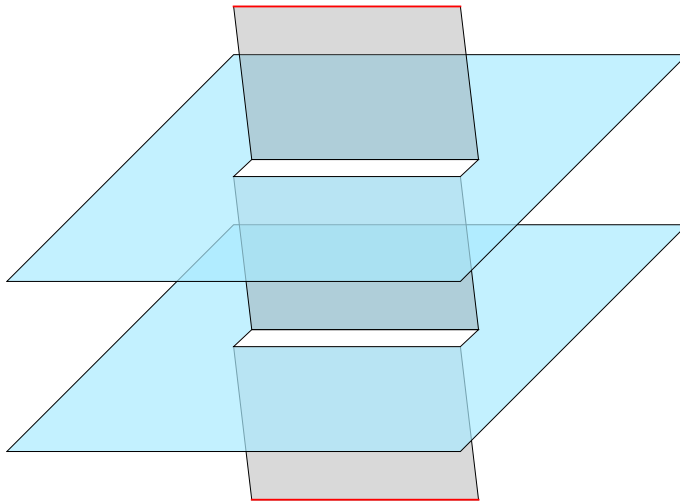


Figure 2.2 – Riemann surface with 2 replicas. The two blue planes are infinite and are stitched together at their cut. Periodic boundary condition is enforced by the trace therefore the two red lines are identified.

The quantity $\text{Tr} \rho_A^N$ corresponds (up to a normalisation factor) to the partition function Z_N on a N -sheeted Riemann surface. The normalisation factor for each ρ_A is the simple partition function Z_1 on a single plane. Therefore we are left with the quantity

$$\text{Tr}_A \rho_A^N = \frac{Z_N}{Z_1^N} \quad (2.12)$$

to compute. This analysis is valid for all integer values of $N > 1$ and the von Neumann entropy can be derived by considering the analytic continuation in the limit $N \rightarrow 1$

$$S_A = - \lim_{N \rightarrow 1} \partial_N \log \left(\frac{Z_N}{Z_1^N} \right). \quad (2.13)$$

In the following, the concept of twist fields is briefly presented. The goal of this section is not to provide a detailed mathematical description of this object and of the cyclic orbifold but to show that computing the partition function on a N -sheeted Riemann surface can be re-expressed as a correlation function of some operators. In particular, the derivation of the conformal dimension of the twist field using Ward identities is not recalled since a different approach using Coulomb gas methods is presented later in this chapter. The simple case of a cut corresponding to a single interval $[u, v]$ is considered. Let us take a very general Lagrangian $\mathcal{L}[\varphi](x, \tau)$ for a field φ . The Lagrangian on the Riemann surface with N replicas reads

$$Z_N = \int_{\mathcal{C}_N} \prod_{i=1}^N d\varphi_i e^{-\int dx d\tau (\sum_{i=1}^N \mathcal{L}[\varphi_i](x, \tau))} \quad (2.14)$$

where the N fields $\{\phi_i\}$ are coupled by the conditions

$$\varphi_i(x, 0^+) = \varphi_{i+1}(x, 0^-), \quad x \in [u, v], \quad i = 1, \dots, N \quad (2.15)$$

that are included in the definition of the domain \mathcal{C}_N . This condition encodes the continuity of the fields in the vicinity of the cuts. This condition on the integral domain can be re-expressed using two fields \mathcal{T}_N and $\tilde{\mathcal{T}}_N$, called twist fields [95], acting respectively at the branch points of the cut. The partition function is now a two-point function where the condition on the integral domain is dropped

$$Z_N = \int \prod_{i=1}^N d\varphi_i \mathcal{T}_N(u) \tilde{\mathcal{T}}_N(v) e^{-\int dx d\tau (\sum_{i=1}^N \mathcal{L}[\varphi_i](x, \tau))}. \quad (2.16)$$

Therefore the task is now to compute the two-point function

$$\frac{Z_N}{Z_1^N} = \langle \mathcal{T}_N(u) \tilde{\mathcal{T}}_N(v) \rangle \quad (2.17)$$

where the conformal dimension of the twist field is left to be determined exactly. In general, this can be done by considering the conformal mapping

$$z \rightarrow \left(\frac{z-u}{z-v} \right)^{1/N} \quad (2.18)$$

that transforms the N -sheeted Riemann surface to a plane (the N cuts are mapped toward infinite lines going from the origin to the infinity). The conformal dimension $h_{\mathcal{T}_N}$ is computed using Ward identities, it was found that

$$h_{\mathcal{T}_N} = \frac{c}{24} \left(N - \frac{1}{N} \right) \quad (2.19)$$

where c is the central charge of the original conformal field theory. The scaling of the entanglement entropy can now be derived since

$$\mathrm{Tr}_A \rho_A^N = \frac{Z_N}{Z_1^N} \propto \ell^{-4h\tau_N} \quad (2.20)$$

with $\ell = |u - v|$ being the length of the cut. Computing the Rényi entropies (2.9) is now straightforward

$$S_A^{(N)} = \frac{1}{1-N} \log \mathrm{Tr}_A \rho_A^N \sim \frac{(N+1)c}{6N} \log \ell/a \quad (2.21)$$

with a a microscopic cut-off. The von Neumann entropy is derived by the analytic continuation for real N and taking the limit $N \rightarrow 1$

$$S_A \sim \frac{c}{3} \log \ell/a. \quad (2.22)$$

2.1.3 The non-unitary case: first observations

The naive extension to non-unitary case is now discussed. Before considering a specific model, we discuss the apparent issues with the scaling (2.22) and review some results found in the literature.

First, as it was hinted earlier, the definition of the density matrix must distinguish between right and left eigenvectors. Indeed, the field theory interpretation holds only if it is possible to write the density matrix as the zero temperature limit of the evolution operator in imaginary time. This definition may seem curious from the point of view of pure quantum information. Indeed the von Neumann entropy measures the entanglement within a given quantum state and it is, *a priori*, acceptable to study a naive entropy where $\rho = |0_R\rangle\langle 0_R|$.

A second apparent difference comes from the prefactor of the scaling law (2.22). In a unitary CFT, a non trivial theory has a strictly positive central charge hence equation (2.22) is in a perfect agreement with the fact that the von Neumann entropy is a positive quantity. However in a non-unitary system, the central charge can be zero or negative. The simplest cases of such systems are the non-unitary minimal models. A famous member of this class of model is the Yang-Lee model [96, 97] with $c = -22/5$. The minimal models $\mathcal{M}(p, p')$ are a series of conformal field theories with a finite number of primary fields with integer p and p' coprime such that $2 \leq p < p'$. The central charge is given by

$$c = 1 - \frac{6(p-p')^2}{pp'} \quad (2.23)$$

and the conformal weights are

$$h_{r,s} = \frac{(pr - p's)^2 - (p-p')^2}{4pp'}, \quad 1 \leq r \leq p' - 1, \quad 1 \leq s \leq p - 1. \quad (2.24)$$

In the non-minimal series $|p - p'| > 1$, it is important to notice that their conformal spectrum contains a negative conformal weight. The smallest conformal weight h_{\min} is given by

$$h_{\min} = \frac{1 - (p - p')^2}{4pp'} < 0. \quad (2.25)$$

Therefore, the ground-state of the theory is no longer the conformal vacuum. The partition function (on a N -sheeted Riemann surface) interpretation as a two points correlation function (2.17) is thus a little bit more subtle. The so-called effective central charge can be defined

$$c_{\text{eff}} = c - 24h_{\min} = 1 - \frac{6}{pp'} \quad (2.26)$$

which is positive. This universal quantity appears for instance in the scaling of the energy per unit of length on a cylinder of circumference L [45]

$$E = -\frac{v_S \pi c_{\text{eff}}}{24L}. \quad (2.27)$$

The scaling of the entanglement entropy was found to hold if c is replaced by c_{eff} within the framework of RSOS models [98]. The goal of this chapter is to revisit this problem in a more general case. In particular we are not restricted to non-unitary minimal models. Connections with loop models are going to be detailed. The twist field analysis in particular is going to be connected to a Coulomb gas analysis.

2.2 The XXZ spin chain

The Potts model is introduced in this section. Its mappings to a loop model and a vertex model are discussed. We show explicitly the connection between both and derive the quantum Hamiltonian associated. The XXZ Hamiltonian is recovered with Hermiticity breaking boundary terms. It is symmetric under the action of the quantum group $U_q sl(2)$, a deformation of $sl(2)$.

2.2.1 Potts model

The Q -state Potts model is a lattice model of interacting spins. Considering a graph $G = (V, E)$ with vertex set V and edge set E . To each vertex $i \in V$ we associate a spin σ_i that can take Q possible states, $\sigma_i = 1, 2, \dots, Q$. The interaction between two spins, σ_i and σ_j , linked by an edge $(ij) \in E$, adds a contribution $-K\delta_{\sigma_i, \sigma_j}$ to the total energy of the system, where δ is the Kronecker symbol. Hence the partition function is

$$Z = \sum_{\{\sigma\}} \prod_{(i,j) \in E} e^{K\delta_{\sigma_i, \sigma_j}}, \quad (2.28)$$

where $\{\sigma\} \equiv \{\sigma_i\}_{i \in V}$ denotes all the possible spin configurations of the system. Let us emphasise that for now we do not make any particular assumptions about the graph G ,

neither about the regularity of the lattice, nor about the number of dimensions d into which it can be embedded.

The above partition function can be expanded in terms of the Fortuin-Kasteleyn (FK) clusters [29]. Since the interaction energy between two spins has only two possible values, we use the identity $e^{K\delta_{\sigma_i, \sigma_j}} = 1 + v\delta_{\sigma_i, \sigma_j}$, with $v = e^K - 1$, to transform the product over the edges into a sum over subsets $A \subseteq E$ of edges. A connected component of the subgraph (V, A) is called an FK cluster. Then, by performing the sum over $\{\sigma\}$, we arrive at

$$Z = \sum_{A \subseteq E} Q^{k(A)} v^{|A|}, \quad (2.29)$$

where $k(A)$ denotes the number of connected components in the subgraph (V, A) with $|A|$ edges.

We notice that all the spins within a same FK cluster take the same spin value. However, the spins of two different clusters are independent; in particular they may take the same value even if the two clusters are adjacent.

Thanks to the formulation (2.29) of the Q -state Potts model, the definition of the partition function can now be extended to real values of Q . This makes it possible to approach physical situations (for which Q is a non-negative integer) via a limiting procedure. The models of main interest stand at $Q = 0$ (spanning trees and forests), $Q = 1$ (percolation) and $Q = 2$ (Ising model). For $Q < 2$ they have non-trivial critical points for $2 \leq d \leq 6$ [99, 100]. In $d = 2$, the model on a regular square lattice can be mapped to a 6-vertex model [101] and is critical for $0 \leq Q \leq 4$ [102].

2.2.2 Loop model formulation

We now study the Potts model in $d = 2$ on a square lattice with open boundary conditions. Starting from its formulation in terms of clusters (2.29), a loop model is obtained by drawing the surroundings (inner and outer) on the medial graph for each cluster. This is illustrated figure 2.3 on an arbitrary configuration.

More precisely, the partition function (2.29) can be written, using topological identities, as

$$Z = Q^{|V|/2} \sum_{A \subseteq E} Q^{\ell(A)/2} \left(\frac{v}{\sqrt{Q}} \right)^{|A|} \quad (2.30)$$

where $\ell(A)$ is the number of closed loops. On a square lattice, the isotropic critical point of the Potts model is obtained at $v = \sqrt{Q}$ simplifying again the partition function which, up to an overall factor, is

$$Z = \sum_{A \subseteq E} n^{\ell(A)} \quad (2.31)$$

with $n = \sqrt{Q}$ the loop fugacity. Still on a square lattice, it is convenient to write the transfer matrix and the Hamiltonian in terms of the Temperley-Lieb (TL) algebra [42]. For M

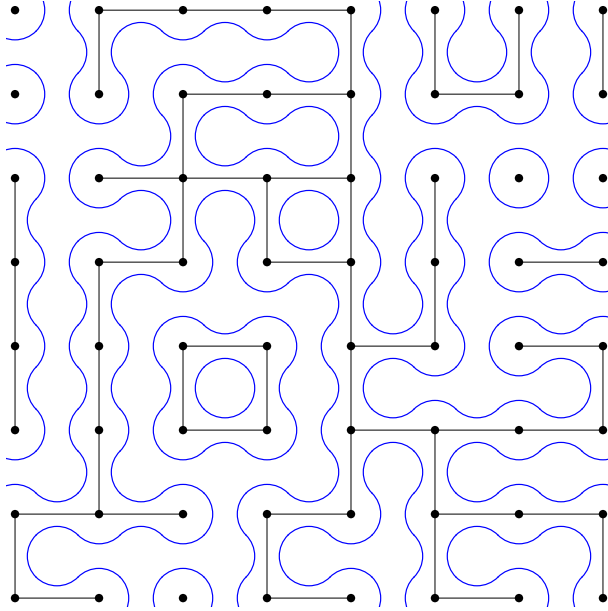


Figure 2.3 – Typical configuration of FK-clusters on a square lattice. The inner and outer boundaries of each cluster form loops on the medial graph.

integer and q a complex number of modulus 1, the TL algebra $TL_{q,2M}$ has $2M - 1$ generators $\{e_i\}_{i=1,\dots,2M-1}$ satisfying the relations

$$[e_i, e_j] = 0, |i - j| \geq 2, \quad (2.32)$$

$$e_i^2 = n e_i, \quad (2.33)$$

$$e_i e_{i\pm 1} e_i = e_i \quad (2.34)$$

with $n = q + q^{-1}$. It has a diagrammatic interpretation allowing a direct connection with the loop configurations of the Potts model. The generator e_i is represented by the diagram

$$e_i = \left| \begin{array}{c} | \\ | \\ \dots \\ \text{---} \cup \text{---} \\ \text{---} \cap \text{---} \\ \dots \\ | \\ | \end{array} \right| \quad (2.35)$$

$i \quad i+1$

Multiplication of words in the algebra is done by stacking the diagrams. Two diagrams are identical if the connectivities are the same. Each time a closed loop is generated, it is removed and a weight n is produced.

2.2.3 The six-vertex model and the XXZ Hamiltonian.

The last useful representation of the Potts model needed in this chapter is the 6-vertex model and its XXZ quantum Hamiltonian. Writing the loop fugacity n as the sum of two conjugate

complex numbers, $n = e^{i\gamma} + e^{-i\gamma}$ with $q = e^{i\gamma}$, leads to an interesting mapping with oriented loops. An un-oriented loop is the superposition of the two orientations

$$\begin{array}{c}
 \text{---} \bigcirc \text{---} \\
 n
 \end{array}
 =
 \begin{array}{c}
 \text{---} \bigcirc \text{---} \\
 q
 \end{array}
 +
 \begin{array}{c}
 \text{---} \bigcirc \text{---} \\
 q^{-1}
 \end{array}
 \quad (2.36)$$

The non-local fugacity of loops can be traded for a local complex weight: a loop turning of an angle $\pm\pi/2$ at a vertex gets a local weight $e^{\pm i\gamma/4}$. At a vertex on the medial square lattice, 6 configurations of arrows are possible due to the conservation of incoming/outgoing arrows. They are given figure 2.4 and generate the 6-vertex model.

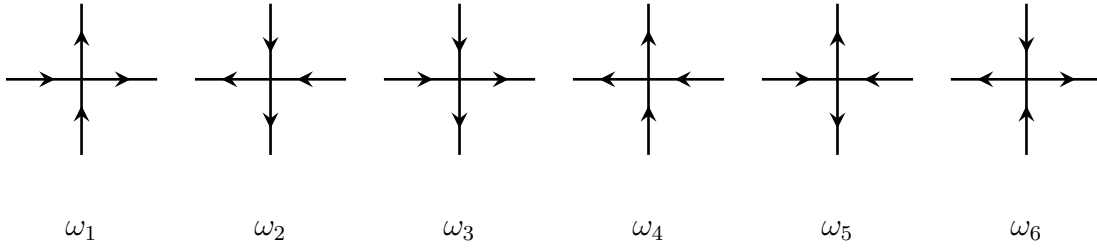


Figure 2.4 – Vertices of the six-vertex model.

The weights obtained by the mapping with the loop models are given by

$$\omega_1, \dots, \omega_6 = 1, 1, x, x, e^{i\gamma/2} + x e^{-i\gamma/2}, e^{-i\gamma/2} + x e^{i\gamma/2}. \quad (2.37)$$

These weights are obtained by drawing all local loop configurations possible with the orientation of the arrows. The parameter x measures the anisotropy in the system (see [42] for details) and is useful to derive the quantum Hamiltonian. The decomposition of the vertices ω_1 and ω_5 are given below as examples.

$$\begin{array}{c}
 \text{---} \bigcirc \text{---} \\
 \omega_1
 \end{array}
 =
 \begin{array}{c}
 \text{---} \curvearrowright \\
 e^{i\gamma/4} \times e^{-i\gamma/4}
 \end{array}
 ,
 \quad
 \begin{array}{c}
 \text{---} \bigcirc \text{---} \\
 \omega_5
 \end{array}
 =
 \begin{array}{c}
 \text{---} \curvearrowleft \\
 x e^{-i\gamma/4} \times e^{-i\gamma/4}
 \end{array}
 +
 \begin{array}{c}
 \text{---} \curvearrowright \\
 e^{i\gamma/4} \times e^{i\gamma/4}
 \end{array}
 \quad (2.38)$$

This reformulation as a vertex model provides a local description where each edge is associated with a two-dimensional vector space $V = \{|\uparrow\rangle, |\downarrow\rangle\}$. The transfer matrix T for a system of size $2M$ with open boundary conditions is

$$T = \prod_{i=1}^{M-1} (1 + x e_{2i+1}) \prod_{i=1}^M (1 + x e_{2i}) \quad (2.39)$$

where e_i are complex matrices acting on site i and $i + 1$. Let $\sigma_i^{x,y,z}$ be Pauli matrices acting on space i , the element e_i is

$$e_i = -\frac{1}{2} \left[\sigma_i^x \sigma_{i+1}^x + \sigma_i^y \sigma_{i+1}^y + \frac{q + q^{-1}}{2} (\sigma_i^z \sigma_{i+1}^z - 1) + \frac{q - q^{-1}}{2} (\sigma_i^z - \sigma_{i+1}^z) \right]. \quad (2.40)$$

In the basis $|\uparrow\uparrow\rangle, |\uparrow\downarrow\rangle, |\downarrow\uparrow\rangle, |\downarrow\downarrow\rangle$ it reads explicitly

$$e_i = \begin{pmatrix} 0 & 0 & 0 & 0 \\ 0 & q & -1 & 0 \\ 0 & -1 & q^{-1} & 0 \\ 0 & 0 & 0 & 0 \end{pmatrix} \quad (2.41)$$

As the notation suggests, these operators satisfy the Temperley-Lieb relations. The anisotropic limit is obtained by considering $x \rightarrow 0$. The 1 + 1D quantum Hamiltonian H associated with this 6-vertex model is obtained from the expansion of the transfer matrix around $x = 0$.

$$T = 1 - xH + O(x^2) \quad (2.42)$$

which gives

$$H = - \sum_{i=1}^{L-1} e_i. \quad (2.43)$$

This Hamiltonian can be written in terms of Pauli matrices

$$H_{\text{XXZ}} = \frac{1}{2} \sum_{i=1}^{L-1} \left(\sigma_i^x \sigma_{i+1}^x + \sigma_i^y \sigma_{i+1}^y + \frac{q + q^{-1}}{2} \sigma_i^z \sigma_{i+1}^z \right) + \frac{q - q^{-1}}{2} (\sigma_1^z - \sigma_L^z) \quad (2.44)$$

up to a constant term. The famous XXZ Hamiltonian can be recognised with anisotropy parameter $\Delta = (q + q^{-1})/2$. Note that, despite its name, Δ is not related at all to the parameter x measuring the anisotropy in the two dimensional lattice description. The only difference with the usual unitary XXZ chain comes from the boundary term. It breaks the Hermiticity of the Hamiltonian but is very important in terms of symmetry since it ensures the commutation of \mathcal{H} with the generators of the quantum group $U_q sl(2)$ [93].

2.2.4 Quantum group

As mentioned, the Hamiltonian (2.43) is symmetric under the action of the quantum group $U_q sl(2)$. This symmetry is essential in the relation between the spin $\frac{1}{2}$ representation of the XXZ spin chain and the loop model. In particular, for q root of unity, the representation theory of $U_q sl(2)$ plays an important role in the analysis of indecomposability.

The generators of $sl(2)$, S^\pm and S_z , satisfy the relations

$$[S^+, S^-] = 2S^z, \quad [S^z, S^\pm] = \pm S^\pm. \quad (2.45)$$

This algebra is the symmetry of the XXX spin chain. The XXZ is a generalisation of this Heisenberg model, the symmetry now being encoded in the quantum-group $U_q sl(2)$, a quantum deformation of $sl(2)$. The generators satisfy the relations

$$[S^+, S^-] = \frac{q^{2S^z} - q^{-2S^z}}{q - q^{-1}}, \quad [S^z, S^\pm] = \pm S^\pm. \quad (2.46)$$

The usual $sl(2)$ algebra is restored in the limit $q \rightarrow 1$. The quantum group can be seen as the universal enveloping algebra of $sl(2)$. In the spin 1/2 representation, the above generators have the form [93]

$$S^z = \frac{1}{2} \sum_i \sigma_i^z \quad (2.47)$$

$$S^+ = \frac{1}{2} \sum_i q^{\sigma_i^z/2} \otimes \dots \otimes q^{\sigma_{i-1}^z/2} \otimes \sigma_i^+ \otimes q^{-\sigma_{i+1}^z/2} \otimes \dots \otimes q^{-\sigma_{2M}^z/2} \quad (2.48)$$

$$S^- = \frac{1}{2} \sum_i q^{\sigma_i^z/2} \otimes \dots \otimes q^{\sigma_{i-1}^z/2} \otimes \sigma_i^- \otimes q^{-\sigma_{i+1}^z/2} \otimes \dots \otimes q^{-\sigma_{2M}^z/2} \quad (2.49)$$

and commutes with the XXZ Hamiltonian $[H_{\text{XXZ}}, S^{+, -, z}] = 0$. Note that quantum groups play an important role in the search of integrable model [103]. Interactions, encoded in the R -matrix satisfying Yang-Baxter equations, can be constructed from its representation theory [104].

2.3 Quantum group entanglement entropy

This first section presents our approach to the entanglement entropy in the XXZ model. A new quantity, called *quantum group entanglement entropy* is introduced. This choice is first motivated by a simple case on two sites for the vertex model. The same calculations are performed in the loop model. In particular, it is shown that the entanglement entropy has a straightforward interpretation with loop connectivities. General definitions are then given and motivated by the correspondance between the two representations. Then a more complex example on four sites is detailed. In the end of the section, a few properties of this modified entanglement entropy are given. First we show that the definition respects the $U_q sl(2)$ symmetry of the model and discuss the several required properties of an entropy.

2.3.1 Pedagogical example on 2 sites

Let us start the discussion with the simple example of $2M = 2$ spin, for pedagogical purposes. The XXZ Hamiltonian is $H = -e_1$, with e_1 the unique TL generator given equation (2.41). The parameter $q = e^{i\gamma}$ is chosen such that $\gamma \in [0, \pi/2[$, leading to a positive loop fugacity $n = 2 \cos \gamma$. In the sector of zero magnetisation, there are 2 distinct eigenenergies $E_0 = -(q + q^{-1}) = -n$ and $E_1 = 0$. The right ground state, defined as $H|0_R\rangle = E_0|0_R\rangle$ reads

$$|0_R\rangle = \frac{1}{\sqrt{2}}(q^{-1/2}|\uparrow\downarrow\rangle - q^{1/2}|\downarrow\uparrow\rangle). \quad (2.50)$$

In this section, we use the (standard) convention that complex numbers are conjugated when calculating the bra associated with a given ket. Therefore $|0_R\rangle$ is normalized: $\langle 0_R|0_R\rangle = 1$. We assume for now that the density matrix is

$$\rho = |0_R\rangle\langle 0_R| = \frac{1}{2} \begin{pmatrix} 0 & 0 & 0 & 0 \\ 0 & 1 & -q^{-1} & 0 \\ 0 & -q & 1 & 0 \\ 0 & 0 & 0 & 0 \end{pmatrix}. \quad (2.51)$$

It is, of course, correctly normalized. Taking subsystem A as the left spin and subsystem B as the right spin, the resulting reduced density operator ρ_A is

$$\rho_A = \frac{1}{2} \begin{pmatrix} 1 & 0 \\ 0 & 1 \end{pmatrix}. \quad (2.52)$$

It leads to a von Neumann entropy (2.7) equal to

$$S_A = \log 2 \quad (2.53)$$

where the entropy of a $\frac{1}{2}$ -spin singlet is recognised. This result is obviously independent of q and identical to the well known result for the XXX case, where the non-Hermiticity problem disappears. However the behaviour of the entanglement is expected to change when the central charge is varied. Since the universality class is a function of q , this simple computation on two sites is not particularly representative. It turns out that for larger systems, the entropy has a weak dependence on q that disappears in the scaling limit.

An alternative definition is now proposed, motivated by the symmetries of the Hamiltonian and its loop model representation. First, as mentioned earlier, the Hamiltonian $H = -e_1$ is not Hermitian. To make the connection with conformal field theory, the distinction between right and left eigenvectors is required. They are defined by $H|E_R\rangle = E|E_R\rangle$ and $\langle E_L|H = E\langle E_L|$ (corresponding to $H^\dagger|E_L\rangle = E|E_L\rangle$ since the energies E are all real). The two eigenvectors in the sector of zero magnetisation ($S^z = 0$) are

$$|0_R\rangle = \frac{1}{\sqrt{q + q^{-1}}} (q^{-1/2}|\uparrow\downarrow\rangle - q^{1/2}|\downarrow\uparrow\rangle) \quad (2.54)$$

$$|1_R\rangle = \frac{1}{\sqrt{q + q^{-1}}} (q^{1/2}|\uparrow\downarrow\rangle + q^{-1/2}|\downarrow\uparrow\rangle) \quad (2.55)$$

where $|0_R\rangle$ denotes the right eigenstate associated with the lowest energy E_0 and $|1_R\rangle$ the right eigenstate associated with excitation E_1 . Similarly the left eigenstates are

$$|0_L\rangle = \frac{1}{\sqrt{q + q^{-1}}} (q^{1/2}|\uparrow\downarrow\rangle - q^{-1/2}|\downarrow\uparrow\rangle) \quad (2.56)$$

$$|1_L\rangle = \frac{1}{\sqrt{q + q^{-1}}} (q^{-1/2}|\uparrow\downarrow\rangle + q^{1/2}|\downarrow\uparrow\rangle). \quad (2.57)$$

The right and left states are carefully normalized such that

$$\langle i_L | i_R \rangle = 1, \quad \langle i_L | j_R \rangle = 0, \quad i \neq j. \quad (2.58)$$

With this choice, the Hamiltonian takes the simple form

$$H = \sum_{i=0,1} E_i |i_R\rangle \langle i_L|. \quad (2.59)$$

Note that $\langle 0_R | 1_R \rangle \neq 0$. A projector on an eigenstate can only be built using left and right eigenstates. The proper density operator is now defined as

$$\tilde{\rho} \equiv |0_R\rangle \langle 0_L| = \frac{1}{q + q^{-1}} \begin{pmatrix} 0 & 0 & 0 & 0 \\ 0 & q^{-1} & -1 & 0 \\ 0 & -1 & q & 0 \\ 0 & 0 & 0 & 0 \end{pmatrix} \quad (2.60)$$

To proceed, let us take the following definition for the reduced density matrix

$$\tilde{\rho}_A = \text{Tr}_B (q^{-\sigma_z} \tilde{\rho}) = \frac{1}{q + q^{-1}} \begin{pmatrix} 1 & 0 \\ 0 & 1 \end{pmatrix}. \quad (2.61)$$

The use of a modified trace is justified in the next sections with geometrical as well as quantum group theoretic considerations. This property is explicitly discussed later in this section. The operator $\tilde{\rho}_A$ is normalized for the modified trace: $\text{Tr}_A (\tilde{\rho}_A q^{\sigma_z}) = 1$. We now define the entanglement as

$$\tilde{S}_A = -\text{Tr}_A (q^{\sigma_z} \tilde{\rho}_A \ln \tilde{\rho}_A) = \ln(q + q^{-1}). \quad (2.62)$$

This entropy value is potentially more appealing than (2.53): not only it depends on q , it involves also explicitly the combination $n = q + q^{-1}$, which is the quantum dimension of the spin 1/2 representation of $U_q sl(2)$.

2.3.2 Entanglement in the loop model and Markov Trace

The same analysis is possible in the loop formalism. On $L = 2$ sites, the Hamiltonian is again given by the only TL generator, which diagrammatically reads

$$H = -e_1 = - \begin{array}{c} \cup \\ \cap \end{array}. \quad (2.63)$$

In loop models, the equivalent of a quantum state is called a link state. It is a non-crossing link pattern where sites are connected by pairs. In fact, a link between two sites represents the formation of a singlet. There are different kinds of link states and it is possible to have defects if a site is not connected in a pair. In the following, only the sector with zero defects (equivalently the sector with zero magnetisation in the vertex model) is considered because

it contains the ground state. For $L = 2$ there is only one link state $|1\rangle$ with zero defect corresponding to an arc connecting the two sites

$$|1\rangle = \frac{1}{\sqrt{n}} \text{---}\cup\text{---} \quad (2.64)$$

In the loop formalism, a bra is obtained from a ket by flipping and stacking the two drawings. The scalar product is obtained by gluing the diagrams and counting the number of closed loops. For instance, it is straightforward that $|1\rangle$ is well normalized.

$$\langle 1|1\rangle = \frac{1}{n} \bigcirc = 1 \quad (2.65)$$

Moreover, $|1\rangle$ is the ground state of the Hamiltonian (2.63) since $H|1\rangle = -n|1\rangle$

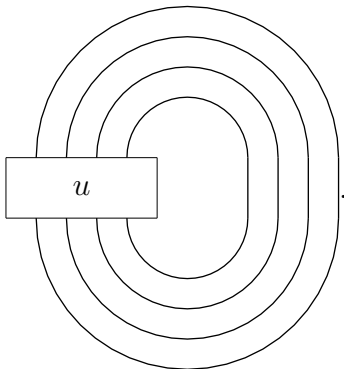
$$H|1\rangle = -e_1|1\rangle = -\frac{1}{\sqrt{n}} \bigcirc = -n \frac{1}{\sqrt{n}} \text{---}\cup\text{---} \quad (2.66)$$

Of course the connection with equations (2.54) and (2.56) comes from H_{XXZ} being a projector on the $U_qsl(2)$ singlet. The loop model provides a compact way to describe the action of the Hamiltonian annihilating and creating $U_qsl(2)$ singlets.

The density matrix, given by $\rho = |1\rangle\langle 1|$, reads in terms of diagrams

$$\rho = \frac{1}{n} \begin{array}{c} \text{---}\cup\text{---} \\ \text{---}\cup\text{---} \end{array} = \frac{1}{n} e_1 \quad (2.67)$$

where equation (2.60) can be recognised. The next task, computing the reduced density matrix, involves the (partial) trace operator. For loop models, tracing is performed by connecting the top and the bottom of a diagram. The resulting number of closed loops gives the value of the trace. It is called the Markov trace (MTr) and for any diagram u it is formally

$$\text{MTr}(u) = \text{---}\boxed{u}\text{---} \quad (2.68)$$


Note that this definition is consistent with the calculation of a scalar product where the link states are glued together (illustrated equation (2.65)). The Markov trace ensures, on a cylinder, that every closed loop has a weight n . The partial Markov trace is defined similarly

by connecting only certain sites. The reduced density matrix ρ_A , obtained by taking the Markov trace over the second site (2.67) reads

$$\rho_A = \text{MTr}_2(\rho) = \frac{1}{n} \left(\text{Diagram: a vertical line with two loops on the right side} \right) = \frac{1}{n} \left| \right. \quad (2.69)$$

A single line in a diagram acts as the identity. The equation (2.61) is thus recognised. The computation to obtain the von Neumann entropy is straightforward, given that the usual trace is replaced by the Markov trace.

$$S_A = -\text{MTr}_A \rho_A \log \rho_A = -\frac{1}{n} \log \frac{1}{n} \times \left(\text{Diagram: a circle} \right) = \log n \quad (2.70)$$

The result found in the last subsection, for the XXZ spin chain, is recovered. The key ingredient is to count the number of loops formed by the trace with the right fugacity n .

2.3.3 Definition of the quantum group entanglement entropy and motivations

The general definition for the modified entanglement entropy in the XXZ spin chain is now discussed. For a chain, with open boundary conditions and L sites, let us consider a subsystem A made of M neighbour spins. Its complement B is made of two parts, B_L on the left and B_R on the right, so that $B = B_L \cup B_R$ and $\mathcal{H} = \mathcal{H}_{B_L} \otimes \mathcal{H}_A \otimes \mathcal{H}_{B_R}$. The right and left ground states are distinguished so the density matrix ρ reads

$$\tilde{\rho} = |0_R\rangle\langle 0_L|, \quad (2.71)$$

with $|0_R\rangle$ and $\langle 0_L|$ the right and left ground states. The modified reduced density $\tilde{\rho}_A$ matrix is defined as

$$\tilde{\rho}_A = \text{Tr}_B q^{2S_{B_L}^z - 2S_{B_R}^z} \tilde{\rho} \quad (2.72)$$

where $S_{B_L}^z = \frac{1}{2} \sum_{i \in B_L} \sigma_i^z$ and $S_{B_R}^z = \frac{1}{2} \sum_{i \in B_R} \sigma_i^z$ are the magnetisations in the respective subsystems. The Quantum Group Entanglement Entropy, or QG EE, is defined by

$$\tilde{S}_A = -\text{Tr} q^{2S_A^z} \tilde{\rho}_A \log \tilde{\rho}_A. \quad (2.73)$$

The phases ensure that all loops, in the mapping to the geometrical representation, have the right fugacity. On a N -sheeted Riemann surface, a loop can propagate on the successive replicas and close on itself without being contractible. This is also the case on a cylinder. The figure 2.5a shows an example of configuration.

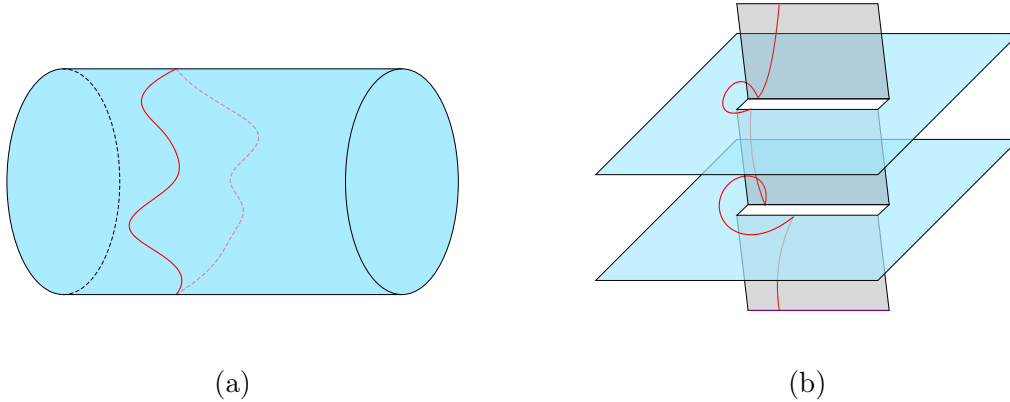


Figure 2.5 – On the left: a non-contractible loop on a cylinder. In the vertex formulation, if no twist is added, this loop gets a weight $\tilde{n} = 2$ instead of n . The right figure show a similar situation on the $N = 2$ -sheeted Riemann surface. A non contractible loop of this form does two full turns and get a weight $\tilde{n} = 2 \cos 2\gamma$ instead of n .

A loop winding around the periodic direction of the cylinder can be decomposed into two oriented loops. Since they are not globally turning to close on themselves, they do not acquire the phase q or q^{-1} but simply 1. In the end the loop fugacity is wrongly counted as $\tilde{n} = 1 + 1 = 2$. On the Riemann surface with N replicas, an oriented loop can wind around a branch point and form a closed loop after a turning of an angle $\pm 2\pi N$. In the vertex model, these oriented loops get a weight $q^{\pm N}$ and the un-oriented loop a fugacity $2 \cos N\gamma$. Ensuring that all loops have the same weight is exactly the role of the Markov Trace. The twist in the trace of the vertex model plays this role. The geometrical definition in terms of loops is thus very natural. The QG EE can be computed exactly in the loop model. Taking $\rho = |0\rangle\langle 0|$ as the density matrix of the system, the reduced density matrix is

$$\rho_A = \text{MTr}_B \rho \quad (2.74)$$

and the entanglement entropy is simply

$$S_A = -\text{MTr}_A \rho_A \log \rho_A \quad (2.75)$$

or for general Rényi entropies

$$S_A^{(N)} = -\frac{1}{N-1} \log \text{MTr}_A \rho_A^N. \quad (2.76)$$

Another important property of the definition (2.72) is that it respects the symmetry of the quantum group restricted on the subsystem A . This is developed further later in this section.

2.3.4 A more complex example: $2M = 4$ sites

As a more complicated example for the loop entanglement entropy, we propose to perform the computation of entanglement in the case of $2M = 4$ sites. The two possible link states with zero defects are.

$$|1\rangle = \text{---} \cup \text{---} \cup \text{---} \cup \text{---} \text{ , } |2\rangle = \text{---} \cup \text{---} \cup \text{---} \cup \text{---} \text{---} \quad (2.77)$$

The hamiltonian $H = -e_1 - e_2 - e_3$ has the following ground state $|0\rangle = \frac{1}{\mathcal{N}}(\alpha|1\rangle + |2\rangle)$, where $\mathcal{N}^2 = n^2\alpha^2 + 2n\alpha + n^2$ and $\alpha = (n + \sqrt{n^2 + 8})/2$. The density matrix ρ is

$$\rho = \frac{1}{\mathcal{N}^2} \left(\alpha^2 \begin{array}{c} \cup \\ \cup \end{array} + \alpha \begin{array}{c} \cup \quad \cup \\ \cup \quad \cup \end{array} + \alpha \begin{array}{c} \cup \quad \cup \\ \cup \quad \cup \end{array} + \begin{array}{c} \cup \quad \cup \\ \cup \quad \cup \end{array} \right).$$

Consider first a bipartition in which A is the first site, and B the remainder. Take the partial Markov trace over the three last sites, the reduced density operator is

$$\rho_A = \frac{1}{\mathcal{N}^2} (\alpha^2 n + 2\alpha + n) \left| \begin{array}{c} | \\ | \end{array} \right| = \frac{1}{n} \left| \begin{array}{c} | \\ | \end{array} \right|. \quad (2.78)$$

This leads to $\tilde{S}_A = \log n$, the same result found for $2M = 2$ spins.

Next, let us take A as the first two sites and compute the entanglement at the middle of the system. We trace the density operator over the two last sites:

$$\begin{aligned} \rho_A &= \frac{1}{\mathcal{N}^2} \left(\left| \begin{array}{c} | \\ | \end{array} \right| + (\alpha^2 n + 2\alpha) \begin{array}{c} \cup \\ \cup \end{array} \right) \\ &= \frac{1}{\mathcal{N}^2} (\mathbb{I} + (\alpha^2 n + 2\alpha) e_1). \end{aligned} \quad (2.79)$$

The logarithm of the operator ρ_A must be computed. The identity

$$\exp(a e_1) = 1 + \frac{1}{n} (\exp(an) - 1) e_1, \quad (2.80)$$

where $e_1 = \begin{array}{c} \cup \\ \cup \end{array}$, can be demonstrated by expanding the exponential. It follows

$$\log \rho_A = -\log \mathcal{N}^2 \mathbb{I} + \frac{2}{n} \log(1 + \alpha n) e_1. \quad (2.81)$$

and thus we can compute $\rho_A \log \rho_A$.

$$\begin{aligned} \rho_A \log \rho_A &= -\frac{\log \mathcal{N}^2}{\mathcal{N}^2} \left| \begin{array}{c} | \\ | \end{array} \right| + \left(\frac{-\log \mathcal{N}^2}{\mathcal{N}^2} (\alpha^2 n + 2\alpha) + \frac{2}{n \mathcal{N}^2} \log(1 + \alpha n) \right. \\ &\quad \left. + \frac{2}{\mathcal{N}^2} (\alpha^2 n + 2\alpha) \log(1 + \alpha n) \right) \begin{array}{c} \cup \\ \cup \end{array}. \end{aligned} \quad (2.82)$$

Tracing over A finally leads to

$$\begin{aligned}
S_A &= -\text{MTr}_A \rho_A \log \rho_A = \frac{n^2 \log \mathcal{N}^2}{\mathcal{N}^2} - n \left(\frac{-\log \mathcal{N}^2}{\mathcal{N}^2} (\alpha^2 n + 2\alpha) \right. \\
&\quad \left. + \frac{2}{n\mathcal{N}^2} \log(1 + \alpha n) + \frac{2}{\mathcal{N}^2} (\alpha^2 n + 2\alpha) \log(1 + \alpha n) \right) \\
&= -\frac{(1 + \alpha n)^2}{\mathcal{N}^2} \log(1 + \alpha n)^2 + \log \mathcal{N}^2.
\end{aligned} \tag{2.83}$$

This expression coincides with the result obtained by using the modified trace in the vertex model. Note also that this results agrees with the computations done in the Potts spin representation for $Q = n^2$ integer, not presented in this thesis [76].

For larger M it is hard to compute this final partial trace directly, since the form of $\log \rho_A$ will be substantially more complicated than (2.81). A much more convenient option is to recall that gluing corresponding sites on top and bottom of any word in the TL algebra means technically to take the so-called Markov trace MTr . This in turn can be resolved as follows

$$\text{MTr} = \sum_j [2j + 1]_q \text{Tr}_{\mathcal{V}_j}, \tag{2.84}$$

where $\text{Tr}_{\mathcal{V}_j}$ is the usual matrix trace over the (standard) module \mathcal{V}_j with $2j$ defect lines, and $[k]_q = \frac{q^k - q^{-k}}{q - q^{-1}}$ are q -deformed numbers such that the loop weight $n = [2]_q = q + q^{-1}$.

In the simple $2M = 4$ case considered above, A has just two sites so that \mathcal{V}_0 and \mathcal{V}_1 are both one-dimensional with bases $\{\cup\}$ and $\{\lfloor \rfloor\}$ respectively. Thus we have the matrices

$$\rho_A|_{\mathcal{V}_0} = \left[\frac{1}{\mathcal{N}^2} (1 + n (\alpha^2 n + 2\alpha)) \right], \quad \rho_A|_{\mathcal{V}_1} = \left[\frac{1}{\mathcal{N}^2} \right]$$

and

$$\begin{aligned}
\text{MTr}_A \rho_A \log \rho_A &= \text{Tr}_{\mathcal{V}_0} \rho_A \log \rho_A \\
&\quad + (n^2 - 1) \text{Tr}_{\mathcal{V}_1} \rho_A \log \rho_A.
\end{aligned} \tag{2.85}$$

We find in the end

$$\begin{aligned}
\text{MTr}_A \rho_A \log \rho_A &= \frac{(1 + \alpha n)^2}{\mathcal{N}^2} \log \frac{(1 + \alpha n)^2}{\mathcal{N}^2} \\
&\quad + (n^2 - 1) \frac{1}{\mathcal{N}^2} \log \frac{1}{\mathcal{N}^2},
\end{aligned} \tag{2.86}$$

which is the same as (2.83) after simplification.

Similar computations were made for $L = 6$ sites, for all choices of the bipartition $A \cup B$, finding again perfect agreement between the results from the loop model (with the Markov trace) and the vertex model (with the modified trace).

2.3.5 Properties of the entropy

In this subsection, two properties of the entanglement entropy are discussed. First the reduced density matrix ρ_A , with the twist in the trace, is found to have the right symmetries with respect to the action of the quantum group restricted to the subsystem A . The second interesting property is the expected relation $\tilde{S}_A = \tilde{S}_B$ that holds with our definition.

Commutation with $U_qsl(2)$ generators The definition of the quantum group entanglement entropy \tilde{S}_A relies on the use of a deformed trace where a twist $q^{-2S_B^z}$ is inserted under the usual trace symbol. To ensure that the resulting reduced density operator $\tilde{\rho}_A$ makes sense in the quantum group formalism, it must commute with the generators of $U_qsl(2)$.

The Hamiltonian commutes with the following generators:

$$S^z = \frac{1}{2} \sum_i \sigma_i^z \quad (2.87)$$

$$S^+ = \frac{1}{2} \sum_i q^{\sigma_i^z/2} \otimes \dots \otimes q^{\sigma_{i-1}^z/2} \otimes \sigma_i^+ \otimes q^{-\sigma_{i+1}^z/2} \otimes \dots \otimes q^{-\sigma_{2M}^z/2} \quad (2.88)$$

$$S^- = \frac{1}{2} \sum_i q^{\sigma_i^z/2} \otimes \dots \otimes q^{\sigma_{i-1}^z/2} \otimes \sigma_i^- \otimes q^{-\sigma_{i+1}^z/2} \otimes \dots \otimes q^{-\sigma_{2M}^z/2} \quad (2.89)$$

The generators and the Hamiltonian share the same right and left eigenvectors. As a consequence they commute with the density operator $\tilde{\rho}$

$$[S^\alpha, \tilde{\rho}] = 0, \quad \tilde{\rho} = |0_R\rangle\langle 0_L|. \quad (2.90)$$

We split the spin chain in two parts A, B and define the reduced density operator $\tilde{\rho}_A$ using a twisted trace over the part B . We consider the case where A is in the middle of the chain between B_L and B_R , so that $B = B_L \cup B_R$ and $\mathcal{H} = \mathcal{H}_{B_L} \otimes \mathcal{H}_A \otimes \mathcal{H}_{B_R}$. Thus

$$\tilde{\rho}_A = \text{Tr}_B q^{2S_{B_L}^z - 2S_{B_R}^z} \tilde{\rho}, \quad \text{with } S_B^z = \sum_{i \in B} \sigma_i^z. \quad (2.91)$$

Let us check that the generators of $U_qsl(2)$ on the subsystem A commute with the reduced density operator $\tilde{\rho}_A$. We have the following relations:

$$\begin{aligned} S^z &= S_{B_L}^z \otimes \mathbb{1}_A \otimes \mathbb{1}_{B_R} + \mathbb{1}_{B_L} \otimes S_A^z \otimes \mathbb{1}_{B_R} + \mathbb{1}_{B_L} \otimes \mathbb{1}_A \otimes S_{B_R}^z, \\ S^\pm &= S_{B_L}^\pm q^{-S_A^z - S_{B_R}^z} + q^{S_{B_L}^z} S_A^\pm q^{-S_{B_R}^z} + q^{S_{B_L}^z + S_A^z} S_{B_R}^\pm. \end{aligned} \quad (2.92)$$

Consider first S_A^z :

$$\begin{aligned} S_A^z \tilde{\rho}_A &= \text{Tr}_B \left(S_A^z q^{2S_{B_L}^z - 2S_{B_R}^z} \tilde{\rho} \right) \\ &= \text{Tr}_B \left((S^z - S_{B_L}^z - S_{B_R}^z) q^{2S_{B_L}^z - 2S_{B_R}^z} \tilde{\rho} \right). \end{aligned} \quad (2.93)$$

Obviously $S_{B_L}^z, S_{B_R}^z, S_A^z$ and S^z commute. Since S^z also commutes with $\tilde{\rho}$:

$$\begin{aligned} S_A^z \tilde{\rho}_A &= \text{Tr}_B \left(q^{2S_{B_L}^z - 2S_{B_R}^z} \tilde{\rho} S^z \right) - \text{Tr}_B \left(q^{2S_{B_L}^z - 2S_{B_R}^z} \tilde{\rho} S_{B_L}^z \right) \\ &- \text{Tr}_B \left(q^{2S_{B_L}^z - 2S_{B_L}^z} \tilde{\rho} S_{B_L}^z \right). \end{aligned}$$

For the two last terms a cyclic permutation under the trace is performed. We can now sum all terms and this proves $[S_A^z, \tilde{\rho}_A] = 0$. Next the same is done for S_A^+ :

$$\begin{aligned} S_A^+ \tilde{\rho}_A &= \text{Tr}_B \left(S_A^+ \tilde{\rho} q^{2S_{B_L}^z - 2S_{B_R}^z} \right) \\ &= \text{Tr}_B \left((q^{-S_{B_L}^z + S_{B_R}^z} S^+ - q^{-S_A^z - S_{B_L}^z} S_{B_L}^+ \right. \\ &\quad \left. - q^{S_A^z + S_{B_R}^z} S_{B_R}^+) \tilde{\rho} q^{2S_{B_L}^z - 2S_{B_R}^z} \right) \\ &\equiv (1) - (2) - (3). \end{aligned} \tag{2.94}$$

The first term (1) of the right-hand side reads

$$\begin{aligned} (1) &= \text{Tr}_B \left(q^{-S_{B_L}^z + S_{B_R}^z} S^+ \tilde{\rho} q^{2S_{B_L}^z - 2S_{B_R}^z} \right) \\ &= \text{Tr}_B \left(q^{2S_{B_L}^z - 2S_{B_R}^z} \tilde{\rho} S^+ q^{-S_{B_L}^z + S_{B_R}^z} \right) \end{aligned}$$

thanks to the cyclic permutation under the trace and the commutation of $\tilde{\rho}$ and S^+ . We then deal with the second term (2) involving $S_{B_L}^+$:

$$\begin{aligned} (2) &= \text{Tr}_B \left(q^{-S_A^z - S_{B_L}^z} S_{B_L}^+ \tilde{\rho} q^{2S_{B_L}^z - 2S_{B_R}^z} \right) \\ &= \text{Tr}_B \left(S_{B_L}^+ q^{-S_A^z} \tilde{\rho} q^{S_{B_L}^z - 2S_{B_R}^z} \right) \\ &= \text{Tr}_B \left(q^{-S^z + S_{B_R}^z + S_{B_L}^z} \tilde{\rho} q^{S_{B_L}^z - 2S_{B_R}^z} S_{B_L}^+ \right) \\ &= \text{Tr}_B \left(q^{-S_{B_R}^z + S_{B_L}^z} \tilde{\rho} q^{-S^z + S_{B_L}^z} S_{B_L}^+ \right) \\ &= \text{Tr}_B \left(q^{-2S_{B_R}^z + 2S_{B_L}^z} \tilde{\rho} S_{B_L}^+ q^{-S_A^z - S_{B_L}^z} \right), \end{aligned}$$

thanks to cyclic permutations of the operators over the subsystem B , the commutation of S^z with $\tilde{\rho}$ and the commutation of $S_{B_L}^z$ with S_A^z and $S_{B_R}^z$. Similarly for the term (3) involving $S_{B_R}^+$:

$$\begin{aligned} (3) &= \text{Tr}_B \left(q^{S_A^z + S_{B_R}^z} S_{B_R}^+ \tilde{\rho} q^{2S_{B_L}^z - 2S_{B_R}^z} \right) \\ &= \text{Tr}_B \left(q^{-2S_{B_R}^z + 2S_{B_L}^z} \tilde{\rho} S_{B_R}^+ q^{S_A^z + S_{B_R}^z} \right). \end{aligned}$$

By regrouping the terms we find the desired property $S_A^+ \tilde{\rho}_A = \tilde{\rho}_A S_A^+$. A very similar computation can be done for S_A^- .

$\tilde{S}_A = \tilde{S}_B$ for the QG EE. A meaningful entanglement entropy must satisfy, at the very least, the symmetry property $S_A = S_B$, meaning that subsystem A is as entangled with B , as B with A . We now show that this is the case for the quantum group entanglement entropy. Let us consider the case $q \in \mathbb{R}$. The proof is then simple and can be extended by analytic continuation to complex q . In this case the Hamiltonian is symmetric, and $|0\rangle \equiv |0_R\rangle = |0_L\rangle$. We again divide our system in two pieces A and B with a cut in the middle (for more complicated cuts the argument is similar) and write the state in the following way:

$$|0\rangle = \sum_{i,j} \psi_{i,j} |i\rangle_A |j\rangle_B. \quad (2.95)$$

The bases $|i\rangle_A$ and $|j\rangle_B$ can be chosen such that they have a well-defined magnetization. As a consequence, since the groundstate $|0\rangle$ is in the zero-magnetization sector, we can define those bases such that the matrix $\psi_{i,j}$ is block-diagonal and where each block correspond to a sector of A and B with a well-defined magnetization. A singular value decomposition (SVD) is performed, leading to the Schmidt decomposition

$$|0\rangle = \sum_{\alpha} s_{\alpha} |\alpha\rangle_A |\alpha\rangle_B, \quad (2.96)$$

where $|\alpha\rangle_A$ and $|\alpha\rangle_B$ are eigenvectors of S_A and S_B ; they form orthonormal bases of A and B . The density matrix $\tilde{\rho}$ is

$$\tilde{\rho} = \sum_{\alpha,\alpha'} s_{\alpha} s_{\alpha'} |\alpha\rangle_A |\alpha\rangle_B \langle\alpha'|_A \langle\alpha'|_B. \quad (2.97)$$

The reduced density matrices $\tilde{\rho}_A$ and $\tilde{\rho}_B$ read

$$\begin{aligned} \tilde{\rho}_A &= \text{Tr}_B q^{-2S_B} \tilde{\rho} = \sum_{\alpha} s_{\alpha}^2 q^{-2S_B^{\alpha}} |\alpha\rangle_A \langle\alpha|_A, \\ \tilde{\rho}_B &= \text{Tr}_A q^{-2S_A} \tilde{\rho} = \sum_{\alpha} s_{\alpha}^2 q^{2S_A^{\alpha}} |\alpha\rangle_B \langle\alpha|_B. \end{aligned}$$

Since the ground state is in the $S = 0$ sector $q^{2S_A^{\alpha}} = q^{-2S_B^{\alpha}}$ and thus the two reduced density operators have the same spectra and define the same entropy. This proves the statement $\tilde{S}_A = \tilde{S}_B$ in the case of a cut in the middle of the system.

2.4 The scaling relation of the quantum group entanglement entropy

This section presents the derivation of the scaling relation for the quantum group entanglement entropy. We start with a brief reminder on Coulomb gas and the computation of the scaling law of the entanglement is performed in this formalism. The quantum group entanglement entropy is shown to behave as expected in unitary conformal field theory with the true central charge. Numerical analysis using DMRG is given at the end of this section.

2.4.1 A brief introduction to Coulomb Gas

The Coulomb gas approach is useful to describe the continuum limit of two-dimensional loop models [28, 31, 105]. In particular, it is particularly powerful to describe systems such as the Potts model (like in this chapter) or the $O(n)$ model. Suppose the system is on a cylinder, the Coulomb gas method describes a soup of oriented loops, that are level lines of a compactified height field. In the continuum, it is described by a field $\phi(x)$ with the action

$$S = \frac{g}{4\pi} \int d^2x (\nabla\phi)^2. \quad (2.98)$$

which is the Euclidean action of a free compactified boson $\phi(x) + 2\pi = \phi(x)$. The parameter g controls the rigidity of the height surface and is related to the loop fugacity by

$$n = -2 \cos \pi g. \quad (2.99)$$

The central charge of this theory is simply $c = 1$. In this formalism, the non-contractible loops encircling the cylinder do not have the fugacity n . This is solved by introducing an electric background charge at both infinite ends of the cylinder, which introduces a term in the action of the form

$$S_B = \frac{ie_0}{4\pi} \int d^2x \phi(x) \mathcal{R}(x) \quad (2.100)$$

where \mathcal{R} is the scalar curvature. On a cylinder, it takes the simple form $S_B = ie_0(\phi(x, \infty) - \phi(x, -\infty))$ where the charges are located at both infinite ends of the cylinder. On the lattice it creates a twist similar to what has been described in different geometries earlier. The central charge of the twisted theory is

$$c = 1 - \frac{6e_0^2}{g} \quad (2.101)$$

with $e_0 = 1 - g$.

2.4.2 The replica trick and the modified scaling relation

We now claim that for the critical quantum group invariant XXZ chain with Hamiltonian $H = -\sum e_i$, the Rényi and Von-Neumann entropies scale as expected in a conformal field theory, with the *true* central charge. The simplest argument for this relies on a field theoretic analysis. We follow the Cardy and Calabrese [94] replica calculation extended to the non unitary case, the density operator is $\tilde{\rho} = |0_R\rangle\langle 0_L|$.

With N replicas in the Coulomb Gas formalism, there are N bosonic fields ϕ_1, \dots, ϕ_N . An essential complication arises because of the cut: the loops winding N times around one of the extremities should still have weight n , while, due to the collection of phases gathered in the winding, the complex Boltzmann weights conspire to give them the weight $\tilde{n} = 2 \cos N\gamma$. This issue was discussed earlier and a picture was given figure 2.5b. The problem of the non-contractible loops fugacity can be repaired by the introduction of electric charges at the two

extremities of the cut. In practice, in the field theory, vertex operators $\exp[ie_{l,r}(\phi_1 + \dots + \phi_N)]$ are inserted at the left and right extremities of the cut. The charges $e_{l,r}$ are respectively the charges of the vertex operators inserted at the left and right of the cuts and are tuned conveniently to compensate the extra phases. An oriented loop surrounding both extremities first gathers a weight $e^{\pm i\pi e_0}$ due to the complex turning weights with a sign depending on the orientation. The two vertex operators provide the additional weight $e^{\pm i\pi(e_l + e_r)}$. The total complex weight must satisfy

$$e^{i\pi(e_0 + e_l + e_r)} = e^{i\pi e_0} \quad \text{or} \quad e^{i\pi(e_0 + e_l + e_r)} = e^{-i\pi e_0} \quad (2.102)$$

to give the correct loop fugacity. In addition, a loop that surrounds only one extremity of the cut gets a weight

$$e^{\pm i e_{l,r} N \pi} e^{\pm i N \pi e_0} = e^{\pm i N \pi (e_{l,r} + e_0)} \quad (2.103)$$

which must also be set to $e^{\pm i\pi e_0}$ or $e^{\mp i\pi e_0}$. A solution to the condition (2.102) is to parametrise the charges as follows

$$e_l = e - e_0, \quad e_r = -e - e_0 \quad (2.104)$$

where e is a free parameter. The condition on equation (2.103) provides the value of e

$$e = e_0/N \quad (2.105)$$

and thus

$$e_l = \frac{e_0}{N} - e_0, \quad e_r = -\frac{e_0}{N} - e_0. \quad (2.106)$$

To evaluate the partition function, the boundary conditions along the cut $\phi_j(e^{2i\pi} z) = \phi_{j+1}(z)$ ($j \bmod N$) must be implemented. To do so, combinations of the fields are formed such that they obey twisted boundary conditions on the cut. For instance, with $N = 2$, the combinations $\phi_+ = \frac{\phi_1 + \phi_2}{\sqrt{2}}$ and $\phi_- = \frac{\phi_1 - \phi_2}{\sqrt{2}}$ can be formed. While ϕ_+ is uniquely defined (and does not see the cut), ϕ_- now is twisted, $\phi_-(e^{2i\pi} z) = -\phi_-(z)$. For arbitrary N , the field $\phi_{sym} \equiv \frac{\phi_1 + \dots + \phi_N}{\sqrt{N}}$ is symmetric, while the others are twisted by angles $e^{2i\pi k/N}$, $k = 1, \dots, N-1$. The k -th twist field in a complex bosonic theory is known to have the conformal weight [106]

$$h_{k/N} = \frac{1}{2} \frac{k}{N} \left(1 - \frac{k}{N} \right). \quad (2.107)$$

The partition function, for a cut of length ℓ , is given by a combination of two-point functions of those fields. We can write their contribution as Z_N^{twist}

$$Z_N^{\text{twist}} \propto \ell^{-2x_{\text{twist}}} \quad (2.108)$$

with

$$x_{\text{twist}} = \sum_{k=1}^{N-1} h_{k/N} = \frac{1}{12} \left(N - \frac{1}{N} \right) \quad (2.109)$$

The second contribution to the partition function comes from the insertion of vertex operators at the ends of the cut. This term is not present for an untwisted theory, as in the continuum limit of the XXX chain. The additional contribution Z_N^{charge} , corresponding to the two-point function of vertex operators with charges $e_{l,r}$, reads

$$Z_N^{\text{charge}} \propto \ell^{-2x_N^{\text{charge}}} \quad (2.110)$$

with

$$x_N^{\text{charge}} = N \frac{e^2 - e_0^2}{2g} = \frac{e_0^2}{2g} \left(\frac{1}{N} - N \right). \quad (2.111)$$

Gathering every term together provides the asymptotic behaviour of the partition function

$$Z_N \propto \ell^{-\frac{1}{6}(N - \frac{1}{N})(1 - \frac{6e_0^2}{g})}. \quad (2.112)$$

Using that $e_0 = \frac{1}{x+1}$ and $g = \frac{x}{x+1}$ for the spin chain with $q = e^{i\pi/x+1}$, this gives us the Reny entropies

$$\tilde{S}_L^{(N)} = \frac{1}{6} \left(N - \frac{1}{N} \right) \left[1 - \frac{6}{x(x+1)} \right] \ln L \quad (2.113)$$

and the entanglement entropy as

$$\tilde{S}_L = \tilde{S}_L^{(1)} = \frac{1}{3} \left[1 - \frac{6}{x(x+1)} \right] \ln L \quad (2.114)$$

hence establishing our claim, with the central charge given in (2.101).

We emphasize that the $U_q sl(2)$ spin chain differs from the usual spin chain simply by the presence of boundary terms. It is expected that the properties of the ordinary entanglement should not be affected by these terms, and that the central charge obtained via the density operator $\rho = |0\rangle\langle 0|$ is $c = 1$, which one can consider in this case as the effective central charge in the vertex representation [107].

2.4.3 Numerical analysis

Those predictions can be checked numerically. They are illustrated on the generic case $q = e^{2i\pi/5}$ with central charge $c = -3/5$ figure 2.6. The ground state is obtained using matrix product state methods. Of course the Hamiltonian being non-Hermitian, it is important to be careful in the numerical scheme. As mentioned in the first chapter, one possibility is simply to take a random state and evolve it in imaginary time. Of course the usual variational approach does not work *a priori*. We are able to reach a length of $2M = 400$ sites. First the naive entropy, obtained by taking the usual trace and a density matrix involving only the right ground state, is considered and shown to scale with $c_{\text{eff}} = 1$. The quantum group entanglement entropy is also computed and shown to scale with the real central charge c . Lastly we show that, putting a twist to non-contractible loops such that their weight \tilde{n} is $\tilde{n} = 2 \cos \pi/5$ leads to the effective central charge obtained in the RSOS model and non-unitary minimal models. This connection with RSOS models is discussed more extensively in the following.

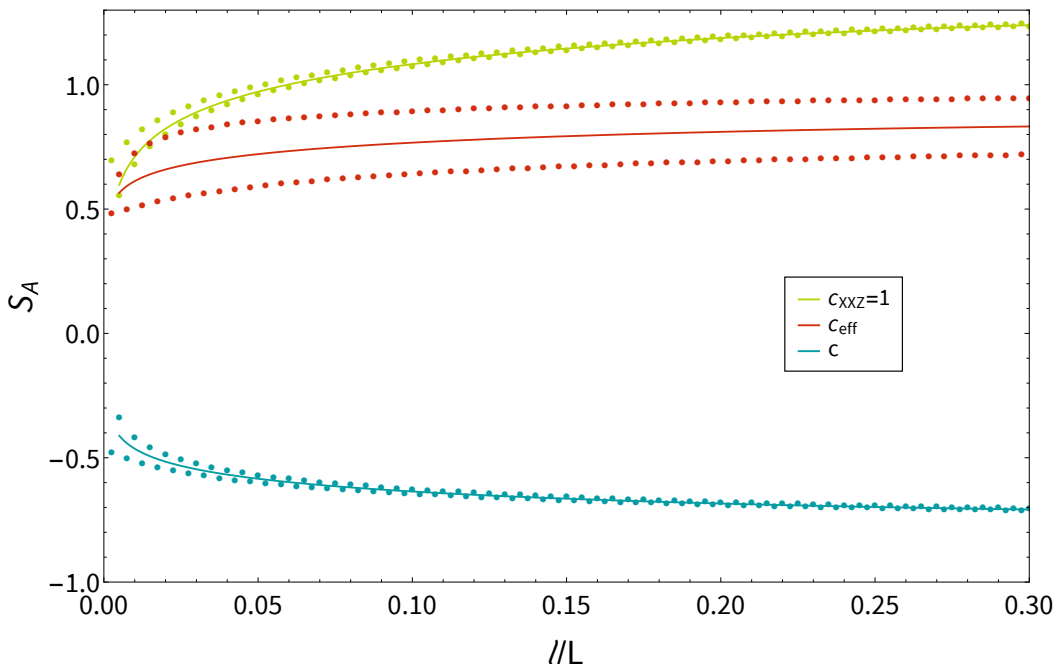


Figure 2.6 – Numerical EE for the non-unitary case $(p, m) = (2, 4)$ ($n = 2 \cos \frac{2\pi}{5}$), versus the (normalised) length of the cut ℓ/M , for a chain with $M = 400$ sites and open boundary conditions. Green dots show the usual EE with the unmodified trace. Averaging over the parity oscillations (solid curve) reveals the scaling with $c_{\text{XXZ}} = 1$. Red dots show the $N = 2$ Rényi entropy, with the modified trace giving weight $\tilde{n} = 2 \cos \pi/5$ to non-contractible loops; this scales with $c_{\text{eff}} = 3/5$. Blue dots again show $\tilde{S}^{(2)}$, but with $\tilde{n} = n$; the scaling then involves the true central charge $c = -3/5$.

2.5 Extensions

In this section, the Coulomb gas approach is applied to several problems. First the case of RSOS models, a lattice discretisation of minimal models, is discussed. The scaling of the entanglement entropy is shown to involve the effective central charge of non-unitary minimal models. A detailed analysis of the mapping between the RSOS model and the loop model on the N -sheeted Riemann surface is given. Our approach can be easily generalised to other kinds of system, in particular the simple case of the supersymmetric $sl(2|1)$ chain is presented. At the end of this section, some ideas and preliminary results are given in the case of non-compact conformal field theories.

2.5.1 Restricted Solid-on-Solid models

The Restricted Solid-On-Solid models (RSOS) provide a discretisation of minimal models on the lattice. This section presents the connection between the Coulomb Gas analysis for the entanglement entropy and the case of minimal models. Before presenting our results we start with a brief description of those systems.

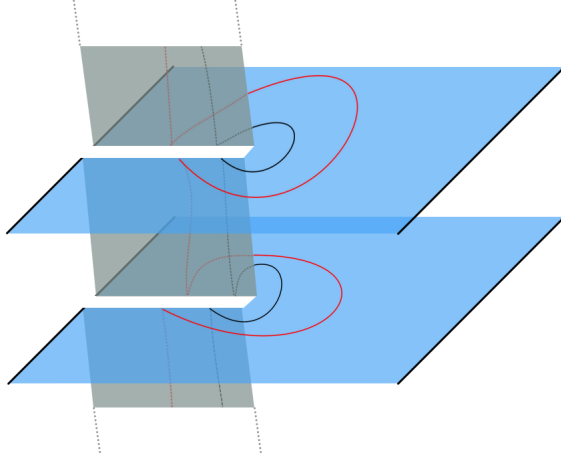


Figure 2.7 – Surface with $N = 2$ replicas. Black edges along the planes represent boundary conditions (height fixed to h_{bdy}). The top and bottom are identified. Non-contractible loops always wind N times. Moreover, only the outermost loop (red here) sees the boundary directly.

RSOS models are labelled by two parameters p and $m + 1$ satisfying $\gcd(p, m + 1) = 1$ and $1 \leq p \leq m$. It provides another representation of the TL algebra with $n = 2 \cos \frac{\pi p}{m+1}$ [108, 109]. The degrees of freedom in this model are heights at the corner of each face in a square lattice. Each site i is associated a height h_i . These heights live on a Dynkin diagram A_m and have m possible values $h_i = 1, \dots, m$. Two neighbouring sites i and j must have a height difference of 1: $|h_i - h_j| = 1$. The weight of a face is

$$W \left(\begin{array}{cc|c} h_k & h_j & \\ \hline h_i & h_l & u \end{array} \right) = \begin{array}{c} h_k \qquad h_j \\ \square \\ h_i \qquad h_l \end{array} = \sin(\lambda - u) \delta_{h_i, h_j} + \sin(u) \delta_{h_k, h_l} \frac{\sqrt{S_{h_i} S_{h_j}}}{S_{h_k}} \quad (2.115)$$

where u is the spectral parameter, $\lambda = \frac{p\pi}{m+1}$ the crossing parameter and $S_h = \sin h\lambda / \sin \lambda$. The right part of the interaction of equation (2.115), $e_i = \delta_{h_{i-1}, h_{i+1}} \sqrt{S_{h_i} S_{h'_i}} / S_{h_{i-1}}$, satisfies the Temperley-Lieb relations. Note that in the quantised formulation time is in the top-right direction and e_i acts on three heights h_{i-1} , h_i and h_{i+1} . With the boundary conditions $h_0 = h_M = 1$, the ground state $|0\rangle$ has the same energy as in the other representations. This holds in the non-unitary cases $p > 1$, provided we resolve the square root as $\sqrt{S_{h_i} S_{h'_i}} = S_{h_i}$ when $S_{h_i} = S_{h'_i} < 0$.

We discuss here in more details the correspondence between the RSOS and loop models for the calculation of the Rényi entropies. For simplicity, only open boundary conditions are considered with the boundary heights h_{bdy} fixed to 1 and the cut is located at the edge of the system (figure 2.7).

Loops surround clusters of constant height. When a loop makes a right (resp. left) turn

by bouncing off a piece of a cluster, it gets a weight $\sqrt{S_a/S_b}$ (resp. $\sqrt{S_b/S_a}$) where a and b are the heights of the adjacent clusters (cluster of height b on the left, and a on the right). The amplitude S_h is defined by

$$S_h = \frac{\sin h\lambda}{\sin \lambda}, \quad (2.116)$$

with $\lambda = \frac{p\pi}{m+1}$. After summing over all possible heights, loops pick a weight

$$n = 2 \cos \frac{p\pi}{m+1} = \frac{S_{h-1} + S_{h+1}}{S_h} \quad (2.117)$$

if they are homotopic to a point. Let us consider the Rényi entropies for $N > 1$. In the replica picture, the weight of loops on the N -sheeted surface, shown in figure 2.5b for $N = 2$, must be carefully computed. The weight of a non-contractible (resp. contractible) loop on this surface, surrounding a cluster of height h and surrounded by a cluster of height h' , is $(S_{h'}/S_h)^N$ (resp. $S_{h'}/S_h$), due to the $2\pi N$ winding of non-contractible loops; this must finally be summed over all possible paths in the Dynkin diagram. For instance, consider the case of figure 2.7, with $N = 2$ and two non-contractible loops. The first loop is the boundary between a cluster of height $h_{\text{bdy}} = 1$ on its left and $h = 2$ on its right. It picks up a factor S_2^2/S_1^2 . The second loop can either surround a cluster of height 1 or 3, therefore it gets a factor $(S_3^2 + S_1^2)/S_2^2$.

In the general case, we consider heights living on the A_m Dynkin diagram, and define the following matrix

$$(\Lambda_N)_{i,j} = \delta_{|i-j|,1} (S_i/S_j)^N \quad i, j = 1, \dots, m. \quad (2.118)$$

Thus, Λ_N is the adjacency matrix with the non-contractible loop weights on N replicas. The matrix element $(\Lambda_N^k)_{h_{\text{bdy}}, h_k}$ is the weight of the configuration with k non-contractible loops, where the boundaries are fixed to h_{bdy} and the last loop surrounds a cluster of height h_k . Since we sum over the height of the last cluster and we fix $h_{\text{bdy}} = 1$, the full weight is $\langle \mathbf{h}_{\text{free}} | \Lambda_N^k | \mathbf{h}_{\text{bdy}} \rangle$ where $\langle \mathbf{h}_{\text{free}} | = (1, \dots, 1)$ and $|\mathbf{h}_{\text{bdy}} \rangle = (1, 0, \dots, 0)^T$. The weight of a set of k contractible loops is then

$$w = \sum_{i=1}^m \langle \mathbf{h}_{\text{free}} | \lambda_i \rangle \langle \lambda_i | \mathbf{h}_{\text{bdy}} \rangle \lambda_i^k, \quad (2.119)$$

where $|\lambda_i \rangle$ and $\langle \lambda_i |$ are the right and left eigenvectors of Λ_N associated to the eigenvalues λ_i , for $i = 1, \dots, m$.

We hence need to sum over sectors where the weight of non-contractible loops is given by the different eigenvalues of Λ_N . Notice that the characteristic polynomial depends only on the products $(\Lambda_N)_{i,j} (\Lambda_N)_{j,i} = 1$ (expand by the minors of the first column). Therefore it remains unchanged if Λ_N is replaced by the usual adjacency matrix, with elements $\Lambda_{i,j} = \delta_{|i-j|,1}$. The spectra of the adjacency matrices of A_m Dynkin diagrams are $\{\lambda_k = 2 \cos \frac{k\pi}{m+1}\}_{k=1, \dots, m}$. The

normalized eigenvectors of Λ_N are found [110] as

$$\begin{aligned} |\lambda_k\rangle_i &= \sqrt{\frac{2}{m+1}} \left(\frac{\sin \frac{ip\pi}{m+1}}{\sin \frac{p\pi}{m+1}} \right)^N \sin \left(\frac{ik\pi}{m+1} \right), \\ \langle \lambda_k|_i &= \sqrt{\frac{2}{m+1}} \left(\frac{\sin \frac{ip\pi}{m+1}}{\sin \frac{p\pi}{m+1}} \right)^{-N} \sin \left(\frac{ik\pi}{m+1} \right) \end{aligned} \quad (2.120)$$

for $i = 1, 2, \dots, m$. Finally, the RSOS partition function with N replicas and a boundary is a sum of loop partition functions $Z_{N,k}^{\text{loop}}$, where non-contractible loops get a weight λ_k , i.e., $Z_N^{\text{RSOS}} = \sum_{k=1}^m \alpha_k Z_{N,k}^{\text{loop}}$. The prefactor α_k can be computed from the eigenvectors of Λ_N :

$$\begin{aligned} \alpha_k &= \langle \mathbf{h}_{\text{free}} | \lambda_k \rangle \langle \lambda_k | \mathbf{h}_{\text{bdy}} \rangle \\ &= \frac{2}{m+1} \left(\sin \frac{h_{\text{bdy}} k \pi}{m+1} \right)^{1-N} \sum_{i=1}^m \left(\sin \frac{ip\pi}{m+1} \right)^N \sin \frac{ik\pi}{m+1}. \end{aligned} \quad (2.121)$$

The dominant contribution comes from non-contractible loop with the largest possible weight, $2 \cos \frac{\pi}{1+m}$; this is because the corresponding sector is associated with the smallest electric charge. In the limit where the system size goes to infinity we thus have $Z_N^{\text{RSOS}} \sim \alpha_1 Z_1^{\text{loop}}$. As a consequence, the scaling of the entanglement entropy is dominated by the partition of the loop model where non-contractible loops have the weight $\tilde{n} = 2 \cos \frac{\pi}{1+m}$. In the Coulomb gas analysis, it can be enforced by choosing the electric charge

$$e = \frac{e_0}{pN}. \quad (2.122)$$

With this choice, the quantity Z_N/Z^N is not well normalized. This quantity in the limit $N \rightarrow 1$ should be 1 but, because the electric charge $e \neq e_0$ at $N = 1$, it is not the case anymore. The partition function Z of the RSOS model on a single plane is not the simple limit $\lim_{N \rightarrow 1} Z_N$. It is chosen here to renormalize Z_N by the formal limit $Z_1 = \lim_{N \rightarrow 1} Z_N$ corresponding to a single copy of the RSOS model with the charges. Doing the same computation, it is found that now

$$\frac{Z_N}{Z_1^N} \propto \ell^{-\frac{1}{6}(N-1/N) \left(1 - \frac{6e_0^2}{p^2 g} \right)} \quad (2.123)$$

and therefore

$$S_A^{(N)} \sim \frac{N+1}{6N} c_{\text{eff}} \log \ell \quad (2.124)$$

with $c_{\text{eff}} = 1 - \frac{6e_0^2}{p^2 g}$ the effective central charge of non-unitary minimal model.

Let us discuss a last aspect of the RSOS models. The detailed coefficient α_k depends on the boundary condition imposed on the left of the system. For fixed height h_{bdy} , the prefactor

in (2.121) contributes a term $\ln\left(\sin\frac{h_{\text{bdy}}k\pi}{m+1}\right)$. Recall now the expression (see e.g. [111]) of the Affleck-Ludwig entropy [112], we restrict here to the unitary case $p = 1$ for simplicity:

$$g_{1h_{\text{bdy}}} = \left[\frac{2}{m(m+1)}\right]^{1/4} \left[2\frac{\sin\frac{\pi}{m}}{\sin\frac{\pi}{m+1}}\right]^{1/2} \sin\frac{\pi h_{\text{bdy}}}{m+1}$$

The h_{bdy} dependence of the $O(1)$ contribution to the Rényi entropy matches the (logarithm of) the degeneracy factor $g_{1h_{\text{bdy}}}$. Meanwhile, it is well known that fixing the RSOS height to h_{bdy} corresponds to the boundary condition ($h_{\text{bdy}} = 1$) in the above notation, while it is also known that the conformal boundary condition contributes to the entanglement by a factor $O(1)$ which is precisely the logarithm of the degeneracy factor—the Affleck-Ludwig entropy [112]. Our calculation thus reproduces this subtle aspect of the entanglement entropy as well.

Note that, despite the relative freedom offered by the coefficients α_k , there does not seem to be any satisfactory way to concoct a boundary condition for which the leading term $\alpha_{k=1}$ cancels out for all N .

2.5.2 A supersymmetric example

Percolation and other problems with supersymmetry have $Z = 1$, hence $c = 0$, and the entanglement entropy scales trivially. Having a quantity that distinguishes the many $c = 0$ universality classes would be very useful. We now show that, by carefully distinguishing left and right eigenstates, and using traces instead of supertraces, one can modify the definition of entanglement entropy to build such a quantity. This is illustrated by the $sl(2|1)$ alternating chain [113] which describes percolation hulls. This chain is encountered later in chapter 4 where the supersymmetric formalism is given. In the following, the focus of the discussion is on the geometrical interpretation of this chain in terms of loops.

The $sl(2|1)$ chain is a representation of the Temperley-Lieb model (2.32) with $n = 1$. The Hilbert space \mathcal{H} , for a chain of length $2M$ is

$$\mathcal{H} = (V \otimes \bar{V})^{\otimes M} \tag{2.125}$$

where V is the fundamental representation $V = \{|1\rangle, |2\rangle, |3\rangle\}$ of $sl(2|1)$ and \bar{V} its conjugate $\bar{V} = \{|\bar{1}\rangle, |\bar{2}\rangle, |\bar{3}\rangle\}$. The states $|1\rangle$ and $|2\rangle$ are bosonic and $|3\rangle$ is fermionic and similarly for \bar{V} . A loop is given a fugacity corresponding to the supertrace on its internal degrees of freedom. The supertrace $\text{STr}(\dots)$ being simply $\text{Tr}((-1)^F \dots)$ (F counts the number of fermion), it gives a weight $+1$ to a bosonic loop and -1 to a fermionic loop. The loop fugacity is thus $n = 1 + 1 - 1 = 1$. The Hamiltonian on two sites is $H = -e_1$ and reads

$$e_1 = (|1\bar{1}\rangle + |2\bar{2}\rangle + |3\bar{3}\rangle)(\langle 1\bar{1}| + \langle 2\bar{2}| + \langle 3\bar{3}|).$$

The eigenvectors are $|0_{\text{R}}\rangle = |1\bar{1}\rangle + |2\bar{2}\rangle + |3\bar{3}\rangle$ and $\langle 0_{\text{L}}| = \langle 1\bar{1}| + \langle 2\bar{2}| + \langle 3\bar{3}|$. Note that, despite its misleading appearance, H is not Hermitian because the state $|\bar{3}\rangle$ has a negative norm: $\langle \bar{3}|\bar{3}\rangle = -1$. The density operator is $\tilde{\rho} = e_1$ and satisfies $\text{STr}\tilde{\rho} \equiv \text{Tr}(-1)^F \tilde{\rho} = 1$. In the

same spirit as for quantum group entanglement entropy of the 6-vertex model, the entropy is defined with the supertrace to give the weight $n = 1$ to all loops. The reduced density operator is

$$\tilde{\rho}_A = \text{STr}_B \tilde{\rho} = |1\rangle\langle 1| + |2\rangle\langle 2| + |3\rangle\langle 3| \quad (2.126)$$

where A is the first site. We can compute the entanglement entropy and first remark that $\text{STr} \tilde{\rho}_A^N = 1$ for all N . Therefore all Rényi entropies are trivial ($S_N^A = 0$) as expected for percolation ($c = 0$). It is instead more interesting to consider the usual normal trace of $\tilde{\rho}_A$. It changes the normalisation to ensure $\text{Tr} \tilde{\rho}_A = 1$. A straightforward computation shows $\tilde{\rho}_A^N = \frac{1}{3^N} (|1\rangle\langle 1| + |2\rangle\langle 2| + |3\rangle\langle 3|)$ and thus $\tilde{S}_A^{(N)} = \ln 3$. This equals the quantum group Rényi entanglement entropy with $n = 3$. This calculation carries over to arbitrary size. One finds that $\tilde{S}_A = \tilde{S}_{A,\ell}$ with weight $n = 1$, *provided* that non-contractible loops winding around one cut end in the replica calculation get the modified weight $\tilde{n} = 3$ instead of n . We can then use the Coulomb gas framework developed in the context of the non-unitary minimal models to calculate the scaling behaviour. For percolation $g = \frac{2}{3}$ ($n = 1$), and $\tilde{n} = 2 \cos \pi e_0$. It follows that e_0 is purely imaginary, in the end

$$S^{(N)} \sim \frac{N+1}{6N} c_{\text{eff}} \log L \quad (2.127)$$

with

$$c_{\text{eff}} = 1 + \frac{9}{\pi^2} \left(\log \frac{3 + \sqrt{5}}{2} \right)^2 \sim 1.84464 \dots \quad (2.128)$$

2.5.3 Entanglement entropy in the non-compact case

The case of non-compact conformal field theories is also interesting from the entanglement entropy point of view. The partition function on a N -sheeted Riemann surface is written as a correlation function of twist fields

$$\frac{Z_N}{Z^N} = \langle \mathcal{T}_N(0) \tilde{\mathcal{T}}_N(\ell) \rangle. \quad (2.129)$$

Correlations on a lattice for non-compact models may involve a continuum of critical exponents. Therefore it is expected, in some cases at least, that the two-points function of twist fields, measured on a lattice, will have the form

$$\langle \mathcal{T}_N(0) \tilde{\mathcal{T}}_N(\ell) \rangle = \int_{x=0}^{\infty} dx \rho(x) \ell^{-2\Delta_{\mathcal{T}_N} + x} \quad (2.130)$$

where $\Delta_{\mathcal{T}_N}$ is the conformal weight of the twist fields and $\rho(x)$ plays the role of a density and is non-universal. In the limit $\ell \rightarrow \infty$, the behaviour is dominated by a term of the form

$$\langle \mathcal{T}_N(0) \tilde{\mathcal{T}}_N(\ell) \rangle \sim \lim_{\ell \rightarrow \infty} \ell^{-2\Delta_{\mathcal{T}_N}} \log \ell^{\alpha\rho} \quad (2.131)$$

where α_ρ depends on the precise behaviour of ρ in the vicinity of $x = 0$. As a consequence, taking the logarithm of this correlation functions leads to a term $\log \log \ell$ in the entanglement entropy. The prefactor seems, *a priori*, non-universal. It is possible to use our study of RSOS models to observe this term. As an example of non-compact CFT we consider the $c = 1$ Liouville theory, which is obtained by taking the $m \rightarrow \infty$ limit of the unitary CFTs based on the A_m RSOS models [114]. Going back to the calculation in the preceding subsection, and writing the contributions from all possible loop weights, we get the partition function for the N -replica model in the form

$$Z_N \propto L^{-\frac{1}{6}(N-\frac{1}{N})(1-6e_0^2/g)} \sum_{k=1}^m c_{k,N} L^{-\frac{e_0^2}{g} \frac{k^2-1}{N}}, \quad (2.132)$$

and

$$Z_1 \propto \sum_{k=1}^m c_{k,1} L^{-\frac{e_0^2}{g}(k^2-1)}. \quad (2.133)$$

The coefficients $c_{k,N}$ are difficult to evaluate: they depend not only on the combinatorics of the model, but also on the normalization in the continuum limit of the different insertions of lattice vertex operators necessary to give the correct weights to non-contractible loops. Recall that $e_0 = \frac{1}{m+1}$ and $g = \frac{m}{m+1}$. The limit $m \rightarrow \infty$ is taken, following the construction of [114]. To this end, we have to make an ansatz for the coefficients $c_{k,N}$. Many comments in the literature suggest that the dependency on N is negligible. Assume for extra simplicity that the $c_{k,N}$ are essentially constant as a function of k (this is all up to a lattice-cutoff power-law dependency, which we put in the L term). Replacing sums by integrals when m is large, the partition function reads

$$\frac{Z_N}{Z_1^N} \sim L^{-\frac{1}{6}(N-\frac{1}{N})} \frac{\int_0^\infty dx L^{-x^2/N}}{(\int_0^\infty dx L^{-x^2})^N}. \quad (2.134)$$

Note that the integral is extended to infinity, while since obviously $x \propto \frac{k}{m}$, it looks like it should run only up to $x = 1$. There are two reasons for this: one is that at large L the behavior is dominated by the region in the vicinity of $x = 0$. The other is that we have in fact neglected all the contributions occurring from electric charges (in the lattice derivation) shifted by integers. Accepting (2.134) and after evaluating the Gaussian integrals, the result reads

$$\frac{Z_N}{Z_1^N} \sim L^{-\frac{1}{6}(N-\frac{1}{N})} (\ln L)^{\frac{N-1}{2}}. \quad (2.135)$$

Note that there are in fact additional factors of m cropping up when the sums (2.132)–(2.133) are transformed into integrals. They will only affect the entanglement by $O(1)$ terms, so we have neglected them.

Finally, taking minus the derivative of (2.135) at $N = 1$ to get the entanglement entropy, we obtain

$$S = \frac{1}{3} \ln L - \frac{1}{2} \ln(\ln L), \quad (2.136)$$

whereas for the Rényi entropy we get

$$S^{(N)} = \frac{N+1}{6N} \ln L - \frac{1}{2} \ln(\ln L). \quad (2.137)$$

The argument hinges crucially on the absence of a non-trivial (power-law) dependency of the $c_{k,N}$ on k . Since these coefficients depend, in part, on the correspondence between lattice and continuum, this may well provide a non-universal contribution to the $\ln(\ln L)$ term. Other examples of $\log \log L$ corrections were found in the case of a free boson [115, 116]

2.6 Comparisons and conclusion

This chapter ends with a brief comparison to other works on this problem. We start by discussing the first approach, by Bianchini and al.'s approach [91]. They studied the entanglement entropy for non-unitary minimal models and more generally PT -symmetric systems. The work of Dupic and al. [117] is also interesting and can be compared with our approach. Using null vector conditions they can compute precisely correlation functions of twist field in the RSOS model.

2.6.1 Entanglement in non-unitary minimal models

In [91] Bianchini, Castro-Alvaredo, Doyon, Levi and Ravanini study the Rényi entanglement entropy in general non unitary conformal field theories. In particular they focus on the case where the ground state breaks conformal invariance. In others words, they assume the existence of a negative conformal weight $h_{\min} < 0$. The Rényi entropy is identified with the correlation function of the twist field

$$\mathrm{Tr} \rho_A^N = \frac{\langle \mathcal{T}_\phi(0) \tilde{\mathcal{T}}_\phi(\ell) \rangle}{\langle \phi(0) \phi(\ell) \rangle^N} \quad (2.138)$$

where ϕ is the field of dimension $h_{\min} < 0$ and \mathcal{T}_ϕ is the twist field associated to ϕ on the N -sheeted Riemann surface. The main result is the modified scaling of the entanglement entropy

$$S_N \sim \frac{c_{\mathrm{eff}}(N+1)}{6N} \log \ell \quad (2.139)$$

with the usual form of the effective central charge $c_{\mathrm{eff}} = c - 24h_{\min}$. A particularly interesting finding is that for logarithmic conformal field theory where the ground state is mixed in a Jordan cell, an additional $\log \log \ell$ terms appear as a subleading factor of (2.139). Our results are in agreement with this formula in the case of RSOS non-unitary minimal models for open boundary conditions.

2.6.2 The null-vector conditions in the cyclic orbifold

A different approach was proposed by Dupic, Estienne and Ikhlef in a recent paper [117]. Similarly to the papers just mentioned, they also consider the case of rational non-unitary

models and, for their lattice regularisation, the RSOS models. Null-vector conditions were originally used to compute the conformal dimension of twist fields but they were able to exploit them fully by computing entanglement entropies as four-point functions. Their results involve much more complicated scaling behaviours than ours. The main restriction of their approach is the limitation to rational CFTs and the computational cost to explicit four-point functions. In particular, they study the Yang-Lee model and their definitions of the entanglement entropies are not simple two-point functions. They consider a mapping of higher power of the reduced density matrix, within the formalism of the orbifold, such that

$$\text{Tr } \rho_A^N = \langle \phi | \mathcal{T}_\phi(0) \tilde{\mathcal{T}}_\phi | \phi \rangle \quad (2.140)$$

where $\phi = \phi^{\otimes N}$. It is a non-trivial function of ℓ . This result seems to be in apparent contradiction with our work. However, there are several differences with the quantities we considered. First in their paper they study the Rényi entropies with periodic boundary conditions. This is an important distinction since our mapping between RSOS and the loop model is done only in the open case. It is indeed more complicated to do the same analysis if there are several types of non-contractible loops. Moreover, in our entropy in the RSOS model, the boundary conditions correspond to the ones of the loop model, selecting effectively the conformal vacuum for the state at infinity instead of $|h_{\min}\rangle$. Thus we indeed have a two-point functions and our analysis holds. However a difference remains. In the section 2.5.1 on RSOS, the reduced density matrix was renormalized such that $\text{Tr } \tilde{q}^{2S_A} \rho_A = 1$ with \tilde{q} the twist related to the weight of non-contractible loops. This normalisation factor is important to take the analytic continuation of the Rényi entropies. In practice, it divides the two-point functions of the twist field by the two-point function of ϕ in one replica such as in equation (2.138). This is artificial and remains an important difference with the work of Dupic, Estienne and Ikhlef where this renormalisation is not done.

3 Truncations of non-compact loop models

This chapter presents our work on non-compact lattice models and the on-site truncation approach. The first system considered here is the Chalker-Coddington model with its first truncation introduced in [37]. We start with a short presentation of the Chalker-Coddington model and its mapping to a supersymmetric model.

3.1 The Chalker-Coddington model

3.1.1 Definition as a one-particle model

The Chalker-Coddington model [12] is a network representation of the discrete time evolution of a single-electronic wave function in a disordered potential subject to a transverse magnetic field (for a review see [118]). An eigenstate has a non-zero wave function amplitude along equipotential lines of the disordered potential. If the energy of this equipotential is lower (resp. higher) than a certain threshold value the electron is trapped around a local minimum (resp. extremum). In both cases, the state is localised and does not contribute to the conductivity. Only at specific energies, close to the centre of Landau bands, the equipotentials percolate and the wave function propagates in the entire system. Such a state is delocalised and contributes to the electric current. It is possible to imagine a classical picture where an electron drifts along an equipotential line because of the strong magnetic field. If two equipotential lines are close enough to each other, the wave function can propagate by quantum tunnelling. In the classical picture, an electron has a non-zero probability to go through a small barrier of potential and jump between two equipotentials. The Chalker-Coddington model is thus a model of quantum percolation.

Let us present the oriented network description of this model. The equipotential lines, along which the magnetic field imposes a directed motion, are modeled by the edges of an oriented square lattice. The vertices represent the saddle points where these lines are close to each others and where quantum tunnelling occurs. Each face of the odd (resp. even) sublattice is a minimum (resp. maximum) of the potential as seen in figure 3.1. Of course, since the potential is random, the length of an edge connecting two saddle points is also a random quantity and the network is drawn as a regular square lattice only for convenience.

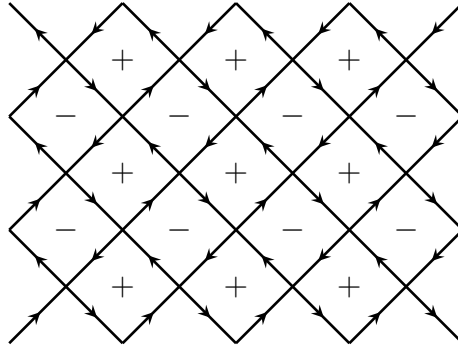


Figure 3.1 – Oriented lattice of the Chalker-Coddington model. Faces are extrema of the random potential. Each edge represents an equipotential line linking two saddle points. An electron, under the action of the strong magnetic field, always drifts in the clockwise direction around maxima and anti-clockwise around minima.

In this model of non-interacting electrons the energy appears as a parameter whose tuning allows to observe the plateau transition via the delocalisation of the wave function. The wave function ψ of a single electron is discretised, each edge e is associated to a complex number ψ_e . Thus ψ is the collection of all amplitudes

$$\psi = \{\psi_e\}_{e \in E} \quad (3.1)$$

with E the set of edges. Near a saddle point, see figure 3.2, the outgoing wave function amplitudes ψ_3 and ψ_4 are related to the incoming amplitudes ψ_1 and ψ_2 by a scattering matrix \mathcal{S}

$$\begin{pmatrix} \psi_3 \\ \psi_4 \end{pmatrix} = \mathcal{S} \cdot \begin{pmatrix} \psi_1 \\ \psi_2 \end{pmatrix} \quad (3.2)$$

where unitary evolution and conservation of probabilities impose \mathcal{S} to be in $SU(2)$. In principle each vertex v can have a different scattering matrix \mathcal{S}_v , but we assume that the dynamic on all vertices of the even sublattice A (resp. odd sublattice B) is given by the matrix \mathcal{S}_A (resp. \mathcal{S}_B). We can take, without any loss of generality, the following matrices

$$\mathcal{S}_S = \begin{pmatrix} t_S & r_S \\ -r_S & t_S \end{pmatrix} \quad (3.3)$$

where $S = A, B$ and t_A, t_B, r_A and r_B are real amplitudes. Conservation of probability imposes $t_A^2 + r_A^2 = 1$ and $t_B^2 + r_B^2 = 1$.

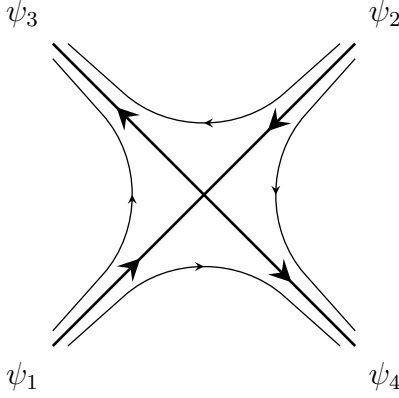


Figure 3.2 – Vertex in the Chalker-Coddington model. The two incoming amplitudes ψ_1 and ψ_2 scatter and are related to ψ_3 and ψ_4 by a scattering matrix \mathcal{S} . The possible oriented trajectories of an electron are drawn.

Finally the disorder of the network is encoded on edges. When an electron moves along an edge e , it acquires an Aharonov-Bohm phase ϕ_e that depends on the length l_e . Assuming that l_e is much larger than the magnetic length $l_B = \sqrt{\hbar/|e|B}$, the phase ϕ_e is a random variable, uniformly distributed between $[0, 2\pi[$. The propagation of the electron is thus characterised by the unitary evolution

$$\psi_e \xrightarrow{e} \psi'_e \quad (3.4)$$

with

$$\psi'_e = e^{i\phi_e} \psi_e. \quad (3.5)$$

A time step $t \rightarrow t + 1$ is encoded by the total evolution operator \mathcal{U}

$$\psi_{t+1} = \mathcal{U} \psi_t \quad (3.6)$$

with matrix element

$$\mathcal{U}_{e',e} = e^{i\phi_e} \mathcal{S}_{e',e}. \quad (3.7)$$

The amplitude $\mathcal{S}_{e',e}$ is the matrix element of the full scattering matrix

$$\mathcal{S} = \bigotimes_{\text{vertex } v} \mathcal{S}_v \quad (3.8)$$

with $\mathcal{S}_v = \mathcal{S}_A$ or $\mathcal{S}_v = \mathcal{S}_B$ depending on the sublattice. It acts on \mathbb{C}^{N_e} where N_e is the number of edges in the two-dimensional lattice. The system is critical for $t_A = t_B$ and at the isotropic point if $t_S = r_S = 1/\sqrt{2}$. Studying this model can be done by computing correlation functions based on the Green's function. The Green's function is defined by

$$G(e_2, e_1, z) = \langle e_2 | (1 - z\mathcal{U})^{-1} | e_1 \rangle \quad (3.9)$$

with z a parameter related to the energy ($z = 1$ at criticality) and $|e\rangle$ is the state of \mathbb{C}^{N_e} associated to the edge e . The Green's function is an important quantity involved in the computation of physical observables.

The point conductance is an important physical observable measuring the transport properties of the system. By cutting two edges of a closed system, the transport properties are measured by injecting a current at a point and draining at the other. It is discussed more extensively in section 3.2.6. Let us state, for now, that the point contact conductance g , between link e_1 and a link e_2 , is defined as

$$g = |t_{e_1 e_2}|^2 \quad (3.10)$$

where $t_{e_1 e_2}$ is the transmission amplitude

$$t_{e_1 e_2} = \langle e_1 | (1 - \mathcal{U})^{-1} | e_2 \rangle. \quad (3.11)$$

Note that, to define the proper point conductance, from e_2 to e_1 , the edges are cut open and the action of the evolution operator becomes $\mathcal{U}|e_1\rangle = \mathcal{U}^\dagger|e_2\rangle = 0$. This is discussed more precisely in 3.2.6. The quantity $t_{e_1 e_2}$ is given by a sum over paths connecting the two edges and is very similar to the Green's function. Moreover, the point contact conductance is a random quantity (it depends on all the phases ϕ_e), we thus average over disorder to get some information about the statistics.

3.1.2 Supersymmetric formulation

The main quantity of interest here is $\overline{|G|^2}$, where the overline denotes the average over each $U(1)$ random phase. We here follow closely [37]. Let us start with the simple Green's function $G(e_2, e_1, z)$. First let us associate a complex number $b(e)$ to each edge e . The Green's function reads

$$G(e_2, e_1, z) = \frac{\int [Db] b^*(e_2) b(e_1) e^{S_b}}{\int [Db] e^{S_b}} \quad (3.12)$$

where the Gaussian measure is

$$Db = \prod_{\text{edge } e} \left[\frac{1}{2\pi} db^*(e) db(e) e^{-b^*(e)b(e)} \right] \quad (3.13)$$

and the action S_b is defined by

$$S_b = z \sum_{e', e} b^*(e') \mathcal{U}_{e', e} b(e). \quad (3.14)$$

The correspondence (3.12) can be simply seen by expanding the Green's function in terms of Feynman path γ from e_1 to e_2

$$G(e_2, e_1, z) = \sum_{k=1}^{\infty} z^k \langle e_2 | \mathcal{U}^k | e_1 \rangle = \sum_{\gamma(e_2, e_1)} W_\gamma(e_2, e_1, z) \quad (3.15)$$

with $W_\gamma(e_2, e_1, z)$ the product of each weight of the form $\mathcal{U}_{e',e}$ gathered along the path γ . The computation of $|G|^2 = GG^*$ is straightforward. We denote by b_+ the bosonic variables of the advanced Green's function $G(e_2, e_1, z)$ and by b_- the bosonic variables of the retarded Green's function $G(e_2, e_1, z)^*$, then

$$|G(e_2, e_1, z)|^2 = \frac{\int [Db_+] [Db_-] b_+^*(e_2) b_-(e_2) b_+(e_1) b_-^*(e_1) e^{S_{b_+} + S_{b_-}^*}}{\int [Db_+] [Db_-] e^{S_{b_+} + S_{b_-}^*}}. \quad (3.16)$$

In order to progress, the average over disorder needs to be computed. However, the partition function

$$Z = \int [Db_+] [Db_-] e^{S_{b_+} + S_{b_-}^*} \quad (3.17)$$

is also dependent on the random $U(1)$ phases at every edge. A computational method, known as *supersymmetric method*, must be employed. Another possibility, known as the *replica trick*, used in this thesis for the computation of the entanglement entropy, can also be used. This was followed by Pruisken [119] and led to a description in terms of a sigma model with a field living on the space $\lim_{n \rightarrow 0} U(2n)/U(n) \times U(n)$. In the following we follow the supersymmetric approach. It consists in writing the inverse of the partition function (3.17) such that

$$\frac{1}{Z} = \int [Df_+] [Df_-] e^{S_{f_+} + S_{f_-}^*} \quad (3.18)$$

where f_+ and f_- are Grassmann (or equivalently fermionic) variables. We recall that two fermionic variables anticommute $f_1 f_2 = -f_2 f_1$ and in particular $f_1^2 = 0$. The measure is simply

$$Df = \prod_{\text{edge } e} \left[\frac{1}{2\pi} df^*(e) df(e) e^{-f^*(e)f(e)} \right] = \prod_{\text{edge } e} \left[\frac{1}{2\pi} df^*(e) df(e) (1 - f^*(e)f(e)) \right] \quad (3.19)$$

and the definition of the fermionic action S_f is very similar to the bosonic one

$$S_f = z \sum_{e',e} f^*(e') \mathcal{U}_{e',e} f(e). \quad (3.20)$$

where complex conjugation for Grassmann variables is $(f_1 f_2)^* = f_2^* f_1^*$. We now have

$$|G(e_2, e_1, z)|^2 = \int [Db_+] [Db_-] [Df_-] [Df_+] b_+^*(e_2) b_-(e_2) b_+(e_1) b_-^*(e_1) e^{S_{b_+} + S_{b_-}^* + S_{f_+} + S_{f_-}^*} \quad (3.21)$$

thus $Z = 1$ and average over disorder can be performed. We thus compute

$$\overline{|G(e_2, e_1, z)|^2} = \int \prod_e \left[\frac{d\phi_e}{2\pi} \right] |G(e_2, e_1, z)|^2 \quad (3.22)$$

by expanding the action in terms of Feynman paths. Considering a specific edge e , the contribution of the integration over ϕ_e for a single term in the decomposition of the exponential reads

$$\int_0^{2\pi} \frac{d\phi_e}{2\pi} e^{i\phi_e(n_{b_+}+n_{f_+}-n_{b_-}-n_{f_-})} = \delta_{n_{b_+}+n_{f_+}, n_{b_-}+n_{f_-}} \quad (3.23)$$

where n_c is the number of instances of the variable c on the edge e . In terms of trajectories, n_c is the number of times a Feynman path of a particle c goes through e . As a consequence, the average over disorder selects only configurations where each edge carries the same number of advanced and retarded particles.

3.1.3 The supersymmetric $gl(2|2)$ spin chain

To proceed, it is convenient to introduce the formulation of the original model as a superspin chain, corresponding to the second quantisation of the network model. In the following, operators without a bar act on the states of even sites and operators with a bar on the states of odd sites. The creation and annihilation operators satisfy the (anti) commutation relations

$$[b_\alpha, b_\beta^\dagger] = \{f_\alpha, f_\beta^\dagger\} = \delta_{\alpha,\beta}, \quad (3.24a)$$

$$[\bar{b}_\alpha, \bar{b}_\beta^\dagger] = -\{\bar{f}_\alpha, \bar{f}_\beta^\dagger\} = \delta_{\alpha,\beta}, \quad (3.24b)$$

where $\alpha, \beta = +, -$. All states can be obtained from the vacuum, denoted $|0\rangle$ on even sites and $|\bar{0}\rangle$ on odd sites, by the action of creation operators. The states for even sites are grouped by quadruplet

$$|4n+1\rangle = \frac{1}{n!} (b_+^\dagger b_-^\dagger)^n f_+^\dagger f_-^\dagger |0\rangle \quad (3.25a)$$

$$|4n+2\rangle = \frac{1}{\sqrt{n!(n+1)!}} (b_+^\dagger b_-^\dagger)^n b_+^\dagger f_-^\dagger |0\rangle \quad (3.25b)$$

$$|4n+3\rangle = \frac{1}{\sqrt{n!(n+1)!}} (b_+^\dagger b_-^\dagger)^n b_-^\dagger f_+^\dagger |0\rangle \quad (3.25c)$$

$$|4n+4\rangle = \frac{1}{(n+1)!} (b_+^\dagger b_-^\dagger)^{n+1} |0\rangle \quad (3.25d)$$

with $n \in \mathbb{N}$ and for odd sites

$$|\overline{4n+1}\rangle = \frac{1}{n!} (\bar{b}_+^\dagger \bar{b}_-^\dagger)^n \bar{f}_+^\dagger \bar{f}_-^\dagger |\bar{0}\rangle \quad (3.26a)$$

$$|\overline{4n+2}\rangle = \frac{1}{\sqrt{n!(n+1)!}} (\bar{b}_+^\dagger \bar{b}_-^\dagger)^n \bar{b}_+^\dagger \bar{f}_-^\dagger |\bar{0}\rangle \quad (3.26b)$$

$$|\overline{4n+3}\rangle = \frac{1}{\sqrt{n!(n+1)!}} (\bar{b}_+^\dagger \bar{b}_-^\dagger)^n \bar{b}_-^\dagger \bar{f}_+^\dagger |\bar{0}\rangle \quad (3.26c)$$

$$|\overline{4n+4}\rangle = \frac{1}{(n+1)!} (\bar{b}_+^\dagger \bar{b}_-^\dagger)^{n+1} |\bar{0}\rangle \quad (3.26d)$$

Note that fermionic states on odd sites have norm squared equal to -1 , as a consequence of the anti-commutation relation for barred fermionic generators. All states in (3.25) and (3.26) satisfy the constraint that comes from averaging over the $U(1)$ disorder

$$b_+^\dagger b_+ + f_+^\dagger f_+ = b_-^\dagger b_- + f_-^\dagger f_-, \quad \text{or} \quad \bar{b}_+^\dagger \bar{b}_+ - \bar{f}_+^\dagger \bar{f}_+ = \bar{b}_-^\dagger \bar{b}_- - \bar{f}_-^\dagger \bar{f}_-. \quad (3.27)$$

The transfer matrix at a node of the sublattice A reads

$$R = (\mathcal{P} \otimes \bar{\mathcal{P}}) e^{zt_A(b_+^\dagger \bar{b}_+^\dagger + f_+^\dagger \bar{f}_+^\dagger) + zt_A(b_-^\dagger \bar{b}_-^\dagger + f_-^\dagger \bar{f}_-^\dagger)} (zr_A)^{(b_+^\dagger b_+ + f_+^\dagger f_+ + b_-^\dagger b_- + f_-^\dagger f_-)} \\ \times (zr_A)^{(\bar{b}_+^\dagger \bar{b}_+ - \bar{f}_+^\dagger \bar{f}_+ + \bar{b}_-^\dagger \bar{b}_- - \bar{f}_-^\dagger \bar{f}_-)} e^{zt_A(\bar{b}_+ b_+ + \bar{f}_+ f_+) + zt_A(\bar{b}_- b_- + \bar{f}_- f_-)} (\mathcal{P} \otimes \bar{\mathcal{P}}) \quad (3.28)$$

The operators $\mathcal{P}/\bar{\mathcal{P}}$ project out states that do not respect the constraints (3.27). The minus sign, in the anti-commutation relation of the fermions on odd sites (3.24b), is unusual but important to ensure that closed fermionic paths have the weight -1 . Indeed creation and annihilation of a pair of fermions by the transfer matrix reads

$$\langle 0, \bar{0} | \bar{f} f f^\dagger \bar{f}^\dagger | 0, \bar{0} \rangle = -1, \quad \text{with} \quad |0, \bar{0}\rangle = |0\rangle \otimes |\bar{0}\rangle. \quad (3.29)$$

3.1.4 Exact results and critical exponents

In the continuum, educated guesses led to the description with the action of a sigma model. The field Q lives on a supersymmetric space $U(1, 1|2)/U(1|1) \otimes U(1|1)$. This target space can be decomposed as the product between a non-compact hyperboloid and a compact sphere. The action reads

$$S = \frac{1}{16g_\sigma^2} \int d^2z \text{STr}(\partial_\mu Q \partial_\mu Q) - \frac{\theta}{16\pi} \int d^2z \epsilon_{\mu\nu} \text{STr}(Q \partial_\mu Q \partial_\nu Q) \quad (3.30)$$

with g_σ and θ some parameters. This action has a topological term, responsible for the criticality of the system in presence of disorder (see [120] for a review).

An important aspect of the problem, where many results were found, is to characterise the multifractal spectrum [121] of the Hall transition [122, 123]. In this context, it is done by studying the moments $|\psi(r)|^{2q}$ of a critical wavefunction. They follow the scaling law

$$L^d \overline{|\psi(r)|^{2q}} \sim L^{-\tau_q} \quad (3.31)$$

with $\tau_q \equiv d(q-1) + \Delta_q$ and L the lattice size. The dimensions Δ_q have been extensively studied and exact results were found based on symmetries [124, 125]. This is connected to a recent approach where lattice observables are studied carefully and the exponent was conjectured to be purely parabolic

$$\Delta_q = Xq(1-q) \quad (3.32)$$

with $X = 1/4$ [126]. The interpretation of the observables in [126, 127] and the quantized models studied in this chapter are discussed section 3.2.6. However, the study of the multifractal spectrum does not give access to the critical exponent ν . More recently, Zirnbauer

proposed in [128] to describe the plateau transition in the IQHE as a deformed $Gl(1|1)_{n=4}$ Wess-Zumino-Witten model. The exponent ν predicted is $\nu = \infty$ and thus, this approach remains at odds with all simulations of this exponent. It is nevertheless not incompatible in the case of an RG-flow converging very slowly towards the fixed point. Very large system sizes would show an increasing exponent ν .

Note also that, to describe the universality class of the IQHE transition, it has been hinted that the disorder of the lattice may be an important qualitative property. In a recent paper [129], the authors studied a network model with a randomised lattice structure and found an exponent ν slightly different, in a better agreement with experience.

Nevertheless, a complete solution to the Chalker-Coddington model remains to be found despite the subject being a very active topic of research. The first reason this model resisted attempts to solve it comes from the infinite-dimensional on-site $gl(2|2)$ representations. It is not always clear how to apply, in general, ideas of integrability to this kind of space. Moreover, the $gl(2|2)$ super-spin chain is presumably not integrable [19, 130]. Of course, an approach directly in the continuum is possible. However, it is hard to narrow down the possibilities to a small set of candidates. The non-unitarity, indecomposability and irrationality of the theory makes this task much harder than in the unitary case. Different approaches must be considered, such as on-site truncations.

3.2 The first truncation as a loop model

The presence of an infinite number of local degrees of freedom makes the model very hard to tackle analytically or numerically. It is a natural idea to investigate instead truncations obtained by restricting the number of states on a given edge. Following Ikhlef et al. [37] we define the truncation at level M by keeping only configurations such that the number of particles on an edge for each type $(+, -)$ is less or equal to M . The original network model is known to be critical for $z = 1$ but the truncated model at this value is gapped, and criticality is restored only in the limit $M \rightarrow \infty$. However it is possible to increase the particle fugacity z such that the model becomes critical for finite M . We assume in the rest of the chapter that z is real.

The original idea of studying such truncations comes from a work of Marston and Tsai [70]. Using DMRG techniques, the authors argued that the successive truncations of the $gl(2|2)$ Hamiltonian model defined by keeping $1 + 4M$ states at each site were not critical. However, they showed that the gap in the spectrum goes to 0 as $M \rightarrow \infty$ and thus criticality is restored in the limit of large order of truncations. However, no attempt was made to tune parameters of the Hamiltonian in order to study these models as a series of critical models. This idea was first discussed in the work of Ikhlef et al. [37], where they tuned the particle fugacity z of the first truncation to restore criticality.

In the following, the first truncation is discussed. We start with a review of its construction and the integrable deformation of Ikhlef, Fendley and Cardy. The symmetries are discussed extensively and their spectrum compared. Then some comments are made on the physics of the dense phase and possible connections with lattice observables are considered.

3.2.1 Truncations as a loop model: the case $M = 1$

The interpretation of the Chalker-Coddington model as a two-color loop model applies naturally to its truncations. We look into the case $M = 1$, already considered in [37]. Since the truncations preserve the symmetry between bosons and fermions, each closed path has weight $n = 1 + (-1) = 0$.

Let us expand the partition function

$$\bar{Z} = \int \prod_e \left[\frac{d\phi_e}{2\pi} \right] [Db_+] [Db_-] e^{S_{b_+} + S_{b_-} + S_{f_+} + S_{f_-}} \quad (3.33)$$

with terms involving the following combination of variables

$$\Gamma_{e_2 \leftarrow e_1}^\sigma = (b_\sigma^*(e_2)b_\sigma(e_1) + f_\sigma^*(e_2)f_\sigma(e_1)) \quad (3.34)$$

where $\sigma = +, -$. Since we have at most 1 particle of each color per site, the expansion of the partition function in terms of the functions Γ defines paths on the oriented lattice. If there is a closed path (a loop), the weight of the configuration vanishes. Indeed

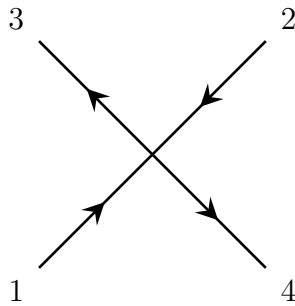
$$\Gamma_{e_1 \leftarrow e_N}^\sigma \Gamma_{e_N \leftarrow e_{N-1}}^\sigma \cdots \Gamma_{e_3 \leftarrow e_2}^\sigma \Gamma_{e_2 \leftarrow e_1}^\sigma = b_\sigma^*(e_1) \left(\prod_{i=2}^N (b_\sigma(e_i)b_\sigma^*(e_i)) \right) b_\sigma(e_1) \quad (3.35)$$

$$+ f_\sigma^*(e_1) \left(\prod_{i=2}^N (f_\sigma(e_i)f_\sigma^*(e_i)) \right) f_\sigma(e_1) \quad (3.36)$$

where we wrote only terms with a non-zero contribution after the integration over the inner edges. When performing the integration over bosonic and fermionic variables, we find the weight $1 + (-1) = 0$ because of the anti-commutation of $f_\sigma(e_1)$ with $f_\sigma^*(e_1)$. Note that the following relation is true

$$\int_{e_2} [Db_\sigma(e_2)] [Df_\sigma(e_2)] \Gamma_{e_3 \leftarrow e_2}^\sigma \Gamma_{e_2 \leftarrow e_1}^\sigma = \Gamma_{e_3 \leftarrow e_1}^\sigma \quad (3.37)$$

so it is obvious that expanding the partition function in terms of these functions Γ is exactly the same as keeping track of the connectivities of a loop model. We now derive the weight of the different vertices. We drop the index σ since the colors interact only by having the same number of strands of either colour at each edge. It suffices to derive the weights for one flavour as the final interaction is a tensor product of the tiles for each colour that respects the constraints. For a vertex



$$(3.38)$$

we have the decomposition

$$\begin{aligned}
e^{S_b+S_v} &= \exp\left(\sum_{i=1,2} \sum_{j=3,4} b^*(e_j) S_{i,j} b(e_i)\right) \exp\left(\sum_{i=1,2} \sum_{j=3,4} f^*(e_j) S_{i,j} f(e_i)\right) \\
&= \exp\left(\sum_{i=1,2} \sum_{j=3,4} S_{i,j} (b^*(e_j) b(e_i) + f^*(e_j) f(e_i))\right) \\
&= \exp\left(\sum_{i=1,2} \sum_{j=3,4} S_{i,j} \Gamma_{e_j \leftarrow e_i}\right) \\
&= 1 + \sum_{i=1,2} \sum_{j=3,4} S_{i,j} \Gamma_{e_j \leftarrow e_i} + S_{13} S_{24} \Gamma_{e_3 \leftarrow e_1} \Gamma_{e_4 \leftarrow e_2} + S_{14} S_{23} \Gamma_{e_4 \leftarrow e_1} \Gamma_{e_3 \leftarrow e_2} \quad (3.39)
\end{aligned}$$

where the terms, in the expansion of the last line, with more than one particle per site have been dropped. The first contribution with weight 1 corresponds to the following empty diagram

$$\begin{array}{c}
\text{◇} \\
1
\end{array} \quad (3.40)$$

The contribution $\sum_{i=1,2} \sum_{j=3,4} S_{i,j} \Gamma_{e_j \leftarrow e_i}$ gives the 4 following diagrams (with their weights)

$$\begin{array}{cccc}
\text{◇} & \text{◇} & \text{◇} & \text{◇} \\
zt & -zr & zt & zr
\end{array} \quad (3.41)$$

and the two last contributions are

$$\begin{array}{cc}
\text{◇} & \text{◇} \\
z^2 t^2 & -z^2 r^2
\end{array} \quad (3.42)$$

The R -matrix encoding the local Boltzmann weights at each vertex is given by the product of the interaction for each type (+/-) that we draw using two colours. The disorder average adds the constraint that an edge is either empty or carrying two paths, one of each colour.

$$\begin{aligned}
R &= \text{◇} + z^2 t^2 \left(\text{◇} + \text{◇} \right) + z^2 r^2 \left(\text{◇} + \text{◇} \right) \\
&\quad - z^4 t^2 r^2 \left(\text{◇} + \text{◇} \right) + z^4 t^4 \text{◇} + z^4 r^4 \text{◇}.
\end{aligned} \quad (3.43)$$

The monomer fugacity z has to be tuned in order for the model to be critical: an empty edge has therefore a weight 1, and an edge with a pair of strands has a weight z^2 . In the $M = 1$ truncated model the critical value z_C of z is not known exactly but was estimated numerically to $z_C \simeq 1.03 > 1$ in [37]. The natural interpretation is that restricting the occupation number on each edge is compensated by weighting occupied edges with a fugacity $z > 1$.

In the following, the generalised watermelon operators are considered. In a loop model, a conformal dimension x_ℓ measures the propagation of ℓ lines between two neighbourhoods. In practice, it corresponds to the critical exponent obtained by considering a transfer matrix sector propagating ℓ through-lines. In the first truncation, we thus defined the watermelon exponents x_{ℓ_1, ℓ_2} propagating ℓ_1 red lines and ℓ_2 blue lines.

3.2.2 An integrable deformation

As discussed in [37], it is possible to slightly modify the truncated model to make it integrable. This makes the use of Bethe ansatz calculations possible, hence allowing a much more accurate and complete identification of the continuum limit. The question is however whether the required “slight” modification matters, and in particular whether it changes the universality class. As shown in [37], the integrable model involves the addition of two tiles where the strands can go straight, with a corresponding integrable \check{R} matrix

$$\begin{aligned}
\check{R}(\varphi) = & t(\varphi) \langle \diamond \rangle + u_1(\varphi) \left(\langle \langle \rangle \rangle + \langle \rangle \langle \rangle \right) + u_2(\varphi) \left(\langle \langle \rangle \rangle + \langle \rangle \langle \rangle \right) \\
& + v(\varphi) \left(\langle \langle \rangle \rangle + \langle \rangle \langle \rangle \right) + x(\varphi) \left(\langle \langle \rangle \rangle + \langle \rangle \langle \rangle \right) + w_1(\varphi) \langle \langle \rangle \rangle + w_2(\varphi) \langle \langle \rangle \rangle
\end{aligned} \tag{3.44}$$

Here the weights are

$$t(\varphi) = -\cos(2\varphi - 3\theta) - \cos 5\theta + \cos 3\theta + \cos \theta \tag{3.45a}$$

$$u_1(\varphi) = -2 \sin 2\theta \sin(\varphi - 3\theta) \tag{3.45b}$$

$$u_2(\varphi) = 2 \sin 2\theta \sin \varphi \tag{3.45c}$$

$$v(\varphi) = -2 \sin 2\theta \varphi \sin(\varphi - 3\theta) \tag{3.45d}$$

$$x(\varphi) = 2 \sin \varphi \sin(\varphi - 3\theta) \tag{3.45e}$$

$$w_1(\varphi) = 2 \sin(\varphi - 2\theta) \sin(\varphi - 3\theta) \tag{3.45f}$$

$$w_2(\varphi) = 2 \sin \varphi \sin(\varphi - \theta) \tag{3.45g}$$

$$n = -2 \cos 2\theta. \tag{3.45h}$$

The weights (3.45) contain an extra parameter θ , allowing to consider loops with a non-zero fugacity n in the range $|n| \leq 2$. The model relevant for the quantum Hall effect is retrieved in the end by setting $n = 0$ for $\theta = \frac{3\pi}{4}$.

The question of the equivalence between the first truncation of the Chalker-Coddington model and this integrable modification is not obvious. This is due in large part to the fact

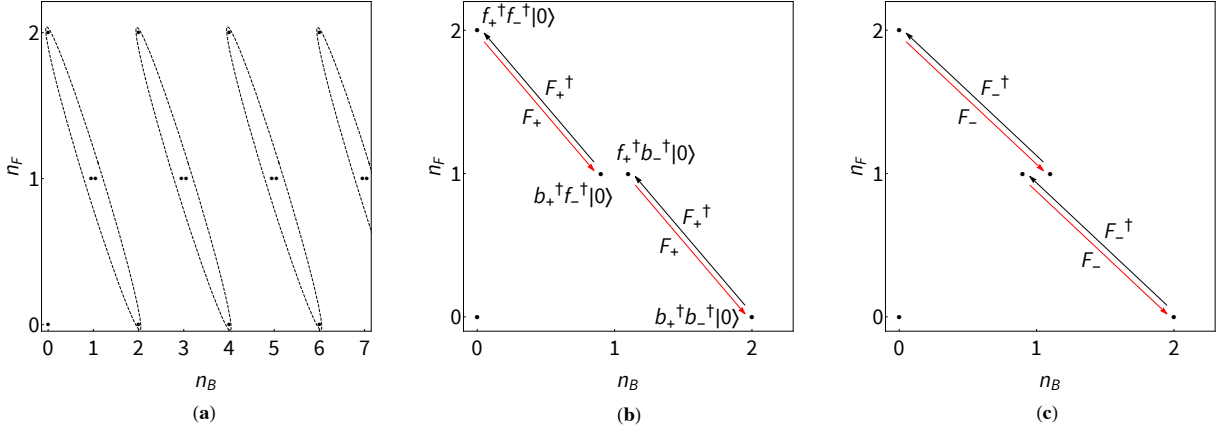


Figure 3.3 – Structure of the Hilbert space on a given edge. The first panel (a) represents the possible states corresponding to the quantum numbers n_B and n_F . The vector space can be divided in quartet of states with an identical number of particles. The second and third panels ((b) and (c)) shows the action of F_+ and F_- within the first quartet (thus corresponding to the first truncation).

that, in the integrable model, the loops can go straight, a fact which is incompatible with the underlying orientation of the original Chalker-Coddington model. It is easier to understand what this means, and how this might affect the universality class, by thinking in terms of symmetries.

Using the Bethe ansatz equations, critical exponents of this integrable model can be obtained analytically [77]. In particular, the watermelon exponents, propagating ℓ_1 strands of the first colour and ℓ_2 strands of the second colour, are

$$x_{\ell_1, \ell_2, s} = \frac{\ell_1^2 + \ell_2^2}{16} - \frac{1}{4} + s^2, \quad \ell_1, \ell_2 \neq 0, s > 0 \quad (3.46)$$

with s a positive real number describing the continuum of critical exponents above a sector with $x_{\ell_1, \ell_2, 0}$ at the bottom.

3.2.3 Symmetries

The truncation at level M only keeps the first $1 + 4M$ states of (3.25) and (3.26). Note that, since after this truncation we need to tune the value of z to make the model critical, the operator \mathcal{P} (resp. $\bar{\mathcal{P}}$) gets modified in such a way that for every state in (3.25) (resp. (3.26)), it gives a weight z^N where $N = n_B + n_F$ is the number of bosons and fermions in the state, $0 \leq N \leq 2M$.

In the untruncated case (and thus $z = 1$), the transfer matrix (3.28) has $gl(2|2)$ symmetry. It is convenient in what follows to represent the Hilbert space on a given edge as in figure 3.3. The state at the origin is the vacuum, while the “quartets” correspond to successive values of n in (3.25) or (3.26), with the corresponding value of $N = n_B + n_F = 2n + 2$.

The four Cartans of $gl(2|2)$ correspond essentially to the numbers of bosons/fermions of type \pm :

$$\text{Cartan} = \left\{ b_+ b_+^\dagger - \frac{1}{2}, f_+ f_+^\dagger - \frac{1}{2}, -b_- b_-^\dagger - \frac{1}{2}, f_- f_-^\dagger - \frac{1}{2} \right\}. \quad (3.47)$$

The other generators of this algebra can be conveniently encoded in matrix form as

$$J = \begin{pmatrix} b_+ b_+^\dagger - \frac{1}{2} & b_+ f_+^\dagger & b_+ b_- & b_+ f_- \\ f_+ b_+^\dagger & f_+ f_+^\dagger - \frac{1}{2} & f_+ b_- & f_+ f_- \\ -b_-^\dagger b_+^\dagger & -b_-^\dagger f_+^\dagger & -b_- b_-^\dagger - \frac{1}{2} & -b_-^\dagger f_- \\ f_-^\dagger b_+^\dagger & f_-^\dagger f_+^\dagger & f_-^\dagger b_- & f_- f_-^\dagger - \frac{1}{2} \end{pmatrix}. \quad (3.48)$$

We see that some of these generators change the total number of particles: on the diagram they would move between different quartets, i.e. different values of n . The first non-trivial truncation is obtained by restricting to the first five states on a given edge, i.e., the vacuum and the first quartet ($n = 1$).

In order to discuss the symmetries of the resulting model we introduce some notion about the $gl(1|1)$ symmetry. It is easy to see that if we denote the particle numbers as

$$b_+^\dagger b_+ + f_+^\dagger f_+ = N_+ \quad (3.49a)$$

$$b_-^\dagger b_- + f_-^\dagger f_- = N_- \quad (3.49b)$$

the new fermion operators defined as

$$F_+ \equiv f_+ b_+^\dagger, \quad F_+^\dagger = b_+ f_+^\dagger, \quad (3.50a)$$

$$F_- \equiv b_-^\dagger f_-, \quad F_-^\dagger = f_-^\dagger b_- \quad (3.50b)$$

obey

$$\{F_+, F_+^\dagger\} = N_+, \quad (3.51a)$$

$$\{F_-, F_-^\dagger\} = N_-. \quad (3.51b)$$

These are well known to be $gl(1|1)$ commutation relations. And of course the $F_\pm^{(\dagger)}$ generators are part of the $gl(2|2)$ symmetry: the matrix elements $J_{1,2}$ and $J_{2,1}$ in (3.48) reproduce the fermionic generators (3.50a) of $gl(1|1)_+$, while $J_{3,4}$ and $J_{4,3}$ reproduce the generators (3.50b) of $gl(1|1)_-$. Therefore we see that each quartet in figure 3.3 can be interpreted as the tensor product of a pair of two-dimensional representations of $gl(1|1)_+ \times gl(1|1)_-$, where each of the $gl(1|1)$ acts on a given colour (\pm). In our model moreover, $N_+ = N_-$, so the two representations are isomorphic.

This is all for one type of edge. Of course, for the other edges, we have the barred generators, with the conjugate action

$$\begin{aligned} \{\bar{F}_+, \bar{F}_+^\dagger\} &= -\bar{N}_+ \\ \{\bar{F}_-, \bar{F}_-^\dagger\} &= -\bar{N}_- \end{aligned} \quad (3.52)$$

which correspond to another (conjugate) pair of two-dimensional representations.

Restricting to $N_+ = N_- = 1$ (i.e., $N = 2$) gives the first non-trivial truncation. We see that it retains the $gl(1|1)_+ \times gl(1|1)_-$ symmetry discussed above, here acting on the tensor product $(V \otimes V^*)^{\otimes L}$, with the five-dimensional representations $V = 1 \oplus (\square_+ \otimes \square_-)$ for even sites and $V^* = 1 \oplus (\bar{\square}_- \otimes \bar{\square}_+)$ for odd sites. We have here denoted the two-dimensional representations of $gl(1|1)$ simply by $\square, \bar{\square}$, without reference to the number N , as representations with different values of $N_{\pm} \neq 0$ are isomorphic.

For higher truncations, the symmetry is the same and acts again on a direct sum of the identity and products of pairs of two-dimensional representations. Note that a key feature of the untruncated model is that the different quartets and the singlet are all related by action of $gl(2|2)$ generators: this extra symmetry disappears in the truncations.

The presence of V and V^* modules is a consequence of the underlying orientation of the Chalker-Coddington (CC) lattice. In geometrical terms, the arrows on the lattice edges define a unique orientation for all the loops.

A key feature of the integrable modification introduced in [37] is that it allows vertices which are not consistent with the CC orientation any more. This is a priori a dangerous manoeuvre, since it breaks an underlying symmetry of the original (truncated as well as non-truncated) model.

To understand more precisely the link between lattice orientation and symmetry breaking, it is useful to consider a simpler version of the problem where only one colour of loop would be allowed. The model consistent with the orientation of the CC lattice would then be a model of dilute self-avoiding loops on an oriented lattice. This model was studied in [131], where it was called the *dilute oriented loop model*. A typical configuration of loops within this model is shown in figure 3.4.

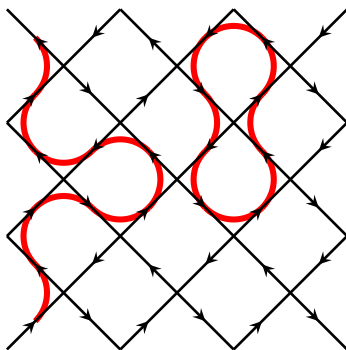


Figure 3.4 – A configuration of the dilute oriented loop model.

The modified model corresponding to this one-colour toy model would then be, by analogy, the ordinary dilute loop model on the square lattice. This modification can be made integrable by making an appropriate choice of the vertex weights.

We now discuss (following [131]) a path-integral description of the one-colour model for n integer. In the oriented case, this is obtained by associating with every edge an n -dimensional complex vector \vec{z} subject to $|\vec{z}|^2 = 1$. Consider a vertex such as the one shown in the first

diagram in figure 3.5. A term $\vec{z}_A^\dagger \cdot \vec{z}_B$ will correspond to the arc drawn as in the second diagram in this figure.

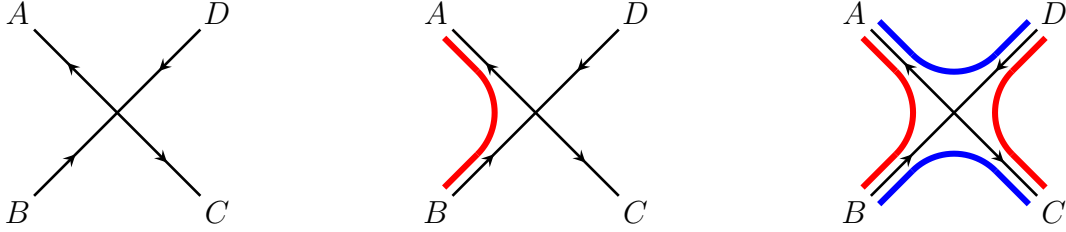


Figure 3.5 – Examples of interactions at a vertex. The left panel shows an oriented vertex with no arc, corresponding to the identity in the action. The panel in the middle has an arc going from the edge B to the edge A corresponding in the action to the term $(\vec{z}_A^\dagger \cdot \vec{z}_B)$. The third panel on the right shows an other configuration with two colours coming from $(\vec{z}_A^\dagger \cdot \vec{z}_B)(\vec{z}_C^\dagger \cdot \vec{z}_D)(\vec{w}_A^\dagger \cdot \vec{w}_D)(\vec{w}_C^\dagger \cdot \vec{w}_B)$

The convention is now that we go around a loop by following the arrows, and we take the dagger (\dagger) vector for the half edge exiting a given vertex, and the non-dagger vector for the half-edge entering the vertex. Each of \vec{z} and \vec{z}^\dagger appears once, due to the definition of loops. It is then possible to express the partition function of the dilute oriented loop model as

$$Z \propto \int \prod_{\text{edges } e} d\vec{z}_e e^{-S}. \quad (3.53)$$

The corresponding action S contains a total of seven terms: in addition to the identity it contains terms of the form $(\vec{z}_A^\dagger \cdot \vec{z}_B)(\vec{z}_C^\dagger \cdot \vec{z}_D)$ and $(\vec{z}_A^\dagger \cdot \vec{z}_D)(\vec{z}_C^\dagger \cdot \vec{z}_B)$, as well as $(\vec{z}_A^\dagger \cdot \vec{z}_B)$, $(\vec{z}_C^\dagger \cdot \vec{z}_D)$, $(\vec{z}_A^\dagger \cdot \vec{z}_D)$ and $(\vec{z}_C^\dagger \cdot \vec{z}_B)$. The loop diagrams corresponding to two of these terms are shown in the first two panels of Figure 3.5. This model has obviously $U(n)$ symmetry. Indeed, once the partition function is expanded in terms of loops, a local change of phase $\vec{z}_e \rightarrow e^{i\phi_e} \vec{z}_e$ does not change Z . As a matter of fact, the model is closely related to the sigma model on the complex projective space $CP^{n-1} = U(n)/U(n-1) \times U(1)$.

Of course this definition works only for n a positive integer. It can be extended to the case $n = 0$ we are interested in after replacing $U(0)$ by the appropriate supergroup $U(p|p)$, with $p \geq 1$ integer. The simplest choice is obviously $U(1|1)$.

It is possible to use, instead of a Euclidian version involving complex vectors, a transfer matrix or Hamiltonian version or the oriented one-colour model. In this case, one needs to put on every edge the direct sum of the trivial and the fundamental representation for one orientation of $gl(1|1)$, and the direct sum of the trivial and the conjugate fundamental for the other. In other words, the ‘‘Hilbert space’’ is $(V \otimes V^*)^{\otimes L}$, with $V = 1 \oplus \square$ for even sites and $V^* = 1 \oplus \bar{\square}$ for odd sites.

Like the unmodified model, the modified one admits a different path-integral description where every edge now carries a real n -dimensional vector \vec{u} . This is because loop pieces can connect either bonds of the CC lattice with compatible orientation, or bonds with opposite

orientations, like those going straight through a vertex. This is only possible if the vectors are self-conjugate. One can then write a model with a similar kind of action, involving instead products of the type $(\vec{u}_A \cdot \vec{u}_B)(\vec{u}_C \cdot \vec{u}_D)$. The possibility of going straight through a vertex will lead to two new interactions, $(\vec{u}_A \cdot \vec{u}_C)$ and $(\vec{u}_B \cdot \vec{u}_D)$, so that the expansion over loops now gives a total of nine diagrams, in accordance with [38]. The model has now $O(n)$ symmetry. Note that it is also possible to add an interaction of the form $(\vec{u}_A \cdot \vec{u}_C)(\vec{u}_B \cdot \vec{u}_D)$ that allows crossing at vertices without breaking this symmetry. Once the partition function is expanded in terms of loops, a local change of sign $\vec{u}_e \rightarrow -\vec{u}_e$ does not change the result. When $n = 0$, $O(0)$ can be given sense using an orthosymplectic supergroup, the smallest of which is $OSp(2|2)$.

Going from the oriented to the non-oriented model therefore breaks the symmetry from $U(n)$ to $O(n)$, or, in the case $n = 0$, from $U(2|2)$ down to $OSp(2|2)$. In general, such explicit symmetry-breaking does change the universality class. It was shown for instance in [131], that, while the non-oriented model is in the universality class of $O(n)$ criticality, the oriented model is in fact in the universality class of $O(2n)$. While these two universality classes are different for general n , they coincide—remarkably—for $n = 0$. The corresponding “self-avoiding walk” universality class is indeed extremely robust: not only is it insensitive to the lattice orientation, it is also known to be unaffected by the introduction of crossing vertices (giving rise to what is called self-avoiding trails [132]), which remains compatible with $O(n)$ symmetry.

The symmetry analysis of the first truncation of the Chalker-Coddington model is very similar. In the Euclidian version, what we need now are two independent complex vectors, \vec{z} and \vec{w} , on each edge. Interactions are simple, but laborious to write down. For instance a diagram such as the third one in figure 3.5 corresponds to $(\vec{z}_A^\dagger \cdot \vec{z}_B)(\vec{z}_C^\dagger \cdot \vec{z}_D)(\vec{w}_A^\dagger \cdot \vec{w}_D)(\vec{w}_C^\dagger \cdot \vec{w}_B)$. The symmetry is obviously $U(n) \times U(n) \times Z_2$, the Z_2 corresponding to the symmetry between the two types of vectors (colours). In terms of spin chain, the Hilbert space for $n = 0$ is

$$\mathcal{H} = ((1 \oplus (\square_+ \otimes \square_-)) \otimes (1 \oplus (\bar{\square}_- \otimes \bar{\square}_+)))^{\otimes L} \quad (3.54)$$

where \square_+, \square_- are now fundamental ($2p$ -dimensional) representations of $U(p|p)$, and the total symmetry is now $U(p|p) \times U(p|p) \times Z_2$. It is then clear that the modification of this two-colour model has lower symmetry, $O(n) \times O(n) \times Z_2$. For $n = 0$ this becomes $OSp(2|2) \times OSp(2|2) \times Z_2$.

While we lose symmetry when we modify the model, interestingly, at its critical point, the modified truncation exhibits another kind of symmetry which is expected in the genuine, untruncated model, but would disappear in the first truncation per se. This symmetry can be seen qualitatively as relating the state with empty edges to the state with occupied edges, and is part of a $U_q so(5)$ symmetry (see [77]), with $q = i$ for the point $n = 0$.

The guess that the modified and unmodified truncated models are in the same universality class can of course be investigated numerically. This will be done in section 3.2.4 below.

Interestingly, we will find later on that the universality class of the modified truncated model is formally the same as the one of another model which *does* respect the symmetry of the CC lattice: the $a_3^{(2)}$ integrable model, which admits a loop formulation with the following

interaction:

$$\check{R} = \left(\begin{array}{c} \text{Diagram 1} \\ \text{Diagram 2} \end{array} \right) + \lambda_c \left(\begin{array}{c} \text{Diagram 3} \\ \text{Diagram 4} \end{array} \right) \quad (3.55)$$

The situation is however a bit subtle because integrable models can in general admit several different *regimes*, corresponding to different ranges of the “crossing parameter”, denoted θ in (3.45). The critical exponents depend analytically on θ within a given regime, but distinct regimes are in general not related by analytical continuation. Therefore each regime gives rise to a different universality class.

The regime of the $a_3^{(2)}$ which is of interest for us is the so-called regime III. This regime, however, does not include the value $n = 0$ of the loop fugacity. Formally, however, the continuation of regime III for this model up to $n = 0$ would give the same universality class as the one we shall find for the modified truncated model. This justifies *a posteriori* that the modification does not affect the continuum limit significantly. Indeed, we will also find later that the continuum limit of the modified truncated model exhibits a $U(n|n) \times U(n|n) \times Z_2$ symmetry in the continuum limit. In many ways, the truncated loop model is a “dilution” of the model in [66, 133]. Like in the case of ordinary (single) loops, the dilution may change the relationship between the bare parameters and the field theories describing their continuum limit, but the two regimes are qualitatively very similar.

As a last remark, we note that, while the original truncated model can, after a gauge transformation, be formulated purely in terms of positive Boltzmann weights, the modified truncated model involves some negative Boltzmann weights. This feature is however shared by higher truncations. It is not clear to what extent it is “unphysical”.

3.2.4 Comparison

We finally turn to a numerical comparison of the exponents in the modified and unmodified truncated model. Conformal dimensions and the critical parameter z_C can be studied using the ground state and excited states of the transfer matrix. Denoting by $\Lambda_{\ell_1, \ell_2}^L$ the largest eigenvalue of the sector (ℓ_1, ℓ_2) propagating ℓ_1 red strands and ℓ_2 blue strands, we define approximations of the associated dimension $x_{\ell_1, \ell_2}(L, z)$ by

$$x_{\ell_1, \ell_2}(L, z) = -\frac{L}{2\pi} \log \frac{\Lambda_{\ell_1, \ell_2}(L, z)}{\Lambda_0(L, z)}, \quad (3.56)$$

where $\Lambda_0(L, z)$ is simply the largest eigenvalue. The critical parameter z_C can be obtained using “phenomenological renormalisation” [37] as the limit $L \rightarrow \infty$ of the series $z_C(L, L+2)$ solution of $x_{2,2}(L, z) = x_{2,2}(L+2, z)$. An estimate of x_{ℓ_1, ℓ_2} finally follows, either using for any L the extrapolated value of z_C found from phenomenological renormalization for the $x_{2,2}$ exponent, or using phenomenological renormalization size by size for the given exponent x_{ℓ_1, ℓ_2} . In the case of the integrable model things are simpler since the critical point is exactly known. The truncated model is not integrable, and due to the large Hilbert space (of dimension 5^L in the supersymmetric representation) only small sizes are reached using exact diagonalization.

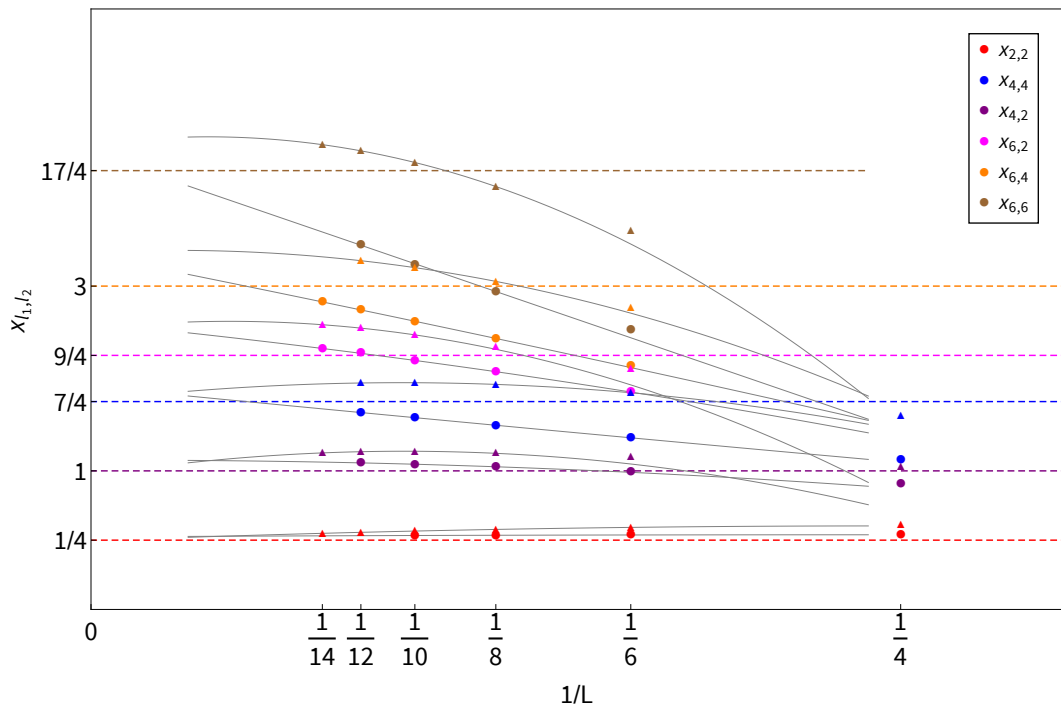


Figure 3.6 – Estimate of dimensions $x_{\ell_1, \ell_2}(L) = -\frac{L}{2\pi} \log \lambda_i / \lambda_0$ in even sectors for the truncated and integrable models. Each colour refers to a different (ℓ_1, ℓ_2) sector that propagates ℓ_1 red strands and ℓ_2 blue strands. Eigenvalues of the diagonal-to-diagonal transfer matrix are computed using exact diagonalisation. The dots are estimates obtained from the integrable model. Triangles are obtained by considering the truncated unmodified model with a loop fugacity z fixed to the estimated critical point $z_C = 1.032$. Dashed coloured lines are the exact dimensions corresponding to the watermelon exponents x_{ℓ_1, ℓ_2} (3.46). Gray lines are polynomial fits of order 2 over the 3 or 4 last data points for each exponent.

Figure 3.6 shows numerical estimates in several sectors for the unmodified truncated model as well as the modified integrable one, up to size $L = 14$. It is clear that despite strong finite-size corrections (expected to be logarithmic, see below) the two models seem to have the same dimensions not only for the thermal state corresponding to the sector $(2, 2)$ but also for higher excitations with even number of lines.

Meanwhile, we see that, while the integrable model has different dimensions for operators inserting an odd number of loop strands, these operators in the unmodified truncated model seem to have the same dimensions as operators in the even sectors (cf Figure 3.7). Similar features have been encountered sometimes in the past [69, 134].

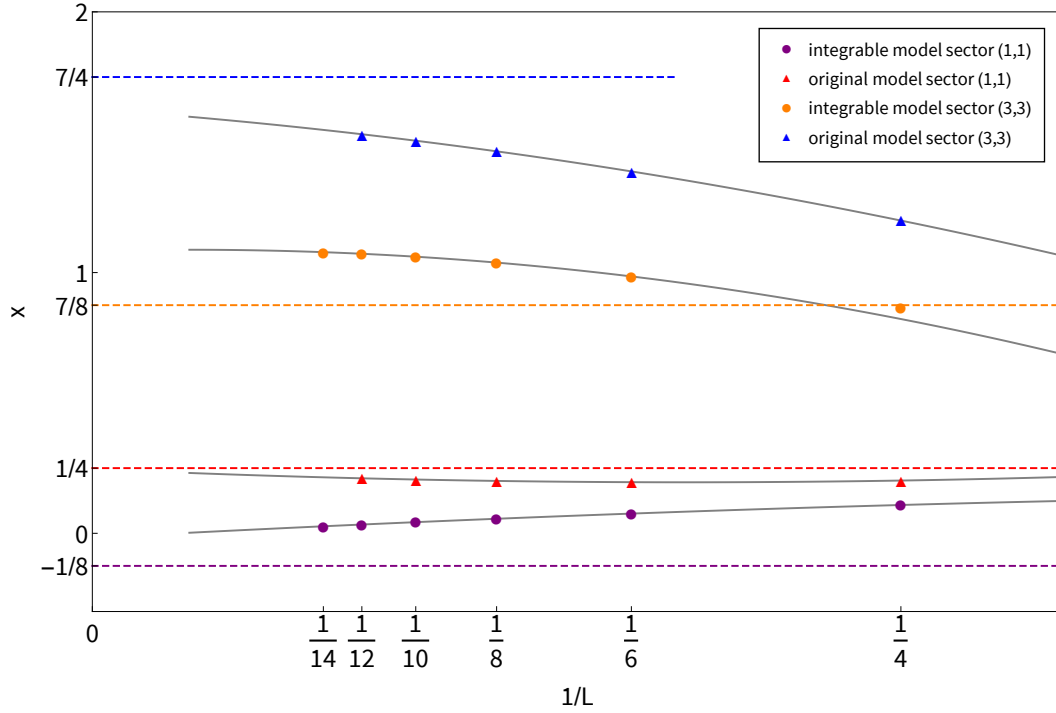


Figure 3.7 – Estimate of dimensions $x_{\ell_1, \ell_2}(L) = -\frac{L}{2\pi} \log \lambda_i / \lambda_0$ in odd sectors for the truncated and integrable models. Eigenvalues of the diagonal-to-diagonal transfer matrix are computed using exact diagonalisation. The dots are estimates obtained from the integrable model. Triangles are obtained by considering the truncated unmodified model with a loop fugacity z fixed to the estimated critical point $z_C = 1.032$. Dashed coloured lines are the exact dimensions corresponding to the watermelon exponents. The propagation of (1, 1) lines corresponds to the purple colour in the integrable model and red colour in the truncated model. The propagation of (3, 3) lines corresponds to the orange colour in the integrable model and blue colour in the truncated model. Gray lines are polynomial fits of order 2 over the 3 or 4 last data points for each exponent. It seems that the sectors (1, 1) and (3, 3) converge toward the exponent (2, 2) and (4, 4) in the truncated unmodified model—with values $\frac{1}{4}$ and $\frac{7}{4}$ respectively.

3.2.5 A word on the dense phase

When z is increased beyond $z_C \sim 1.032$, the system stays critical but the physics—like in the ordinary self-avoiding walk case [135]—is very different and the model is in a new universality class. The ground state is no longer a state of dilute polymers but becomes dense. The largest eigenvalue of the vacuum sector is no longer 1 and does not contain the vacuum. The new ground state corresponds to the energy of the sector $(2, 2)$. Numerical data show that as soon as we go higher than z_C , the system has a unique phase with central charge $c = -4$ (figure 3.8). This can be understood in the limit $z \rightarrow \infty$. The R -matrix in this limit is greatly simplified and corresponds to two decoupled dense polymers (one for each colour). In particular, it reads

$$R = \left(\begin{array}{c} \text{red loop} \\ \text{red loop} \end{array} - \begin{array}{c} \text{red loop} \\ \text{red loop} \end{array} \right) \otimes \left(\begin{array}{c} \text{blue loop} \\ \text{blue loop} \end{array} - \begin{array}{c} \text{blue loop} \\ \text{blue loop} \end{array} \right) \quad (3.57)$$

at the isotropic point, where we kept separated the two colours for clarity and to emphasize that the system is decoupled. Note that the minus sign can be switched (indeed in the Temperley-Lieb algebra, the relations between the generators e_i are also satisfied by $-e_i$ if the loop weight is vanishing.)

The central charge is hence twice the central charge of one dense polymer, $2 \times (-2) = -4$. Watermelon exponents for dense polymers are

$$x_\ell^D = \frac{\ell^2}{16} - \frac{1}{4}. \quad (3.58)$$

Since in the $z \rightarrow \infty$ limit the blue and red degrees of freedom are independent, the exponents in this limit are obtained simply by summing the dense values for each of the two colours. So for instance for the $(\ell_1 = 4, \ell_2 = 4)$ operator we have $x_{44} = 2 x_4^D = \frac{3}{2}$, a result we have checked numerically (Figure 3.9).

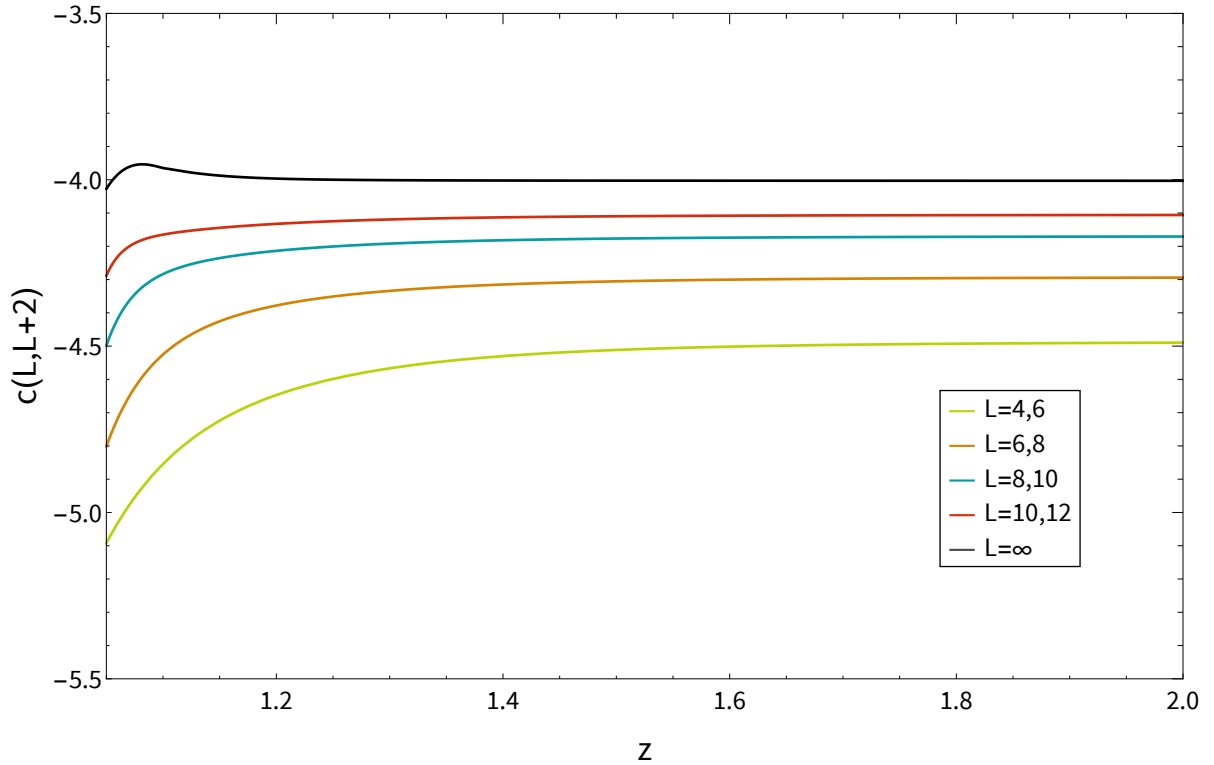


Figure 3.8 – Estimate of the central charge for successive sizes as a function of the fugacity z . Using two sizes L and $L + 2$ at fixed z we obtain an estimate of $c(L, L + 2)$ that converges as L increases. The model seems to have $c = -4$ for all z higher than the critical value z_C . The ground state that we use comes from the sector with zero magnetization. The eigenvalue is exactly the same as for the sector propagating $(2, 2)$ loops.

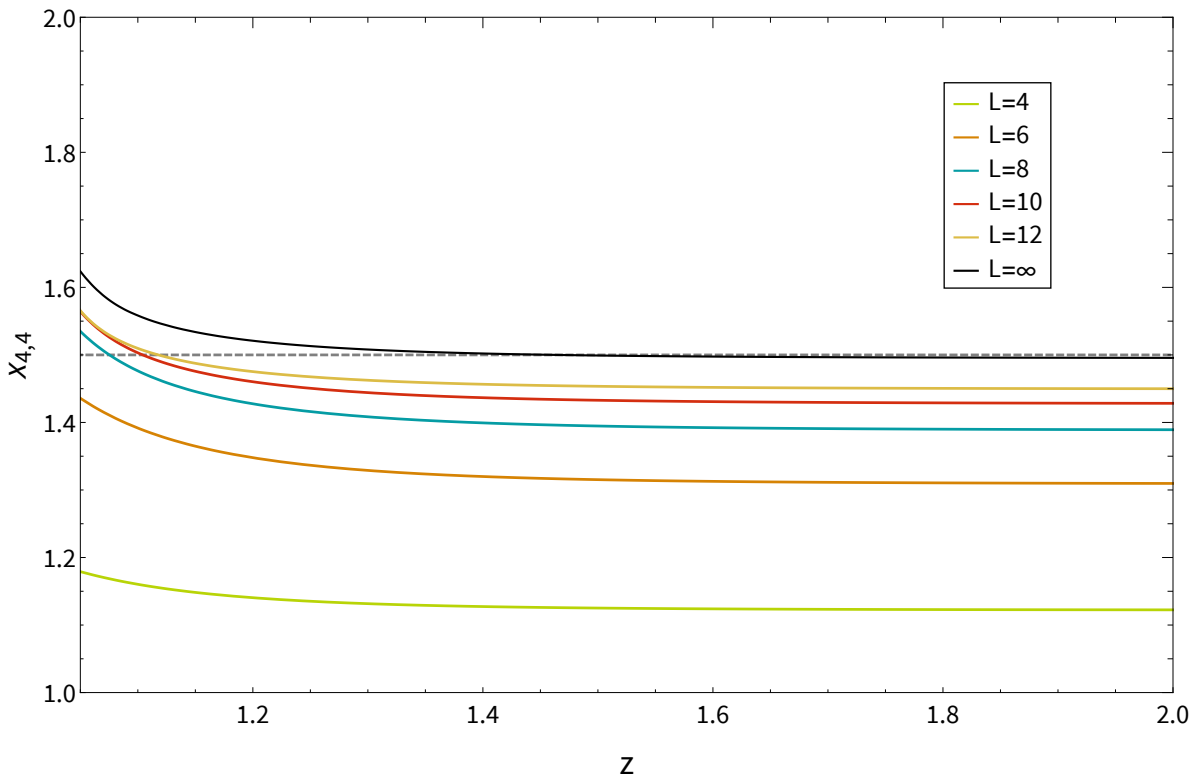


Figure 3.9 – Estimate of the exponent $x_{4,4}$ corresponding to the propagation of $(4, 4)$ through-lines. It converges toward the value $3/2$. The dimension is twice the value expected in the dense polymer model because of the two colours.

3.2.6 Lattice observables in the network model

In this subsection we recall some aspects of the network observables constructed in [126, 127]. Let \mathcal{U} be the discrete-time evolution operator of a single-electronic wave function on the Chalker-Coddington network:

$$\mathcal{U} = \bigotimes_{\text{edge } e} \mathcal{U}_e \bigotimes_{\text{vertex } v} \mathcal{U}_v. \quad (3.59)$$

The observables of [126, 127] are defined by introducing a set of *point-contacts* \mathbf{c}_k , $k = 1, \dots, r$, which amount to cut edges open at which current can enter or exit the system. They are encoded by the projector

$$\mathcal{Q} = \prod_k (1 - |\mathbf{c}_k\rangle\langle\mathbf{c}_k|) = 1 - \sum_{k=1}^r |\mathbf{c}_k\rangle\langle\mathbf{c}_k|, \quad (3.60)$$

such that the stationary wave function (“scattering state”) associated with current injected at the point contact \mathbf{c}_k reads

$$|\psi_{\mathbf{c}_k}\rangle = \mathcal{Q}\mathcal{U}(1 - \mathcal{Q})|\mathbf{c}_k\rangle. \quad (3.61)$$

Let \mathbf{r}_i , $i = 1, \dots, \ell$ be a set of *observation points* lying in the bulk of the system, that is, distinct from the point-contacts. In this framework the observables of Bondesan *et al.* are then defined as

$$\begin{aligned} Z_{1,q} &= \mathbb{E}(|\psi_{\mathbf{c}_k}(\mathbf{r}_1)|^{2q}) \\ Z_{\ell,q} &= \mathbb{E} \left(\left| \begin{array}{ccc} \psi_{\mathbf{c}_1}(\mathbf{r}_1) & \dots & \psi_{\mathbf{c}_1}(\mathbf{r}_\ell) \\ \vdots & & \vdots \\ \psi_{\mathbf{c}_\ell}(\mathbf{r}_1) & \dots & \psi_{\mathbf{c}_\ell}(\mathbf{r}_\ell) \end{array} \right|^{2q} \right), \end{aligned} \quad (3.62)$$

where $\mathbb{E}(\dots)$ is used here to denote the average over disorder.

Following the construction of [126, 127], the observables $Z_{\ell,q}$ are expected to become pure-scaling ones in a continuum limit of the network model which takes the contact and observation regions to single points, namely $\mathbf{c}_k \rightarrow \mathbf{c}$ and $\mathbf{r}_k \rightarrow \mathbf{r}$ while \mathbf{r} and \mathbf{c} remain distinct:

$$Z_{\ell,q} \sim |\mathbf{r} - \mathbf{c}|^{-2X\ell q(\ell-q)}, \quad (3.63)$$

with $X \simeq 1/4$. A particular case is that of $Z_{1,1}$, which is shown to be trivial:

$$Z_{1,1} = 1. \quad (3.64)$$

It is easy to relate these observables to the geometric formulation used in this chapter. Proceeding as in section 3.1.2, the amplitudes $\psi_{\mathbf{c}_k}(\mathbf{r}_i) \equiv \langle \mathbf{r}_i | \psi_{\mathbf{c}_k} \rangle$ can be decomposed as a sum over (advanced) Feynman paths starting at \mathbf{c}_k and ending at \mathbf{r}_i while avoiding all point-contacts,

$$\psi_{\mathbf{c}_k}(\mathbf{r}_i) = \sum_{\omega: \mathbf{c}_k \rightarrow \mathbf{r}_i} W(\omega), \quad (3.65)$$

where the statistical weights $W(\omega)$ collects all phases accumulated by the path ω at the visited edges as well as the weight coming from scattering at vertices. Similarly, the complex conjugate $\psi_{\mathbf{c}_k}(\mathbf{r}_i)^*$ is written as a sum over retarded Feynman paths $\bar{\omega}$ starting at \mathbf{r}_k and ending at \mathbf{c}_k , with weight $W(\bar{\omega})^*$. From there, a geometrical interpretation can be given to the observables (3.62), when $q \equiv n$ is an integer. For instance, let us take the case of only one contact point \mathbf{c} and one observation point \mathbf{r} ,

$$\begin{aligned} Z_{1,n} &= \mathbb{E} (|\psi_{\mathbf{c}}|^{2(q=n)}) \\ &= \sum_{\omega_1, \dots, \omega_n: \mathbf{c} \rightarrow \mathbf{r}} \sum_{\bar{\omega}_1, \dots, \bar{\omega}_n: \mathbf{r} \rightarrow \mathbf{c}} \prod_e \delta \left(\sum_{i=1}^n n_e(\omega_i) - \sum_{i=1}^n n_e(\bar{\omega}_i) \right) \\ &\quad \times W'(\omega_1) \dots W'(\omega_n) W'(\bar{\omega}_1)^* \dots W'(\bar{\omega}_n)^*, \end{aligned} \quad (3.66)$$

where $n_e(\omega)$ is the number of times ω visits the edge e and the weights W' correspond to W with random phases removed. The observable $Z_{1,1}$ for instance is given by a sum over configurations of one advanced (resp. one retarded) path going from \mathbf{r} to \mathbf{c} (resp. from \mathbf{c} to \mathbf{r}) with the constraint that the path never visits the edge \mathbf{c} except at the end (resp. at the beginning). Similarly, for higher values of $q = n$ an integer, we get q paths (in advanced/retarded pairs) relating \mathbf{r} to \mathbf{c} with the constraint that each of these paths visits \mathbf{c} only once.

We note that instead of $Z_{1,q}$, one can also define another observable involving two contact points \mathbf{c}_1 and \mathbf{c}_2

$$\tilde{Z}_{1,q} = \mathbb{E} (|\psi_{\mathbf{c}_1}(\mathbf{c}_2)|^{2q}). \quad (3.67)$$

The geometric interpretation of $\tilde{Z}_{1,q}$ now involves q paths (in advanced /retarded pairs) relating points c_1 and c_2 with the constraint that these paths pass only once through c_1 and c_2 . This is in contrast with $Z_{1,q}$ where c_2 is replaced by an observation point r_2 , where the paths can pass an arbitrary number of times.

It was argued in [122] that the behaviour of $\tilde{Z}_{1,q}$ for $|q| \geq 1/2$ is

$$\tilde{Z}_{1,q} = \Gamma(q)^{-2} \int_0^\infty |\Gamma(q - 1/2 - i\lambda/2)| r^{-2x_\lambda} \mu(\lambda) d\lambda \quad (3.68)$$

with $\mu(\lambda) = \frac{\lambda}{2} \tanh \frac{\pi\lambda}{2}$. Unlike $Z_{1,q}$, this is not a pure-scaling variable. At large distances, for all $q \geq 1/2$ the integral is dominated by the contribution of the same scaling dimension $x_{\lambda=0} = X/4$ corresponding to $p = 0$ and $q = 1/2$ in [126].

In the first truncation, edges can be occupied at most once. Watermelon observables involve ℓ paths (coming in advanced/retarded pairs), and their two-point functions are essentially truncated versions of $Z_{1,q}$ or $\tilde{Z}_{1,q}$ with $q = \ell$ —it is not clear which.¹ Since for watermelons $q \geq 1$, the interpretation in terms of $\tilde{Z}_{1,q}$ would lead to exponents at the bottom of the continuum, while we find the watermelon exponents in the discrete part of the

¹The paths in the watermelon observables start and finish at neighbouring points instead of exactly at the same point, but this does not affect the scaling behaviour.

spectrum, the interpretation in terms of $Z_{1,q}$ seems more natural.² For higher truncations, a difference between contact points and observation points can be introduced in the lattice model: for instance for $Z_{1,1}$ it is possible, for the second and higher truncations, to impose that the paths go only once on the contact-edges, while they can go once or more over the observation edges. This, however, does not seem to make much difference: in all cases, the correlation function is dominated by the $x_{1,1}$ dimension, and we do not know how to build objects corresponding to different $Z_{1,1}$ and $\tilde{Z}_{1,1}$.

3.3 Higher truncations

In the following, the definition of higher truncations is presented. We start with the instructive case $M = 2$ before giving a proper generalisation. Some preliminary numerical results are presented.

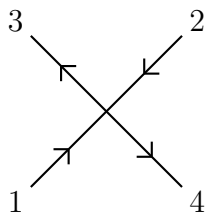
3.3.1 The second truncation

Higher truncations are now discussed with the results of some numerical studies. In the following we use the combination of variables

$$\Gamma_{e_2 \leftarrow e_1}^\sigma = (b_\sigma^*(e_2)b_\sigma(e_1) + f_\sigma^*(e_2)f_\sigma(e_1)) \quad (3.69)$$

where e_2 and e_1 are edges. This term geometrically represents a loop of colour σ going from e_1 to e_2 .

We start with the second truncation $M = 2$. Each edge can carry at most 2 strands of each colour. The partition function is expanded in terms of the functions Γ representing connectivities. The interaction is still the tensor product of individual tiles respecting the constraint of having the same number of strands per colour at every edge. The interaction, at a vertex



$$(3.70)$$

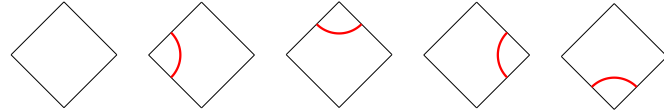
for one colour is

$$e^{S_v^+} = \exp \left(\sum_{j=1,2} \sum_{i=3,4} \mathcal{S}_{i,j} \Gamma_{e_i \leftarrow e_j}^+ \right), \quad (3.71)$$

where i and j refer to the number of the edges in the vertex (3.70). We expand this expression such that only terms with at most 2 strands on each e_i and e_j are kept. The exponential

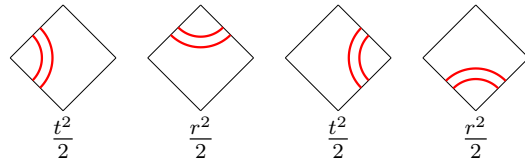
²Note however that the value $x_{1,1} = \frac{1}{4}$ for Z_{11} is precisely at the bottom of the continuum! But this is not the case for higher values of q .

is developed to fourth order in S to get all contributions and all terms are represented by diagrams. First the contribution of order 0 and the four ones of order 1, that also appear in the first truncation, have the weights



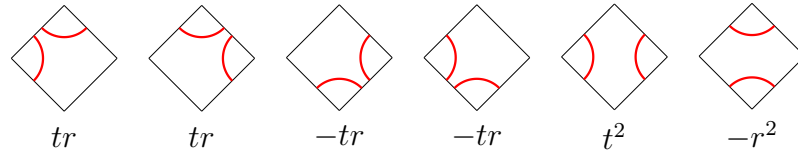
$$1 \quad t \quad -r \quad t \quad r \quad . \quad (3.72)$$

At order 2 are present the tiles where the same path is picked twice in the expansion



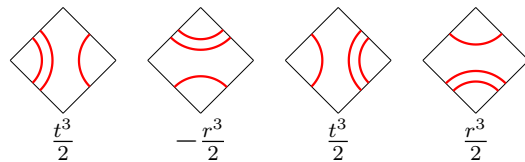
$$\frac{t^2}{2} \quad \frac{r^2}{2} \quad \frac{t^2}{2} \quad \frac{r^2}{2} \quad (3.73)$$

but also the tiles with two distinct paths. They come with an extra factor 2 cancelling the one from the expansion of the exponential function:



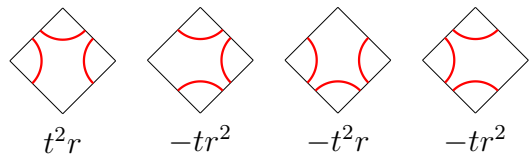
$$tr \quad tr \quad -tr \quad -tr \quad t^2 \quad -r^2 \quad (3.74)$$

At third order in S , there are four contributions with a path picked twice:



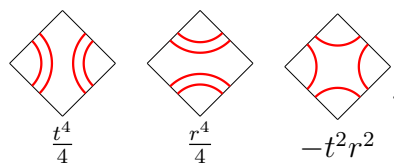
$$\frac{t^3}{2} \quad -\frac{r^3}{2} \quad \frac{t^3}{2} \quad \frac{r^3}{2} \quad (3.75)$$

and four with 3 different paths:



$$t^2r \quad -tr^2 \quad -t^2r \quad -tr^2 \quad (3.76)$$

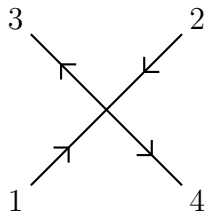
Finally, at fourth order, we find



$$\frac{t^4}{4} \quad \frac{r^4}{4} \quad -t^2r^2 \quad (3.77)$$

3.3.2 Generalisation

The generalisation of the above procedure for all M is obtained as follows. The M -th truncation is obtained by expanding $e^{\mathcal{S}_v}$ using the functions Γ to the order $2M$ in \mathcal{S} . Directly in the loop model, the weight of a tile can be computed in the following way. Denote by k_{ij} the number of strands joining the edge i and j of the following vertex (here the arrows are irrelevant)


(3.82)

The weight w of a loop tile (with one colour) \mathcal{T} is given by

$$w(\mathcal{T}) = \frac{(-1)^{k_{14}}}{k_{13}!k_{14}!k_{23}!k_{24}!} t^{k_{13}+k_{24}} \gamma^{k_{14}+k_{23}}. \quad (3.83)$$

Moreover, gluing two edges together with n strands is done by summing over the $n!$ permutations. The R -matrix of the model is obtained in the end by taking the tensor product of tiles from each colour that have the same number of strands at each edge.

3.3.3 Preliminary numerical results

The full Chalker-Coddington model is critical if z is equal to the special value $z_C = 1$. The modification of the critical parameter to $z_C \sim 1.032$ in the first truncation ($M = 1$) changes the symmetries to $gl(1|1) \otimes gl(1|1)$ instead of the full $gl(2|2)$ algebra. This observation remains true in the higher truncations. For instance in the second truncation ($M = 2$), the critical value of z is approximately $z_C \sim 1.014$ which again breaks the symmetries between the vacuum and the bosons/fermions. We expect that for the full series of truncated models, the critical value of the parameter z stays strictly greater than 1 and converge to 1 for $M \rightarrow \infty$. As a consequence, the symmetry of the Chalker-Coddington model is only recovered in the limit of $M \rightarrow \infty$.

We can then investigate the value of the dimension corresponding to the first excited state in the sector of the vacuum. As observed by Ikhlef et al. [37], the energy of the first excited state corresponds to the sector propagating two strands of each colour. This property remains true for higher truncations. We can track the evolution of its associated critical dimension; see Figure 3.10. While it is hard to carry out the numerics for higher truncations and large size, it looks like the dimension decreases as the level of truncation increases.

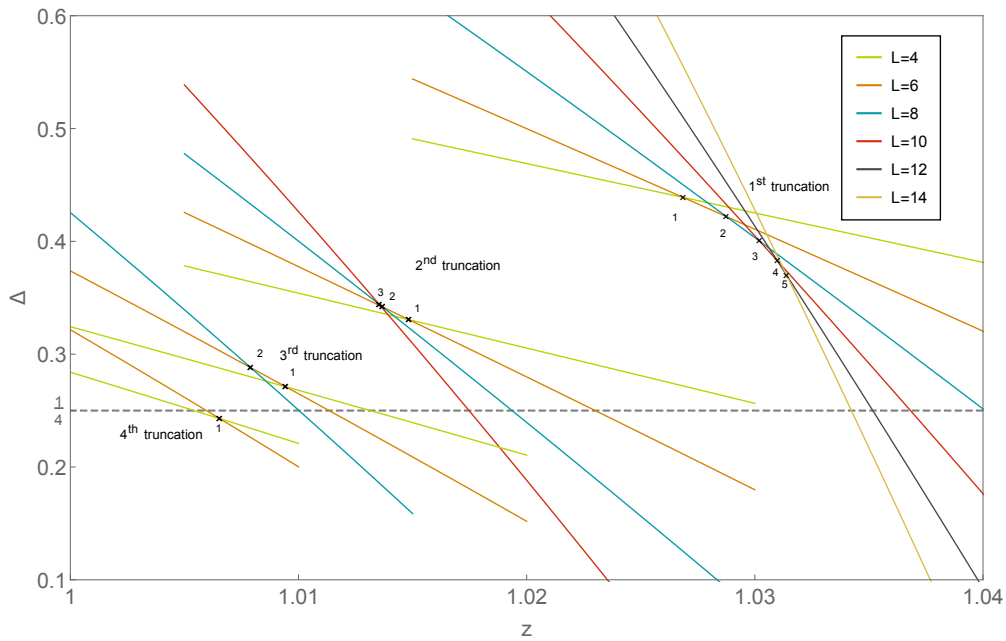


Figure 3.10 – Estimate of dimensions of $x_{2,2}$ as a function of z in the first four truncations with periodic boundary conditions. The dotted line represents the scaling dimension $x_{2,2} = 1/4$, the exact value in the first truncation. The crosses are the intersections between successive sizes and define, via the phenomenological renormalisation scheme, series converging toward the conformal dimensions.

3.4 Truncations of the Brownian motion

In this section, the supersymmetric approach for the Brownian motion is proposed. This model has many properties in common with the Chalker-Coddington model. It is useful to study a different example of this truncation approach to understand qualitatively the connections between a model and its truncations. The transfer matrix and Hamiltonian are written in terms of a boson and a fermion, providing a one-colour version of the model previously discussed.

We recall a couple of classical results. Consider the discrete Laplacian on the square lattice with $\Delta_{ii} = 4$ and $\Delta_{ij} = -1$ if $i \neq j$ are neighbors, 0 otherwise. The expansion for the Green's function is (here m^2 stands for $m^2\text{Id}$)

$$(m^2 - \Delta)_{ij}^{-1} = \sum_{\omega:i \rightarrow j} \left(\frac{1}{4 + m^2} \right)^{|\omega|} \quad (3.84)$$

where the sum runs over all random walks connecting i to j , and $|\omega|$ is the length of the walk - that is, the number of sites visited, each counted with their multiplicity³. There is a similar expansion for the ‘‘partition function’’

$$\frac{1}{\text{Det}(m^2 - \Delta)} = (4 + m^2)^{-\mathcal{N}} \exp \left(\sum_{\underline{\omega}} (4 + m^2)^{-|\underline{\omega}|} \right). \quad (3.85)$$

Here $\underline{\omega}$ denotes configurations of random loops, with the convention that loops equivalent up to a cyclic permutation of their visited sites are counted only once. \mathcal{N} is the total number of sites of the lattice. We see that (3.85) generates a set of possible overlapping and self-intersecting loops somewhat analogous to what one gets in the expansions for the $O(n)$ loop model. Once drawn as a succession of steps (i_k, i_{k+1}) , a loop is counted twice in (3.85) because it can be obtained by clockwise or counterclockwise propagation.

Note that the results (3.84,3.85) do not depend on the topology of the lattice: they hold in particular if the system is on a torus. In this case, loops can be contractible, or wrap around the torus.

A result akin to (3.85) holds for the determinant itself [136]

$$\text{Det}(m^2 - \Delta) = \sum_{\underline{F}} (m^2)^{|\underline{F}|} \quad (3.86)$$

where the sum runs over rooted spanning forests and $|\underline{F}|$ is the number of trees in a particular forest. This expression of the determinant is related, in the following supersymmetric approach, to the fermionic part of the partition function.

We now consider the square lattice, and associate with every vertex i a pair of complex bosonic variables b_i, b_i^* as well as pair of Grassmann variables f_i, f_i^* . Result of Gaussian

³If we think of the walk as a series of steps $(i_1, i_2), (i_2, i_3), \dots (i_{N-1}, i_N)$, the number of times a given i is visited is the number of occurrences of $i_j = i$. A single site i is considered as a walk of length one.

integration gives immediately:

$$\int \prod_i \frac{[db_i^* db_i]}{2\pi} \exp \left[- \sum_{i,j} b_i^* (m^2 \delta_{ij} - \Delta_{ij}) b_j \right] = \frac{1}{\text{Det}(m^2 - \Delta)} \quad (3.87)$$

as well as

$$\int \prod_i [df_i^* df_i] \exp \left[- \sum_{i,j} \bar{f}_i (m^2 \delta_{ij} - \Delta_{ij}) f_j \right] = \text{Det}(m^2 - \Delta) \quad (3.88)$$

The propagator in (3.84) can be obtained as

$$(m^2 - \Delta)_{kl}^{-1} = \frac{\int b_k^* b_l \prod_i \frac{[db_i^* db_i]}{2\pi} \exp \left[- \sum_{i,j} b_i^* (m^2 \delta_{ij} - \Delta_{ij}) b_j \right]}{\int \prod_i \frac{[db_i^* db_i]}{2\pi} \exp \left[- \sum_{i,j} b_i^* (m^2 \delta_{ij} - \Delta_{ij}) b_j \right]} \quad (3.89)$$

Using the fermionic integral, it can also be written without denominators in a ‘‘supersymmetric’’ formulation:

$$(m^2 - \Delta)_{kl}^{-1} = \int b_k^* b_l \prod_i \frac{[db_i^* db_i]}{2\pi} [df_i^* df_i] \exp \left[- \sum_{i,j} b_i^* (m^2 \delta_{ij} - \Delta_{ij}) b_j - \sum_{i,j} f_i^* (m^2 \delta_{ij} - \Delta_{ij}) f_j \right] \quad (3.90)$$

Writing the Boltzmann weight in (3.90) as the exponential of the action e^{-A} , the action in (3.90) is invariant under global $OSP(2/2)$ symmetry, where $OSP(2/2)$ is the group preserving the form $b^* b + f^* f$ [137]. The straightforward continuum limit of the action is

$$A = \int d^2 z [b^* (m^2 - \Delta) b + f^* (m^2 - \Delta) f] \quad (3.91)$$

where now the fields depend on z, \bar{z} and $\Delta = 4\partial\bar{\partial}$. Field theory (3.91) is made of two non-compact bosons and a pair of symplectic fermions. The theory becomes conformal after $m^2 \rightarrow 0$. The corresponding total central charge is $c = 2 - 2 = 0$, as expected since the partition function is equal to unity.

In the following, the quantised supersymmetric description of the Brownian motion is discussed. We show that the oriented Brownian motion is in fact equivalent to a Brownian motion on an un-oriented square lattice. The truncations are discussed, starting with the first one which corresponds to a model of self-avoiding walks. This model is shown to have a symmetry $osp(2|2)$, restored in the continuum limit. Numerical results on higher truncations are presented. There is a strong crossover where critical exponents change with the order of truncation. However higher truncations seem to, at large size, flow ultimately to the universality class of the self-avoiding walks. It is possible to add, in the action of the second truncation, a new interaction such that a multicritical point is reached.

3.4.1 Brownian motion as a supersymmetric spin chain

The partition function of the Brownian system on a square lattice is

$$Z = \int [Db] [Df] \exp \left(\sum_{e_i \rightarrow e_j} b(e_j)^* \mathcal{S}_{e_j, e_i} b(e_i) + f(e_j)^* \mathcal{S}_{e_j, e_i} f(e_i) \right) \quad (3.92)$$

where the matrix \mathcal{S} is

$$\mathcal{S}_S = \begin{pmatrix} T_S & R_S \\ R_S & T_S \end{pmatrix} \quad (3.93)$$

with $S = A, B$ depending on the sublattice. The parameters T_S and R_S , related by $T_S + R_S = 1$, correspond to the probability of a trajectory to turn right or left on the sublattice S . We follow the approach presented in section 3.1.2 and write the second quantisation using bosonic and fermionic oscillators. The transfer matrix acts on $(V \otimes \bar{V})^{\otimes L}$. The space V is the infinite dimensional space with the states

$$|2n+1\rangle = \frac{1}{\sqrt{(n+1)!}} (b^\dagger)^{n+1} |0\rangle \quad (3.94)$$

$$|2n+2\rangle = \frac{1}{\sqrt{n!}} (b^\dagger)^n f^\dagger |0\rangle \quad (3.95)$$

with $n \in \mathbb{N}$ plus $|0\rangle$ the vacuum state. The operators f^\dagger and b^\dagger satisfy the usual commutation relations $[b, b^\dagger] = 1$, $\{f, f^\dagger\} = 1$. The space \bar{V} is its dual with the doublets

$$|\overline{2n+1}\rangle = \frac{1}{\sqrt{(n+1)!}} (\bar{b}^\dagger)^{n+1} |\bar{0}\rangle \quad (3.96)$$

$$|\overline{2n+2}\rangle = \frac{1}{\sqrt{n!}} (\bar{b}^\dagger)^n \bar{f}^\dagger |\bar{0}\rangle \quad (3.97)$$

($n \in \mathbb{N}$) plus $|\bar{0}\rangle$ the vacuum state. The operators \bar{f}^\dagger and \bar{b}^\dagger satisfy the commutation relations $[\bar{b}, \bar{b}^\dagger] = 1$, $\{\bar{f}, \bar{f}^\dagger\} = -1$. The transfer matrix at a node of the sublattice A is the operator $R : V \otimes \bar{V} \rightarrow V \otimes \bar{V}$ encoding the weights of the interaction:

$$R = e^{T_A(b^\dagger \bar{b}^\dagger + f^\dagger \bar{f}^\dagger)} R_A^{b^\dagger b + f^\dagger f + \bar{b}^\dagger \bar{b} - \bar{f}^\dagger \bar{f}} e^{T_A(\bar{b} b + \bar{f} f)}. \quad (3.98)$$

A similar operator is obtained for the sublattice B. Note that the isotropic point is $R_S = T_S = 1/2$.

Hamiltonian: The Hamiltonian is obtained in the anisotropic limit $T_A \rightarrow 0$ with $R_A = 1 - T_A$, $R_B = R_A$ and $T_B = T_A$. The interaction is expanded, the Hamiltonian between two sites H_{node} is defined by

$$R \sim_{T_A \rightarrow 0} 1 - T_A H_{\text{node}} \quad (3.99)$$

where

$$H_{\text{node}} = -b^\dagger \bar{b}^\dagger - f^\dagger \bar{f}^\dagger - \bar{b}b - \bar{f}f + b^\dagger b + f^\dagger f + \bar{b}^\dagger \bar{b} - \bar{f}^\dagger \bar{f} \quad (3.100)$$

hence the full Hamiltonian can be written

$$H = - \sum_i \left[b_i^\dagger b_{i+1}^\dagger + b_i b_{i+1} + f_i^\dagger f_{i+1}^\dagger + f_{i+1} f_i - b_i^\dagger b_i - (-1)^i f_i^\dagger f_i - b_{i+1}^\dagger b_{i+1} - (-1)^{i+1} f_{i+1}^\dagger f_{i+1} \right] \quad (3.101)$$

with $[b_i, b_j^\dagger] = \delta_{i,j}$ and $\{f_i, f_j^\dagger\} = (-1)^i \delta_{i,j}$.

Supersymmetric truncations: The truncation procedure is similar to the Chalker-Coddington case. The M -th truncation is obtained by restricting the on-site spaces V and \bar{V} to states with at most M particles (the $2M + 1$ first ones). A parameter z is introduced to counterbalance the removal of states with a higher particle number.

$$R^{(M)} = (\mathcal{P}_M \otimes \bar{\mathcal{P}}_M) e^{zT_A(b^\dagger \bar{b}^\dagger + f^\dagger \bar{f}^\dagger)} (zR_A)^{b^\dagger b + f^\dagger f + \bar{b}^\dagger \bar{b} - \bar{f}^\dagger \bar{f}} e^{zT_A(\bar{b}b + \bar{f}f)} (\mathcal{P}_M \otimes \bar{\mathcal{P}}_M). \quad (3.102)$$

with \mathcal{P}_M and $\bar{\mathcal{P}}_M$ the projectors over the $2M + 1$ states of V and \bar{V} . The Hamiltonian limit is obtained in the joint limit $T_A \rightarrow 0$, $z \rightarrow 1$. The precise relation between T_A and z on the critical line is unknown. Nevertheless, a formal parametrisation $z(T_A)$ is considered. The Hamiltonian has an additional term

$$H_{\text{node}}^{(M)} = H_{\text{node}} + \alpha_M \left(b^\dagger b + f^\dagger f + \bar{b}^\dagger \bar{b} - \bar{f}^\dagger \bar{f} \right) \quad (3.103)$$

with α_M an unknown amplitude that must be fine-tuned to recover the gapless regime. The contribution H_{node} is given in the above equation (3.100) and the on-site truncation of the Hilbert space is implicit.

3.4.2 Equivalence between oriented/unoriented lattice

In this subsection, the equivalence between a Brownian path on an oriented lattice and on an unoriented lattice is shown at the isotropic point $\mathcal{S}_{e_i, e_j} = \mathcal{S} = 1/2$ if $e_j \rightarrow e_i$. This shows explicitly that the model possesses an $osp(2|2)$ symmetry despite the orientation of the lattice. The bosonic partition function for the Brownian motion on the oriented lattice is

$$Z = \int \left(\prod_e [Db(e)] \right) \exp \left(\sum_{e_i \rightarrow e_j} b^*(e_i) \mathcal{S}_{e_i, e_j} b(e_j) \right). \quad (3.104)$$

where we recall that the integration measure for the complex bosonic variables is

$$\int [Db(e)] (\dots) = \frac{1}{2\pi} \int db(e) db(e)^* e^{-b(e)^* b(e)} (\dots). \quad (3.105)$$

The partition function is first rewritten in terms of bosons at the vertices (and not the edges). Let us consider one vertex v :



Its contribution to the action e^{S_v} is

$$e^{S_v} = e^{\mathcal{S}(b_3^*+b_4^*)(b_1+b_2)} \quad (3.107)$$

where in this equation and the rest of the section, we write b_e to denote the variable $b(e)$ for the sake of lighter notation. It can be rewritten, by introducing a new complex bosonic variable b_v ,

$$e^{S_v} = \int [Db_v] e^{\mathcal{S}(b_3^*+b_4^*)b_v+b_v^*(b_1+b_2)}. \quad (3.108)$$

This identity comes from the following calculation

$$e^{S_v} = \int [Db_v] e^{\mathcal{S}(b_3^*+b_4^*)b_v+b_v^*(b_1+b_2)} \quad (3.109)$$

$$= \frac{1}{\pi} \int db_v db_v^* e^{-b_v^* b_v} \sum_{n,m=0}^{\infty} \frac{\mathcal{S}^n}{n!m!} (b_v^*)^m (b_v)^n (b_3^* + b_4^*)^n (b_1 + b_2)^m \quad (3.110)$$

$$= \sum_{n=0}^{\infty} \frac{\mathcal{S}^n}{(n!)^2} (b_3^* + b_4^*)^n (b_1 + b_2)^n \frac{1}{\pi} \int db_v db_v^* e^{-b_v^* b_v} (b_v^* b_v)^n \quad (3.111)$$

$$= \sum_{n=0}^{\infty} \frac{\mathcal{S}^n}{n!} (b_3^* + b_4^*)^n (b_1 + b_2)^n \quad (3.112)$$

$$= e^{\mathcal{S}(b_3^*+b_4^*)(b_1+b_2)}. \quad (3.113)$$

The next step is to integrate the edge contributions. Let us consider e , an edge going from v_1 to v_2 , its contribution is

$$\int [Db_e] e^{\mathcal{S}b_e^* b_{v_1} + b_{v_2}^* b_e} = e^{\mathcal{S}b_{v_2}^* b_{v_1}}. \quad (3.114)$$

We now integrate over all the variables of one sub-lattice. Consider a vertex

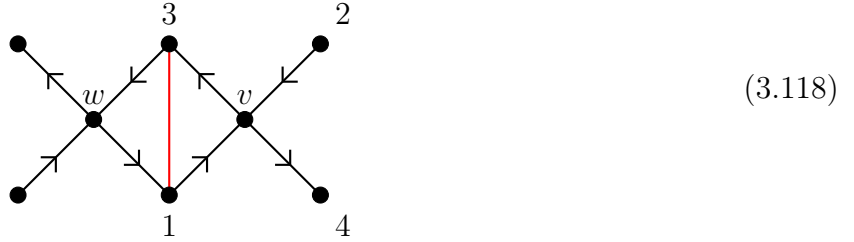


where 1, 2, 3 and 4 are its four neighbour vertices. Integrating over the variable b_v, b_v^* , we get the following contribution:

$$e^{S_v} = \int [Db_v] e^{\mathcal{S}(b_3^*+b_4^*)b_v + \mathcal{S}b_v^*(b_1+b_2)} \quad (3.116)$$

$$= e^{\mathcal{S}^2(b_3^*+b_4^*)(b_1+b_2)}. \quad (3.117)$$

Hence there is an effective interaction $e^{\mathcal{S}^2 b_3^* b_1}$ between the vertices 1 and 3. Similarly the partial integration over the vertex w at the left of 1 and 3



provides an effective interaction $e^{\mathcal{S}^2 b_1^* b_3}$. In the end the partition function can be written over a square lattice (corresponding to a sublattice of the original L lattice).

$$Z = \int \left(\prod_v [Db_v] \right) \exp \left(\sum_{(i,j) \text{ neighbors}} \mathcal{S}^2 (b_i^* b_j + b_j^* b_i) \right) \quad (3.119)$$

where \prod_v is a product over all vertices of the square lattice. The exact same transformation can be done with the supersymmetric partition function. The identity (3.107) holds for its fermionic counterpart:

$$e^{\mathcal{S}(f_3^*+f_4^*)(f_1+f_2)} = \int [Df_v] e^{\mathcal{S}(f_3^*+f_4^*)f_v + f_v^*(f_1+f_2)}. \quad (3.120)$$

Then again, the integration over the odd sub-lattice provides an effective interaction between the vertices of the even sub-lattice. The supersymmetric partition function is

$$Z_{\text{SUSY}} = \int \left(\prod_v [Db_v][Df_v] \right) \exp \left(\sum_{(i,j) \text{ neighbors}} \mathcal{S}^2 (b_i^* b_j + b_j^* b_i + f_i^* f_j + f_j^* f_i) \right) \quad (3.121)$$

Equation (3.119) shows that this model, where loops have a weight 1 on an unoriented lattice with an on-site fugacity \mathcal{S} , is equivalent to a loop model on an un-oriented square lattice, with a loop weight 2 and a monomer fugacity \mathcal{S}^2 . Note that this mapping works only at the isotropic point. A similar correspondence is found in the context of the $O(n)$ model [131] where no exact mapping exists. The Gaussian description of the present model allows us to explicitly show this equivalence.

3.4.3 The first truncation: self-avoiding walks

The transfer matrix of the first truncation is directly obtained from the loop interpretation of the path integral. We follow the procedure described in section 3.3.1 to obtain a loop model. Let us keep the subset of trajectories where each link is visited at most once. As in the Chalker-Coddington truncations, a new parameter z , corresponding to the fugacity of one monomer, is introduced to obtain a critical point. The vertices of the loop model, at the isotropic point, are

$$\begin{array}{ccccccc}
 \text{◇} & \text{◇} & \text{◇} & \text{◇} & \text{◇} & \text{◇} & \text{◇} \\
 & \text{red arc} & \text{red arc} & \text{red arc} & \text{red arc} & \text{red arcs} & \text{red arcs} \\
 1 & z & z & z & z & z^2 & z^2
 \end{array} \tag{3.122}$$

and each closed loop has a weight 0. This model is a particular case of the $O(n)$ model with $n = 0$ [38]. It is expected to be critical for a value $z = z_c$ and in the universality class of self-avoiding walks. Using the transfer matrix formalism, the conformal dimensions of some well-known operators are extracted in finite-size. The smallest gap in the spectrum is used to determine the critical parameter z_c via phenomenological renormalisation. The sequence $\{z_c(L)\}_{L \in 2\mathbb{N}}$ is defined as the series of solutions of

$$\frac{\xi_L(z_c(L))}{L} = \frac{\xi_{L+2}(z_c(L))}{L+2}, \quad \xi_L(z) = -\log \frac{\Lambda_1(z)}{\Lambda_0} \tag{3.123}$$

where ξ_L is the (un-normalized) correlation length of the system of size L , Λ_1 the second largest eigenvalue of the transfer matrix and Λ_0 the largest eigenvalue of the transfer matrix (which is always 1 in the dilute case because of supersymmetry). Two sequences are obtained: $\{z_c(L)\}_{L \in 2\mathbb{N}}$ converging towards z_c and $\{x_1(L, z_c(L))\}_{L \in 2\mathbb{N}}$ with

$$x_1(L, z) = -\frac{1}{2\pi L} \log \Lambda_1(z) \tag{3.124}$$

converging towards the conformal dimension of the 1-leg watermelon operator. The first terms of this sequence are computed numerically, see Figure 3.11. The estimated critical parameter $z_c = 0.5774$ is used to compute other critical exponents. Examples for x_2 and x_3 are also reported Figure 3.11 and are in good agreement with the exact known values of the watermelon dimensions

$$x_\ell = \frac{9\ell^2 - 4}{96}. \tag{3.125}$$

Despite a good agreement with CFT predictions, the finite-size scaling corrections are quite severe. In the case of the integrable point of the $O(n)$ mode, the convergence is much faster. Indeed integrable models have infinitely more conserved quantities and the finite-size corrections are expected to be smaller. Moreover the unknown exact value of the critical parameter z_C makes it harder to obtain precise estimates with small sizes.

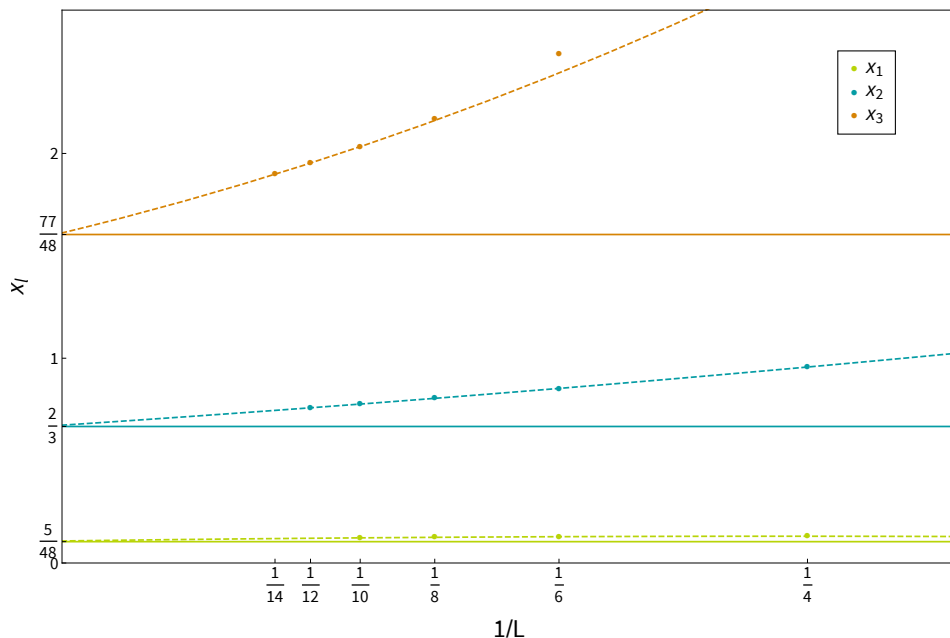


Figure 3.11 – Numerical estimates of the ℓ -leg watermelon exponents for $\ell = 1, 2, 3$ in the case of oriented self-avoiding walks for a periodic system of size L . The exact values are $x_1 = 5/48$, $x_2 = 2/3$ and $x_3 = 77/48$. Our results are in very good agreement with these predictions.

3.4.4 Hamiltonian limit

In this subsection, the Hamiltonian of the first truncation is numerically studied. The two-sites interaction is

$$H_{\text{node}}^{(1)} = H_{\text{node}} + \alpha_1 \left(b^\dagger b + f^\dagger f + \bar{b}^\dagger \bar{b} - \bar{f}^\dagger \bar{f} \right) \quad (3.126)$$

and the boundary conditions are chosen such that $f_{2N+1}^\dagger = (-1)^{N+1} f_1^\dagger$ and $f_{2N+1} = (-1)^{N+1} f_1$. It is gapless for an unknown value $\alpha = \alpha_c$. Because of supersymmetry, at the critical dilute point, the ground state E_0 satisfies exactly $E_0 = 0$. Hence the finite-size corrections formula to the i -th excited state reads

$$E_i = \frac{2\pi v_S}{L} x_i + o\left(\frac{1}{L}\right) \quad (3.127)$$

where X_i is the conformal dimension corresponding to the i -th state (or operator in the state-operator correspondence) and v_S is the velocity of sound. The parameter v_S is first measured and then the spectrum is shown to be corresponding to the $O(n)$ model in the limit $n \rightarrow 0$.

A model with conformal symmetry possesses, in the sector of the identity operator, a state associated with $L_{-1}\mathbb{1}$ with conformal weights $(h, \tilde{h}) = (1, 0)$, thus $x = h + \tilde{h} = 1$. This state can be found by looking at transfer matrix eigenstates with pseudo-momentum ± 1 corresponding to operators with conformal spin $|h - \tilde{h}| = 1$. After having identified the

corresponding state, phenomenological renormalisation is used to obtain estimates of α_c and v_S (see Figure 3.12).

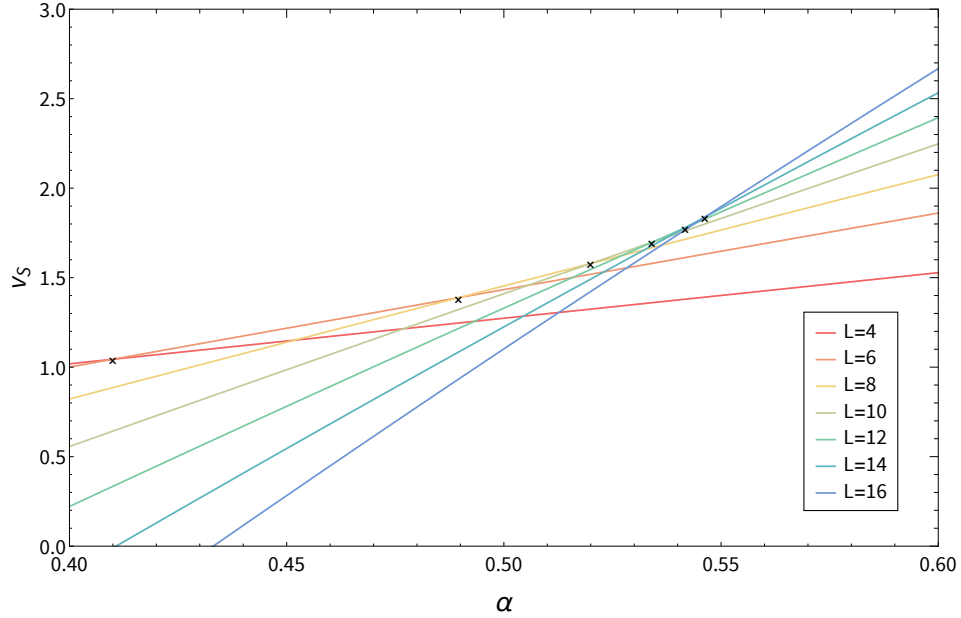


Figure 3.12 – Evolution of $v_S(L, \alpha) = \frac{L}{2\pi} E_1(L, \alpha)$ where $E_1(L, \alpha)$ is the energy of the states corresponding to $(h, \tilde{h}) = (1, 0)$ (at $\alpha = \alpha_c$), in a system of size L . The crossing point, where the estimated v_S does not depend on L , gives estimates of the critical value of α and the sound velocity at that point.

Using a second order polynomial fit as a function of $1/L$, the estimates $v_S \approx 2.213\dots$ and $\alpha_c \approx 0.5577\dots$ are found (see figure 3.12). These values, together with equation (3.127), are useful to compute scaling dimensions. Numerical results are in a very good agreement with the expected dimensions of the self-avoiding walks. Figure 3.13 presents numerical estimates for the watermelon exponents x_ℓ . The 2-leg watermelon operator, corresponding to the propagation of two distinct self-avoiding walks on the cylinder, can be defined in two ways. The two brownian paths can move on sites with the same or distinct parity. This difference is non-trivial since our model is oriented. We thus denote by the subscript e and o if a path is created on an even or odd site. For instance the exponent x_{ee} is the 2-leg watermelon exponent with 2 walks on sites with the same parity and x_{eo} the 2-leg watermelon exponent with 2 walks on sites with different parities. Of course $x_{ee} = x_{oo}$ and $x_{eo} = x_{oe}$.

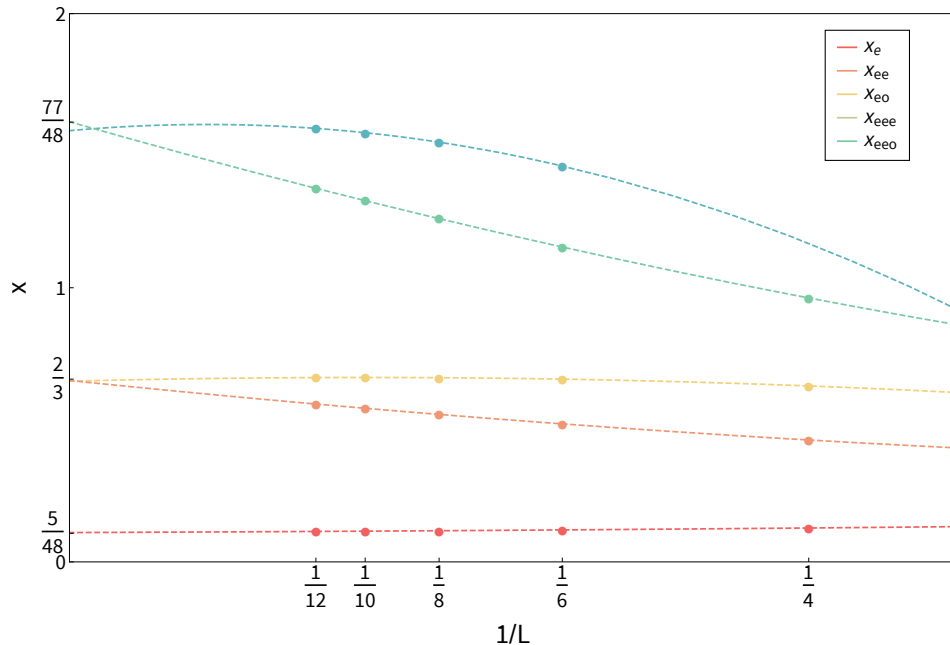


Figure 3.13 – Finite-size scaling of different exponents as a function of $1/L$. Exact values are the expected dimensions of self-avoiding walks. The exponents are obtained in the Hamiltonian formulation of the first truncation with the parameters $v_S \approx 2.213\dots$ and $\alpha_c \approx 0.5577\dots$

3.4.5 Symmetries in the continuum limit

The truncation procedure breaks the $osp(2|2)$ symmetry of the original model down to the $gl(1|1)$ symmetry (the analysis is very similar to what has been done in section 3.2.3 for the Chalker-Coddington model). As a result, the transfer matrix (or equivalently the Hamiltonian) only commutes with $gl(1|1)$. In finite size, the degeneracies of the model are therefore those of $gl(1|1)$: levels occur only with multiplicities 1, 2, 4. Furthermore, we have seen numerically that the critical exponents are those of ordinary self-avoiding walks, which are described by the critical point of the $O(n)$ model for $n = 0$. The value $n = 0$ can be made sense of using a supersymmetric description, where SAWs appear as the critical point of an $OSp(2|2)$ symmetric Φ^4 field theory. On the lattice, the SAW universality class can be obtained with an $osp(2|2)$ spin chain carrying the fundamental, four-dimensional representation on every site. In other words, we find that the critical properties of our $gl(1|1)$ model are the same as those of an $osp(2|2)$ model. In fact, the symmetry is *enhanced* in the continuum limit. We believe that the generating function of (scaled) levels for our $gl(1|1)$ model in the continuum coincides with the generating function of the $osp(2|2)$ spin chain considered in [113]. To define the generating functions we take the transfer matrix or Hamiltonian and calculate the object

$$Z_{gl(1|1)} = \text{Tr } q^{L_0^{(L)}} \bar{q}^{\bar{L}_0^{(L)}} \quad (3.128)$$

where q, \bar{q} are formal parameters, and $L_0^{(L)}$ (resp. $\bar{L}_0^{(L)}$) are the lattice approximations of the L_0, \bar{L}_0 generators, whose eigenvalues are obtained from diagonalization of the Hamiltonian (or logarithm of the transfer matrix) and lattice momentum as in (3.127). Note that we take the trace and not the supertrace. This means that, when decomposing the space onto representations of $gl(1|1)$, the multiplicities will be given by dimensions of the representations (the superdimensions all vanish except for the trivial representation).

The identity with $h = \bar{h} = 0$ comes with multiplicity one in (3.128), as it does in the $osp(2|2)$ model of [113]. The one-leg operator comes with multiplicity $2 + 2 = 4$ due to the degeneracy between the exponents x_e and x_o even in finite size. This is the same multiplicity as in the $osp(2|2)$ model, where it corresponds to the dimension of the fundamental representation. Next, we find that, although the exponents x_{ee} and x_{eo} are different in finite size, they become equal as $L \rightarrow \infty$, as illustrated on figure 3.13. Since each of these exponents comes with a multiplicity 4 in the $gl(1|1)$ model, this means the two-leg operator appear in the spectrum with a degeneracy of 8 in the continuum limit, just like for the $osp(2|2)$ model in [113].

After checking on low-lying levels the emergence of the $osp(2|2)$ spectrum in the continuum limit, we can also give an argument for the symmetry restoration by focussing on large conformal weights instead. It is well known indeed that in a unitary conformal field theory the density of states at high values of the dimension $x = h + \bar{h}$ is related with the central charge through the formula $D(x) \sim \exp(4\pi\sqrt{\frac{cx}{12}})$, a result that follows from modular invariance [3]. In the case of a theory with supergroup symmetry, one has to be a bit careful with this argument. The density of states being obtained by counting with the trace (and not the supertrace), its asymptotic behavior will come from the effective central charge obtained from the ground state energy for a system where loops wrapping around the cylinder will come with fugacity 2 (the dimension of the modules V, \bar{V}). Measurements of this central charge are reported in figure 3.14.

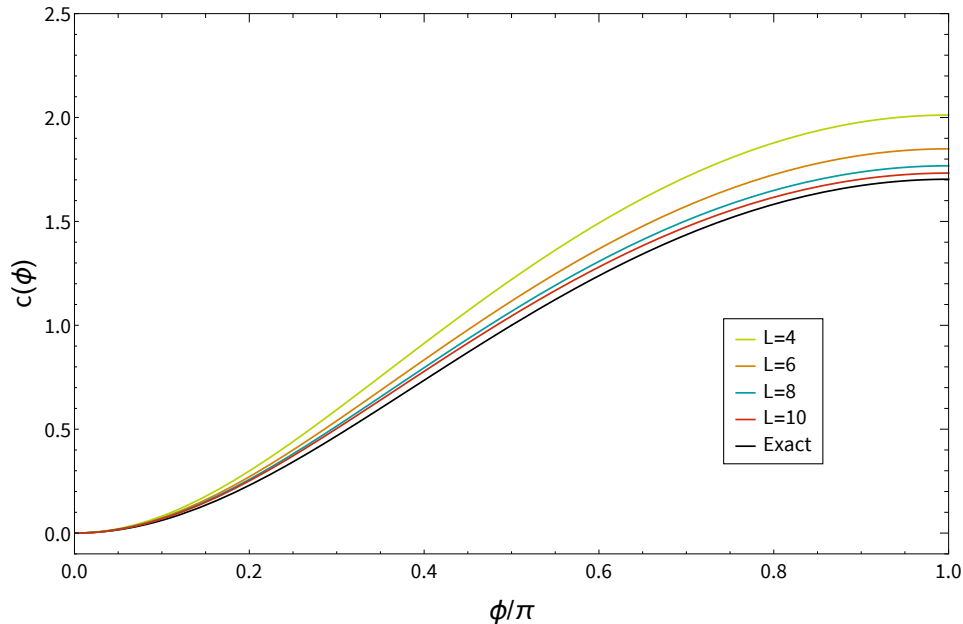


Figure 3.14 – Central charge obtained for the first truncation with twisted boundary conditions. Fermions are twisted by a phase $\exp(\pm i(\phi + \pi))$ depending on the orientation of the edge. Anti-symmetric boundary conditions are obtained at $\phi = \pi$. The graph shows that the extracted value of the central charge corresponds to the one obtained in the $O(n)$ model where non-contractible loops have a fugacity $\tilde{n} = 2 + 2 \cos(\pi + \phi)$. The central charge is given by a Coulomb gas analysis $c(\phi) = 1 + (4/\pi^2) \text{ArcCosh}^2(\tilde{n}(\phi)/2)$. Thus the effective central charge ($\phi = \pi$) is obtained by giving non-contractible loops a weight $\tilde{n} = 4$ in the Coulomb gas analysis. On the oriented lattice, at $\phi = \pi$, non contractible loops have a weight 2. This is again a consequence of the restoration of the $osp(2|2)$ symmetry. The model on the oriented lattice is equivalent to the $O(2n)$ model [131].

They converge to the same value one would get for the $osp(2|2)$ model of [113]. In this model indeed, the asymptotic density of states is controlled by the effective central charge obtained from the ground state energy where non-contractible loops have fugacity 4 - the dimension of the fundamental $osp(2|2)$ representation. This central charge can be calculated using Coulomb gas techniques for a twisted free boson. The coupling constant of this boson is $g = \frac{3}{2}$. For a fugacity $\tilde{n} = 2 \cos \pi e$, the effective central charge will be $c_{\text{eff}} = 1 - \frac{6e^2}{g} = 1 - 4e^2$. We recover $c = 0$ for $\tilde{n} = 0$, the usual fugacity in the $O(n = 0)$ model. Setting $\tilde{n} = 4$ gives

$$c_{\text{eff}} = 1 + \frac{4}{\pi^2} \text{ArcCosh}^2 2 \approx 1.70292 \quad (3.129)$$

The coincidence of the effective central charge in the two models shows their densities of states are identical at large values of the dimension x . Combined with the results in the limit of low dimensions this strongly suggests the two models are in the same universality class.

3.4.6 Higher truncation of the Brownian motion

We believe that the second (and presumably, the higher) truncations is, when unmodified, in the universality class of the first truncation. This is expected if we think of the truncations as some sort of short range repulsion: it is a well known [138] fact that pretty much any kind of repulsion drives random walks into the universality class of ordinary self-avoiding walks (SAWs). This fact can easily be interpreted in the Landau-Ginzburg and ϵ expansion approach. Consider theories with $O(n)$ symmetry and action

$$A = \int d^2x \left[\frac{1}{2} (\partial_\mu \vec{\Phi})^2 + V(\vec{\Phi}^2) \right] \quad (3.130)$$

where $\vec{\phi}$ has n components, and V is an even potential

$$V(\vec{\Phi}^2) = \sum_{p=1}^{k+1} g_p \vec{\Phi}^{2p} \quad (3.131)$$

Following [36], the formal limit $n \rightarrow 0$ in (3.130) provides a description of interacting polymers in dimension D : as seen earlier in this section, the limit can be avoided if one extends the formalism to supergroups. Note that in this description the length of the polymers is not fixed: rather, (3.130) corresponds to a grand canonical ensemble, where lengths are summed over, with the appropriate fugacity for monomers. The Gaussian fixed point ($V = 0$) corresponds to critical random walks: changing the fugacity of monomers corresponds to adding a mass term ($g_2 > 0$ in (3.131)). The Gaussian fixed point is unstable in dimensions $D < 4$. A short range repulsive interaction translates into some potential $V(\vec{\Phi}^2)$, and, for generic coefficients, a critical point is reached when the amplitude of the $\vec{\Phi}^2$ term vanishes. The resulting universality class is determined by the remaining leading $\vec{\Phi}^4$ interaction. For a given order of truncation, the observed exponents will thus eventually converge to those of SAWs as the size of the system is increased.

It is nonetheless also clear that important crossover effects must be expected. After all, the critical untruncated model is described by the free theory. It is thus natural to expect that for a high (but finite) order of truncation, the coefficients of the potential V will be skewed towards the higher powers $\vec{\phi}^{2p}$ for small sizes. In other words, we expect the observed exponents to get closer to those of Brownian motion when the order of truncation is increased at fixed system size. It is not known how the crossover between system size and order of truncation is happening precisely. Nevertheless, it seems reasonable to think of the truncated models as some kind of asymptotic approximation.

For small sizes, we can diagonalise the transfer matrix and look at the gap in the vacuum sector for different levels of truncation. For each level of truncation, using phenomenological renormalisation since we do not know the associated critical parameter z_C (that of course depends on the level of truncation), we obtain a sequence $\{x_{eo}(k, L)\}_{L \in 2\mathbb{N}}$ converging towards the exponent of the k -th truncation. Results can be found in figure 3.15. It seems at first that different truncations belong to different universality classes where x_{eo} corresponds to the Flory exponent $2/(k+2)$. However only very small systems are accessible through exact

diagonalisation. This is due to the very large vector space that we obtain as k increases (the dimension is $(1 + 2k)^L$). Numerical evidence, for other exponents and in a more general setting that will be presented in the next section, suggests that the naive higher levels of truncation are subject to severe finite-size scaling and belong to the universality class of self-avoiding walks.

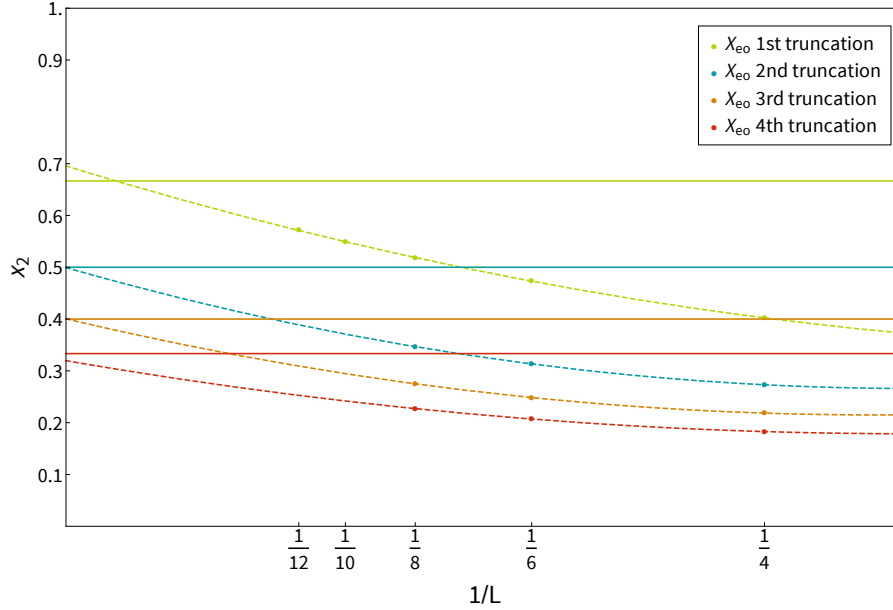


Figure 3.15 – Exponent x_{eo} for different sizes and level of truncations. The exponents seems for small sizes to converge toward the values $x = 2/(k + 2)$ corresponding to the Flory exponents.

3.4.7 The multicritical point of the second truncation

Additional interactions can be introduced in the second truncation. In the original model, an edge with n particles has a weight z^n (with $z = 1/2$ for the critical theory) or equivalently the presence of n particles in a state corresponds simply to a term of the form $e^{-n\epsilon}$ in the action. In the second truncation, we introduce μ , a parameter that changes the fugacity of an edge carrying two particles. A link with zero (resp. one and two) particle has a weight 1 (resp. z and μz^2). For $\mu < 1$, this interaction is a repulsion of two polymers on the same edge whereas, for $\mu > 1$, it corresponds to an attraction. The phase diagram of this model can be investigated numerically and is given Figure 3.16.

High values of z and μ correspond to a critical phase where polymers fill the lattice. The ground state is no longer given by the physical supersymmetric vacuum with $\Lambda_0 = 1$. This phase is described by dense polymers with $c = -2$. For small values of z and μ , the system is in a dilute phase and not critical. In between, there is a critical line of critical dilute polymers. The nature of the critical line can be studied by looking at certain exponents.

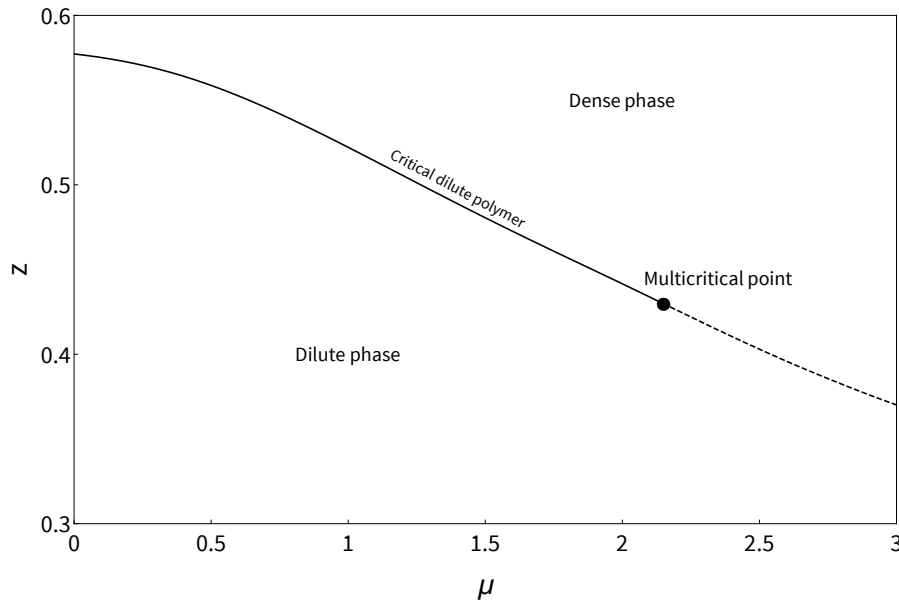


Figure 3.16 – Phase diagram of the second truncation in the (μ, z) plane. The non-critical dilute regime is separated from the dense regime by a critical line. The universality class on this line is the self-avoiding walks except at some particular point corresponding to a multicritical model. The dotted line represents a first order transition.

Let us study the 1-leg watermelon exponent x_1 . It is defined as the ground state of the sector propagating one polymer. In terms of supersymmetric particles, it corresponds to the propagation of one boson or fermion. The exact value for self-avoiding walks is $x_1 = 5/48$. Using again the phenomenological renormalisation procedure, the critical value of z_c and exponent X_1 are extracted for successive sizes. Numerical results obtained with exact diagonalisation of the isotropic row-to-row transfer matrix can be found Figure 3.17.

In the domain $\mu < 1.5$, the evolution of the conformal dimension becomes flatter as the size L increases. Extrapolations are compatible with a value of the conformal dimension near $5/48$ (the dotted straight line). In the range $1.5 < \mu < 2.15$, the convergence is not very good. However the extent of this domain seems to shrink as the system size increases. There is a very peculiar point near $\mu \sim 2.15$ where all curves are crossing. Such a behaviour suggests strongly the existence of a multicritical point. It is known that approaching a multicritical point can lead to important finite-size effects explaining the bad estimates of the critical exponent for $1.5 < \mu < 2.15$. Using three consecutive sizes we can measure the successive crossings:

	$L = 4, 6, 8$	$L = 6, 8, 10$	$L = 8, 10, 12$	$L = \infty$
μ_c	2.15201...	2.166144...	2.167705...	2.15...
x_1	0.126728...	0.128409...	0.128658...	0.127...

(3.132)

Numerical data suggest strongly that $x_1 = 1/8$. Several difficulties are encountered to provide

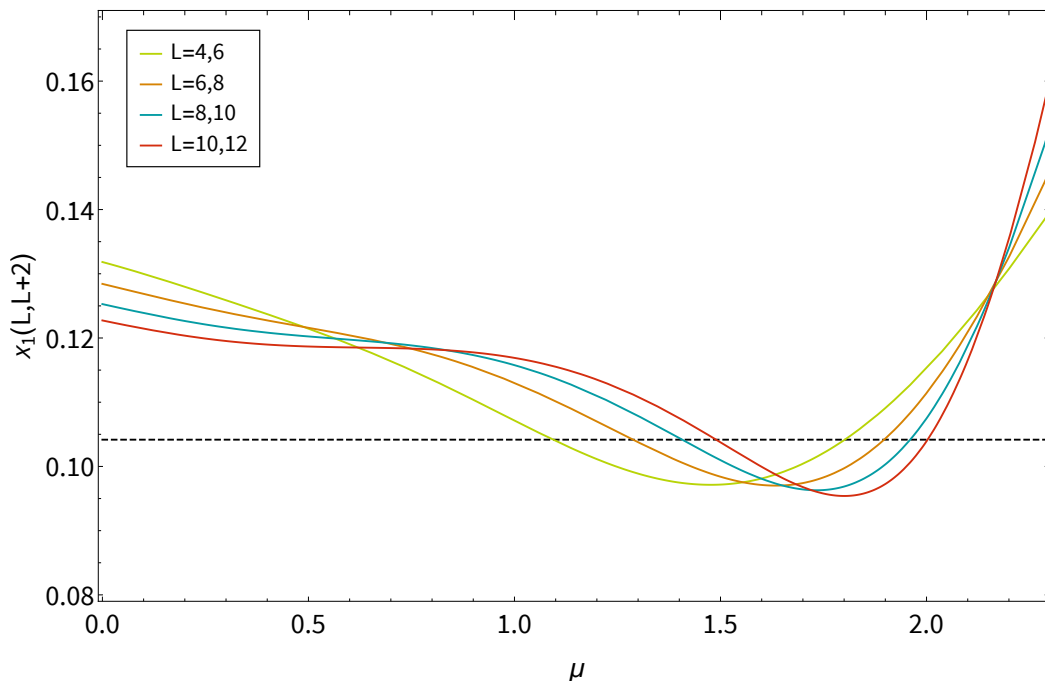


Figure 3.17 – 1-leg watermelon exponents x_e on the critical line. Numerical data are obtained by exact diagonalisation of the transfer matrix in the row-to-row geometry and periodic boundary conditions. Each curve is drawn using two consecutive sizes with phenomenological renormalisation. The $\mu = 0$ point describes usual self-avoiding walks and the successive measured exponents converge toward the black line $x_1 = 5/48$.

better estimates. First, very few sizes are available for exact diagonalisation because of the large Hilbert space of our model (5^L). Moreover, small sizes are severely affected by finite-size effects where quantities are not even monotonic. The multicritical point is localised approximatively at the parameters $(z, \mu) = (0.4287, 2.165)$ and conformal dimensions can be estimated for higher watermelon operators.

	$L = 4$	$L = 6$	$L = 8$	$L = 10$
x_{ee}	0.2863...	0.3027...	0.31286...	0.31583
x_{eo}	0.1583...	0.1455...	0.1399...	...

(3.133)

This table shows the values of the two possible 2-leg watermelon exponents at the multicritical point for small sizes. An important observation is that x_{ee} and x_{eo} do not seem to correspond to the same dimension in the CFT, $x_{ee} \neq x_{eo}$ in the thermodynamic limit, contrary to what we observed the self-avoiding walks. This is problematic since, if this multicritical model is better approximation of the full untruncated theory, then we expect that the symmetry between odd and even sites is restored in the continuum since it is the case for the brownian motion (and the self-avoiding walks).

4 A flow between class A and class C

In the previous chapter, we studied several aspects of the Chalker-Coddington model [12] and its truncations, relevant to the plateau transition in the integer quantum Hall effect. In this section the possibility of having a lattice model describing the flow between two different theories of the quantum Hall effect is discussed. In the Anderson localisation [139], Atland and Zirnbauer identified ten symmetry classes [140] corresponding to distinct sets of random matrices. In these ten classes, several can have a plateau transition in two dimensions and this chapter focusses on two of them. The Chalker-Coddington model is in the class A where disorder is encoded in $U(N)$ matrices ($N = 1$ in this model). The goal of this chapter is to start the study of a renormalisation-group flow between class A and the so-called class C.

The class C describes the physics of the plateau transition in the spin quantum Hall effect mentioned in the first chapter. This transition is very similar to the plateau transition in class A where the charge current is replaced by a spin current. On a lattice, its network model is similar to the Chalker-Coddington model but the wave function has two components: one for each state of a $1/2$ spin (\uparrow, \downarrow). Moreover the disorder comes from random $SU(2)$ matrices [20, 21] instead of the random $U(1)$ phase of class A. In general, class C is characterised by Sp_{2N} matrices that becomes simply $SU(2)$ for $N = 1$.

Class C was found to be related to a well-known phenomena: percolation. In a letter [141], Gruzberg, Ludwig and Read identified several critical exponents of this network model with the ones of percolation thanks to a mapping to an $sl(2|1)$ supersymmetric spin chain. It led to many exact results [23, 142, 143] since many properties (exponents, logarithmic features) of percolation are known. Perturbations around the fixed point of class C have already been studied [144] but here a different approach is proposed. The existence of an RG-flow between class A and class C is interesting from the point of view of field theory because the continuum limit of the Chalker-Coddington model involves non-compact fields whereas percolation has a discrete spectrum. It is tempting to think that, by studying class A as a perturbation of class C, we can learn something about the Chalker-Coddington model.

This chapter starts by a brief review of the class C network model and shows that its form is very close to the Chalker-Coddington model introduced in section 3.1.1. Different approaches to interpolate between the two universality classes are discussed. One of them is chosen because of its simple lattice interpretation and similarities with the truncations introduced in the last chapter 3.3. After discussing the symmetries, we show that our model is defined as a two-colour loop model with a new operator mixing colours. The evolution of the critical exponents ν is studied along the interpolating critical line directly in the network model formulation using Lyapunov exponents. At the end of the chapter, a similar analysis is done for the interpolation between the first truncation of the Chalker-Coddington model and class C.

4.1 Lattice model interpolating between class A and class C

The first task is to find a model interpolating between the two universality classes. We are going to take advantage of their similarities as network models. This section first introduces

the network in class C describing the plateau transition in the spin quantum Hall. Next the second quantisation and its Hamiltonian limit, leading to the $sl(2|1)$ supersymmetric spin chain, are presented. Different options are then discussed to define an interpolating model on the lattice. We choose an approach that interpolates the measure over the disorder such that the correlation functions can reproduce the ones of class A and class C. At the end of this section, the interpretation in terms of a loop model is discussed. In particular our approach leads to a formulation of percolation as a dilute loop model with two colours.

4.1.1 The Spin Quantum Hall Effect as a network model

The network model describing the plateau transition in the spin quantum Hall effect is defined on an oriented lattice exactly as in the Chalker-Coddington model discussed in section 3.1.1. The wave function ψ is discrete and each edge e carries a doublet

$$\psi_e = (\psi_{e,\uparrow}, \psi_{e,\downarrow}) \in \mathbb{C}^2 \quad (4.1)$$

corresponding to the up and down spin states. Time evolution involves two parts. First there is an operator propagating the state along the edges. The class C is characterised by random $SU(2)$ matrices (instead of the simple $U(1)$ phases in the Chalker-Coddington model) hence

$$\begin{pmatrix} \psi'_{e,\uparrow} \\ \psi'_{e,\downarrow} \end{pmatrix} = U \cdot \begin{pmatrix} \psi_{e,\uparrow} \\ \psi_{e,\downarrow} \end{pmatrix}, \quad U \in SU(2) \quad (4.2)$$

which is mixing the up and down components. The natural measure over the $SU(2)$ group is the Haar measure. To be precise, consider a unit vector $\vec{n} \in S^2$, an angle $\alpha \in [0, \pi[$ and the $SU(2)$ matrix defined by $U = \cos \alpha + i \sin \alpha (\vec{\sigma} \cdot \vec{n})$ where $\vec{\sigma} = (\sigma_x, \sigma_y, \sigma_z)$ encodes the Pauli matrices. The Haar measure $\nu_{SU(2)}$ is defined by

$$d\nu_{SU(2)} = \frac{2}{\pi} \sin^2 \alpha \, d\alpha \, d\vec{n}. \quad (4.3)$$

The second part of the time evolution operator corresponds to the scattering of the wave function at vertices. It is now given by two scattering matrices, one for each spin component.

$$S_P = S_{P,\uparrow} \oplus S_{P,\downarrow}, \quad S_{P,\sigma} = \begin{pmatrix} r_{P,\sigma} & t_{P,\sigma} \\ -t_{P,\sigma} & r_{P,\sigma} \end{pmatrix} \quad (4.4)$$

where $P = A, B$ depending whether we consider even or odd sublattices. The amplitudes satisfy $r_{P,\sigma}^2 + t_{P,\sigma}^2 = 1$ and the model is critical when

$$t_{A,\uparrow} = t_{A,\downarrow} = t_{B,\uparrow} = t_{B,\downarrow}. \quad (4.5)$$

The primary object of interest is the Green's function

$$G(e_2, e_1, z) = \langle e_2 | (1 - z\mathcal{U})^{-1} | e_1 \rangle \quad (4.6)$$

that is now a 2×2 matrix since each edge has two channels. The parameter z plays the same role as in the previous chapter, the model is critical for $z = 1$. The Green's function can be expanded in terms of Feynman paths leading to a formulation in terms of Gaussian variables. The process is identical here except that there are now two types of particles: \uparrow and \downarrow . To compute the conductance $|\bar{G}|^2$, we need a priori to introduce advanced and retarded Green's functions. In the end there are twice as many variables as in the Chalker-Coddington case.

At this point, it is important to use a simplification and realise that conductance can be computed in an easier way. The transmission matrix t is

$$t_{\sigma_1, \sigma_2} = \langle e_2, \sigma_2 | (1 - z\mathcal{U})^{-1} | e_1, \sigma_1 \rangle \quad (4.7)$$

and the conductance reads

$$g = \sum_{\sigma_1, \sigma_2} |t_{\sigma_1, \sigma_2}|^2 = \text{Tr}(tt^\dagger) \quad (4.8)$$

Indeed advanced and retarded Green's functions are related by so called particle-hole symmetry and the point conductance is thus

$$g = 2\text{Det}(t). \quad (4.9)$$

This property comes from the evolution operator being a linear combination of $SU(2)$ matrices. It is not the case for the conductance in the Chalker-Coddington model since random matrices are in $U(1)$. Let us now give the path integral description for the spin quantum Hall effect. The supersymmetric method is used and the Green's functions can be expanded in terms of Feynman paths to obtain

$$G(e_2, e_1, z) = \int [Db_{\uparrow, \downarrow}] [Df_{\uparrow, \downarrow}] b_{L, \uparrow}(e_2) b_{L, \uparrow}^*(e_1) b_{L, \downarrow}^*(e_2) b_{L, \downarrow}(e_1) e^{S_{b, \downarrow} + S_{f, \downarrow} + S_{b, \uparrow} + S_{f, \uparrow}} \quad (4.10)$$

where $b_{\bullet, \bullet}$ are usual complex variables and $f_{\bullet, \bullet}$ are complex Grassman variables. Note that this time, to separate explicitly the edge contributions from the vertex contributions, variables with the indice R (resp. L) is associated to the beginning (resp. end) of an oriented edge. The Gaussian measure is

$$\int [Db_{\uparrow, \downarrow}] [Df_{\uparrow, \downarrow}] (\dots) = \int \prod_{\substack{\text{edge } e \\ X \in R, L \\ \sigma \in \{\uparrow, \downarrow\}}} db_{X, \sigma}^*(e) db_{X, \sigma}(e) \frac{1}{2\pi} e^{-b_{X, \sigma}^*(e) b_{X, \sigma}(e)} \prod_{\substack{\text{edge } e \\ X \in R, L \\ \sigma \in \{\uparrow, \downarrow\}}} df_{X, \sigma}^*(e) df_{X, \sigma}(e) e^{-f_{X, \sigma}^*(e) f_{X, \sigma}(e)} \quad (4.11)$$

and the action for bosons

$$S_b = z \sum_{\text{edge } e} \sum_{\sigma_1, \sigma_2} b_{L, \sigma_1}^*(e) (U_e)_{\sigma_1, \sigma_2} b_{R, \sigma_2}(e) + \sum_{\sigma} \sum_{\text{vertex } v} \sum_{j \rightarrow i} b_{R, \sigma}^*(e_i) S_{ij} b_{L, \sigma}(e_j) \quad (4.12)$$

where $\sigma_1, \sigma_2 \in \{\uparrow, \downarrow\}$.

Averaging an edge e over the disorder gives a factor ψ_e^{SQHE} :

$$\begin{aligned} \psi_e^{\text{SQHE}} \equiv & \int_{SU(2)} d\nu_{SU(2)} \exp \left(z \sum_{\sigma_1, \sigma_2} b_{L, \sigma_1}^*(e) (U_e)_{\sigma_1, \sigma_2} b_{R, \sigma_2}(e) \right. \\ & \left. + z \sum_{\sigma_1, \sigma_2} f_{L, \sigma_1}^*(e) (U_e)_{\sigma_1, \sigma_2} f_{R, \sigma_2}(e) \right) \end{aligned} \quad (4.13)$$

The exact computation of this integral shows that only 3 states can propagate on an edge

$$\begin{aligned} \psi_e^{\text{SQHE}} = & 1 + \frac{z^2}{2} (b_{L, \uparrow}^*(e) f_{L, \downarrow}^*(e) - b_{L, \downarrow}^*(e) f_{L, \uparrow}^*(e)) (b_{R, \uparrow}(e) f_{R, \downarrow}(e) - b_{R, \downarrow}(e) f_{R, \uparrow}(e)) \\ & + z^2 f_{L, \uparrow}^*(e) f_{L, \downarrow}^*(e) f_{R, \uparrow}(e) f_{R, \downarrow}(e). \end{aligned} \quad (4.14)$$

In other words, the edge is either not visited, visited by an anti-symmetric pair of boson/fermion or a pair of fermions. This is a very important simplification compared to what has been obtained for the Chalker-Coddington model since there are only a finite number of states on each edge. It corresponds effectively to an on-site truncation of the model.

4.1.2 Second quantisation and the Hamiltonian limit

The quantised description of the model is given by a transfer matrix [25]. Similarly to the Chalker-Coddington model, the node transfer matrix is

$$T_{A, \text{node}} = \prod_{\substack{\sigma=\uparrow, \downarrow \\ a=b, f}} e^{t a_{\sigma}^{\dagger} \bar{a}_{\sigma}^{\dagger} a_{\sigma}^{\dagger} a_{\sigma} + (-1)^{|a|} \bar{a}_{\sigma}^{\dagger} \bar{a}_{\sigma}} e^{-t \bar{a}_{\sigma} a_{\sigma}} \quad (4.15)$$

for the even sublattice A and

$$T_{B, \text{node}} = \prod_{\substack{\sigma=\uparrow, \downarrow \\ a=b, f}} e^{t \bar{a}_{\sigma}^{\dagger} a_{\sigma}^{\dagger} a_{\sigma}^{\dagger} a_{\sigma} + (-1)^{|a|} \bar{a}_{\sigma}^{\dagger} \bar{a}_{\sigma}} e^{-t a_{\sigma} \bar{a}_{\sigma}} \quad (4.16)$$

in the case of the odd sublattice. The operators $b_{\uparrow}, b_{\downarrow}, \bar{b}_{\uparrow}, \bar{b}_{\downarrow}, f_{\uparrow}, f_{\downarrow}, \bar{f}_{\uparrow}, \bar{f}_{\downarrow}$ (plus their Hermitian conjugates) are harmonic oscillators satisfying

$$[b_{\sigma_1}, b_{\sigma_2}^{\dagger}] = \{f_{\sigma_1}, f_{\sigma_2}^{\dagger}\} = [\bar{b}_{\sigma_1}, \bar{b}_{\sigma_2}^{\dagger}] = -\{\bar{f}_{\sigma_1}, \bar{f}_{\sigma_2}^{\dagger}\} = \delta_{\sigma_1, \sigma_2}, \quad \sigma_1, \sigma_2 \in \{\uparrow, \downarrow\}. \quad (4.17)$$

The minus sign in front of the fermions on the odd sublattice is needed to set the weight of closed Feynman paths to zero. This is perfectly analogous to what is done in section 3.1.1. The node transfer matrix encodes the scattering at vertices. The average over the $SU(2)$ disorder is a projector on the following two subspaces

$$V_3 = \left\{ |0\rangle, \frac{1}{\sqrt{2}} \left(b_{\uparrow}^{\dagger} f_{\downarrow}^{\dagger} - f_{\uparrow}^{\dagger} b_{\downarrow}^{\dagger} \right) |0\rangle, f_{\uparrow}^{\dagger} f_{\downarrow}^{\dagger} |0\rangle \right\} \quad (4.18)$$

at an even site and

$$V_{\bar{3}} = \left\{ |0\rangle, \frac{1}{\sqrt{2}} \left(\bar{b}_{\uparrow}^{\dagger} \bar{f}_{\downarrow}^{\dagger} - \bar{f}_{\uparrow}^{\dagger} \bar{b}_{\downarrow}^{\dagger} \right) |0\rangle, \bar{f}_{\uparrow}^{\dagger} \bar{f}_{\downarrow}^{\dagger} |0\rangle \right\} \quad (4.19)$$

at an odd site. The sets V_3 and $V_{\bar{3}}$ correspond respectively to the $sl(2|1)$ fundamental representation and its conjugate. Later in section 4.2.1, the symmetries will be described more precisely. Let us write \mathbb{P}_3 and $\mathbb{P}_{\bar{3}}$ for the projectors on these two spaces. The node transfer matrices $R_{P=A,B}$ that include edge contributions read

$$\begin{aligned} R_A &= (\mathbb{P}_3 \otimes \mathbb{P}_{\bar{3}}) \cdot T_{A, \text{node}} \cdot (\mathbb{P}_3 \otimes \mathbb{P}_{\bar{3}}) \\ R_B &= (\mathbb{P}_{\bar{3}} \otimes \mathbb{P}_3) \cdot T_{B, \text{node}} \cdot (\mathbb{P}_{\bar{3}} \otimes \mathbb{P}_3) \end{aligned} \quad (4.20)$$

They are 9×9 matrices thanks to the on-site truncation, much more convenient than the infinite dimensional ones in class A. The transfer matrix T on a strip of length $2N$ is given by

$$T = \prod_{i=0}^{N-2} R_{B,2i+1} \prod_{i=0}^{N-1} R_{A,2i} \quad (4.21)$$

in the diagonal-to-diagonal geometry. Periodic boundary conditions can also be considered and will be used in later in this chapter. The associated quantum Hamiltonian is obtained by taking the continuum limit of the system in the time direction. We take the anisotropic limit $t \rightarrow 0$. The amplitude r is related to t by $r = \sqrt{1-t^2}$ and in the Hamiltonian \mathcal{H} is defined by

$$T = 1 - t^2 \mathcal{H}_C + o(t^2). \quad (4.22)$$

where

$$\mathcal{H}_C = \sum_{i=0}^{L-2} \left(\sum_{a=1}^4 g_a S_i^a S_{i+1}^a + (-1)^j \sum_{a=5}^8 g_a S_i^a S_{i+1}^a \right) \quad (4.23)$$

with $\{g_a\} = \{2, -2, 1, 1, -2, -2, 2, 2\}$ and

$$S^1 = b_+^\dagger b_+ + b_-^\dagger b_- + 1 \quad S^2 = b_+^\dagger f_+ + f_-^\dagger f_- + 1 \quad (4.24)$$

$$S^3 = 2f_+^\dagger f_-^\dagger \quad S^4 = 2f_+ f_- \quad (4.25)$$

$$S^5 = (b_+^\dagger f_-^\dagger - b_-^\dagger f_+^\dagger) \quad S^6 = (b_+ f_- - b_- f_+) \quad (4.26)$$

$$S^7 = (b_+^\dagger f_+ - b_-^\dagger f_-) \quad S^8 = (b_+ f_+^\dagger - b_- f_-^\dagger) \quad (4.27)$$

4.1.3 Choosing an interpolation

Different approaches are possible in order to obtain a crossover between class A and class C. This section discusses successively different options. The option that we shall choose is motivated by the possibility to use our knowledge about truncations and especially the first truncations of the Chalker-Coddington model.

The first idea is to introduce a uniform Zeeman field in the network model of class C. It would break the global spin-rotation symmetry and split the SQH transition into two class A transitions. This can be done by taking $t_{P,\uparrow} \neq t_{P,\downarrow}$. Two perturbations are introduced, Δ and ϵ , the parameters of the network models are given by

$$\begin{aligned} t_{A,\uparrow} &= t(1 + \epsilon + \Delta), & t_{A,\downarrow} &= t(1 + \epsilon - \Delta) \\ t_{B,\uparrow} &= t(1 - \epsilon + \Delta), & t_{B,\downarrow} &= t(1 - \epsilon - \Delta) \end{aligned} \tag{4.28}$$

with $t = 1/\sqrt{2}$. The parameter Δ is breaking the spin-rotation symmetry by changing the parameters for each spin value in different ways. The parameter ϵ has already been introduced and corresponds to a staggering of the lattice.

A simple perturbation $\Delta \neq 0$, $\epsilon = 0$ is relevant and leads the system to a non-critical phase. Nevertheless it is possible to couple this Δ -perturbation with the ϵ term in a specific way $\epsilon = \pm f(\Delta)$ such that we obtain a crossover with a class A transition [20]. It turns out this approach has a few drawbacks. First the inter-dependence between ϵ and Δ is not known exactly and must be determined numerically such that the system stays critical. Moreover, since we have in mind to use the truncation approach for this problem, it is important to obtain a model as close as possible the Chalker-Coddington model. Here, since the spin-rotation symmetry is broken, we need to introduce advanced and retarded variables of the up and down spin components. This process leads to a description with twice as many variables.

A second option, proposed by Tsai [145], is to work directly in the Hamiltonian language and consider the operator

$$\mathcal{H} = \mathcal{H}_A + g\mathcal{H}_C = \mathcal{H}_A + g\mathbb{P}_{sl(2|1)} \cdot \mathcal{H}_A \cdot \mathbb{P}_{sl(2|1)} \tag{4.29}$$

where $\mathbb{P}_{sl(2|1)}$ is the product of each local projector on the fundamentals of $sl(2|1)$ and g is an amplitude which perturbs the $gl(2|2)$ Hamiltonian with the $sl(2|1)$ Casimir. This approach is more convenient since it interpolates between the two usual Hamiltonians, taking advantage of their similar generators.

In the following, a new approach inspired by this last option is presented. It is very convenient to have the possibility to work either in the Hamiltonian limit or directly in a 2D system. However it is not obvious which 2D transfer matrix corresponds to the Hamiltonian (4.29). The rest of this section focusses on exhibiting a flow between the network models. The resulting Hamiltonian description is discussed later.

Let us first write \uparrow and \downarrow with $+$ and $-$ as indices to emphasise the similarities with the quantity $|G(e_2, e_1, z)|^2$ computed in the last chapter (equation (3.10)) for the Chalker-Coddington model. The physical nature of those indices are very different since in the former case they correspond to the spin components and in the latter case they correspond to advanced and retarded particles. Nevertheless, the correlation functions have exactly the same form given the following change of variables in the Chalker-Coddington correlation functions

$$\Phi : \begin{cases} b_{X,+} \rightarrow b_{X,+} & b_{X,+}^* \rightarrow b_{X,+}^* \\ b_{X,-} \rightarrow b_{X,-}^* & b_{X,-}^* \rightarrow b_{X,-} \\ f_{X,+} \rightarrow f_{X,+} & f_{X,+}^* \rightarrow f_{X,+}^* \\ f_{X,-} \rightarrow f_{X,-}^* & f_{X,-}^* \rightarrow -f_{X,-} \end{cases} \quad (4.30)$$

The only difference comes from the set of random matrices. In other words, replacing the random $SU(2)$ matrices with the Haar measure by diagonal matrices $\text{diag}(e^{i\phi}, e^{-i\phi})$ where ϕ is a uniform random variable in the interval $[0, 2\pi[$, gives exactly the correlation functions of the Chalker-Coddington model. Formally it corresponds to having a measure $\nu_{U(1)}$ such that

$$d\nu_{U(1)} \propto \delta(n_z^2 - 1) d\alpha d\vec{n} \quad (4.31)$$

up to the overall normalisation constant.

If the Haar measure of $SU(2)$ is deformed continuously such that $\nu_{U(1)}$ is obtained then we have a model that describes either the correlation functions in class A or class C. There is no obvious (physical) way to do it thus a linear interpolation between the two measures is chosen for convenience. The measure $d\nu(\mu)$ is defined as the composite measure

$$d\nu(\mu) = (1 - \mu) d\nu_{U(1)} + \mu d\nu_{SU(2)} \quad (4.32)$$

reproducing class A (resp. class C) for $\mu = 0$ (resp. $\mu = 1$). On each edge of the lattice, there is a probability μ of having a $SU(2)$ matrix (drawn from the Haar measure) and a probability $(1 - \mu)$ to have a matrix drawn using $\nu_{U(1)}$. In the gaussian formulation of the model, averaging over disorder leads simply to

$$\psi_e(\mu) \equiv \int_{SU(2)} d\nu(\mu) e^{z \sum_{\sigma_1, \sigma_2} b_{L, \sigma_1}^*(e)(U_e)_{\sigma_1, \sigma_2} b_{R, \sigma_2}(e)} = (1 - \mu) \psi_e^I + \mu \psi_e^S. \quad (4.33)$$

The equation (4.33) shows that on each edge any state can propagate like in the Chalker-Coddington model with a probability $(1 - \mu)$ or there is an on-site truncation to the three $sl(2|1)$ states with probability μ . The node transfer matrix encoding the behaviour of the scattering at vertices is not modified in our description. The equation (4.33) can be directly translated as an operator on every edge in the second quantisation formalism. Each edge carries an operator

$$\mathbb{P}(\mu) = (1 - \mu)\mathbb{I} + \mu\mathbb{P}_3 \quad (4.34)$$

on even sites and

$$\bar{\mathbb{P}}(\mu) = (1 - \mu)\bar{\mathbb{I}} + \mu\bar{\mathbb{P}}_3 \quad (4.35)$$

on odd sites, where \mathbb{I} and $\bar{\mathbb{I}}$ are the projector on the $gl(2|2)$ modules. The transfer matrix is effectively given by

$$T = \prod_{i=0}^{N-2} R_{B, 2i+1}(\mu) \prod_{i=0}^{N-1} R_{A, 2i}(\mu) \quad (4.36)$$

with

$$\begin{aligned} R_A &= (\mathbb{P}(\mu) \otimes \bar{\mathbb{P}}(\mu)) \cdot T_{A, \text{node}} \\ R_B &= (\bar{\mathbb{P}}(\mu) \otimes \mathbb{P}(\mu)) \cdot T_{B, \text{node}} \end{aligned} \quad (4.37)$$

where the action of the projectors can act before and after the node contribution if one takes the square root of the operator $\mathbb{P}(\mu)$. This form is extremely similar to what has been done in the last chapter when the on-site Hilbert space is softly truncated. The Hamiltonian description is obtained by taking an anisotropic limit $t \rightarrow 0$. At order 0 the transfer matrix must become the identity thus the operator $\mathbb{P}(\mu)$ must tend towards the identity. The only non trivial contribution to the Hamiltonian coming from the operators $\mathbb{P}(\mu)$ is a term proportional to the $sl(2|1)$ projector. As a consequence the interpolating model is expected to be described by the following Hamiltonian

$$\mathcal{H} = \mathcal{H}_A + g \left(\sum_{i=0}^{N-1} \mathbb{P}_3^{2i} + \sum_{i=0}^{N-2} \mathbb{P}_3^{2i+1} \right) \quad (4.38)$$

since the vertex contribution is unchanged. This Hamiltonian shares some similarities with (4.29) since it has the same symmetries. The role of the second term is similar because it favors the states in V_3 and $V_{\bar{3}}$.

4.1.4 Loop formulation of the model

On one hand, the Chalker-Coddington model is known to have a loop formulation that we fully described in the last chapter. It is a two-colour dilute loop model with loop fugacity equal to zero. On the other hand, percolation is described by dense loops of fugacity one as discussed in the introductory chapter. The model defined in the last section can be mapped exactly to the Chalker-Coddington model at $\mu = 0$ and percolation at $\mu = 1$. Its description, at any value of μ , in terms of loops is thus interesting. Let us rewrite the edge contribution (4.33) in the gaussian representation:

$$\begin{aligned} \psi_e(\mu) &= 1 + (1 - \mu)z^2 (b_{L,+}^* b_{R,+} + f_{L,+}^* f_{R,+}) (b_{L,-}^* b_{R,-} + f_{L,-}^* f_{R,-}) \\ &\quad + \mu \frac{z^2}{2} (b_{L,+}^* f_{L,-}^* - b_{L,-}^* f_{L,+}^*) (b_{R,+} f_{R,+} - b_{R,-} f_{R,+}) \\ &\quad + \mu z^2 f_{L,+}^* f_{L,-}^* f_{R,-} f_{L,-} + (1 - \mu)(\text{higher states}) \\ &= 1 + \left(1 - \frac{\mu}{2}\right) z^2 (b_{L,+}^* b_{R,+} + f_{L,+}^* f_{R,+}) (b_{L,-}^* b_{R,-} + f_{L,-}^* f_{R,-}) \\ &\quad - \frac{\mu}{2} z^2 (b_{L,+}^* b_{R,-} + f_{L,+}^* f_{R,-}) (b_{L,-}^* b_{R,+} + f_{L,-}^* f_{R,+}) \\ &\quad + (1 - \mu)(\text{higher states}) \end{aligned} \quad (4.39)$$

where (higher states) represents all the states with more than two particles. The first term of (4.39) is the weight associated with an empty edge. The second term takes into account the propagation of a pair of each type $(+, -)$ on an edge. The third one is new, it switches the flavours $(+, -)$ of the pair. Replacing types of particles by colours, the loop interpretation is as follows:

- an empty edge has a weight 1,
- a pair of strands simply propagates with a weight $(1 - \mu/2)$,
- a pair of strands has their colours exchanged with a weight $-\mu/2$
- and more than one pair propagate with a weight $(1 - \mu)$.

For the first truncation, this is represented by the following operator:

$$\text{---}\bullet\text{---} = \text{.....} + \left(1 - \frac{\mu}{2}\right) \text{====} - \frac{\mu}{2} \text{====} \quad (4.40)$$

The following drawing provides an example of a typical configuration.

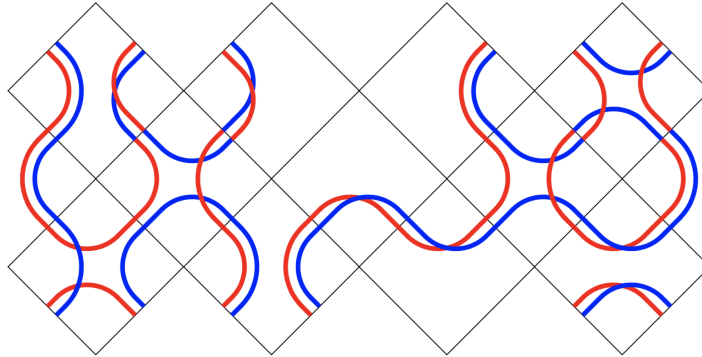


Figure 4.1 – Typical configuration of the interpolating loop model at $\mu > 0$. Edge can carry an arbitrary number of pair of strands but for simplicity here we restricted it to one. Strands can have their colour switched at an edge.

The weight of a closed loop, independently of the number of colours switches along it, is still zero because of supersymmetry.

$$\text{O} = 0 \quad (4.41)$$

Note that it is a highly inefficient way to simulate a percolation system ($\mu = 1$) since the number of configurations is very high. In fact it is somewhat surprising that percolation in this loop representation requires a larger Hilbert space whereas it is much simpler in the supersymmetric formulation.

For higher truncations or the full, untruncated model, the situation is very similar. The operator on the edge is identical to (4.40) for states with a pair of paths and is $(1 - \mu)$ times the identity when there are two or more pair of paths going through the edge. It is interesting to consider the spin quantum Hall case $\mu = 1$ since it should eventually correspond to the percolation loop model [141]. This description provides a surprising formulation of

percolation as a two-colours dilute loop model with vanishing loop fugacity whereas in its usual formulation using the Temperley-Lieb algebra, it is a dense one colour-loop model with loop fugacity one.

In the following, we change the parametrisation of μ and use $\mu \rightarrow 1 - (1 - \mu)^4$. Indeed, we observe that in the vicinity of $\mu = 1$, at least four perturbations must be inserted on the lattice to obtain a non-trivial contribution, otherwise the states out of the 3-dimensional representation of $sl(2|1)$ are annihilated immediately. As a consequence, with the natural parametrisation of μ , all physical quantities have their first three derivatives vanishing at $\mu = 1$. The above parametrisation distributes the interesting crossover region on the whole range $0 < \mu < 1$.

4.1.5 Percolation as a two-colours loop model

In this section, the interpretation of percolation as a two-colours loop model is discussed. For $\mu = 1$, the edge operator is

$$\text{---}\bullet\text{---} = \text{.....} + \frac{1}{2} \begin{array}{c} \text{---} \\ \text{---} \end{array} - \frac{1}{2} \begin{array}{c} \text{---} \\ \text{---} \end{array}. \quad (4.42)$$

An edge is either empty or carries a pair of strands with an antisymmetric exchange of colour. Note that this operator is a projector as expected since it represents the action of \mathbb{P}_3 or $\mathbb{P}_{\bar{3}}$ in the quantised formulation. In the rest of this section, μ is assumed to be equal to 1 and for simplicity the operator $\mathbb{P}(\mu)$ is not drawn on the tiles. For instance the following equation is true

$$\begin{array}{c} \diagup \diagdown \\ \diagdown \diagup \end{array} = \begin{array}{c} \diagup \diagdown \\ \diagdown \diagup \end{array}. \quad (4.43)$$

Each time two tiles are glued together it is important to remember that colours are antisymmetrized. The tiles of the model can be grouped into 3 operators

$$\text{I} = \begin{array}{c} \diagup \diagdown \\ \diagdown \diagup \end{array} + \begin{array}{c} \diagup \diagdown \\ \diagdown \diagup \end{array} + \begin{array}{c} \diagup \diagdown \\ \diagdown \diagup \end{array} + \begin{array}{c} \diagup \diagdown \\ \diagdown \diagup \end{array} \quad (4.44)$$

$$\text{E} = \begin{array}{c} \diagup \diagdown \\ \diagdown \diagup \end{array} + \begin{array}{c} \diagup \diagdown \\ \diagdown \diagup \end{array} + \begin{array}{c} \diagup \diagdown \\ \diagdown \diagup \end{array} + \begin{array}{c} \diagup \diagdown \\ \diagdown \diagup \end{array} \quad (4.45)$$

$$\text{K} = \begin{array}{c} \diagup \diagdown \\ \diagdown \diagup \end{array} + \begin{array}{c} \diagup \diagdown \\ \diagdown \diagup \end{array} + \begin{array}{c} \diagup \diagdown \\ \diagdown \diagup \end{array} + \begin{array}{c} \diagup \diagdown \\ \diagdown \diagup \end{array} \quad (4.46)$$

where I is the identity. The transfer matrix at a node can be written in the following form

$$T_{\text{node}} = r^2 I + t^2 E - t^2 r^2 K \quad (4.47)$$

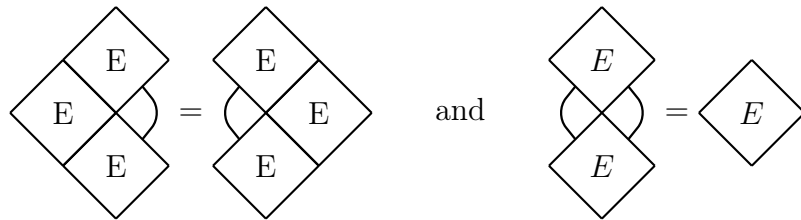
which at the isotropic point simply gives

$$T_{\text{node}} = \frac{1}{2} I + \frac{1}{2} E - \frac{1}{4} K. \quad (4.48)$$

In the anisotropic limit $t \rightarrow 0$, the Hamiltonian H can be computed:

$$H = - \sum_{i=0}^{2N} (E_i - K_i). \quad (4.49)$$

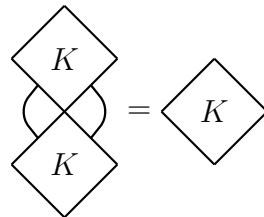
Let us first discuss the nature of the operators E and K . The first operator, as the notation suggests, is a Temperley-Lieb generator. It satisfies in particular the relations



$$(4.50)$$

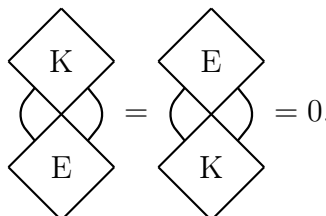
where the black line just acts as the identity. The generators $\{E_i\}$ are thus Temperley-Lieb generators with loop fugacity 1. Notice that this mapping between a dilute loop model with fugacity n and a dense loop model of fugacity $n + 1$ is very similar to what happens with the θ_{DS} point [146]. Empty edges can be interpreted as strands with loop fugacity 1 because of a symmetry between the vacuum and the particles.

Let us now discuss a little bit the nature of the operator K . A quick computation shows that K , like E , is a projector.



$$(4.51)$$

Moreover K and E are orthogonal



$$(4.52)$$

The interpretation of the operators E and K within the $sl(2|1)$ algebra can be studied in the alternated spin chain (4.21). In this representation, it can be computed that K, acting on $V_3 \otimes V_{\bar{3}}$, is exactly $K = 0$. Indeed the Hilbert space is

$$\mathcal{H} = (V_3 \otimes V_{\bar{3}})^{\otimes N} \quad (4.53)$$

and the tensor product of the fundamental representation of $sl(2|1)$ with its conjugate is

$$V_3 \otimes V_{\bar{3}} = \{0\} \oplus \{0, 1\}. \quad (4.54)$$

The Temperley-Lieb generator is known to project on the singlet state of the tensor product. It is not surprising to find that $K = 0$ since, in the tensor product (4.54), there are not much room for a projector on another $sl(2|1)$ representation. Thus the Hamiltonian (4.53) is effectively reduced to the well-known form

$$H = - \sum_{i=0}^{2N} E_i. \quad (4.55)$$

Obviously the action of K is no trivial in terms of loops. The spectrum of the loop model can be computed exactly in finite-size and compared with the $sl(2|1)$ alternated spin chain. The spectrum of the supersymmetric spin chain is found to be included in the spectrum of the loop model. However there are additional eigenvalues in the loop transfer matrix that are related to the non-trivial action of K in terms of connectivities.

The rest of this section does not aim at providing an exhaustive study of the role of K. However we show that the additional spectrum and role of K can be understood in terms of higher representations of $sl(2|1)$. The idea is to change the quantisation scheme of the loop model and associate more types of particle to an edge. In the fundamental $sl(2|1)$ representation we have on even sites the states

$$\{|0\rangle, \epsilon^{\sigma_1, \sigma_2} a_{\sigma_1}^\dagger b_{\sigma_2}^\dagger |0\rangle \quad a, b = f, b\} \quad (4.56)$$

where $\epsilon^{\sigma_1, \sigma_2}$ is the anti-symmetric tensor. A possibility is to double the number of particles on an edge. Two types of bosons and fermions are introduced b^1, b^2, f^1, f^2 with the usual commutation relations. The antisymmetrization of the colours reduces the $1 + 4 \times 4 = 17$ dimensional vector space to a space V_9 of dimension 9 with the states

$$\begin{aligned} |0\rangle &= |\text{vacuum}\rangle \\ |1\rangle &= f_+^{1\dagger} f_-^{1\dagger} |0\rangle & |2\rangle &= \frac{1}{\sqrt{2}} \left(f_+^{1\dagger} f_-^{2\dagger} + f_+^{2\dagger} f_-^{1\dagger} \right) |0\rangle \\ |3\rangle &= f_+^{2\dagger} f_-^{2\dagger} |0\rangle & |4\rangle &= \frac{1}{\sqrt{2}} \left(b_+^{1\dagger} b_-^{2\dagger} - b_+^{2\dagger} b_-^{1\dagger} \right) |0\rangle \\ |5\rangle &= \frac{1}{\sqrt{2}} \left(b_+^{1\dagger} f_-^{1\dagger} - f_+^{1\dagger} b_-^{1\dagger} \right) |0\rangle & |6\rangle &= \frac{1}{\sqrt{2}} \left(b_+^{1\dagger} f_-^{2\dagger} - f_+^{2\dagger} b_-^{1\dagger} \right) |0\rangle \\ |7\rangle &= \frac{1}{\sqrt{2}} \left(b_+^{2\dagger} f_-^{1\dagger} - f_+^{1\dagger} b_-^{2\dagger} \right) |0\rangle & |8\rangle &= \frac{1}{\sqrt{2}} \left(b_+^{2\dagger} f_-^{2\dagger} - f_+^{2\dagger} b_-^{2\dagger} \right) |0\rangle \end{aligned}$$

Similarly on odd sites ($\{\bar{f}_\sigma, \bar{f}_\sigma^\dagger\} = -1$), the vector space $V_{\bar{9}}$ is:

$$\begin{aligned}
|\bar{0}\rangle &= |\text{vacuum}\rangle \\
|\bar{1}\rangle &= f_+^{1\dagger} f_-^{1\dagger} |0\rangle & |\bar{2}\rangle &= \frac{1}{\sqrt{2}} \left(\bar{f}_+^{1\dagger} \bar{f}_-^{2\dagger} + \bar{f}_+^{2\dagger} \bar{f}_-^{1\dagger} \right) |0\rangle \\
|\bar{3}\rangle &= \bar{f}_+^{2\dagger} \bar{f}_-^{2\dagger} |0\rangle & |\bar{4}\rangle &= \frac{1}{\sqrt{2}} \left(\bar{b}_+^{1\dagger} \bar{b}_-^{2\dagger} - \bar{b}_+^{2\dagger} \bar{b}_-^{1\dagger} \right) |0\rangle \\
|\bar{5}\rangle &= \frac{1}{\sqrt{2}} \left(\bar{b}_+^{1\dagger} \bar{f}_-^{1\dagger} - \bar{f}_+^{1\dagger} \bar{b}_-^{1\dagger} \right) |0\rangle & |\bar{6}\rangle &= \frac{1}{\sqrt{2}} \left(\bar{b}_+^{1\dagger} \bar{f}_-^{2\dagger} - \bar{f}_+^{2\dagger} \bar{b}_-^{1\dagger} \right) |0\rangle \\
|\bar{7}\rangle &= \frac{1}{\sqrt{2}} \left(\bar{b}_+^{2\dagger} \bar{f}_-^{1\dagger} - \bar{f}_+^{1\dagger} \bar{b}_-^{2\dagger} \right) |0\rangle & |\bar{8}\rangle &= \frac{1}{\sqrt{2}} \left(\bar{b}_+^{2\dagger} \bar{f}_-^{2\dagger} - \bar{f}_+^{2\dagger} \bar{b}_-^{2\dagger} \right) |0\rangle.
\end{aligned}$$

The following operators B , Q^z , Q^+ , Q^- , V^+ , V^- , W^+ , W^- satisfy the (anti)commutation relations of $sl(2|1)$.

$$\begin{aligned}
B &= \frac{n_{b^1} - n_{b^2}}{2} & Q^3 &= \frac{n_{f^1} - n_{f^2}}{2} \\
Q^- &= f_\sigma^{2\dagger} f_\sigma^1 & Q^+ &= f_\sigma^{1\dagger} f_\sigma^2 \\
V^+ &= \frac{1}{\sqrt{2}} \left(\alpha b_\sigma^{1\dagger} f_\sigma^2 + f_\sigma^{1\dagger} b_\sigma^2 \right) & V^- &= \frac{1}{\sqrt{2}} \left(-b_\sigma^{1\dagger} f_\sigma^1 + f_\sigma^{2\dagger} b_\sigma^2 \right) \\
W^+ &= \frac{1}{\sqrt{2}} \left(f_\sigma^{1\dagger} b_\sigma^1 + b_\sigma^{2\dagger} f_\sigma^2 \right) & W^- &= \frac{1}{\sqrt{2}} \left(f_\sigma^{2\dagger} b_\sigma^1 - b_\sigma^{2\dagger} f_\sigma^1 \right)
\end{aligned}$$

where the summation over the colours (+ and -) is implicit. For instance:

$$f_\sigma^{2\dagger} f_\sigma^1 \equiv f_+^{2\dagger} f_+^1 + f_-^{2\dagger} f_-^1 \quad (4.57)$$

The quantities α , β , and b are free parameters. Changing the values of α and β leads to an equivalent representation of $sl(2|1)$. The generators are also defined on odd sites

$$\begin{aligned}
\bar{B} &= -\frac{n_{\bar{b}^1} - n_{\bar{b}^2}}{2} & \bar{Q}^3 &= -\frac{n_{\bar{f}^1} - n_{\bar{f}^2}}{2} \\
\bar{Q}^- &= \bar{f}_\sigma^{1\dagger} \bar{f}_\sigma^2 & \bar{Q}^+ &= \bar{f}_\sigma^{2\dagger} \bar{f}_\sigma^1 \\
\bar{V}^+ &= -\frac{1}{\sqrt{2}} \left(\bar{f}_\sigma^{2\dagger} \bar{b}_\sigma^1 + \bar{b}_\sigma^{2\dagger} \bar{f}_\sigma^1 \right) & \bar{V}^- &= \frac{1}{\sqrt{2}} \left(\bar{f}_\sigma^{1\dagger} \bar{b}_\sigma^1 - \frac{1-b}{2\beta} \bar{b}_\sigma^{2\dagger} \bar{f}_\sigma^2 \right) \\
\bar{W}^+ &= -\frac{1}{\sqrt{2}} \left(\bar{b}_\sigma^{1\dagger} \bar{f}_\sigma^1 + \beta \bar{f}_\sigma^{2\dagger} \bar{b}_\sigma^2 \right) & \bar{W}^- &= \frac{1}{\sqrt{2}} \left(-\bar{b}_\sigma^{1\dagger} \bar{f}_\sigma^2 + \beta \bar{f}_\sigma^{1\dagger} \bar{b}_\sigma^2 \right)
\end{aligned}$$

The on-site vector space is the direct sum of the trivial representation (the vacuum) and the typical irreducible representation $\{0, 1\}$: $V = \mathbf{1} \oplus \{0, 1\}$ In the following the notation used for representation of $sl(2|1)$ is taken from [147]. The transfer matrix at a node is acting on

the tensor product $V \otimes V^*$. From the representation theory of $sl(2|1)$ the decomposition is found to be

$$V_{\mathfrak{g}} \otimes V_{\mathfrak{g}} = \mathbf{1} \oplus \{0, 1\} \oplus \{0, 1\} \oplus \{0, 1\} \otimes \{0, 1\} \quad (4.58)$$

where we have, for general representations $\{b, 1\}$ $\{-b, 1\}$:

$$\{b, 1\} \otimes \{-b, 1\} = \{0, 2\} \oplus \{0, 1\} \oplus \{0, 1\} \oplus \left\{ \frac{1}{2}, \frac{3}{2} \right\} \oplus \left\{ -\frac{1}{2}, \frac{3}{2} \right\} \oplus \left\{ 0, -\frac{1}{2}, \frac{1}{2}, 0 \right\} \quad (4.59)$$

involving a not fully reducible nontypical representation. The operator E corresponding to a Temperley-Lieb generator is still a projector over a singlet state. The operator K is a projector on a space of dimension 48. Numerical analysis shows that it projects a state on the representation:

$$\{0, 2\} \oplus \{0, 1\} \oplus \left\{ \frac{1}{2}, \frac{3}{2} \right\} \oplus \left\{ -\frac{1}{2}, \frac{3}{2} \right\} \quad (4.60)$$

Because of the previous interpretation of the operators E and K as projectors over subrepresentations, it is clear that the transfer matrix at one node (4.47) preserves the $sl(2|1)$ -symmetry. If J is a generator defined above and \bar{J} its dual counterpart:

$$[J + \bar{J}, T_{\text{node}}] = 0 \quad (4.61)$$

This supersymmetric model reproduces indeed some of the additional eigenvalues of the loop transfer matrix. They could be related to eigenvalues with certain inner symmetries between strands in the loop model. A similar construction is studied in a different context chapter 5 for the Potts model where observables acting on N clusters are classified in terms of representation of the symmetric group with N elements.

4.2 The untruncated model

This section discusses the nature of the lattice model in the untruncated case. Because of the edge operator $\mathbb{P}(\mu)$ ((4.34),(4.35)), the vector space is effectively infinite-dimensional except at $\mu = 1$ where only 3 states per edge survive. As a consequence, we cannot rely on exact diagonalisation or DMRG techniques. Instead we use directly the network model and extract Lyapunov exponents. Before doing so, the symmetries along the interpolating line ($0 \leq \mu \leq 1$) are first discussed. Then evidence of a flow towards class C is given and discussed.

4.2.1 Symmetries

Let us start the discussion by summarising the symmetry algebra at each end of the critical line. For the Chalker-Coddington model at $\mu = 0$, as discussed more extensively in section 3.2.3, the model has a $gl(2|2)$ symmetry. The generators are encoded in the following matrix

$$J = \begin{pmatrix} b_+ b_+^\dagger - \frac{1}{2} & b_+ f_+^\dagger & b_+ b_- & b_+ f_- \\ f_+ b_+^\dagger & f_+ f_+^\dagger - \frac{1}{2} & f_+ b_- & f_+ f_- \\ -b_-^\dagger b_+^\dagger & -b_-^\dagger f_+^\dagger & -b_- b_-^\dagger - \frac{1}{2} & -b_-^\dagger f_- \\ f_-^\dagger b_+^\dagger & f_-^\dagger f_+^\dagger & f_-^\dagger b_- & f_- f_-^\dagger - \frac{1}{2} \end{pmatrix}. \quad (4.62)$$

for even sites. There are four conserved quantities, one for each particle type. In the network model, the randomness is introduced by the U(1) phases or equivalently, as explained previously, by matrices U_e of the form

$$U_e = \begin{pmatrix} e^{i\phi_e} & 0 \\ 0 & e^{-i\phi_e} \end{pmatrix} \quad (4.63)$$

where the first channel corresponds to advanced particles and the second one to retarded particles. On the other hand, at the Spin Quantum Hall end ($\mu = 1$), the transfer matrix has additional projectors on all edges. Hence only the generators (3.48) that commute with the projector \mathbb{P}_3 are going to be symmetries of the model. For even sites the generators are

$$B = \frac{1}{2} (b_+^\dagger b_+ + b_-^\dagger b_- + 1) \quad Q^z = \frac{1}{2} (f_+^\dagger f_+ + f_-^\dagger f_- - 1) \quad (4.64)$$

$$Q^+ = f_+^\dagger f_-^\dagger \quad Q^- = f_- f_+ \quad (4.65)$$

$$V^+ = \frac{1}{\sqrt{2}} (b_+^\dagger f_-^\dagger - b_-^\dagger f_+^\dagger) \quad W^- = (V^+)^\dagger \quad (4.66)$$

$$V^- = -\frac{1}{\sqrt{2}} (b_+^\dagger f_+^\dagger + b_-^\dagger f_-^\dagger) \quad W^+ = -(V^-)^\dagger \quad (4.67)$$

and they are of course linear combination of the $gl(2|2)$ ones. In other words, the $sl(2|1)$ symmetry is a subalgebra of $gl(2|2)$. The bosonic generators satisfy

$$[B, Q^3] = 0, \quad (4.68)$$

$$[B, Q^\pm] = 0, \quad (4.69)$$

$$[Q^+, Q^-] = 2Q^z, \quad (4.70)$$

$$[Q^z, Q^\pm] = \pm Q^\pm, \quad (4.71)$$

the fermionic generators have the following anti-commutation relations

$$\{V^+, V^-\} = \{W^+, W^-\} = 0 \quad (4.72)$$

$$\{V^\pm, W^\pm\} = \pm Q^\pm \quad (4.73)$$

$$\{V^\pm, W^\mp\} = \pm B - Q^z \quad (4.74)$$

and finally

$$[Q^z, V^\pm] = \pm \frac{1}{2} V^\pm \quad (4.75)$$

$$[Q^z, W^\pm] = \pm \frac{1}{2} W^\pm \quad (4.76)$$

$$[Q^\pm, V^\pm] = [Q^\pm, W^\pm] = 0 \quad (4.77)$$

$$[Q^\pm, V^\mp] = V^\pm \quad (4.78)$$

$$[Q^\pm, W^\mp] = W^\pm \quad (4.79)$$

. In principle the $gl(2|2)$ module can even be decomposed over $sl(2|1)$ representations:

$$V = \left\{ \frac{1}{2} \right\}_+ \oplus \left\{ \frac{1}{2}, \frac{1}{2} \right\} \oplus \left\{ \frac{3}{2}, \frac{1}{2} \right\} \oplus \dots \quad (4.80)$$

For generic μ , the generators of the symmetry have to commute with

$$\mathbb{P}(\mu) = (1 - \mu)\mathbb{P}_{gl(2|2)} + \mu\mathbb{P}_3. \quad (4.81)$$

The generators of $sl(2|1)$ still commute with the transfer matrix thus this symmetry is never broken. This also can be understood from the point of view of the network model. In principle, the universality class can change with the set of random matrices. For any value of μ , the matrices are always in $SU(2)$. Even at the Chalker-Coddington point the matrix (4.63) is in $SU(2)$ but only a small subset of this group is covered by the measure (only diagonal matrices). Therefore at the point $\mu = 0$, class C is not expected to describe the behaviour of the model. It is natural to expect the following behaviour.

$$\begin{array}{ccc} \text{IQHE} & \longrightarrow & \text{SQHE} \\ \bullet & & \bullet \\ \mu = 0 & & \mu = 1 \end{array} \quad (4.82)$$

4.2.2 Lyapunov exponents

Because of the infinite-dimensional Hilbert space at generic values of μ , it is not possible to use exact diagonalisation or other methods to study numerically the model. The only possible simulation is to use the random network model and Lyapunov exponents. In this section, numerical simulations are presented and estimate of the exponents ν along the critical line is given.

In the network model, a transfer matrix is a random object and average over disorder is done by taking a very long system. The widths considered are $2N = 4, 8, 16, 32, 64$. Given

a collection of random transfer matrices $\{T_i, i = 1, \dots, L\}$ where L is typically of order $L = 10^7 - 10^8$, two quantities are defined

$$T = \prod_{i=1}^L T_i, \quad \Omega = \log(T^\dagger T). \quad (4.83)$$

The matrix T is the transfer matrix on the full cylinder and Ω is a Hermitian matrix with pairs of eigenvalues $\{\lambda_1, \dots, \lambda_N, -\lambda_N, \dots, \lambda_1\}$. The smallest positive Lyapunov exponent is denoted γ and defined as the quantity

$$\gamma = \lim_{L \rightarrow \infty} \frac{\lambda_N}{2L} \quad (4.84)$$

which converges for large values of system length. In practice, this quantity cannot be computed directly because of a loss of precision due to round-off error. In order to properly simulate the system, it must be decomposed in small slices using QR-factorisations. This section does not enter into the detail of the numerical scheme and we refer to [148] for an extensive discussion. The quantity $\Gamma_N = \gamma/N$ is believed to obey a universal scaling law of the form

$$\Gamma_N = F(N^{1/\nu}(x - x_c)) \quad (4.85)$$

where F is unknown. In practice, in order to get more precise results, one needs to take into account less relevant fields. The form of the scaling law considered is then

$$\Gamma_N = F(N^{1/\nu}u_0(x), N^y u_1(x)) \quad (4.86)$$

where u_0 and u_1 are the relevant and irrelevant scaling variables and y is related to the irrelevant field with $y < 0$. To get a precise estimate of ν , it is very important to determine F using Γ_N with many successive widths. However, because the focus of the study is to observe the RG-flow as N increases, it is not the strategy adopted here. It is more convenient to use two successive sizes to obtain an effective exponent $\nu_N(\mu)$. Its evolution as N increases shows the direction of the flow.

Let us now give a few details about the numerical scheme used. Systems of width $2N = 4, 8, 16, 32, 64$ are considered. Numerical estimates of $\Gamma_N(x)$ are computed for different values of μ . The behaviour of $\Gamma_N(x)$ around $x = 0$ is fitted with a polynomial P of the form $P(x) = a_0 + \frac{a_2}{2}x^2 + \frac{a_4}{24}x^4$. Typically we choose the range of x to be $|x| < 0.1$ to avoid contributions of higher order. The second derivative of Γ_N , a_2 , can be used to extract an estimate for ν . Deriving twice the scaling formula and evaluating it in $x = 0$ gives

$$\Gamma_N''(0) = N^{2/\nu} F''(0) \quad (4.87)$$

and thus, using two sizes $N, 2N$:

$$\nu_N = 2 \times \frac{\log 2}{\log \Gamma_N''(0)/\Gamma_{2N}''(0)}. \quad (4.88)$$

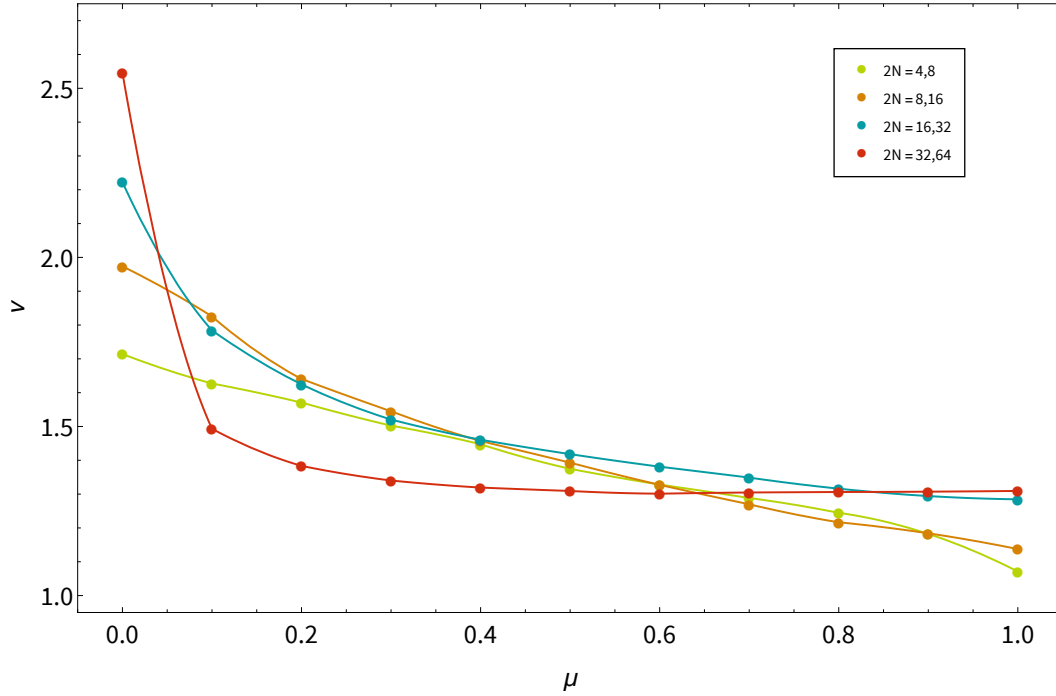


Figure 4.2 – Estimates of ν_N for sizes $N = 2, 4, 8, 16$ as a function of μ . The limit at $\mu = 0$ is the value of the Chalker-Coddington model around $\nu = 2.6$ [13] whereas the value at the percolation end $\mu = 1$ is known exactly to be $\nu = 4/3$. In order to obtain those estimates, equation (4.88) is used with two successive sizes. The second derivative of Γ_N around $x = 0$ is obtained by a fit of the form $\Gamma_N(x) \sim A + Bx^2 + Cx^4$ for $x < 0.15$. Each Lyapunov exponent is computed by diagonalising the transfer matrix on a strip of length 10^8 . It has been reported elsewhere [148] that one should use smaller values of x ($|x| < 0.05$) in order to increase the precision of the fit but with the length considered here, the results already show the direction of the flow.

It is possible to use two successive sizes N and $N + 1$ but, as N becomes large, this scheme produces some instabilities since the term $\log(N/(N + 1))$ and the denominator tend to zero. The exact value for percolation is $\nu = 4/3$. Indeed, we know that the thermal perturbation is associated with the two-hull operator of dimension $X_2 = 5/4$ and the scaling relation is $X = 2 - 1/\nu$. On the contrary, the exact value at the Hall point is unknown, many numerical simulations report a value in the range $[2.5 - 2.6]$. Results are given Figure 4.2 and are discussed in the next section.

From the Lyapunov exponents, additional information can be extracted to understand the perturbation around the spin quantum Hall point at $\mu = 1$. The exponent ν_μ is introduced to describe the behaviour of the universal function

$$\Gamma(1 - \delta\mu) = F_\mu(\delta\mu L^{1/\nu_\mu}). \quad (4.89)$$

In the case of an irrelevant perturbation, the exponent ν_μ is negative. Moreover, since the perturbation is of order $O(\delta\mu^4)$ in the action, we can expect a scaling relation between X_μ , its associated conformal dimension, and ν_μ of the form

$$X_\mu = 2 - \frac{4}{\nu_\mu}. \quad (4.90)$$

The hull-exponents of percolation are recalled to be

$$X_k = \frac{4k^2 - 1}{12} \quad (4.91)$$

and the two first irrelevant dimensions are $X_3 = 35/12$ and $X_4 = 21/4$. If equation (4.90) holds then the possible associated values for ν_μ are respectively $-48/11 \sim -4.36$ or $-16/13 \sim -1.23$. We find a good collapse of the curve for the first value as can be seen in the figure 4.3.

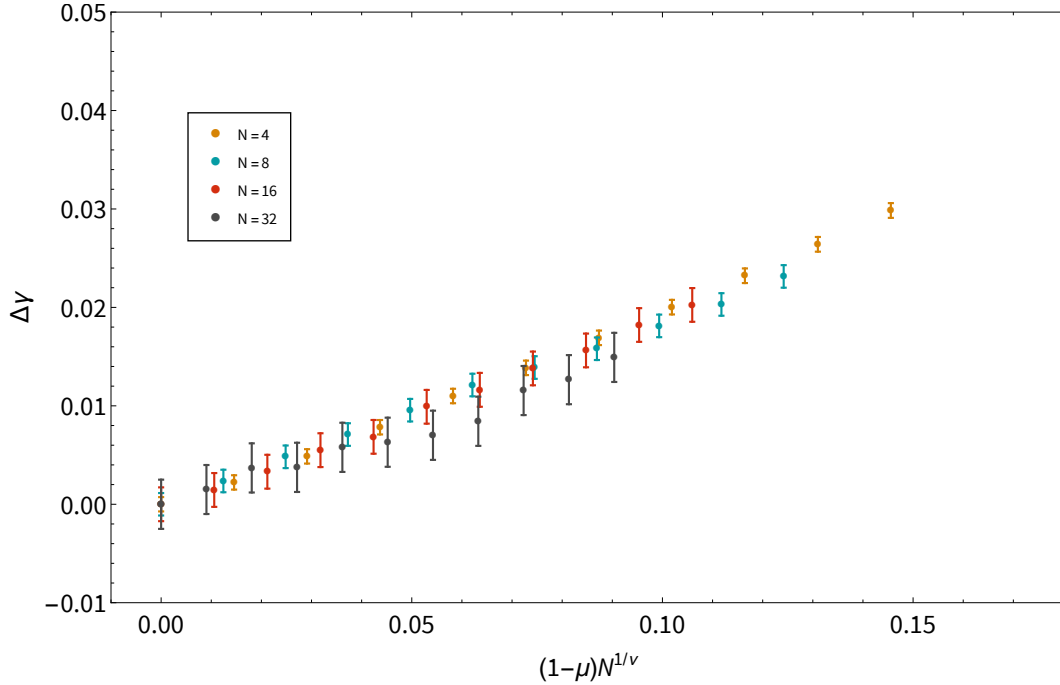


Figure 4.3 – Evolution of the smallest Lyapunov exponent of the transfer matrix along the perturbation μ . Because of the important finite-size corrections at $\mu = 0$ for successive sizes we decided to plot the difference between $\Delta_\gamma = \Gamma(\mu) - \Gamma(\mu = 1)$ such that all curves start at the origin. The perturbation axis is rescaled by a size-dependent factor N^{1/ν_μ} . The curves are supposed to collapse for some value of ν_μ . Here we chose to use the conjecture $\nu_\mu = -48/11$ corresponding to the operator X_3 . This value provides a relatively good collapse of the curves. The error bars are estimated in the network model as 3 times the dispersion of each value of the Lyapunov exponents. Each point corresponds to a simulation on a cylinder of length 10^8 . The curve for the smallest size $N = 2$ has been discarded since it was subject to enormous finite-size corrections for small perturbations of μ .

This result that the percolation point is indeed stable and the perturbation along the critical line $z_c(\mu)$ is associated to the 3-hull operator.

4.3 Truncations

Truncating the model has the advantage of reproducing the series of models discussed in the last chapter at the end point $\mu = 0$. In particular, the first truncation provides an interpolating model between class C and the first truncation of the Chalker-Coddington model. Therefore, it is natural to study this flow since we have a better understanding of the continuum limit of the truncated model. Predictions about the direction of the flow are far from being obvious because truncating the model already breaks several symmetries and, in particular, the $sl(2|1)$ sub-algebra of the $gl(2|2)$ symmetry for $\mu < 1$. Notice that the model at $\mu = 1$ is actually not modified by a hard truncation since it has already an on-site truncation to three states in the supersymmetric formalism. On the contrary, in the original model the space at each edge is infinite-dimensional, hence the truncation affects it in a non-trivial way.

Working with truncations instead of the full model has several advantages. It is for instance possible to use numerical methods such as exact diagonalisation (or more advanced methods like matrix product state). First of all, the phase diagram has to be determined in terms of the parameter (μ, z) .

This section is structured as follows. First the phase diagram is obtained numerically thanks to a phenomenological renormalisation scheme. The parameter z have to be reintroduced in order to reach critical points. This part is very much analogous to what has been shown in the section 3.3 for the second truncation of the brownian motion. Then the symmetries of the critical model are discussed. In particular, contrary to the untruncated model, it appears that the $sl(2|1)$ symmetry is broken in finite-size for $\mu < 1$. We also discuss the nature of the dense phase, obtained for high fugacity z . Later, numerical evidence for the direction of the flow is given by studying the critical exponents.

4.3.1 The phase diagram

The parameter z , corresponding to the fugacity of monomers, is reintroduced as in the last chapter. The model is already known to be critical at two points $(\mu, z) = (1, 1)$ and $(\mu, z) \sim (0, 1.032)$. The first critical point corresponds to the class C universality class discussed above and the second is the critical first truncation of the Chalker-Coddington model. Actually, a critical line between those two points can be parametrised by a function $z_C(\mu)$. A numerical estimate can be obtained by phenomenological renormalisation using the first gap in the transfer matrix spectrum. A good alternative, chosen here, is to use the gap between the groundstate of the periodic transfer matrix and the groundstate of the transfer matrix with anti-periodic boundary conditions. This latter state, useful for determining the effective central charge c_{eff} , is easily computed and converges nicely. There are two types of boundary conditions on a cylinder. The first one, called simply periodic boundary condition, wraps the system on a cylinder by taking care that closed non-contractible loops get the

right fugacity zero. The second one uses an anti-periodic condition for the fermions which, in practice, gives a weight 2 to non-contractible loops. For a cylinder of width $2N$ the two sets of conditions are

- periodic boundary conditions:

$$b_{\sigma,2N} = b_{\sigma,0} \text{ and } f_{\sigma,2N} = -(-1)^N f_{\sigma,0} \quad (4.92)$$

- anti-periodic boundary conditions:

$$b_{\sigma,2N} = b_{\sigma,0} \text{ and } f_{\sigma,2N} = (-1)^N \cdot f_{\sigma,0} \quad (4.93)$$

For most physical purposes, we are interested in the usual periodic boundary conditions but quantities such as the effective central charge also has a high physical interest. The phase diagram obtained is drawn Figure 4.4.

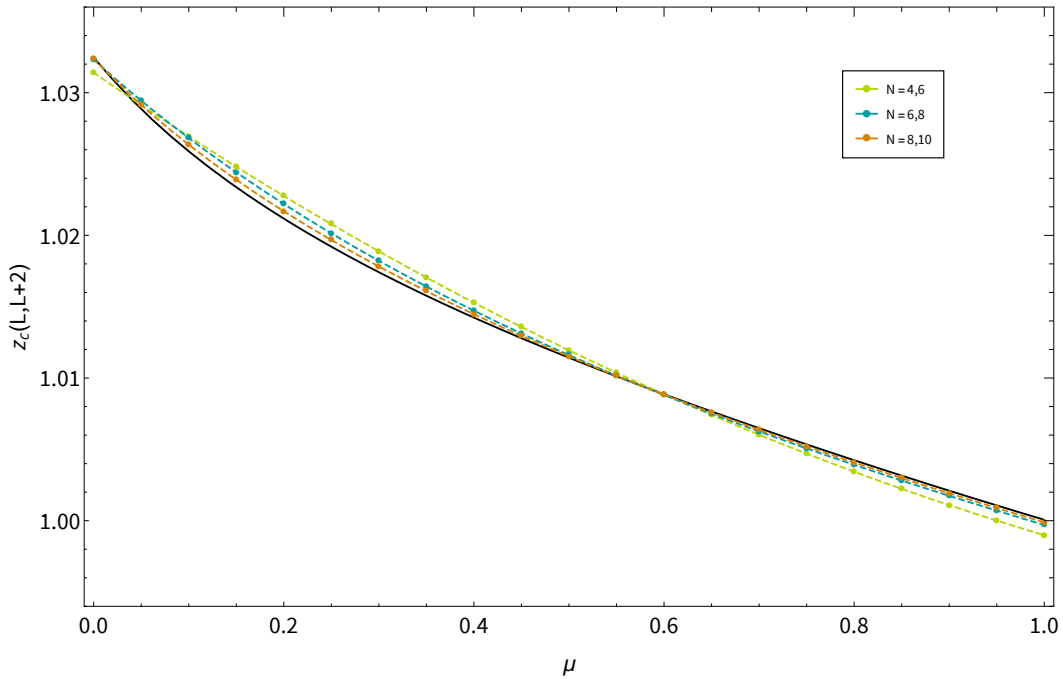


Figure 4.4 – Phase diagram for the lattice model. The critical line $z_C(\mu)$ is obtained using phenomenological renormalisation for a system on a cylinder and describes the dilute critical phase at $c = 0$. On the end point at the right the model describes percolation whereas on the far left the system describes the first truncation of the Chalker-Coddington model. The domain below the critical line is a dilute non-critical phase. Above, the phase is critical but in a different universality class where the lattice is filled with loops.

In particular it is clear that indeed $z_C(\mu = 1) = 1$ for percolation and we recover the estimate for z_C in the first truncation of the Chalker-Coddington model $z_C(\mu = 0) \sim 1.032$.

All the domain under the line $z_C(\mu)$ is a non-critical dilute phase and is not discussed here. As already partially discussed in the last chapter, the domain above $z_C(\mu)$ is dense and critical. It has already been shown in section 3.2.5 that, at $\mu = 0$, this dense phase is composed of two dense polymers with central charge $c = -4$. The section 4.3.3 discuss in details the universality class at generic values of μ .

4.3.2 Symmetries

The symmetries of the first truncation of the Chalker-Coddington model are discussed extensively in the section 3.2.3. It was found that for $\mu = 0$ the model has a $gl(1|1)_+ \times gl(1|1)_-$ symmetry in finite-size. The edges carry a five-dimensional representations of this algebra,

$$V_5 = 1 \oplus (\square_+ \otimes \square_-) \quad (4.94)$$

for even sites and

$$V_5 = 1 \oplus (\bar{\square}_- \otimes \bar{\square}_+) \quad (4.95)$$

for odd sites. For simplicity, the following discussion focusses on an even site, the analysis about odd sites is perfectly similar. The generators of $gl(1|1)_\sigma$ are

$$N_\sigma = n_{F_\sigma} = f_\sigma^\dagger f_\sigma, \quad \psi_\sigma^+ = f_\sigma^\dagger b_\sigma, \quad \psi_\sigma^- = b_\sigma^\dagger f_\sigma. \quad (4.96)$$

For values of $\mu > 0$, an interaction between $+$ and $-$ generators appears. This interdependence, coming from the \mathbb{P}_3 projector in the edge contribution, can be interpreted with loops. Indeed the model at $\mu > 0$ is not made of two independent polymers since the mixing of colours allows a polymer to go through the same edge twice. As a consequence it is expected that the symmetry algebra is no longer two independent copies of $gl(1|1)$ but only one. The generators of the symmetry on a site are

$$N = N_+ + N_-, \quad \psi^+ = \psi_+^+ + \psi_-^+, \quad \psi^- = \psi_+^- + \psi_-^- \quad (4.97)$$

for even sites and the odd sites generators have a similar expressions. Moreover the on-site Hilbert space is now decomposed as

$$V_5 = 1 \oplus \langle 2, 1 \rangle \oplus \langle 2, 2 \rangle \quad (4.98)$$

in terms of representation of $gl(1|1)$. Thus the symmetry algebra for $0 < \mu < 1$ is indeed reduced to $gl(1|1)$.

The situation is very different for $\mu = 1$. The model is described by the an alternating supersymmetric $sl(2|1)$ spin chain. The critical parameter z is known exactly to be $z = 1$ (independently of the order of truncation). As a consequence, the action of the transfer matrix allows a symmetry between particle states and the vacuum encoded in the generators Q^+, Q^-, V^+ and W^- of (4.64). The $sl(2|1)$ actually contains one copy of $gl(1|1)$. Indeed the generator N can be related to Q^z in (4.64), ψ^+ to V^- and ψ^- to W^+ , all up to trivial

normalisations and shifts. It is important to notice that the $gl(1|1)$ symmetry in the range $0 < \mu < 1$ is actually precisely the $gl(1|1)$ sub-algebra of $sl(2|1)$ at $\mu = 1$.

Let us summarise the symmetry content of the model. Starting from $\mu = 1$ and $z = 1$, with a $sl(2|1)$ symmetry, the system is perturbed along $z_C(\mu)$. This perturbation breaks, in finite-size, the relations encoded in $sl(2|1)$ between the vacuum and particle states. Hence only $gl(1|1)$ is left, mixing the fermions and bosons together. On the other end of the critical line, at $\mu = 0$, the symmetry between the vacuum state and the particles is already broken since $z_C > 1$ (it is also broken by the truncation). Therefore, from the original $gl(2|1)$ symmetry, only the sub-algebra $gl(1|1)_+ \times gl(1|1)_-$ is left and, as the system is perturbed along $z_C(\mu)$, the two $gl(1|1)$ copies are coupled and leaving only $gl(1|1)$.

$$\begin{array}{ccc}
 \text{1st trunc CC} & ? & \text{Class C} \\
 \bullet \text{-----} \bullet & & \\
 \mu = 0 & gl(1|1) & \mu = 1 \\
 gl(1|1)_+ \otimes gl(1|1)_- & & sl(2|1)
 \end{array} \tag{4.99}$$

From the point of view of symmetries, it is perfectly reasonable to expect that the model, in the regime $0 < \mu < 1$, has a distinct universality class. However, it is also possible that symmetries are restored in the continuum limit. In particular, the case of the self-avoiding walks model of the last section provides an example of a symmetry between the vacuum and particle states restored in the continuum. If this is the case, a flow towards class C in the regime $0 < \mu < 1$ is again expected.

4.3.3 The dense phase

The identification of the dense phase is discussed here in the same way as in 3.2.5. In this subsection the values of the parameters (μ, z) always satisfy $z > z_C(\mu)$. As we cross the threshold $z_C(\mu)$ and enter into the dense phase, dominant configurations are filled with loops. In terms of the Hamiltonian or the transfer matrix, the supersymmetric vacuum changes and the largest eigenvalue Λ_0 of the transfer matrix is no longer $\Lambda_0 = 1$.

As discussed earlier, the dense phase of the first truncation of the Chalker Coddington model $\mu = 0$ is two decoupled dense polymers with central charge $c = -4$. Indeed the two $gl(1|1)$ copies are preserved and give one dense polymer each. Considering now the case $\mu = 1$ increasing $z > z_C(\mu = 1) = 1$ breaks the $sl(2|1)$ symmetry to its $gl(1|1)$ sub-algebra as discussed already earlier. The dense phase is thus expected to be a simple dense polymer. This situation is very similar to the case of the $O(n = 0)$ model at the θ_{DS} point. The same behaviour is expected from the regime $0 < \mu < 1$ since the $sl(2|1)$ is already broken to the same $gl(1|1)$ symmetry. The loop model provides a nice picture of this phenomena. Since two polymers with distinct colours can in fact be connected for $\mu > 0$, a single polymer filling the lattice by going through each edge twice is effectively obtained. To summarise, the dense phase for $\mu > 0$ is expected to be a unique dense polymer with central charge $c = -2$.

A transfer matrix simulation is performed in order to obtain numerical estimate of the central charge. The ground state energy per site is known to have universal finite-size corrections

$$f_0(L) = -\frac{1}{L} \log(\Lambda_0) = f_{\text{bulk}} - \frac{\pi c}{6L^2} + o(L^{-2}) \quad (4.100)$$

where Λ_0 is the largest eigenvalue of the transfer matrix and f_{bulk} is a non-universal constant. From this law we extract a series of values of c using two successive sizes and obtain the figure 4.5.

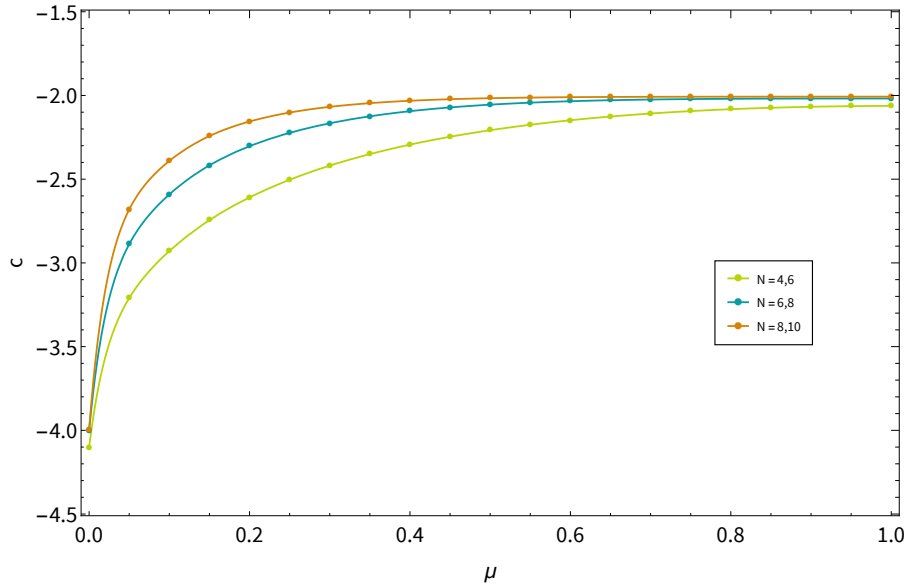


Figure 4.5 – Numerical estimation of the central charge in the dense phase along the critical line. Each value is computed thanks to 2 successive lengths. We chose the value $z = 1.1$ for all value of μ but other values could have been chosen if $z(\mu) > z_c(\mu)$ is respected. The central charge converges towards $c = -4$ for $\mu = 0$ corresponding to two independent dense polymers whereas $c = -2$ for $\mu > 0$ corresponding to one dense polymer.

The action of the renormalisation group provides a flow going from the dense phase of the Chalker-Coddington model first truncation towards the dense phase of the percolation. Note that this is consistent with a c_{eff} theorem since the effective central charge are related by $c_{\text{eff}}(\mu = 0) = 2c_{\text{eff}}(\mu = 1) > 0$ hence $c_{\text{eff}}(\mu)$ decreases along the RG flow. Similar observations can also be made on critical exponents and the same conclusion are reached.

4.3.4 Critical exponents of the critical dilute phase

The focus of this section is to illustrate the direction of the RG-flow by looking at several critical exponents. In the following the choice is made to look at the effective central charge and a few conformal dimensions. Another option is to measure the critical exponent ν

corresponding to a staggering of the lattice. However, it was found that for generic values of μ , its value is hard to obtain precisely. We propose a few explanations. In the spin chain formulation, using exact diagonalisation, we are restricted by the very large vector space of dimension 5 per site. Moreover the critical line $z_C(\mu)$ is not known exactly and if the value is not precise enough, the system is perturbed by a relevant operator (corresponding to X_{eo} as defined in the previous chapter). In practice, larger size of the system must be reached in order to produce a reasonable estimate of ν .

Effective central charge. The first quantity to compute is the effective central charge. It is obtained by measure the central charge of the system with anti-periodic boundary conditions defined equation (4.93). The free energy per site $f_{0,\text{antiperiodic}}$ can be computed from the largest eigenvalue of the transfer matrix $\Lambda_{0,\text{antiperiodic}}$ and its finite-size corrections is

$$f_{0,\text{antiperiodic}}(L) = -\frac{1}{L} \log(\Lambda_{0,\text{antiperiodic}}) = -\frac{\pi c_{\text{eff}}}{6L^2} + o(L^{-2}). \quad (4.101)$$

The figure 4.6 shows the evolution of c_{eff} measured with two successive sizes. Its predicted value is $c_{\text{eff}} = 3$ [77] for the first truncation of the Chalker-Coddington model. The numerical estimate at $\mu = 0$ is a little bit far from this prediction. Moreover the value for percolation is exactly

$$c_{\text{eff}} = 1 + \frac{9}{\pi^2} \left(\log \frac{3 + \sqrt{5}}{2} \right)^2 \sim 1.8446 \dots \quad (4.102)$$

with excellent agreement with our data at $\mu = 1$. We observe a crossover in the intermediate regime. As L increases, the effective centrale charge forms a plateau in the regime $\mu > 0$ at the percolation value. This observation provides further evidence of a flow from the first truncation towards class C.

Vacuum sector. The periodic boundary conditions are now considered in the sector of the supersymmetric groundstate. There are two $gl(1|1)$ conserved charges

$$Q_b = \sum_{i=0}^{N-1} n_b^{2i} - \sum_{i=0}^{N-1} \bar{n}_b^{2i+1} \quad Q_f = \sum_{i=0}^{N-1} n_f^{2i} - \sum_{i=0}^{N-1} \bar{n}_f^{2i+1} \quad (4.103)$$

where n_b^j (resp. n_f^j) is the number of bosons (resp. fermions) on site j . The vaccum sector is the one with $Q_b = Q_f = 0$. The first exponent X_t , corresponding to the creating of a pair of loop arc, is not a good candidate to study naively the RG-flow. Indeed it is known for percolation that X_t corresponds to the one hull exponent, $X_{k=1}$ of equation (4.91), giving $X_t = 1/4$ whereas in the first truncation of the Chalker-Coddington model we also have $X_t = X_{2,2} = 1/4$ as discussed in the last chapter.

Nevertheless it is interesting to look at the evolution of the degeneracies of X_t since we know that the $gl(1|1)$ symmetry is broken around $\mu = 0$. If this symmetry is present in

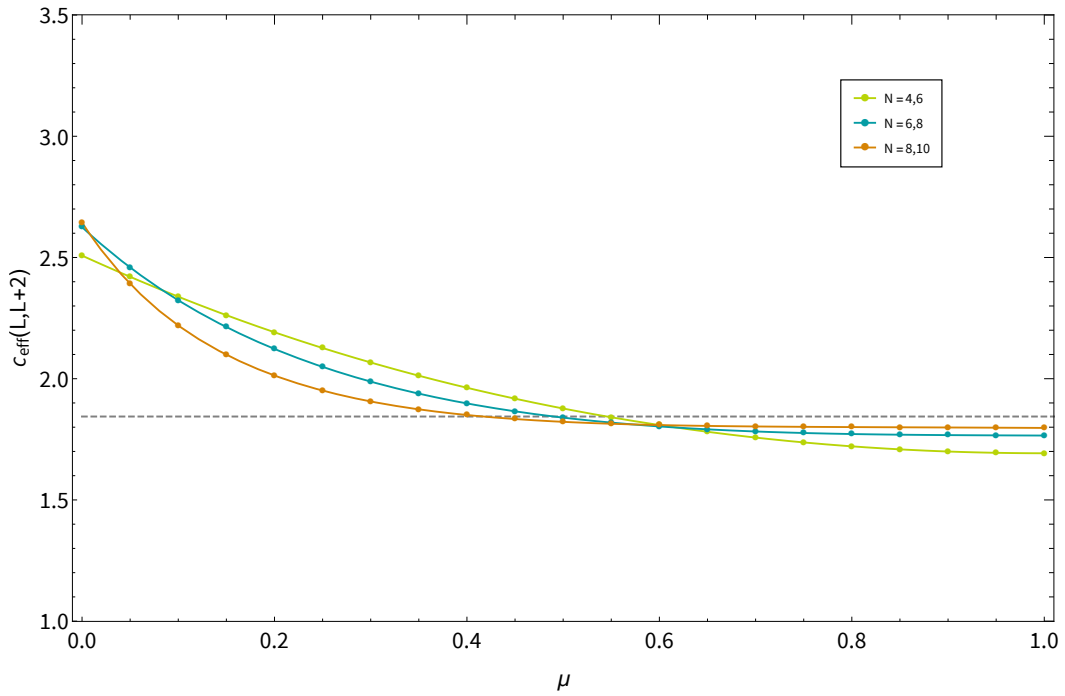


Figure 4.6 – Numerical estimate of the effective central charge for successive sizes. The values are obtained using a phenomenological renormalisation scheme, determining effectively z_C at the same time. The dotted line is the exact value for percolation (4.102).

the continuum limit (in the case of a flow from class C towards the first truncation), the degeneracies are expected to be restored by increasing the size of the system. In the figure 4.7, the first eigenvalue at $\mu = 0$ is plotted and, moving along the critical line $z_C(\mu)$, each degeneracy is followed. Some eigenvalues diverges as the size increases providing an other piece of evidence supporting a flow towards class C, as in the untruncated model.

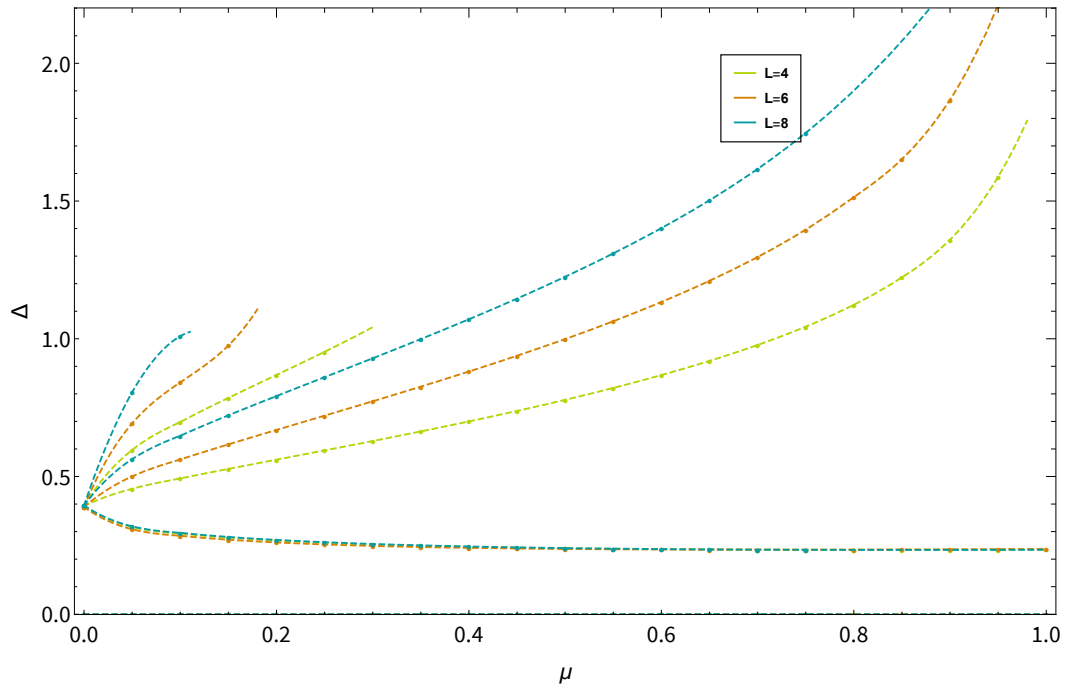


Figure 4.7 – Numerical estimate of the low-energy spectrum for successive sizes in the sector $(Q_b, Q_f) = (0, 0)$. The plot are obtained by exact diagonalisation along the critical line $z_C(\mu)$ and only shows the eigenvalues that correspond to X_t around $\mu = 0$. The degeneracies at the first truncation of the Chalker-Coddington model are lifted and some states disappear under the action of the RG-group by flowing to infinity.

5 Operators in the Potts model

Logarithmic Conformal Field Theories (LCFTs) are characterised by having a non-diagonalisable dilatation operator L_0 . This structure leads to logarithms in the correlations of the fields that transform inside a Jordan cell of L_0 . Some features of the LCFTs can be understood by taking a limiting procedure [149–151] through a continuous family of ordinary (i.e., not indecomposable, but still non-unitary) CFT. If the model is subject to additional discrete symmetries, insight on these logarithmic correlation functions is obtained by studying operators that transform irreducibly under this symmetry. In contradistinction to most of usual techniques in CFT, this approach is *not* limited to two dimensions.

The Q -state Potts model is an interesting statistical physics system, since it contains several important special cases, such as the Ising model ($Q = 2$), percolation ($Q \rightarrow 1$), or spanning trees and forests ($Q \rightarrow 0$ limits) [99, 152–155]. This model is invariant under the action of the discrete symmetric group \mathcal{S}_Q . Even though the original definition supposes Q to be a positive integer, the partition function can be reformulated in terms of non-local geometrical objects and analytically continued to Q real [29] in terms of an irrational model. More details can be found in section 5.1 below. In two dimensions, the Potts model can be solved exactly thanks to a mapping to a 6-vertex model [101] or an associated loop model [42]. Very little is known about the field theory in higher dimensions. A first approach to the logarithmic scale invariant theory for the Potts model has been proposed in [151], and subsequently investigated more systematically in [156]. It successfully predicts Jordan cells in the dilatation operator, independently of the dimension. Recently, progress has been made to determine the general form of correlation functions and conformal blocks in any dimension [157].

In this chapter we generalise the construction of [156] to classify local observables of N spins that transform irreducibly under the action of the symmetric group, taking into account the \mathcal{S}_Q symmetry and also the \mathcal{S}_N symmetry that describes the behaviour of the observables under an exchange of the spins. Only observables symmetric under such exchange were previously considered in [156], corresponding to a trivial action by \mathcal{S}_N and a zero conformal spin. Here we consider arbitrary irreducible observables, including those with non-zero conformal spin, in a more transparent group theoretical setup. The structure and the correlation functions of this new class of observables is discussed. In particular, we underline the consequences for bulk LCFT and identify the critical exponents in two dimensions.

5.1 Observables in the Q -state Potts model

The Q -state Potts model is a quite simple model of statistical physics with \mathcal{S}_Q symmetry, which nevertheless conceals deep algebraic structures and a rich variety of critical behaviour. It can be written in different representations, some of which are specific to two dimensions, and others which hold in arbitrary dimensions. Among the latter, a very appealing choice amounts to rewriting the partition function and correlation functions in terms of non-local objects known as Fortuin-Kasteleyn clusters [29]. Each such cluster carries a Boltzmann weight of Q , which immediately allows us to extend the definition of the model to non-

integer Q . This is particularly useful in the LCFT context, because we can then access particular indecomposable values of Q through a limiting procedure.

In the following, we first provide a brief review of the definition of the Potts model. We then explain the construction of local observables within a particular representation of \mathcal{S}_Q and discuss the structure relevant to LCFT. The previous results for scalar (spinless) observables [156] are recovered within our new framework.

5.1.1 Potts model and Fortuin-Kasteleyn clusters

The Potts model and its Fortuin-Kasteleyn formulation were introduced in the section 2.2.1. We are going to study the so-called N -cluster operators.⁴ Consider a small neighbourhood \mathcal{D}_i containing N spins that belong to N distinct FK clusters. We are interested in the probability that these N clusters extend to another similar neighbourhood \mathcal{D}_j . A *cluster-operator* \mathcal{O}_i —which will be defined precisely below in a more appropriate notation—acts on the N spins in \mathcal{D}_i so as to impose that they belong to *distinct* FK clusters. The clusters thus inserted at \mathcal{D}_i are therefore obliged to propagate until they terminate at another cluster operator.⁵ The probability of having N distinct clusters extending from \mathcal{D}_i to \mathcal{D}_j can thus be related to the two-point function $\langle \mathcal{O}_i \mathcal{O}_j \rangle$.

We shall see below that the N -cluster operator \mathcal{O}_i are functions of the N Potts spins in \mathcal{D}_i . It can therefore be represented explicitly as an N -component tensor (e.g., a vector for $N = 1$ and a matrix for $N = 2$) of coefficients that are algebraic functions of Q . The *N -cluster operators* are strictly speaking observables. We also use the term *operator* here in a looser sense, because in the continuum limit correlation functions of such observables correspond to two-points functions of fields that, in a field-theory terminology, are called operators. For that reason we shall often use the words operator, observable and tensor interchangeably in the sequel.

The correlation functions in the Potts model at criticality involve power laws of the distance between the small neighbourhoods considered. If Q takes the particular values $Q = 4 \cos^2(\pi/p)$ with $p = 2, 3, \dots$ integer (these values are known as Beraha numbers) in $d = 2$, or $Q \in \mathbb{N}$ in higher dimensions, we will find that these power laws are multiplied by logarithms. In two dimensions, these logarithmic contributions have been fixed [47]. In [156], all the tensors acting on an arbitrary number of spins and transforming according to a class of irreducible representations of the symmetric group are constructed. More precisely, they have computed the form of all possible tensors $t(\sigma_1, \dots, \sigma_N)$, acting on N spins, which are irreducible under \mathcal{S}_Q and invariant under arbitrary permutations of the N spins σ_i .

⁴In $d = 2$, the N -cluster operators coincide with the $2N$ -leg watermelon (or fuseau) operators in the loop model representation. However, this latter representation makes crucial use of planarity and duality, and hence is not available in higher dimensions.

⁵The use of words such as “insert”, “propagate” and “terminate” does not imply that these clusters have been equipped with a direction of any kind.

5.1.2 Definitions and representation theory of \mathcal{S}_Q

The symmetric group \mathcal{S}_n is the group of permutations of n objects. We would like to classify the observable content of the Potts model in terms of representation of \mathcal{S}_Q . We need to construct an observable of N spins, $t(\sigma_1, \dots, \sigma_N)$. Let us denote by $L_Q^{(N)}$ the space of $\underbrace{Q \times \dots \times Q}_N$ tensors. We decompose it in terms of the basis elements $\mathcal{O}_{a_1, a_2, \dots, a_N}$ defined by

$$\mathcal{O}_{a_1, a_2, \dots, a_N}(\sigma_1, \sigma_2, \dots, \sigma_N) = \delta_{a_1, \sigma_1} \delta_{a_2, \sigma_2} \dots \delta_{a_N, \sigma_N}, \quad (5.1)$$

where $\{a_i\}$ and $\{\sigma_i\}$ are sets of integers between 1 and Q . A permutation $p \in \mathcal{S}_Q$ has a natural action on this basis:

$$p \mathcal{O}_{a_1, a_2, \dots, a_N} = \mathcal{O}_{p(a_1), p(a_2), \dots, p(a_N)}. \quad (5.2)$$

We can also define the action of \tilde{p} , a permutation in \mathcal{S}_N , by

$$\tilde{p} \mathcal{O}_{a_1, a_2, \dots, a_N} = \mathcal{O}_{a_{\tilde{p}^{-1}(1)}, a_{\tilde{p}^{-1}(2)}, \dots, a_{\tilde{p}^{-1}(N)}}, \quad (5.3)$$

which implies:

$$\tilde{p} \mathcal{O}_{a_1, a_2, \dots, a_N}(\sigma_1, \dots, \sigma_N) = \mathcal{O}_{a_1, a_2, \dots, a_N}(\sigma_{\tilde{p}(1)}, \dots, \sigma_{\tilde{p}(N)}). \quad (5.4)$$

It is straightforward to show that if we act with $p \in \mathcal{S}_Q$ and $\tilde{p} \in \mathcal{S}_N$ on a tensor, the order does not matter because the transformations commute.

To make the presentation self-contained, we start by briefly recalling all the necessary definitions and properties. We refer to [158] for more details. In the following, a permutation is always represented by its decomposition in terms of cycles. A very convenient way to study the representations of \mathcal{S}_n is to use the bijection between irreducible representations and Young diagrams. Let us consider a partition of the integer n , with k integers λ_i ($\sum_{i=1}^k \lambda_i = n$) that we reorder such that $\lambda_1 \geq \lambda_2 \geq \dots \geq \lambda_k$. We use the standard notation for Young diagrams, where $[\lambda_1, \lambda_2, \dots]$ denotes the diagram with λ_i boxes in the i 'th row (counted from the top). The normal Young tableau corresponding to a Young diagram is obtained by filling the n boxes with the integers $\{1, 2, \dots, n\}$, so that the order is increasing in each row (read from left to right) and in each column (read from top to bottom). We henceforth refer to rows also as horizontal lines, and to columns as vertical lines. An arbitrary Young tableau is obtained by acting with a permutation q on the numbers in the boxes of the normal tableau. Therefore the quantities that refer to a particular Young tableau of shape λ will be denoted with a superscript (q) .

We now define a linear operator which will project a tensor in a certain irreducible representation of the symmetric group. Given a Young tableau λ of size n boxes, let $h_\lambda^{(q)}$ (resp. $v_\lambda^{(q)}$) be the subset of permutations that leave invariant the set of numbers in each horizontal (resp. vertical) line of the Young tableaux of shape λ and filled thanks to the permutation q . We then define the symmetriser $s_\lambda^{(q)}$, the anti-symmetriser $a_\lambda^{(q)}$ and the irreducible symmetriser $e_\lambda^{(q)}$ by

$$s_\lambda^{(q)} = \sum_{h \in h_\lambda^{(q)}} h, \quad a_\lambda^{(q)} = \sum_{v \in v_\lambda^{(q)}} \epsilon(v) v, \quad e_\lambda^{(q)} = s_\lambda^{(q)} a_\lambda^{(q)}, \quad (5.5)$$

where $\epsilon(v)$ is the signature of the permutation v . The idea is the following: when we act with the operator $e_\lambda^{(q)}$ on a set of indices, first all the indices in the same column are anti-symmetrised, and then we symmetrise all the indices in the same row. Notice that the quantity that we obtain is a priori not anti-symmetric in the indices that belong to the same column, since $s_\lambda^{(q)}$ and $a_\lambda^{(q)}$ do not commute. Examples of irreducible symmetrisers will be given when we will construct the tensors. Finally, notice that

$$e_\lambda^{(q)} = q e_\lambda q^{-1}, \quad (5.6)$$

which is a relation that relates the irreducible symmetriser of any Young tableau of shape λ to the irreducible symmetriser of the normal Young tableau of the same shape. The operator $e_\lambda^{(q)}$ is a projector (if normalized correctly). In order to get an invariant subset of a vector space (which will be our tensor space) that generates an irreducible representation, we act with $e_\lambda^{(q)}$ on an arbitrary vector. All the other generators are obtained by acting with permutations on this first generator. A very important fact is that if one changes the order of the numbers appearing in the boxes of the diagram λ , we end up with an equivalent representation. Later we will choose those numbers conveniently.

Let us finally recall the *hook formula* that gives the dimension d_λ of an irreducible representation λ of \mathcal{S}_Q :

$$d_\lambda = \frac{n!}{\prod_{(i,j) \in \lambda} h_\lambda(i,j)}, \quad (5.7)$$

where the hook length $h_\lambda(i,j)$ of the box labelled (i,j) in the Young diagram λ is the number of boxes to its right, plus the number of boxes below it, plus the box itself.

We are now ready to act with an irreducible symmetriser on the tensor space to obtain a family of observables in an arbitrary representation of \mathcal{S}_Q . Let us summarise the ‘‘recipe’’. First we choose a Young diagram λ_Q of size Q . We consider a realisation of a Young tableau filled with the permutation q and compute the irreducible symmetriser $e_{\lambda_Q}^{(q)}$. The action of this operator on a tensor t gives us a generator $e_{\lambda_Q}^{(q)} t$ of an invariant subspace V_{λ_Q} . We get all the generators of V_{λ_Q} that transform with the \mathcal{S}_Q irreducible representation associated to λ_Q by acting with some permutations:

$$V_{\lambda_Q} = \left\{ p \left(e_{\lambda_Q}^{(q)} t \right) : p \in \mathcal{S}_Q \right\}. \quad (5.8)$$

In the following, we review the simplest examples of this procedure, recovering some of the results of [156], before generalising the method.

5.1.3 Observables of one spin

First we consider the tensor space $L_Q^{(1)} = \{\mathcal{O}_a : a = 1, \dots, Q\}$ of observables functions of one spin σ . In [151, 156], the authors decomposed this space in two tensors, namely the identity

and the magnetisation. In their notation, these observables read

$$t^{(0,1)}(\sigma) = \sum_{a=1}^Q \delta_{a,\sigma} = 1, \quad (5.9)$$

$$t_a^{(1,1)}(\sigma) = \delta_{a,\sigma} - \frac{1}{Q} t^{(0,1)} = \delta_{a,\sigma} - \frac{1}{Q}. \quad (5.10)$$

These expressions were found in [151, 156] by imposing the constraint

$$\sum_a t_a^{(1,1)} = 0. \quad (5.11)$$

Below we shall rederive them (in our own notation), using a procedure that allows us to consider more complicated cases later. To this end, we consider the irreducible symmetriser $e_\lambda^{(q)}$ for a given Young tableau λ . It is easy to see that only two Young diagrams give a non-zero action: $[Q]$ and $[Q-1, 1]$. These diagrams are respectively associated to the trivial and standard representations. Their respective dimensions (1 and $Q-1$), as found from (5.7), justifies the constraint (5.11).

Invariant tensor. The irreducible symmetriser for $[Q]$ is

$$e_{[Q]} = \sum_{h \in \mathcal{S}_Q} h. \quad (5.12)$$

Its action on any tensor \mathcal{O}_a gives the invariant tensor $t^{[Q]}$:

$$t^{[Q]} \equiv \frac{1}{(Q-1)!} e_{[Q]} \mathcal{O}_a = \sum_{i=1}^Q \mathcal{O}_i. \quad (5.13)$$

The tensor acting on a spin σ is explicitly

$$t^{[Q]}(\sigma) = 1, \quad (5.14)$$

and so we have recovered (5.9).

Standard representation. Let us now move to a more interesting case with the Young diagram $[Q-1, 1]$ and consider the following Young tableau

$$\begin{array}{|c|c|c|c|} \hline i_1 & i_2 & \dots & i_{Q-1} \\ \hline a & & & \\ \hline \end{array} \quad (5.15)$$

with a a specific index (with $a = 1, \dots, Q$) and i_1, \dots, i_{Q-1} arbitrary indices in order to fill the Young tableau. The particular choice $\{i_k\} = \{1, 2, \dots, a-1, a+1, \dots, Q\}$ gives the normal Young tableau for the given value of a . We will also denote by a the permutation

that produces the particular tableau (5.15) from the corresponding normal Young tableau. The corresponding irreducible symmetriser $e_{\lambda_Q}^{(a)}$ is

$$e_{\lambda_Q}^{(a)} = \left(\sum_{h \in \tilde{h}_\lambda^{(a)}} h \right) (1 - (i_1, a)), \quad (5.16)$$

where $\tilde{h}_\lambda^{(a)}$ is the subset of permutations within \mathcal{S}_Q that leave the first line of the Young tableau invariant or, in other words, the permutations leaving a invariant. Also, (i_1, a) denotes the transposition of the indices i_1 and a . Acting on the basis element \mathcal{O}_a we get

$$\begin{aligned} e_{\lambda_Q}^{(a)} \mathcal{O}_a &= \left(\sum_{h \in \tilde{h}_\lambda^{(a)}} h \right) (\mathcal{O}_a - \mathcal{O}_{i_1}) \\ &= (Q-1)! \mathcal{O}_a - (Q-2)! \sum_{\substack{i=1 \\ i \neq a}}^Q \mathcal{O}_i \\ &= Q(Q-2)! \mathcal{O}_a - (Q-2)! \sum_{i=1}^Q \mathcal{O}_i. \end{aligned} \quad (5.17)$$

We define the normalised tensor $t_a^{[Q-1,1]}$ by

$$t_a^{[Q-1,1]} = \frac{1}{Q(Q-2)!} e_{\lambda_Q}^{(a)} \mathcal{O}_a = \mathcal{O}_a - \frac{1}{Q} \sum_{i=1}^Q \mathcal{O}_i = \mathcal{O}_a - \frac{1}{Q} t^{[Q]}. \quad (5.18)$$

We can generate the whole family of tensors by acting with a permutation $p \in \mathcal{S}_Q$, but we find that this family is just given by the previous formula for any a , because of (5.6). We can satisfy that it has dimension $Q-1$, because of the following identity

$$\sum_{a=1}^Q t_a^{[Q-1,1]} = 0, \quad (5.19)$$

which of course is nothing but (5.11) in our notation. The tensor acting on a spin σ is explicitly

$$t_a^{[Q-1,1]}(\sigma) = \delta_{a,\sigma} - \frac{1}{Q}, \quad (5.20)$$

so we have recovered also the magnetisation operator (5.10).

Summarising, the space $L_Q^{(1)}$ has been decomposed as a direct sum of two irreducible representations of \mathcal{S}_Q :

$$L_Q^{(1)} = [Q] \oplus [Q-1, 1]. \quad (5.21)$$

5.1.4 Observables of two spins

We next consider the space $L_Q^{(2)}$ of observable of 2 spins, σ_1 and σ_2 . The subspace of $L_Q^{(2)}$ of observables for which $\sigma_1 = \sigma_2$ reads $\{\mathcal{O}_{a,a} : a = 1, \dots, Q\}$ and is stable under the action of \mathcal{S}_Q . It is isomorphic to $L_Q^{(1)}$ and can therefore be decomposed as the direct sum $[Q] \oplus [Q-1, 1]$, as we have just seen. We thus consider henceforth only observables for which $\sigma_1 \neq \sigma_2$.

In [156] the authors studied only the case of symmetric tensors, i.e., those satisfying $t(\sigma_1, \sigma_2) = t(\sigma_2, \sigma_1)$. They enforced constraints on the sum of coefficients to find three irreducible tensors, which we first discuss using the notation of [156]. The first one, $t^{(0,2)}$, can be identified with the energy operator. The second one, $t_a^{(1,2)}$, has the same \mathcal{S}_Q symmetry as the magnetisation operator. And the last tensor, $t_{a,b}^{(2,2)}$, is the two-cluster operator. The three tensors are found to have the following expressions [151, 156]:

$$t^{(0,2)}(\sigma_1, \sigma_2) = 1 - \delta_{\sigma_1, \sigma_2}, \quad (5.22)$$

$$t_a^{(1,2)}(\sigma_1, \sigma_2) = t_a^{(1,1)}(\sigma_1) + t_a^{(1,1)}(\sigma_2) = \delta_{a, \sigma_1} + \delta_{a, \sigma_2} - \frac{2}{Q}, \quad (5.23)$$

$$t_{a,b}^{(2,2)}(\sigma_1, \sigma_2) = \delta_{a, \sigma_1} \delta_{b, \sigma_2} + \delta_{a, \sigma_2} \delta_{b, \sigma_1} - \frac{1}{Q-2} \left(t_a^{(1,2)}(\sigma_1, \sigma_2) + t_b^{(1,2)}(\sigma_1, \sigma_2) \right) - \frac{2}{Q(Q-1)} t^{(0,2)}, \quad (5.24)$$

where we have omitted writing an overall factor $(1 - \delta_{\sigma_1, \sigma_2})$ multiplying the last two expressions.

As in the previous section we now show how to recover these expression using Young projectors. We also extend the set of operators by considering tensors which are antisymmetric under the permutation of the two spins, i.e., those satisfying $t(\sigma_1, \sigma_2) = -t(\sigma_2, \sigma_1)$. To this end, we first notice that any projector on a representation associated with a Young diagram with more than two boxes below the first line is the null operator. We thus have to consider the following diagrams: $[Q]$, $[Q-1, 1]$, $[Q-2, 2]$ and $[Q-2, 1, 1]$.

Invariant tensor. Let us again first consider the case of $[Q]$. The space $L_Q^{(2)}$ contains an additional invariant observable. When acting with $e_{[Q]}$ on the tensor $\mathcal{O}_{a,b}$ with $a \neq b$ we find:

$$t^{[Q]} \equiv \frac{1}{(Q-2)!} e_{[Q]} \mathcal{O}_{a,b} = \sum_{\substack{i,j=1 \\ i \neq j}}^Q \mathcal{O}_{i,j}. \quad (5.25)$$

In terms of the spins, σ_1 and σ_2 , we have the expression

$$t^{[Q]}(\sigma_1, \sigma_2) = 1 - \delta_{\sigma_1, \sigma_2}, \quad (5.26)$$

and so we have recovered (5.22) in our own notation.

Representation $[Q-1, 1]$. We now turn to the more interesting case of the Young diagram $[Q-1, 1]$. We consider once again the following Young tableau:

$$\begin{array}{|c|c|c|c|} \hline i_1 & i_2 & \dots & i_{Q-1} \\ \hline a & & & \\ \hline \end{array} \quad (5.27)$$

One could act with the same $e_{\lambda_Q}^{(a)}$ as before on an element of the type $\mathcal{O}_{a,b}$:

$$\begin{aligned} e_{\lambda_Q}^{(a)} \mathcal{O}_{a,i_{Q-1}} &= \left(\sum_{h \in \tilde{h}_\lambda^{(a)}} h \right) (\mathcal{O}_{a,i_{Q-1}} - \mathcal{O}_{i_1,i_{Q-1}}) \\ &= (Q-2)! \sum_{\substack{i=1 \\ i \neq a}}^Q \mathcal{O}_{a,i} - (Q-3)! \sum_{\substack{i,j=1 \\ i \neq j \neq a}}^Q \mathcal{O}_{i,j} \\ &= (Q-1)(Q-3)! \sum_{\substack{i=1 \\ i \neq a}}^Q \mathcal{O}_{a,i} + (Q-3)! \sum_{\substack{i=1 \\ i \neq a}}^Q \mathcal{O}_{i,a} - (Q-3)! \sum_{\substack{i,j=1 \\ i \neq j}}^Q \mathcal{O}_{i,j}. \end{aligned}$$

We define the corresponding tensor $t_a^{[Q-1,1],1}$:

$$\begin{aligned} t_a^{[Q-1,1],1} &\equiv \frac{1}{(Q-1)(Q-3)!} e_{\lambda_Q}^{(a)} \mathcal{O}_{a,i_{Q-1}} \\ &= \sum_{\substack{i=1 \\ i \neq a}}^Q \mathcal{O}_{a,i} + \frac{1}{Q-1} \sum_{\substack{i=1 \\ i \neq a}}^Q \mathcal{O}_{i,a} - \frac{1}{Q-1} \sum_{\substack{i,j=1 \\ i \neq j}}^Q \mathcal{O}_{i,j}. \end{aligned} \quad (5.28)$$

However, we could also consider the following non-equivalent operation and define $t_a^{[Q-1,1],2}$:

$$\begin{aligned} t_a^{[Q-1,1],2} &\equiv \frac{1}{(Q-1)(Q-3)!} e_{\lambda_Q}^{(a)} \mathcal{O}_{i_{Q-1},a} \\ &= \sum_{\substack{i=1 \\ i \neq a}}^Q \mathcal{O}_{i,a} + \frac{1}{Q-1} \sum_{\substack{i=1 \\ i \neq a}}^Q \mathcal{O}_{a,i} - \frac{1}{Q-1} \sum_{\substack{i,j=1 \\ i \neq j}}^Q \mathcal{O}_{i,j}. \end{aligned} \quad (5.29)$$

A problematic feature in the definitions (5.28)–(5.29) is that there is no manifest symmetry upon exchanging the two spins, σ_1 and σ_2 . It thus appears natural to classify the observables acting also in terms of the group \mathcal{S}_N permuting the N spins. In the present case, with $N=2$, one possibility is to choose the symmetric representation [2] of \mathcal{S}_2 and define the observable $t_a^{[Q-1,1],[2]}$:

$$\begin{aligned} t_a^{[Q-1,1],[2]} &\equiv \frac{Q-1}{Q} (t_a^{[Q-1,1],1} + t_a^{[Q-1,1],2}) \\ &= \sum_{\substack{i=1 \\ i \neq a}}^Q (\mathcal{O}_{i,a} + \mathcal{O}_{a,i}) - \frac{2}{Q} \sum_{\substack{i,j=1 \\ i \neq j}}^Q \mathcal{O}_{i,j} \end{aligned} \quad (5.30)$$

When expressed explicitly in terms of the spins, this observable reads

$$t_a^{[Q-1,1],[2]}(\sigma_1, \sigma_2) = \begin{cases} \delta_{\sigma_1, a} + \delta_{\sigma_2, a} - \frac{2}{Q} & \text{for } \sigma_1 \neq \sigma_2, \\ 0 & \text{for } \sigma_1 = \sigma_2. \end{cases} \quad (5.31)$$

This precisely coincides with (5.23), which was obtained in [151, 156] by imposing the symmetry between σ_1 and σ_2 .

The other possibility is to choose the representation $[1, 1]$ of \mathcal{S}_2 in which the two spins, σ_1 and σ_2 , are antisymmetric. We therefore define the corresponding normalised tensor $t_a^{[Q-1,1],[1,1]}$:

$$\begin{aligned} t_a^{[Q-1,1],[1,1]} &\equiv \frac{Q-1}{Q-2} (t_a^{[Q-1,1],1} - t_a^{[Q-1,1],2}) \\ &= \sum_{\substack{i=1 \\ i \neq a}}^Q (\mathcal{O}_{i,a} - \mathcal{O}_{a,i}). \end{aligned} \quad (5.32)$$

In terms of the spins this observable reads simply:

$$t_a^{[Q-1,1],[1,1]}(\sigma_1, \sigma_2) = \begin{cases} \delta_{\sigma_1, a} - \delta_{\sigma_2, a} & \text{for } \sigma_1 \neq \sigma_2, \\ 0 & \text{for } \sigma_1 = \sigma_2. \end{cases} \quad (5.33)$$

This is our first example of a non-scalar observable (operator) that was not considered in the previous work [156].

It is straightforward to satisfy that the subsets

$$\{t_a^{[Q-1,1],[2]} : a = 1, \dots, Q\} \quad (5.34)$$

and

$$\{t_a^{[Q-1,1],[1,1]} : a = 1, \dots, Q\} \quad (5.35)$$

are indeed stable under the action of \mathcal{S}_Q , and of dimension $Q - 1$. We can rewrite the definition of both observables using an irreducible symmetriser of \mathcal{S}_N (here with $N = 2$) as

$$t_a^{[Q-1,1],\lambda_N} = \frac{1}{\mathcal{N}} e_{\lambda_Q}^{(a)} \tilde{e}_{\lambda_N}^{(a)} \mathcal{O}_{a, i_{Q-1}}, \quad (5.36)$$

where \mathcal{N} is a normalisation constant. The operator $\tilde{e}_{\lambda_N}^{(a)}$ acts according to (5.3) and is the irreducible symmetriser of the following Young tableau (depending on the two possible choices of λ_N):

$$\begin{array}{|c|c|} \hline 1 & 2 \\ \hline \end{array} \quad \text{or} \quad \begin{array}{|c|} \hline 1 \\ \hline 2 \\ \hline \end{array} \quad (5.37)$$

Representation $[Q-2, 2]$. We now construct the tensors with 2 symmetric indices acting on 2 spins. This corresponds to the Young diagram $\lambda_Q = [Q-2, 2]$. Let us consider the following tableau

$$\begin{array}{|c|c|c|c|} \hline i_1 & i_2 & \dots & i_{Q-2} \\ \hline a_1 & a_2 & & \\ \hline \end{array} \quad (5.38)$$

where we again denote the permutation associated with this configuration by a . The irreducible symmetriser is

$$e_{[Q-2,2]}^{(a)} = \left(\sum_{h \in \tilde{h}_\lambda^{(a)}} h \right) (1 + (a_1, a_2)) (1 - (i_1, a_1)) (1 - (i_2, a_2)) , \quad (5.39)$$

where $\tilde{h}_\lambda^{(a)}$ now denotes the subset of \mathcal{S}_Q consisting of all the permutations that leave a_1 and a_2 invariant. To generate the tensor we act with the irreducible symmetriser on \mathcal{O}_{a_1, a_2} :

$$\begin{aligned} e_{[Q-2,2]}^{(a)} \mathcal{O}_{a_1, a_2} &= \left(\sum_{h \in \tilde{h}_\lambda^{(a)}} h \right) (\mathcal{O}_{a_1, a_2} + \mathcal{O}_{a_2, a_1} - \mathcal{O}_{a_1, i_2} - \mathcal{O}_{a_2, i_2} - \mathcal{O}_{i_1, a_2} - \mathcal{O}_{i_1, a_1} + 2\mathcal{O}_{i_1, i_2}) \\ &= (Q-2)! (\mathcal{O}_{a_1, a_2} + \mathcal{O}_{a_2, a_1}) - (Q-3)! \sum_{\substack{i=1 \\ i \neq a_1, a_2}}^Q (\mathcal{O}_{a_1, i} + \mathcal{O}_{a_2, i} + \mathcal{O}_{i, a_2} + \mathcal{O}_{i, a_1}) \\ &\quad + 2(Q-4)! \sum_{\substack{i, j=1 \\ i \neq j \\ i, j \neq a_1, a_2}}^Q \mathcal{O}_{i, j} . \end{aligned}$$

To get a nice expression we need to complete each sum with the missing terms, leading us to different prefactors. We normalise the resulting observable and define the corresponding tensor $t_{a_1, a_2}^{[Q-2,2]}$. The end result is:

$$\begin{aligned} t_{a_1, a_2}^{[Q-2,2]} &= \mathcal{O}_{a_1, a_2} + \mathcal{O}_{a_2, a_1} - \frac{1}{Q-2} \left(\sum_{\substack{i=1 \\ i \neq a_1}}^Q (\mathcal{O}_{a_1, i} + \mathcal{O}_{i, a_1}) + \sum_{\substack{i=1 \\ i \neq a_2}}^Q (\mathcal{O}_{a_2, i} + \mathcal{O}_{i, a_2}) \right) \\ &\quad + \frac{2}{(Q-1)(Q-2)} \sum_{\substack{i, j=1 \\ i \neq j}}^Q \mathcal{O}_{i, j} . \end{aligned} \quad (5.40)$$

Note that despite of (5.38), this expression can be extended to any values a_1, a_2 , provided that $a_1 \neq a_2$, by permuting the indices as required. The explicit expression of this tensor, omitting an overall factor of $(1 - \delta_{\sigma_1, \sigma_2})$, is

$$\begin{aligned} t_{a_1, a_2}^{[Q-2,2]}(\sigma_1, \sigma_2) &= \delta_{a_1, \sigma_1} \delta_{a_2, \sigma_2} + \delta_{a_2, \sigma_1} \delta_{a_1, \sigma_2} \\ &\quad - \frac{1}{Q-2} (\delta_{a_1, \sigma_1} + \delta_{a_1, \sigma_2} + \delta_{a_2, \sigma_1} + \delta_{a_2, \sigma_2}) + \frac{2}{(Q-1)(Q-2)} . \end{aligned} \quad (5.41)$$

This coincides with (5.24), as first found in [151, 156]. It is readily checked that the subspace $\left\{ t_{a_1, a_2}^{[Q-2, 2]} : 1 \leq a_1 \neq a_2 \leq Q \right\}$ has the correct dimension $Q(Q-3)/2$, as given by the hook formula (5.7) applied to the Young tableau $[Q-2, 2]$.

It should be stressed that to obtain (5.41) we did not specify any representation of S_2 for the spins σ_1 and σ_2 . Indeed, for this tensor the chosen representations of \mathcal{S}_Q and \mathcal{S}_N are not independent: we cannot find observables with symmetric indices a_1, a_2 which are not symmetric for the spins σ_1, σ_2 as well. In fact, the symmetry of the spins σ is partially or totally dictated by the Young diagram λ_Q with the first line removed. The general result about the relation between the \mathcal{S}_Q and \mathcal{S}_N symmetries will be stated below.

Observables with anti-symmetric indices. To complete the discussion of observables of $N = 2$ spins, we finally consider the tensors with two anti-symmetric indices. They correspond to the irreducible representation $[Q-2, 1, 1]$. Let us consider the following Young tableau

$$\begin{array}{|c|c|c|c|} \hline i_1 & i_2 & \dots & i_{Q-2} \\ \hline a_1 & & & \\ \hline a_2 & & & \\ \hline \end{array} \tag{5.42}$$

with its corresponding irreducible symmetriser:

$$e_{[Q-2, 1, 1]}^{(a)} = \left(\sum_{h \in \tilde{h}_\lambda^{(a)}} h \right) (1 - (i_1, a_1) - (i_1, a_2) - (a_1, a_2) + (i_1, a_1, a_2) + (i_1, a_2, a_1)) , \tag{5.43}$$

where $\tilde{h}_\lambda^{(a)}$ denotes the subset of \mathcal{S}_Q consisting of all permutations that leave a_1 and a_2 invariant. We recall that we represent a permutation in terms of its cycles. Thus, for instance, (a, b, c) is the permutation that cyclically permutes a, b and c and leaves invariant all other elements. Acting on \mathcal{O}_{a_1, a_2} yields

$$\begin{aligned}
 e_{[Q-2, 1, 1]}^{(a)} \mathcal{O}_{a_1, a_2} &= (Q-2)! (\mathcal{O}_{a_1, a_2} - \mathcal{O}_{a_2, a_1}) - (Q-3)! \sum_{\substack{i=1 \\ i \neq a_1, a_2}}^Q (\mathcal{O}_{a_1, i} - \mathcal{O}_{i, a_1} + \mathcal{O}_{i, a_2} - \mathcal{O}_{a_2, i}) \\
 &= Q(Q-3)! (\mathcal{O}_{a_1, a_2} - \mathcal{O}_{a_2, a_1}) \\
 &\quad - (Q-3)! \sum_{\substack{i=1 \\ i \neq a_1}}^Q (\mathcal{O}_{a_1, i} - \mathcal{O}_{i, a_1}) - (Q-3)! \sum_{\substack{i=1 \\ i \neq a_2}}^Q (\mathcal{O}_{i, a_2} - \mathcal{O}_{a_2, i}) .
 \end{aligned}$$

We define the corresponding normalised observable $t_{a_1, a_2}^{[Q-2, 1, 1]}$:

$$\begin{aligned}
 t_{a_1, a_2}^{[Q-2, 1, 1]} &= \frac{1}{Q(Q-3)!} e_{[Q-2, 1, 1]}^{(a)} \mathcal{O}_{a_1, a_2} \\
 &= \mathcal{O}_{a_1, a_2} - \mathcal{O}_{a_2, a_1} - \frac{1}{Q} \left(\sum_{\substack{i=1 \\ i \neq a_1}}^Q (\mathcal{O}_{a_1, i} - \mathcal{O}_{i, a_1}) + \sum_{\substack{i=1 \\ i \neq a_2}}^Q (\mathcal{O}_{i, a_2} - \mathcal{O}_{a_2, i}) \right) .
 \end{aligned} \tag{5.44}$$

Omitting again the factor $(1 - \delta_{\sigma_1, \sigma_2})$, the explicit expression corresponding to (5.44) is

$$t_{a_1, a_2}^{[Q-2, 1, 1]}(\sigma_1, \sigma_2) = \delta_{\sigma_1, a_1} \delta_{\sigma_2, a_2} - \delta_{\sigma_1, a_2} \delta_{\sigma_2, a_1} - \frac{1}{Q} (\delta_{\sigma_1, a_1} - \delta_{\sigma_1, a_2} + \delta_{\sigma_2, a_2} - \delta_{\sigma_2, a_1}). \quad (5.45)$$

Also in this case the representation of \mathcal{S}_Q here fully enforces the symmetry between the spins. This is a consequence of the fact that the number of boxes under the first line of $[Q - 2, 1, 1]$ is 2 and equal to the number of spins.

Decomposition of $L_Q^{(2)}$. In the end we have the following decomposition of observables of 2 spins:

$$L_Q^{(2)} = \underbrace{[Q] \oplus [Q - 1, 1]}_{L_Q^{(1)}} \oplus [Q] \oplus \underbrace{[Q - 1, 1]}_{[2]} \oplus \underbrace{[Q - 1, 1]}_{[1, 1]} \oplus [Q - 2, 2] \oplus [Q - 2, 1, 1]. \quad (5.46)$$

The total dimension is seen to be Q^2 , as it should. Two new observables were constructed, namely $t_{a_1, a_2}^{[Q-2, 1, 1]}$ and $t_a^{[Q-1, 1], [1, 1]}$. These observables were not discussed in [151, 156], and omitting their contribution to (5.46) would give the dimension $Q(Q + 1)/2$, corresponding to the number of generators of symmetric $Q \times Q$ matrices. Similarly, the contribution of the two new observables to the dimension is $Q(Q - 1)/2$, that is, the number of generators of anti-symmetric $Q \times Q$ matrices.

5.1.5 Procedure for general representations

The case of observables of 2 spins in the representation $[Q - 1, 1]$ highlighted the need of taking into account the representation of the group \mathcal{S}_N that dictates the symmetries of the N spins. We need to be careful when choosing a representation of \mathcal{S}_N because the representation λ_Q already imposes symmetry constraints. We recall in particular the case $[Q - 2, 2]$ involving 2 spins, where the constructed tensor (5.41) automatically came out as being symmetric in σ_1 and σ_2 , whereas the tensor of representation $[Q - 1, 1]$ acting on 2 spins did not impose any \mathcal{S}_2 symmetry, which therefore needed to be subsequently imposed.

Let us consider now a Young diagram λ_Q containing $Q - n$ boxes in the first row and a total of n boxes in the remaining rows. From this diagram we are going to define a tensor with n indices a_1, \dots, a_n . We would like to define an observable of N spins. This is obviously only possible if $N \geq n$, since we need a sufficient number of spins to act upon.

Primal operator. If the condition $n = N$ is satisfied, the symmetry of the spins σ_i is entirely dictated by the Young diagram of shape λ_Q with the first row removed. In this case we do not need to specify any λ_N representation. We shall call such an observable/operator *primal*. We consider the Young tableau of shape λ_Q where we insert all of the indices a_1, \dots, a_N in the boxes under the first row of λ_Q . This define a Young operator (irreducible symmetriser) via (5.5). We impose that $a_1 \neq a_2 \neq \dots \neq a_N$ in order to avoid redundancy with other representations, but we can relax this constraint in principle.

We now define the tensor $t_{a_1, \dots, a_N}^{\lambda_Q}$ such that

$$t_{a_1, \dots, a_N}^{\lambda_Q} = \frac{1}{\mathcal{N}} e_{\lambda_Q}^{(a)} \mathcal{O}_{a_1, \dots, a_N}, \quad (5.47)$$

where \mathcal{N} is an overall normalisation factor. Of course the normalisation is not fixed by representation theory and must be conveniently chosen (see later).

Secondary operator. If $N > n$, we need to specify as well the Young diagram λ_N that fixes the \mathcal{S}_N representation. The corresponding observable/operator will be referred to as *secondary*. In order to obtain a non-zero tensor, λ_N must obey a rule of consistency. Let us denote by $\widetilde{\lambda}_Q$ the Young diagram built from λ_Q by removing its first row. We need to have the inclusion $\widetilde{\lambda}_Q \subseteq \lambda_N$, or, in other words, $\widetilde{\lambda}_Q$ must be obtained by removing some boxes of λ_N . We fix the representation of \mathcal{S}_N by acting with the corresponding projector $\tilde{e}_{\lambda_N}^{(a)}$, as in (5.36). In order to be coherent with the \mathcal{S}_Q representation we need to change the definition of the latter projector with respect to (5.5). We take, only for the \mathcal{S}_N representation, the following definition: $\tilde{e}_{\lambda_N}^{(a)} = a_{\lambda_N}^{(a)} s_{\lambda_N}^{(a)}$, where we note that the order of symmetrisation and anti-symmetrisation is now the opposite of that used in (5.5) (whence the tilde). Note that for the previous case of \mathcal{S}_2 (5.36) the two choices are equivalent. The operator $t_{a_1, \dots, a_n}^{\lambda_Q, \lambda_N}$ is then defined by

$$t_{a_1, \dots, a_n}^{\lambda_Q, \lambda_N} = \frac{1}{\mathcal{N}} e_{\lambda_Q}^{(a)} \tilde{e}_{\lambda_N}^{(a)} \mathcal{O}_{a_1, \dots, a_n, b_1, \dots, b_{N-n}}, \quad (5.48)$$

where \mathcal{N} is an overall normalisation factor and b_1, \dots, b_{N-n} is a set of unspecified indices. Once again, the normalisation is not fixed by representation theory, but is conveniently chosen so that the observable stays finite when Q goes to infinity. We impose that $a_1 \neq a_2 \neq \dots \neq a_n \neq b_1 \neq \dots \neq b_{N-n}$ in order to avoid redundancy with other representations, but again we can relax this constraint in principle.

We still need to specify the Young tableaux corresponding to the shapes λ_Q and λ_N . First for λ_Q , we order a_1, \dots, a_N in the boxes strictly below the first row and place all the remaining values (including the b 's) in the first row. The exact values of the b 's are not important, since we symmetrise the indices which do not appear in the set $\{a_1, \dots, a_n\}$.

Let us give an example with $\lambda_Q = [Q - 3, 2, 1]$. The tensors have 3 indices, a_1, a_2 and a_3 , and the Young tableau has the form

$$\begin{array}{|c|c|c|c|c|}
 \hline
 & & & \dots & \\
 \hline
 a_1 & a_2 & & & \\
 \hline
 a_3 & & & & \\
 \hline
 \end{array} \quad (5.49)$$

The tableau of shape λ_N must respect the inner symmetry between $\sigma_1, \dots, \sigma_n$ induced by λ_Q . As previously discussed, the n first spins (among the N defining the tensor) have already acquired a given symmetry, due to the action of λ_Q . To construct the tableau λ_N , we thus

place the n first indices as if we were considering the previous tableau of \mathcal{S}_Q with its first row removed, and we choose an arbitrary index for each of the remaining $N - n$ boxes. For instance, if we want to act on $N = 5$ spins with symmetry $[3, 2]$ of \mathcal{S}_N with a tensor belonging to the \mathcal{S}_Q representation $[Q - 3, 2, 1]$, we would have to choose a tableau of the following type

$$\begin{array}{|c|c|c|} \hline 1 & 2 & \\ \hline 3 & & \\ \hline \end{array} \tag{5.50}$$

and put arbitrarily the indices 4 and 5 in the blank boxes.

Consistency between \mathcal{S}_Q and \mathcal{S}_N representations. Even though the symmetries \mathcal{S}_N and \mathcal{S}_Q are different, they interact with each other and the two Young diagrams that we use to define a tensor must somehow be *compatible*. Consider a tensor acting on N spins with a given symmetry \mathcal{S}_N associated to a Young tableau λ_N . We take λ_Q to be a Young diagram with Q boxes and define $\tilde{\lambda}_Q$ as the diagram obtained by removing the boxes in the first line of λ_Q . A representation of \mathcal{S}_Q leads to a non-trivial result if $\tilde{\lambda}_Q$ can be obtained from λ_N by *removing at most one box in each column*.

For instance consider the Young diagram $\lambda_N = [2, 1]$. The only possible representations $\lambda_Q \in \mathcal{S}_Q$ that are compatible with λ_N are $[Q - 3, 2, 1]$, $[Q - 2, 2]$, $[Q - 2, 1, 1]$ and $[Q - 1, 1]$. There are no tensors in the representation $[Q]$ since to obtain the corresponding $\tilde{\lambda}_Q = \emptyset$ from λ_N we would have to remove 2 boxes from its the first column.

This consistency criterion can be understood from the following observation. Consider a pair of representations λ_N and λ_Q where λ_Q is not compatible with λ_N according to the previous rule. We construct a tensor t^{λ_Q, λ_N} from the following definition:

$$t^{\lambda_Q, \lambda_N} = e_{\lambda_Q} \tilde{e}_{\lambda_N} \mathcal{O}_{a_1, a_2, \dots, a_N}. \tag{5.51}$$

In general, \tilde{e} is given by its definition in terms of the action of permutations of \mathcal{S}_N but if we act first with \tilde{e} we can write this operator in terms of permutations of \mathcal{S}_Q . We can interpret \tilde{e}_{λ_N} a sort of Young operator with a tableau of N boxes filled with the indices a_1, \dots, a_N instead of the indices $1, \dots, N$.

For the sake of illustration, we consider $\lambda_N = [2, 2]$ and $\lambda_Q = [Q - 2, 1, 1]$. The tensor reads

$$t^{\lambda_Q, \lambda_N} = e_{\lambda_Q} \tilde{e}_{\lambda_N} \mathcal{O}_{a_1, a_2, i_{Q-3}, i_{Q-4}} \tag{5.52}$$

and we use the following tableaux

$$\begin{array}{|c|c|c|c|} \hline i_1 & i_2 & \dots & i_{Q-2} \\ \hline a_1 & & & \\ \hline a_2 & & & \\ \hline \end{array} \quad \begin{array}{|c|c|} \hline 1 & 3 \\ \hline 2 & 4 \\ \hline \end{array} \tag{5.53}$$

for \mathcal{S}_Q and \mathcal{S}_N respectively. We can write \tilde{e} as permutations of \mathcal{S}_Q with the operator associated to

$$\begin{array}{|c|c|} \hline a_1 & i_{Q-3} \\ \hline a_2 & i_{Q-2} \\ \hline \end{array} \quad (5.54)$$

Of course this tableau is not a Young tableaux corresponding to a representation of \mathcal{S}_Q , but it defines an operator with permutations in a subgroup of \mathcal{S}_Q equivalent to \mathcal{S}_4 .

Since λ_Q is not compatible with λ_N , there are 2 indices a_i and a_j that are anti-symmetrised by \tilde{e} but belong to the first line of the tableau defining e_{λ_Q} (here i_{Q-3} and i_{Q-2}). We consider Q large enough, so that those indices are pushed by definition somewhere in the first row of the tableau of shape λ_Q . This means that they are first antisymmetrised by \tilde{e}_{λ_N} and then symmetrised by e_{λ_Q} . The result of these operations is exactly the null tensor, and hence justifies the consistency rule.

It is obvious that the argument carries over to the general case. If λ_N contains a column having at least two more boxes than $\widetilde{\lambda}_Q$, then the corresponding indices will be antisymmetrised by \tilde{e}_{λ_N} and symmetrised by e_{λ_Q} , so that $t^{\lambda_Q, \lambda_N} = 0$ in (5.51).

5.1.6 Internal structure and LCFT

The structure of observables acting symmetrically on all their spins was initiated in [151] and fully discussed in [156]. The logarithmic features of the LCFT that arise in the continuum limit were studied by analysing how the divergences in the definition of the operators could be removed by mixing operators of the same scaling limit into Jordan cells.

For instance, the 2-cluster operator with Young tableau $[Q-2, 2]$ acting on $N=2$ spins is ill-defined for particular values of Q , as witnessed by the poles on the right-hand side of (5.41). The mechanism explaining the logarithmic nature of correlation functions cures those divergences by mixing two operators [151, 156]. For instance, (5.41) can be put into the form

$$t_{a,b}^{[Q-2,2]} = \mathcal{O}_{a_1, a_2} + \mathcal{O}_{a_2, a_1} - \frac{1}{Q-2} \left(t_a^{[Q-1,1],[2]} + t_b^{[Q-1,1],[2]} \right) - \frac{2}{Q(Q-1)} t^{[Q]}, \quad (5.55)$$

in which the operator is obtained from the basis elements (5.1) by subtracting off components that belong to tensors with another symmetry. The equation (5.55) is ill-defined for percolation ($Q=1$) and this observation leads to the prediction that $t_{a,b}^{[Q-2,2]}$ is mixed with the energy operator $t^{[Q]}$ (5.25) in a Jordan cell of the dilatation operator for the CFT describing percolation.

In order to make further progress on the LCFT structure of the Potts model we need to decompose all operators in a similar way. Consider a primal operator corresponding to a Young diagram λ_Q . All the tensors that are subtracted are called in the following subtensors and obey a simple rule. To be a subtensor (associated with a primal), its Young diagram λ'_Q must be obtained by removing boxes of λ_Q from the rows 2, 3, ... and adding them to the first row. In particular, the subtensors are secondary to the primal from which they are subtracted. For example, in the case of $\lambda_Q = [Q-3, 2, 1]$ all the Young diagram satisfying this condition are $[Q-2, 2]$, $[Q-2, 1, 1]$, $[Q-1, 1]$ and $[Q]$. Moreover, if a subtensor corresponds

to a diagram where *two or more* boxes were removed in the *same* column of λ_Q it would not appear in the structure of the primal. In the example of $\lambda_Q = [Q - 3, 2, 1]$, there is thus no subtensor with the symmetry of $\lambda'_Q = [Q]$ because in order to go from λ_Q to λ'_Q two boxes must be removed from the first column. This requirement can be understood in terms of anti-symmetrisation/symmetrisation in the associated Young operator, using an argument similar to the one given in section 5.1.5.

The subtensors have the same λ_N symmetry as the primal from which they are subtracted. Recall that we do not always need to express the λ_N symmetry explicitly; see (5.55) for an example. In particular, for a primal operator, λ_N is simply obtained by removing the first row of λ_Q .

The internal structure that generalises (5.55) can thus be written in the symbolic form

$$t^{\lambda_Q} = (\mathcal{O}) - \sum_{\lambda'_Q} \frac{1}{A_{\lambda_Q, \lambda'_Q}(Q)} t^{\lambda'_Q} \quad (5.56)$$

where the sum is over all the Young diagram satisfying the subtensor condition given above, $A_{\lambda_Q, \lambda'_Q}(Q)$ is a ratio of polynomials in Q , and (\mathcal{O}) is a combination of basis elements (5.1) that does not depend on Q and whose exact form dictated by the Young tableau λ_Q of the primal operator.

The exact form of (\mathcal{O}) and $t^{\lambda'_Q}$ can be computed in terms of Young operators, but it is actually not necessary to do those explicit computations in order to make LCFT predictions. Rather, only the zeros of the functions $A_{\lambda_Q, \lambda'_Q}(Q)$ are needed in order to understand the mixing between operators.

For two Young diagrams $\lambda^1 = [\lambda_0^1, \lambda_1^1, \dots, \lambda_N^1]$ and $\lambda^2 = [\lambda_0^2, \lambda_1^2, \dots, \lambda_N^2]$, where λ_j^i denotes the number of boxes⁶ in the $(j + 1)$ -th row of λ^i , we conjecture that—up to a multiplicative constant—the polynomial function $A_{\lambda^1, \lambda^2}(Q)$ is

$$A_{\lambda^1, \lambda^2}(Q) \propto \prod_{i=1}^N \frac{(Q - n + i - 1 - \lambda_i^2)!}{(Q - n + i - 1 - \lambda_i^1)!} \quad (5.57)$$

The multiplicative constant depends on the normalisation convention that we use in our definition (5.48).

The amount of evidence supporting the conjecture (5.57) will be discussed in section 5.2.4 below.

5.2 Correlation functions

We now compute the two-point functions of the observables that we constructed in section 5.1 from symmetry considerations. The dependence of the correlation functions on the tensorial indices is fully determined by the irreducible representations of the group \mathcal{S}_Q . All the results

⁶We use the convention of padding with zeros. More precisely, if λ^i has $n + 1$ rows with $n < N$, we set $\lambda_j^i = 0$ for $j > n + 1$.

will be related to the probability that two groups of spins, each comprising N spins, are connected together by FK clusters in a particular way.

For the purpose of taking the continuum limit, and for the physical interpretation as a two-point function to make sense, we imagine that each group of spins is confined to a small neighbourhood on the lattice. It should nevertheless be stressed that this constraint is completely irrelevant for the applicability of the representation theory. For simplicity, we consider only observables that vanish if two spins are equal, and so an FK cluster can at most contain one spin from each group.

Let us introduce the notation used all along this section. Consider a correlation function of two observables, each of which acts on a group of N spins situated in a small neighbourhood, centered at two points in space, that we denote r_1 and r_2 respectively. The correlations will involve the geometrical probability that some pairs of spins—always one from each neighbourhood—are connected in an FK cluster. In order to represent such a probability we draw two groups of N dots, the first group representing the spins $\sigma_1^{(r_1)}, \dots, \sigma_N^{(r_1)}$ near r_1 , and the other $\sigma_1^{(r_2)}, \dots, \sigma_N^{(r_2)}$ near r_2 . We draw a line between one spin at r_1 and one spin at r_2 if they belong to the same FK cluster. Of course two spins in the same neighbourhood cannot be connected, since we consider exclusively observables that vanish if anyone of the N spins acted upon coincide.

For instance, let us illustrate this with a tensor $t(\sigma_1, \sigma_2, \sigma_3)$ acting on $N = 3$ spins and its two-point correlation function $\langle t(r_1)t(r_2) \rangle$. The symbol $\mathbb{P} \left(\begin{array}{c} \cdot \\ \cdot \\ \cdot \\ \cdot \end{array} \right)$ denotes the probability of the following situation: the spin $\sigma_1^{(r_1)}$ and the spin $\sigma_2^{(r_2)}$ are not connected to the four others through an FK cluster, whereas $\sigma_2^{(r_1)}$ (resp. $\sigma_3^{(r_1)}$) and $\sigma_1^{(r_2)}$ (resp. $\sigma_3^{(r_2)}$) are in the same FK cluster. This geometrical dependence, of major importance for the physical system, will depend on all the information concerning the lattice, in particular the number of dimensions d in which it lives. Unfortunately, computing such a quantity exactly for very general cases is out of reach,⁷ but thanks to representation theory, and later scale invariance, we are still able to understand some features.

In order to compute the correlation function between two observables, we list all possible connectivities and compute their respective amplitudes. The average is taken by summing the explicit expressions of the product of observables over independent groups of spins. In other words, if two spins are connected by an FK cluster, we set them equal, and the average is taken by independently summing over the resulting set of FK clusters.

Our results comprise the two-point correlation functions found in [156], except that we now extend the procedure to our new, non-scalar operators. We will find interesting properties that do not appear when one considers only symmetric observables. On the other hand, [156] discussed also some cases of three-point correlation functions—although this can also be done in the present context, we have chosen to focus on two-point functions only.

⁷Exact expressions exist for simple cases in two dimensions, such as for the Ising model. But even this is often restricted to specific regular lattices (such as the square lattice) with specific boundary conditions (free, cylindrical, toroidal, *etc*). However, in $d = 2$, CFT can often predict the power-law asymptotic form of such correlation functions, and this turns out to be universal (i.e., independent of lattice details). The appearance of logarithms will be discussed below.

Let us first investigate the simplest new case corresponding to an anti-symmetric tensor acting on 2 spins. This example will also serve to illustrate the way in which correlation functions are computed. We will then comment briefly on the case of tensors with mixed symmetry (i.e., neither fully symmetric, nor fully anti-symmetric).

5.2.1 Symmetric observables of two spins

The two-point function of the 2-cluster operator was computed in [151, 156]. We compute it again here in order to illustrate the method and emphasise a particular feature. Let us thus consider the average

$$\left\langle t_{a_1, a_2}^{[Q-2, 2]}(\sigma_1, \sigma_2) t_{b_1, b_2}^{[Q-2, 2]}(\sigma_3, \sigma_4) \right\rangle. \quad (5.58)$$

We first compute the amplitude over the probability that σ_1 and σ_3 are in the same cluster, but that σ_2 and σ_4 are in distinct independent clusters. This probability is represented by $\mathbb{P}\left(\begin{array}{c} \bullet \\ \bullet \\ \bullet \\ \bullet \end{array}\right)$. Its amplitude is

$$\frac{1}{Q^3} \sum_{\sigma_1, \sigma_2, \sigma_4} t_{a_1, a_2}^{[Q-2, 2]}(\sigma_1, \sigma_2) t_{b_1, b_2}^{[Q-2, 2]}(\sigma_1, \sigma_4) = 0 \quad (5.59)$$

The computation is straightforward; one only needs to insert the expression (5.41) and remember that $t^{[Q-2, 2]}(\sigma_1, \sigma_2) = 0$ when $\sigma_1 = \sigma_2$.⁸ Computing in the same way the amplitude of each possible probability of having the 4 spins connected in any specific way, we see that only two amplitude are non-zero. They correspond to the probabilities $\mathbb{P}\left(\begin{array}{c} \bullet \\ \bullet \\ \bullet \\ \bullet \end{array}\right)$ and $\mathbb{P}\left(\begin{array}{c} \bullet \\ \bullet \\ \bullet \\ \bullet \end{array}\right)$. They have the same amplitude, which is

$$\begin{aligned} & \frac{1}{Q^2} \sum_{\sigma_1, \sigma_2} t_{a_1, a_2}^{[Q-2, 2]}(\sigma_1, \sigma_2) t_{b_1, b_2}^{[Q-2, 2]}(\sigma_1, \sigma_2) = \\ & \frac{2}{Q^2} \left(\delta_{a_1, b_1} \delta_{a_2, b_2} + \delta_{a_1, b_2} \delta_{a_2, b_1} - \frac{1}{Q-2} \left(\delta_{a_1, b_1} + \delta_{a_2, b_2} + \delta_{a_1, b_2} + \delta_{a_2, b_1} \right) + \frac{2}{(Q-2)(Q-1)} \right). \end{aligned}$$

In the end the correlation function is

$$\begin{aligned} & \left\langle t_{a_1, a_2}^{[Q-2, 2], [2]}(r_1) t_{b_1, b_2}^{[Q-2, 2], [2]}(r_2) \right\rangle = \frac{2}{Q^2} \left(\delta_{a_1, b_1} \delta_{a_2, b_2} + \delta_{a_1, b_2} \delta_{a_2, b_1} \right. \\ & \left. - \frac{1}{Q-2} \left(\delta_{a_1, b_1} + \delta_{a_2, b_2} + \delta_{a_1, b_2} + \delta_{a_2, b_1} \right) + \frac{2}{(Q-2)(Q-1)} \right) \left(\mathbb{P}\left(\begin{array}{c} \bullet \\ \bullet \\ \bullet \\ \bullet \end{array}\right) + \mathbb{P}\left(\begin{array}{c} \bullet \\ \bullet \\ \bullet \\ \bullet \end{array}\right) \right), \quad (5.60) \end{aligned}$$

where r_1 and r_2 are respectively the position of the neighbourhood of (σ_1, σ_2) and (σ_3, σ_4) .

5.2.2 Anti-symmetric observables of two spins

Next consider the correlation function for a tensor with $N = 2$ spins in the symmetry corresponding to the representation of \mathcal{S}_N given by the anti-symmetric Young tableau [1, 1].

⁸Alternatively, one simply notices that $\sum_{\sigma_2} t_{a_1, a_2}^{[Q-2, 2]}(\sigma_1, \sigma_2) = 0$.

It can be computed using the same procedure as above. Note that in the decomposition of $t_{a,b}^{[Q-2,1,1],[1,1]}$ given by (5.45) appears the subtensor $t_a^{[Q-1,1],[1,1]}$ given by (5.33); the latter corresponds to a tensor in the standard representation, but acting on two anti-symmetric spins.⁹ We also compute its correlation function for completeness. We find

$$\begin{aligned} & \left\langle t_a^{[Q-1,1],[1,1]}(r_1) t_b^{[Q-1,1],[1,1]}(r_2) \right\rangle = & (5.61) \\ & \frac{1}{Q} \left(\delta_{a,b} - \frac{1}{Q} \right) \left(2 \mathbb{P} \left(\begin{array}{c} \uparrow \\ \uparrow \\ \uparrow \end{array} \right) - 2 \mathbb{P} \left(\begin{array}{c} \times \\ \times \\ \times \end{array} \right) + \left(\mathbb{P} \left(\begin{array}{c} \uparrow \\ \cdot \\ \cdot \end{array} \right) + \mathbb{P} \left(\begin{array}{c} \cdot \\ \uparrow \\ \cdot \end{array} \right) - \mathbb{P} \left(\begin{array}{c} \times \\ \cdot \\ \cdot \end{array} \right) - \mathbb{P} \left(\begin{array}{c} \cdot \\ \times \\ \cdot \end{array} \right) \right) \end{aligned}$$

$$\left\langle t_{a_1, a_2}^{[Q-2,1,1],[1,1]}(r_1) t_{b_1, b_2}^{[Q-2,1,1],[1,1]}(r_2) \right\rangle = & (5.62)$$

$$\begin{aligned} & \frac{8}{Q^2} \left(\delta_{a_1, b_1} \delta_{a_2, b_2} - \delta_{a_1, b_2} \delta_{a_2, b_1} - \frac{1}{Q} \left(\delta_{a_1, b_1} + \delta_{a_2, b_2} - \delta_{a_1, b_2} - \delta_{a_2, b_1} \right) \right) \left(\mathbb{P} \left(\begin{array}{c} \uparrow \\ \uparrow \\ \uparrow \end{array} \right) - \mathbb{P} \left(\begin{array}{c} \times \\ \times \\ \times \end{array} \right) \right), \\ & \left\langle t_{a_1, a_2}^{[Q-2,1,1],[1,1]}(r_1) t_b^{[Q-1,1],[1,1]}(r_2) \right\rangle = 0. & (5.63) \end{aligned}$$

Before commenting on this result, let us again explain carefully how we can compute these quantities. Consider the two-point function $\left\langle t_{a_1, a_2}^{[Q-2,1,1],[1,1]}(r_1) t_{b_1, b_2}^{[Q-2,1,1],[1,1]}(r_2) \right\rangle$ of observables whose expression was computed previously in (5.45):

$$t_{a_1, a_2}^{[Q-2,1,1],[1,1]}(\sigma_1, \sigma_2) = \delta_{a_1, \sigma_1} \delta_{a_2, \sigma_2} - \delta_{a_1, \sigma_2} \delta_{a_2, \sigma_1} - \frac{1}{Q} \left(\delta_{a_1, \sigma_1} + \delta_{a_2, \sigma_2} - \delta_{a_1, \sigma_2} - \delta_{a_2, \sigma_1} \right).$$

When we compute the correlation function, three cases appear. First, supposing that the spins around r_1 are not connected to the spins around r_2 , the two-point function is proportional to the probability $\mathbb{P} \left(\begin{array}{c} \cdot \\ \cdot \\ \cdot \end{array} \right)$. The amplitude of this probability is obtained after averaging the product of the two tensors summed independently over all the spins:¹⁰

$$\frac{1}{Q^2} \sum_{\sigma_1, \sigma_2} t_{a_1, a_2}^{[Q-2,1,1],[1,1]}(\sigma_1, \sigma_2) \frac{1}{Q^2} \sum_{\sigma_3, \sigma_4} t_{b_1, b_2}^{[Q-2,1,1],[1,1]}(\sigma_3, \sigma_4) = 0. & (5.64)$$

The second case involves situations where a unique spin around r_1 is connected to another spin around r_2 . There are four such situations, related to $\mathbb{P} \left(\begin{array}{c} \uparrow \\ \cdot \\ \cdot \end{array} \right)$, $\mathbb{P} \left(\begin{array}{c} \cdot \\ \uparrow \\ \cdot \end{array} \right)$, $\mathbb{P} \left(\begin{array}{c} \cdot \\ \cdot \\ \uparrow \end{array} \right)$ and $\mathbb{P} \left(\begin{array}{c} \cdot \\ \cdot \\ \times \end{array} \right)$. Let us illustrate the first case. In order to compute the amplitude of this probability appearing in the correlation function, we need to consider the product

$$t_{a_1, a_2}^{[Q-2,1,1],[1,1]}(\sigma_1, \sigma_2) t_{b_1, b_2}^{[Q-2,1,1],[1,1]}(\sigma_3, \sigma_4), & (5.65)$$

average independently over σ_2 and σ_4 , and average over σ_1 and σ_3 with the constraint that they are in the same FK cluster (whence $\sigma_1 = \sigma_3$). It follows that

$$\frac{1}{Q^3} \sum_{\sigma_1, \sigma_2, \sigma_4} t_{a_1, a_2}^{[Q-2,1,1],[1,1]}(\sigma_1, \sigma_2) t_{b_1, b_2}^{[Q-2,1,1],[1,1]}(\sigma_1, \sigma_4) = 0. & (5.66)$$

⁹In this section we have set $t_{a,b}^{[Q-2,1,1],[1,1]} \equiv t_{a,b}^{[Q-2,1,1]}$, adding a superfluous $[1,1]$ to the general notation for extra clarity.

¹⁰Alternatively, one simply notices that $\sum_{\sigma_2} t_{a_1, a_2}^{[Q-2,1,1],[1,1]}(\sigma_1, \sigma_2) = 0$.

The corresponding amplitude in (5.62) is thus zero. However, if we consider the two-point correlation function involving two tensors $t_a^{[Q-2,1],[1,1]}$ as in (5.61), we find a non-trivial result for that same amplitude:

$$\frac{1}{Q^3} \sum_{\sigma_1, \sigma_2, \sigma_4} t_a^{[Q-1,1],[1,1]}(\sigma_1, \sigma_2) t_b^{[Q-1,1],[1,1]}(\sigma_1, \sigma_4) = \frac{1}{Q} \left(\delta_{a,b} - \frac{1}{Q} \right). \quad (5.67)$$

Finally, consider the case with two pairwise connections by FK clusters: $\mathbb{P} \left(\begin{array}{c} | \\ | \\ | \end{array} \right), \mathbb{P} \left(\begin{array}{c} \times \\ | \\ | \end{array} \right)$. Averaging the tensor product over the spins with these constraints, we get

$$\begin{aligned} & \frac{1}{Q^2} \sum_{\sigma_1, \sigma_2} t_{a_1, a_2}^{[Q-2,1,1],[1,1]}(\sigma_1, \sigma_2) t_{b_1, b_2}^{[Q-2,1,1],[1,1]}(\sigma_1, \sigma_2) = \\ & \frac{8}{Q^2} \left(\delta_{a_1, b_1} \delta_{a_2, b_2} - \delta_{a_1, b_2} \delta_{a_2, b_1} - \frac{1}{Q} \left(\delta_{a_1, b_1} + \delta_{a_2, b_2} - \delta_{a_1, b_2} - \delta_{a_2, b_1} \right) \right), \end{aligned} \quad (5.68)$$

or the same expression with the opposite sign if we permute σ_1 and σ_2 in one of the two tensors. Performing a similar computation for the two-point function of $t_a^{[Q-2,1],[1,1]}$ completes the proof of (5.61)–(5.62). The crossed correlator (5.63) of the two different tensors with $[1, 1]$ symmetry turns out to vanish identically.

We notice that an observable that corresponds to a representation of \mathcal{S}_Q having n tensorial indices, involves only probabilities that have at least n FK clusters. This result is generally true for any representation of \mathcal{S}_Q and \mathcal{S}_N (and was already noticed for the symmetric case in [156]). In particular, when a tensor acts on the minimum number of spins (i.e., when $n = N$), such as in (5.62), the result involves only probabilities with all the spins connected in a certain FK configuration. In other words, primal tensors of rank N (i.e., with N tensor indices) are precisely the N -cluster operators discussed in section 5.1.1, having a symmetry given by the corresponding Young diagram $\lambda_Q \in \mathcal{S}_Q$.

The major difference between (5.62) and the correlation function (5.60) found for the symmetric tensor with $N = 2$ [151, 156], is that the dominant term is not the probability to get a cluster that expands from 0 to r , but a sub-leading contribution to that probability. Indeed, the minus sign between the two FK diagrams cancels out the dominant power law decay of the two-cluster operator, leaving only a much smaller correction term. A similar situation will appear in the next section when we consider a mixed symmetry.

5.2.3 Observables with mixed symmetry: $[Q - 3, 2, 1]$

Briefly, and without giving the details of the computations, we present here the simplest case of mixed symmetry, namely the representation of \mathcal{S}_Q $[Q - 3, 2, 1]$ with $\lambda_N = [2, 1]$. After computation we find

$$\begin{aligned} & \left\langle t_{a_1, a_2, a_3}^{[Q-3,2,1],[2,1]}(r_1) t_{b_1, b_2, b_3}^{[Q-3,2,1],[2,1]}(r_2) \right\rangle = \\ & \frac{9}{Q^3} \left(\delta^3 + \frac{1}{2(Q-1)} \delta_s^2 - \frac{3}{2(Q-3)} \delta_a^2 + \frac{1}{(Q-1)(Q-3)} \delta^1 \right) \\ & \times \left(2 \mathbb{P} \left(\begin{array}{c} | \\ | \\ | \end{array} \right) + \mathbb{P} \left(\begin{array}{c} \times \\ | \\ | \end{array} \right) + \mathbb{P} \left(\begin{array}{c} | \\ \times \\ | \end{array} \right) - 2 \mathbb{P} \left(\begin{array}{c} \times \\ \times \\ | \end{array} \right) - \mathbb{P} \left(\begin{array}{c} \times \\ | \\ \times \end{array} \right) - \mathbb{P} \left(\begin{array}{c} \times \\ \times \\ \times \end{array} \right) \right), \end{aligned} \quad (5.69)$$

where δ_i^n is a short-hand notation for a sum of products of n Kronecker functions. The terms δ^3 , δ_s^2 , δ_a^2 and δ^1 involve respectively 6, 18, 8 and 9 terms.

Let us clarify the important features of this result. First, there is an overall (and rather unimportant) constant which is not fixed by symmetry considerations. This multiplies a factor containing an appropriate function of the tensor indices, and another factor which is an appropriate linear combination of FK probabilities. These two factors are entirely determined by the representation in which the tensor being considered lives. These factors are seen to be more complicated than in the fully symmetric case (5.60) or the anti-symmetric case (5.62). We notice that, as we have discussed before, since the considered tensor has an \mathcal{S}_Q representation that is fully redundant with its \mathcal{S}_N representation ($n = N$), we only get probabilities where all the spins at r_1 are connected through FK clusters to another spin at r_2 . In other words, there are no terms such as $\mathbb{P}\left(\begin{array}{c} \cdot \\ \cdot \\ \cdot \\ \cdot \\ \cdot \\ \cdot \end{array}\right)$ or $\mathbb{P}\left(\begin{array}{c} \cdot \\ \cdot \\ \cdot \\ \cdot \\ \cdot \\ \cdot \\ \cdot \end{array}\right)$, etc.

Again the mixed correlation functions of two observables, living in the same \mathcal{S}_N representation but with a different \mathcal{S}_Q symmetry, are exactly vanishing:

$$\begin{aligned} \left\langle t_{a_1, a_2, a_3}^{[Q-3, 2, 1], [2, 1]}(r_1) t_{b_1, b_2}^{[Q-2, 2], [2, 1]}(r_2) \right\rangle &= 0, \\ \left\langle t_{a_1, a_2, a_3}^{[Q-3, 2, 1], [2, 1]}(r_1) t_{b_1, b_2}^{[Q-2, 1, 1], [2, 1]}(r_2) \right\rangle &= 0, \\ \left\langle t_{a_1, a_2, a_3}^{[Q-3, 2, 1], [2, 1]}(r_1) t_b^{[Q-1, 1], [2, 1]}(r_2) \right\rangle &= 0. \end{aligned}$$

We can also compute the correlation functions involving the two other observables corresponding to the \mathcal{S}_Q representations $[Q - 3, 3]$ and $[Q - 3, 1, 1, 1]$. They again vanish:

$$\begin{aligned} \left\langle t_{a_1, a_2, a_3}^{[Q-3, 2, 1], [2, 1]}(r_1) t_{b_1, b_2, b_3}^{[Q-3, 3], [3]}(r_2) \right\rangle &= 0, \\ \left\langle t_{a_1, a_2, a_3}^{[Q-3, 2, 1], [2, 1]}(r_1) t_{b_1, b_2, b_3}^{[Q-3, 1, 1, 1], [1, 1, 1]}(r_2) \right\rangle &= 0. \end{aligned} \tag{5.70}$$

Let us mention that in general the correlation function between two observables in the *same* \mathcal{S}_Q representation but with a different λ_N Young tableaux is non-vanishing. When we compute $\left\langle t_{a_1, a_2}^{[Q-2, 2], [2, 1]}(r_1) t_{b_1, b_2}^{[Q-2, 2], [3]} \right\rangle$ we find a result with probabilities involving 2 propagating FK clusters. On the other hand, the vanishing of correlation functions between field in *different* \mathcal{S}_Q representations is consistent with general representation theoretical expectations.

5.2.4 Generic case

Considering the fact that (5.69) is the easiest two-point function of tensors with a mixed symmetry, it is clear that other cases cannot easily be computed by hand. We have therefore used exact symbolic computations in MATHEMATICA extensively in order to construct the tensors in higher representations and their corresponding two-point functions. In this way, we have computed all tensor acting on up to $N = 5$ spins. We have extensive evidence for the conjecture (5.57) since we are able to compute numerically the exact decomposition to obtain the poles.

For tensors corresponding to primal operators, the correlation function of two identical fields is generically found to be composed of two factors, apart from the overall normalisation. The first factor depends on the tensor indices and is entirely fixed by the chosen \mathcal{S}_Q representation. The second factor is a linear combination of probabilities that N distinct FK clusters propagate from one neighbourhood to the other, and where the order of the cluster end points depends also on the representation. This latter part depends on the specific lattice, and the dimension d . Computing the decay of this linear combination of probabilities determines the corresponding critical exponent, and is amenable to numerical work (see below). The required linear combination can be obtained for generic λ_N very easily by acting with the irreducible symmetriser \tilde{e}_{λ_N} on cluster end points.

5.3 Physical interpretation

5.3.1 Primal and secondary operators

In $d = 2$ dimensions, operators in conformal field theories can be classified as primaries, quasi-primaries and descendants, according to their covariance properties under (local) conformal transformations. In $d > 2$, the conformal algebra is finite-dimensional and strictly speaking operators are at most quasi-primaries. The operators that we labelled *primal* are believed to correspond to primaries in $d = 2$ or quasi-primaries in $d > 2$. This interpretation is supported by the vanishing two-point functions between two different primal operators. The operators labelled as secondary will in general correspond to descendants or sub-leading operators in $d > 2$.

There appears to be at least one exception to this general correspondence. The energy operator corresponds [156] to the secondary tensor discussed in section 5.1.4, with $\lambda_Q = [Q]$ and $\lambda_N = [2]$, which is well-known to be a primary operator in $d = 2$ CFT.

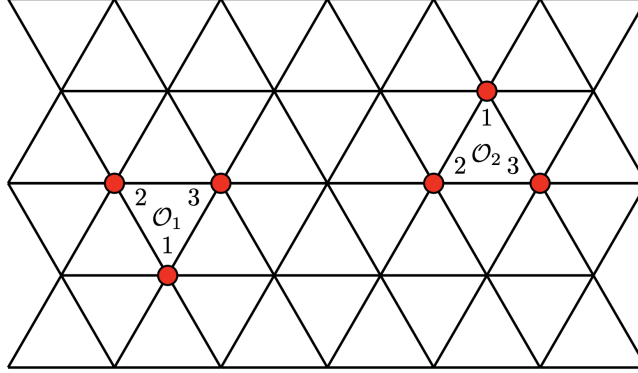
5.3.2 Critical exponents on a cylinder

In this section we discuss the identification of the tensors constructed in section 5.1 with conformal fields in $d = 2$ dimensions. The operators with $n = N$ that we have dubbed primal will be shown to correspond to primary fields in the sense of CFT. All the corresponding scaling dimensions will be identified exactly. We shall also see that the $d = 2$ case conceals a subtlety with respect to the case of arbitrary dimension, $d > 2$. Namely, depending on the precise lattice regularisation used to define the FK probabilities, that enter into the two-point correlators, it is in some cases possible to obtain different results for the critical exponents.

The key remark is that in $d = 2$, some configurations of connectivities between clusters are not possible. Consider the usual situation with two small neighbourhoods, \mathcal{D}_1 and \mathcal{D}_2 , each containing N spins. We shall suppose each neighbourhood \mathcal{D} to be a simply connected domain, and the N marked points to reside at its boundary $\partial\mathcal{D}$. On a given lattice, if the N marked points cover the boundary of \mathcal{D} sufficiently tightly, the FK cluster emanating from some particular marked point $i \in \partial\mathcal{D}$ will be unable to enter the interior of \mathcal{D} and exit it in-between two other marked points, j and k . Thus, since clusters cannot cross each other

in $d = 2$, this implies that the N marked FK clusters will only be able to permute cyclically in the space outside \mathcal{D} . In particular, the clusters cannot undergo arbitrary permutations.

To appreciate this remark, consider the specific example shown below, on the triangular lattice. We take each of \mathcal{D}_1 and \mathcal{D}_2 to consist of the 3 vertices around an elementary triangle. Consider now a pair of 3-cluster operators, \mathcal{O}_1 and \mathcal{O}_2 :



It is clear that in this setup the probabilities $\mathbb{P} \left(\begin{array}{c} \diagup \\ \diagdown \end{array} \right)$, $\mathbb{P} \left(\begin{array}{c} \diagdown \\ \diagup \end{array} \right)$ and $\mathbb{P} \left(\begin{array}{c} \diagup \\ \diagup \end{array} \right)$ are exactly 0. This would not be the case in higher dimensions, since the clusters could cross freely to realise arbitrary permutations, by “entering the third dimension”.

While this setup is relevant for numerical simulations of the Monte Carlo type, the same conclusion applies to transfer matrix diagonalisations. Indeed, in the latter, the two boundaries, $\partial\mathcal{D}_1$ and $\partial\mathcal{D}_2$ are pushed to opposite extremities of an infinite cylinder, by means of a conformal mapping. So also in this geometry, only cyclic permutations of the marked clusters can be realised, because the clusters propagate from one cylinder extremity to the other and can only interchange by winding around the periodic boundary condition.

In other words, the permutation group is not fully relevant in $d = 2$ dimensions. Therefore, if we consider for instance the mixed Young diagram $[Q-3, 2, 1]$, the corresponding two-point function will only involve the following linear combination of probabilities:

$$\left\langle t_{a_1, a_2, a_3}^{[Q-3, 2, 1], [2, 1]}(r_1) t_{b_1, b_2, b_3}^{[Q-3, 2, 1], [2, 1]}(r_2) \right\rangle \propto \left(2 \mathbb{P} \left(\begin{array}{c} \parallel \\ \parallel \\ \parallel \end{array} \right) - \mathbb{P} \left(\begin{array}{c} \diagup \\ \diagdown \end{array} \right) - \mathbb{P} \left(\begin{array}{c} \diagdown \\ \diagup \end{array} \right) \right) \quad (5.71)$$

as opposed to (5.69) in the general case.

Following these observations, consider now an irreducible representation of \mathcal{S}_N . Within the subgroup \mathbb{Z}_N , this is reducible and can be decomposed into a direct sum of irreducible representations of \mathbb{Z}_N . The operators corresponding to each term in this decomposition are well known, so we will obtain in particular an identification of the critical exponents of our operators within $d = 2$ CFT. We recall that irreducible representations of \mathbb{Z}_N are all of dimension 1 and labelled by an integer p , with $0 \leq p \leq N - 1$, where the first cyclic permutation is represented by $\exp \left(i \frac{2\pi p}{N} \right)$.

A procedure for decomposing an irreducible representation of \mathcal{S}_N into representations of \mathbb{Z}_N is given for a more general case in [159]. Given a Young diagram $\lambda_N \in \mathcal{S}_N$ the procedure in our case is the following:

- List all the D standard Young tableaux corresponding to the Young diagram λ_N . Here, D denotes the dimension of the irreducible representation corresponding to λ_N , which can be computed from (5.7).
- Compute the *index* of each standard Young tableau. It is defined as the sum of the *descents* of the Young tableau. A number i is a descent, if $i + 1$ appears in a row strictly below i in the tableau.
- Let p denote the index modulo N , so that it obeys $\frac{-N}{2} < p \leq \frac{N}{2}$.
- Repeating this for all D standard Young tableaux, we obtain D such integers: p_1, p_2, \dots, p_D . An irreducible representation of \mathcal{S}_N restricted to the cyclic group \mathbb{Z}_N can then be decomposed as follows:

$$\lambda_N = \exp\left(i\frac{2\pi p_1}{N}\right) \oplus \exp\left(i\frac{2\pi p_2}{N}\right) \oplus \dots \oplus \exp\left(i\frac{2\pi p_D}{N}\right). \quad (5.72)$$

We call p/N the pseudo-momentum. The critical exponents of the operator within this representation of \mathbb{Z}_N are known [113, 160].

They can be written in terms of an extended Kac table [2] of conformal weights

$$h_{r,s} = \frac{(r(x+1) - sx)^2 - 1}{4x(x+1)}, \quad (5.73)$$

with Kac labels (r, s) of the form $(r, s) = (\pm \frac{p}{N}, N)$, as follows:

$$\Delta_{p,N} = h_{\frac{p}{N},N} + h_{-\frac{p}{N},N} = \frac{N^2(N^2x^2 - 1) + p^2(x+1)^2}{2N^2x(x+1)}, \quad (5.74)$$

$$\ell = h_{-\frac{p}{N},N} - h_{\frac{p}{N},N} = p. \quad (5.75)$$

Here $\Delta_{p,N}$ denotes the scaling dimension, and ℓ is the conformal spin. The number of states in the Potts model corresponds to the parameter x via

$$Q = 4 \cos^2\left(\frac{\pi}{x+1}\right). \quad (5.76)$$

In the end, the operator corresponding to the irreducible representation λ_N will have a dominant scaling dimension corresponding to the smallest exponent in the set $\{\Delta_{|p_i|,N}\}$, where the p_i correspond to the decomposition of λ_N restricted to the cyclic group \mathbb{Z}_N . Since $p \rightarrow \Delta_{p,N}$ is an increasing function for p positive, we find that the leading contribution comes from the smallest absolute value of the p 's.

For instance, the representation of \mathcal{S}_2 with Young diagram $[1, 1]$ is of dimension 1 and has only one standard Young tableau:

$$\begin{array}{|c|} \hline 1 \\ \hline 2 \\ \hline \end{array} \quad (5.77)$$

We find that $p = 1$, so the scaling dimension is $\Delta_{1,2}$ and its spin is $\ell = 1$.

Let us give a slightly more complicated example, from \mathcal{S}_4 , with the Young diagram $[2, 2]$. There are two standard tableaux:

$$\begin{array}{|c|c|} \hline 1 & 2 \\ \hline 3 & 4 \\ \hline \end{array}
 \quad
 \begin{array}{|c|c|} \hline 1 & 3 \\ \hline 2 & 4 \\ \hline \end{array}
 \tag{5.78}$$

We find $p = 2$ for the first tableau and $p = 0$ for the second. The dominant contribution to the two-point function of the operator associated with this representation, in $d = 2$ CFT, will have scaling dimension $\Delta_{0,4}$ and spin $\ell = 0$. The scaling dimension $\Delta_{2,4}$, corresponding to the first tableau, is a sub-leading exponent.

The only exception to this rule is for the case $N = 1$ where the magnetisation operator is given by $(r, s) = (\frac{1}{2}, 0)$ instead of $(r, s) = (0, 1)$ [156]. Indeed, the N -cluster operator corresponds generically (i.e., for $N > 1$) to a $2N$ -leg watermelon operator in $d = 2$, but this is not true for $N = 1$.

5.3.3 Numerics

Numerical checks of the analytically predicted critical exponents can be performed by using several methods.

We first investigate the case of percolation, corresponding to $Q = 1$. Using Monte Carlo simulations, we have studied the scaling behavior of the $N = 2$ two-points function of the tensors $t^{[Q-2,2]}$ and $t^{[Q-2,1,1]}$. The scaling dimensions of the associated fields are predicted by (5.74) to be $\Delta_s = 2h_{0,2} = 5/4$ and $\Delta_a = h_{1/2,2} + h_{-1/2,2} = 23/16$ for the symmetric and anti-symmetric tensor, respectively. The averaging was done over 10^8 configurations. The results, shown in figure 5.1, are in good agreement with the exact values.

In order to measure the exponents for tensors of higher order, the transfer matrix formalism is helpful. By exact diagonalisation of transfer matrices on a cylinder, we are able to extract the conformal data from finite-size scaling corrections to the free energies [161, 162]. We use the Fortuin-Kasteleyn cluster representation. The state for a row of L spins within a time slice is encoded by specifying the way in which the spins are connected through the (parts of) FK clusters constructed at previous times [162]. The transfer matrix adds a row to the system. In order to take into account the non-local weight Q for each cluster, the transfer matrix multiplies by the Boltzmann weight Q whenever it acts on the last (in the time direction) spin of a cluster.

To compute interesting quantities, we place ourselves in sectors where $N \geq 1$ clusters are marked. The marked clusters are constrained to propagate at every step of the action of the transfer matrix, so they cannot be left behind by the time evolution. This means that N distinct clusters propagate from one end to the other of the cylinder. The case $N = 1$ corresponds to the magnetisation, and the finite-size scaling of the free energy in this sector provides an estimate of the magnetisation exponent. In general, we extract estimates of critical exponents from the finite-size scaling of the largest eigenvalues in each sector,

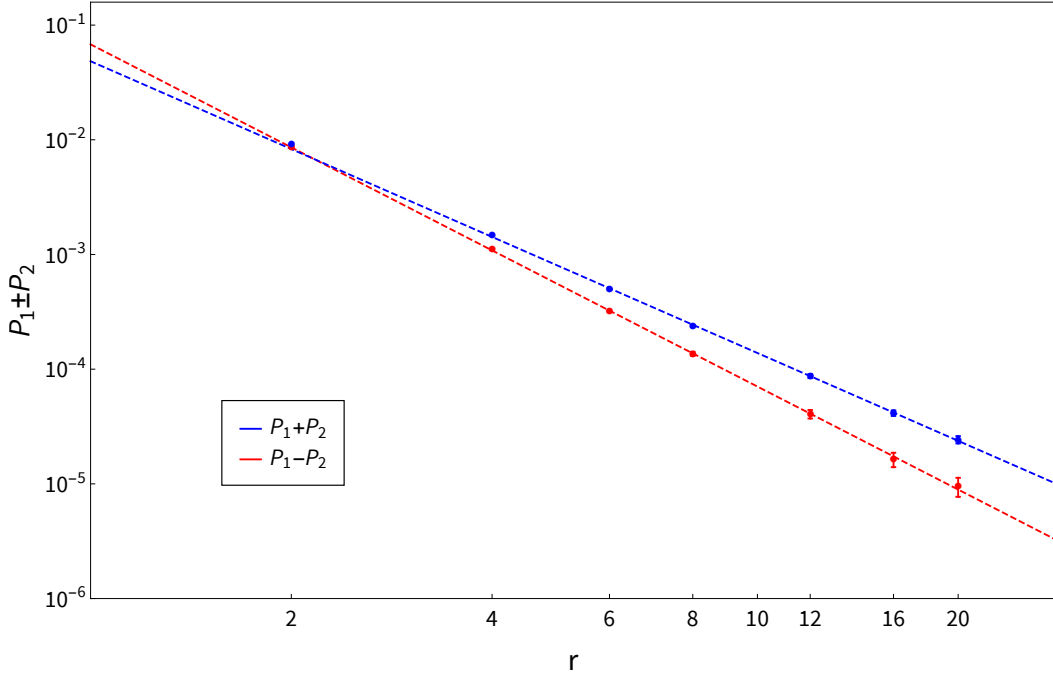


Figure 5.1 – Linear combination $P = P_1 \pm P_2$, where $P_1 = \mathbb{P} \left(\begin{array}{c} \uparrow \\ \uparrow \\ \downarrow \\ \downarrow \end{array} \right)$ and $P_2 = \mathbb{P} \left(\begin{array}{c} \times \\ \times \\ \times \\ \times \end{array} \right)$, of probabilities for the propagation of $N = 2$ clusters in percolation ($Q = 1$, or $x = 2$) obtained in Monte Carlo simulations. The quantity r is the distance between the two operators in lattice spacing. The red plot corresponds to (5.60) and the blue plot to (5.62). The critical exponents correspond to slopes $2\Delta_{0,2} = \frac{5}{2} = 2.5$ and $2\Delta_{1,2} = \frac{23}{8} = 2.875$. Numerically we find $2\Delta_{0,2} = 2.54(8)$ and $2\Delta_{1,2} = 2.9(1)$.

following [161]. We have only considered the critical exponents of primaries (i.e., $N = n$) where each marked spin is connected to a propagating cluster.

For a state with N marked clusters, the Young symmetriser acts on the labeling of the clusters. This provides a state in the N -cluster sector of the transfer matrix with a well-defined \mathcal{S}_Q symmetry. Since the Young symmetriser is idempotent and commutes with the transfer matrix, we can avoid numerical instabilities by letting it act every time a row has been added by the transfer matrix.

For instance, consider a state with $N = 2$ marked clusters, A and B , that we denote symbolically as $v = |X, X, A, B, X, X\rangle$. The vector v corresponds to a state of width $L = 6$ sites, where the third and fourth spins belong respectively to the clusters marked A and B , and the others are not specified in our notation (X). They can be initialised, for instance, so that each X corresponds to a different unmarked cluster. The action of the anti-symmetriser (5.44) gives the vector $v = |X, X, A, B, X, X\rangle - |X, X, B, A, X, X\rangle$ that generates a sector of the transfer matrix.

The largest eigenvalue of each sector is then computed from a standard iterative scheme, and we can extract the scaling dimension of the associated operator. We are able to extract

very precise numerical data using this formalism. The numerical extrapolation for the critical exponents, as function of Q , is shown in figure 5.2.

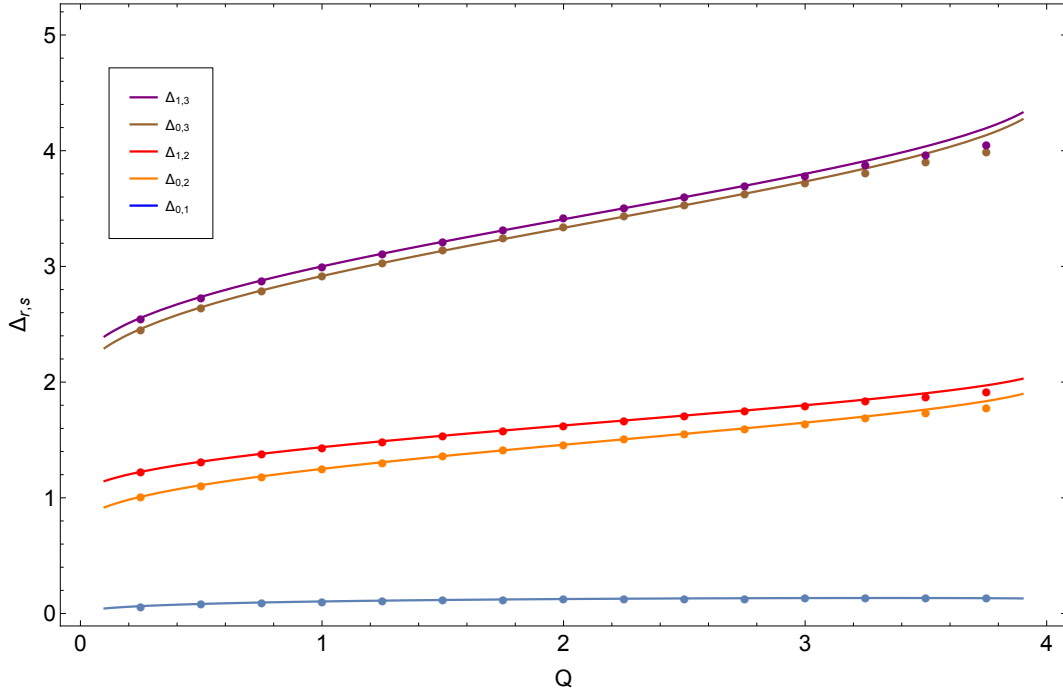


Figure 5.2 – Critical exponents for the propagation of two anti-symmetric clusters, as a function of Q . We computed all conformal dimensions corresponding to the propagation of $N = 1, 2, 3$ FK-clusters. The lines are the theoretical values $\Delta_{p,N} = h_{p/N,N} + h_{-p/N,N}$ for $N > 1$ and $\Delta_{0,1} = 2h_{1/2,0}$ for the magnetisation operator. The points are the data extrapolated from a numerical diagonalisation of the transfer matrix using finite-size scaling on a cylinder. We observe a very good agreement, as long as we do not take Q too close to 4. In the latter case the convergence is impeded by logarithmic terms appearing in the finite-size corrections [163].

5.3.4 Spin

It is also possible to satisfy the predictions for the conformal spin in numerical simulations. Let us consider, for instance, the two-point function corresponding to the tensor (5.44). From the previous section, we expect that $t_{a_1, a_2}^{[Q-2, 1, 1], [1, 1]}$ corresponds, in $d = 2$ CFT, to a field of spin 1. It acts on two sites in the same neighbourhood, whose relative orientation defines a unit vector u^μ , which corresponds to the direction of the vector going from the first to the second site. The general correlation function of a vector field \mathcal{O}_μ is predicted by conformal invariance to be [164, 165]

$$\langle \mathcal{O}_\mu(x) \mathcal{O}_\nu(y) \rangle = \frac{\delta_{\mu, \nu} - 2 \frac{(x-y)_\mu (x-y)_\nu}{(x-y)^2}}{|x-y|^{2\Delta}}. \quad (5.79)$$

We define also $\mathcal{O}_u = u^\mu \mathcal{O}_\mu$. Thus, the correlation function evaluated at the points $x = 0$ and $y = (r, 0)$ reads

$$\langle \mathcal{O}_{u_1}(x) \mathcal{O}_{u_2}(y) \rangle = -\frac{\cos(\theta_1 + \theta_2)}{r^{2\Delta}}, \quad (5.80)$$

where $u_1 = (\cos \theta_1, \sin \theta_1)$ and $u_2 = (\cos \theta_2, \sin \theta_2)$.

It is readily shown that if we keep u_1 and u_2 fixed, and rotate x around y through an angle θ , the above expression is multiplied by an angular factor $\cos 2\theta$. This last property is amenable to numerical verification. Because of the lattice discretisation, it is in fact easier to move one of the points, take the orientation fixed (figure 5.3), rather than to apply a local rotation. Figure 5.4 shows that we can measure this rotation effect on the lattice using Monte Carlo simulations.

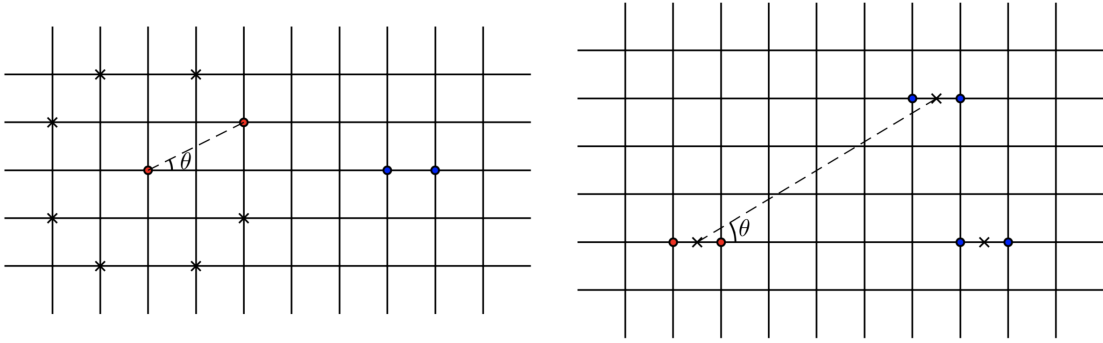


Figure 5.3 – Rotations performed on the lattice to measure the spin of an operator acting on $N = 2$ sites. *Left panel:* One operator acts on the two red sites. We measure the correlation function with another operator (corresponding to the two blue sites) with Monte Carlo simulations. We can move the right red dot around the other one to measure the spin of the operator through the correlation function but this is very restricted by the lattice discretisation (the usable positions are marked with a cross). A first solution to this issue is to increase the distance between the two red sites (this is allowed if the two red points are close enough compared to the distance with the blue sites). *Right panel:* A simpler solution is to keep the relative orientation of each pair of sites fixed and move globally the blue sites around the red ones. This rotation defines the angle θ . Those correlations are easier to measure, since we are less affected by the lattice discretisation.

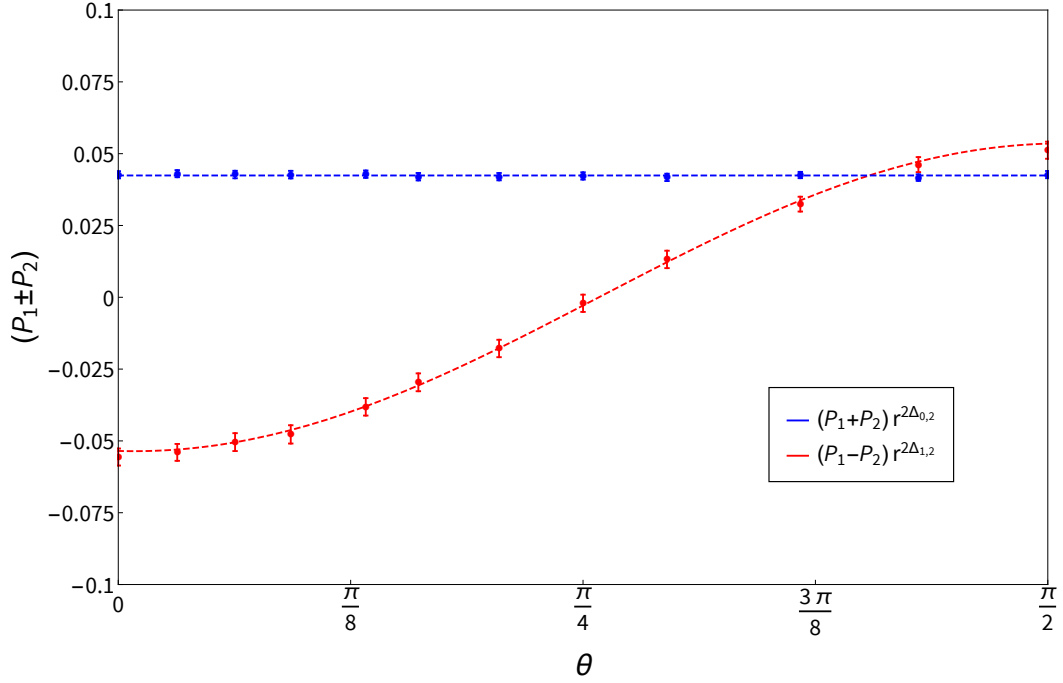


Figure 5.4 – Linear combination $P = P_1 \pm P_2$, where $P_1 = \mathbb{P} \left(\begin{array}{c} \bullet \\ \bullet \\ \bullet \\ \bullet \end{array} \right)$ and $P_2 = \mathbb{P} \left(\begin{array}{c} \bullet \\ \bullet \\ \bullet \\ \bullet \end{array} \right)$, of renormalised probabilities for the propagation of $N = 2$ clusters in percolation ($Q = 1$, or $x = 2$). A rotations corresponding to the one described on the right panel of figure 5.3 is performed and parametrized by θ . The red plot corresponds to (5.60) and the blue plot to (5.62), whose angular dependence is proportional to 1 and $\cos 2\theta$, respectively.

5.4 Logarithmic correlations in 3D percolation

Since all our predictions are independent of the dimension, it is possible to satisfy the validity of the logarithmic structure in 3D. For percolation, in the limit $Q \rightarrow 1$, the scaling dimensions of the two-cluster operator and the local energy operator collide [57]. The classification of the observables (these are scalars) leads to the prediction

$$F(r) = \frac{\mathbb{P} \left(\begin{array}{c} \bullet \\ \bullet \\ \bullet \\ \bullet \end{array} \right) + \mathbb{P} \left(\begin{array}{c} \bullet \\ \bullet \\ \bullet \\ \bullet \end{array} \right) + \mathbb{P} \left(\begin{array}{c} \bullet \\ \bullet \\ \bullet \\ \bullet \end{array} \right) + \mathbb{P} \left(\begin{array}{c} \bullet \\ \bullet \\ \bullet \\ \bullet \end{array} \right) + \mathbb{P} \left(\begin{array}{c} \bullet \\ \bullet \\ \bullet \\ \bullet \end{array} \right) - \mathbb{P} \left(\begin{array}{c} \bullet \\ \bullet \\ \bullet \\ \bullet \end{array} \right)^2}{\mathbb{P} \left(\begin{array}{c} \bullet \\ \bullet \\ \bullet \\ \bullet \end{array} \right) + \mathbb{P} \left(\begin{array}{c} \bullet \\ \bullet \\ \bullet \\ \bullet \end{array} \right)} \sim \delta \log(r) \quad (5.81)$$

where

$$\delta = 2 \times \lim_{Q \rightarrow 1} \frac{\Delta_2 - \Delta_\epsilon}{Q - 1}, \quad (5.82)$$

with Δ_2 and Δ_ϵ the conformal dimensions of the two-cluster and energy operators. In two dimensions, the exact values are known

$$\Delta_2 = 2h_{0,2}, \quad \Delta_\epsilon = 2h_{2,1} \quad (5.83)$$

and $\delta = 2\sqrt{3}/\pi \sim 1.1027\dots$. The quantity δ is proportional to the indecomposability parameter b in (1.18) and a universal quantity. In particular, it does not depend on the microscopic details and has the same value for different lattices. The scaling (5.81) is predicted to be true in higher dimensions and the formula (5.82) holds. Numerical evidence is presented in figure 5.5.

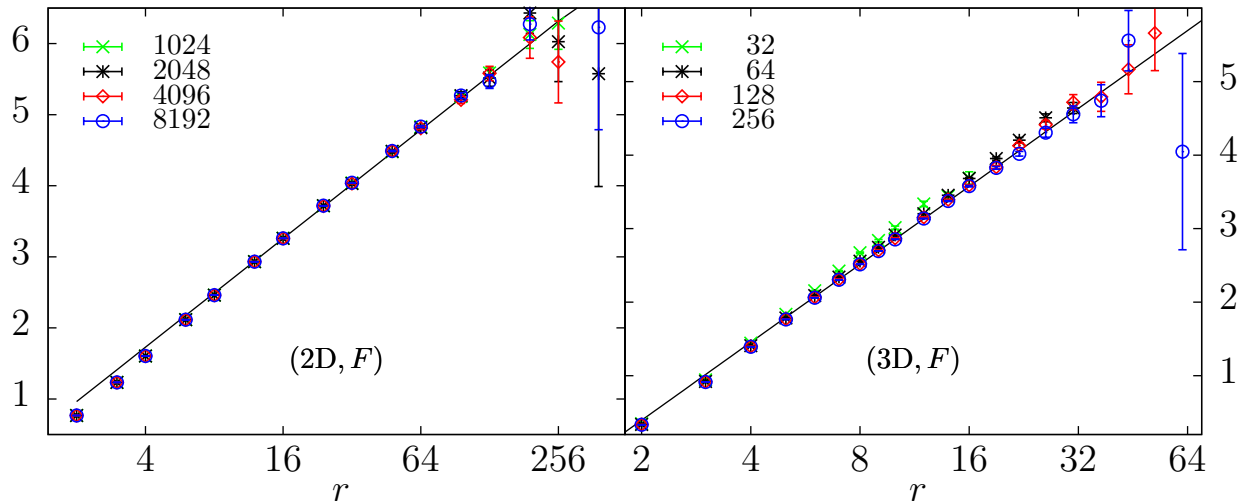


Figure 5.5 – Semi-log plot of the logarithmic correlation $F(r)$ for 2D and 3D. The slopes of the straight lines are universal, and the values are respectively $2\sqrt{3}/\pi$ and $1.53(3)$. Figure taken from [79].

Obviously the exact conformal dimensions for percolation (and even less as a function of Q) are only known for two dimensions. We can nonetheless give a rough estimate of δ from (5.82) by using the numerical values $\Delta_2 \approx 2.243(2)$ and $\Delta_\varepsilon \approx 1.413(1)$ for the 3D Ising model ($Q = 2$) [166, 167]. This gives $\delta \approx 2(\Delta_2(Q = 2) - \Delta_\varepsilon(Q = 2)) = 1.66$. The agreement with $\delta(3D)$ is surprisingly good, showing that $\Delta_2(Q)$ and $\Delta_\varepsilon(Q)$ have little curvature (as in 2D). This result is the first direct measurement of the indecomposability parameter for percolation in higher dimension.

Note that the primal operators, at a given N , also have distinct dimensions in higher dimensions. We thus have an infinite family of observables with new critical exponents in 3D. The dimensions are computed numerically (using Monte-Carlo simulations) in [79] up to $N = 4$ in 2D and $N = 3$ in 3D.

Conclusion

In this thesis, we investigated various aspects relevant to irrational non-unitary critical models. The nature of truncations for infinite-dimensional supersymmetric chains is discussed for the plateau transition in the integer quantum Hall effect and the Brownian motion. The naive second truncation of the latter is found to be in the universality class of self-avoiding walks. Numerics hints at the same conclusion for all truncations and the Chalker-Coddington model is expected to behave similarly. A strong crossover is observed for higher truncations where critical exponents, for small sizes, seem to be in a different universality classes. Multicritical points are found by fine-tuning various fugacities. In the Brownian motion, whether a series of multicritical points, that are less and less stable under the RG, provides an asymptotic description of the non-compact full theory is still an open question. These truncations are also a good playground to observe RG-flow between $c = 0$ theories. We have given examples of flows between the Chalker-Coddington model (and its first truncation) and class C (corresponding to percolation). It is a first step in the investigation of flows between non-compact and compact theories.

An important role is played by the effective central charge as a measurement of the degrees of freedom. This quantity also appears in the context of entanglement. We have generalised the definition of the entanglement entropy in the context of several non-unitary models and have seen that the formalism of Coulomb gas can be applied successfully to compute the entanglement entropy scaling in loop models. The examples in our work show that, for the usual entanglement entropy, the effective central charge may dictate the amount of entanglement in the model. It is of high interest for tensor network simulations that rely on a low amount of entanglement in the encoded states.

Lastly, in the context of the Q -state Potts model, we have shown that the classification of observables, using the discrete S_Q symmetry, could be extended to non-scalar operators where additional predictions for the logarithmic structure of the CFT are given. Remarkably, these simple considerations, based on symmetry, remain valid in arbitrary dimension. We provided the first evidence that percolation in three dimensions is a logarithmic conformal field theory.

The work presented in this manuscript opens many future possible directions of research.

- The entanglement entropy in the case of non-compact models is expected to behave differently. This was shown in this thesis for a certain limit of the unitary minimal models leading to a $\log \log \ell$ term as a sub-leading contribution. Of course this example cannot be directly investigated numerically since RSOS models become infinite-dimensional in this limit. Since very large sizes must be considered, it would be very interesting to perform DMRG simulations for a simple non-compact model such as the staggered XXZ spin chain (with bond dimension 2). It is related, in the continuum, to the black hole CFT and is already quite well understood. In particular, it is not clear whether or not the prefactor of the $\log \log \ell$ term is universal. Some results are already known for a free boson where it is universal but this is maybe not the case with interactions. New developments about non-compact theories with boundaries [168] are interesting for practical reasons in tensor network simulations.

- Our work on the entanglement entropy for non-unitary models was only valid for open systems with a single cut. The generalisation to multiple cuts and periodic boundary conditions is far from obvious. The quantum group symmetry is lost in the closed XXZ spin chain. The trace cannot be modified easily to tune the fugacity of non-contractible loops. Difficulties, in the definition of the twists, arise with multiple cuts since the topology of the loops can be much more complicated. However, the generalisation for loop models is straightforward since only the connectivities must be tracked down. Preliminary results shows that indeed, the loop representation is somehow more fundamental and allows easily to perform computations on the entanglement. Note that loop diagrams are however no longer planar and generalisation of the Temperley-Lieb algebra must be considered where crossings of strands is allowed.
- Some features of higher truncations for the Chalker-Coddington model and Brownian motion remain mysterious. The precise characterisation of the crossover, as the order of truncation increases, is not understood. In particular, it would be very interesting to understand the nature of the multicritical points that these truncations approximate at small sizes. For the second truncation of the Brownian motion, our work lacks a proper understanding of the continuum limit. Good candidates exist such as a model from the $N = 2$ supersymmetric minimal series. It is known to describe, in different limits, the self-avoiding walks and a non-compact free field. Moreover It may be possible to find an integrable deformation of the second truncation to compute exactly critical exponents.
- To continue our work on the flow between $c = 0$ theories, several problems must be considered to complete our understanding of these systems. How non-compact degrees of freedom behave precisely along the flow was not investigated in this thesis. Additionally, the $gl(2|2)$ spin chain, the first truncation of the Chalker-Coddington model and percolation are all three logarithmic conformal field theories in the continuum limit. It is thus very natural to study the flow also from the point of view of the indecomposable structure of the theory. Lastly, we would like to obtain a description, in the continuum limit, to understand how the free boson becomes compactified or massive along a flow would be an interesting and important future prospect.
- The study of logarithmic conformal fields theories in higher dimensions could be continued. The Jordan cell for percolation between the energy operator and the two-leg operator was studied but we predict such structure to appear for non-scalar operators as well. The case of Ising ($Q = 2$) and trees and forests ($Q = 0$) are also possible future directions. The percolation can also be studied in 4 and 5 dimensions.
- Lastly, since many of our models are quite hard to simulate because of their large Hilbert space (especially for higher truncations), it seems important to develop better numerical tools. We witnessed, in the last years, an increased interest in tensor network techniques. Many of these methods cannot be applied to non-unitary spin chain since they rely on variational principles only valid for Hermitian hamiltonians. It is possible to get around these difficulties in some cases but the numerical scheme may be less efficient. However,

a very efficient numerical method to simulate lattice models is called *tensor network renormalisation* [169]. It performs very efficiently successive RG transformations in the spirit of spin-blocking for the Ising model. In general, this method does not rely on the positivity of Boltzmann weights and can easily be generalised to local interactions with complex weights. A recent implementation, called *Gilt-TNR* [170], was proposed with very impressive results. Applying these techniques to supersymmetric spin chains may lead to an important improvement of numerical simulations for non-unitary models.

References

- [1] A. Belavin, A. Polyakov, and A. Zamolodchikov, “Infinite conformal symmetry in two-dimensional quantum field theory,” *Nuclear Physics B*, vol. 241, no. 2, pp. 333 – 380, 1984.
- [2] D. Friedan, Z. Qiu, and S. Shenker, “Conformal invariance, unitarity, and critical exponents in two dimensions,” *Phys. Rev. Lett.*, vol. 52, pp. 1575–1578, 1984.
- [3] J. L. Cardy, “Operator content of two-dimensional conformally invariant theories,” *Nuclear Physics B*, vol. 270, pp. 186 – 204, 1986.
- [4] K. G. Wilson, “Renormalization Group and critical phenomena. I. Renormalization Group and the Kadanoff scaling picture,” *Phys. Rev. B*, vol. 4, pp. 3174–3183, 1971.
- [5] K. G. Wilson, “Renormalization group and critical phenomena. II. Phase-space cell analysis of critical behavior,” *Phys. Rev. B*, vol. 4, pp. 3184–3205, 1971.
- [6] [https://www.nobelprize.org/prizes/physics/1998/press release/](https://www.nobelprize.org/prizes/physics/1998/press%20release/)
- [7] K. v. Klitzing, G. Dorda, and M. Pepper, “New method for high-accuracy determination of the fine-structure constant based on quantized Hall resistance,” *Phys. Rev. Lett.*, vol. 45, pp. 494–497, 1980.
- [8] J. K. Jain, *Composite Fermions*. Cambridge University Press, 2007.
- [9] B. Huckestein, “Scaling theory of the integer quantum Hall effect,” *Rev. Mod. Phys.*, vol. 67, pp. 357–396, 1995.
- [10] W. Li, G. A. Csáthy, D. C. Tsui, L. N. Pfeiffer, and K. W. West, “Scaling and universality of integer quantum Hall plateau-to-plateau transitions,” *Phys. Rev. Lett.*, vol. 94, p. 206807, 2005.
- [11] W. Li, C. L. Vicente, J. S. Xia, W. Pan, D. C. Tsui, L. N. Pfeiffer, and K. W. West, “Scaling in plateau-to-plateau transition: A direct connection of quantum hall systems with the Anderson localization model,” *Phys. Rev. Lett.*, vol. 102, p. 216801, 2009.
- [12] J. T. Chalker and P. D. Coddington, “Percolation quantum tunnelling and the integer Hall effect,” *J. Phys. C*, vol. 21, p. 2665, 1988.
- [13] K. Slevin and T. Ohtsuki, “Critical exponent for the quantum Hall transition,” *Phys. Rev. B*, vol. 80, no. 4, p. 041304(R), 2009.
- [14] H. Obuse, A. R. Subramaniam, A. Furusaki, I. A. Gruzberg, and A. W. W. Ludwig, “Conformal invariance, multifractality, and finite-size scaling at Anderson localization transitions in two dimensions,” *Phys. Rev. B*, vol. 82, p. 035309, 2010.

- [15] J. P. Dahlhaus, J. M. Edge, J. Tworzydło, and C. W. J. Beenakker, “Quantum Hall effect in a one-dimensional dynamical system,” *Phys. Rev. B*, vol. 84, p. 115133, 2011.
- [16] M. Amado, A. V. Malyshev, A. Sedrakyan, and F. Domínguez-Adame, “Numerical study of the localization length critical index in a network model of plateau-plateau transitions in the quantum Hall effect,” *Phys. Rev. Lett.*, vol. 107, p. 066402, 2011.
- [17] K. Slevin and T. Ohtsuki, “Finite size scaling of the Chalker-Coddington model,” in *Localisation 2011*, pp. 60–69.
- [18] E. Bettelheim, I. A. Gruzberg, and A. W. W. Ludwig, “Quantum Hall transitions: An exact theory based on conformal restriction,” *Phys. Rev. B*, vol. 86, p. 165324, 2012.
- [19] M. R. Zirnbauer, “Toward a theory of the integer quantum Hall transition: Continuum limit of the Chalker-Coddington model,” *Journal of Mathematical Physics*, vol. 38, no. 4, pp. 2007–2036, 1997.
- [20] V. Kagalovsky, B. Horovitz, Y. Avishai, and J. T. Chalker, “Quantum Hall plateau transitions in disordered superconductors,” *Phys. Rev. Lett.*, vol. 82, p. 3516, 1999.
- [21] V. Kagalovsky, B. Horovitz, Y. Avishai, and J. T. Chalker, “Spin quantum Hall effect in unconventional superconductors,” *Phys. Rev. B*, vol. 60, p. 4245, 1999.
- [22] E. J. Beamond, J. Cardy, and J. T. Chalker, “Quantum and classical localization, the spin quantum Hall effect, and generalizations,” *Phys. Rev. B*, vol. 65, p. 214301, 2002.
- [23] J. Cardy, “Network models in class C on arbitrary graphs,” *Communications in Mathematical Physics*, vol. 258, no. 1, pp. 87–102, 2005.
- [24] S. Bhardwaj, V. V. Mkhitarian, and I. A. Gruzberg, “Supersymmetry approach to delocalization transitions in a network model of the weak-field quantum Hall effect and related models,” *Phys. Rev. B*, vol. 89, p. 235305, 2014.
- [25] I. A. Gruzberg, N. Read, and S. Sachdev, “Scaling and crossover functions for the conductance in the directed network model of edge states,” *Phys. Rev. B*, vol. 55, pp. 10593–10601, 1997.
- [26] B. Duplantier and H. Saleur, “Exact surface and wedge exponents for polymers in two dimensions,” *Phys. Rev. Lett.*, vol. 57, pp. 3179–3182, 1986.
- [27] H. Saleur and B. Duplantier, “Exact determination of the percolation hull exponent in two dimensions,” *Phys. Rev. Lett.*, vol. 58, pp. 2325–2328, 1987.
- [28] B. Nienhuis, “Critical behavior of two-dimensional spin models and charge asymmetry in the Coulomb gas,” *Journal of Statistical Physics*, vol. 34, no. 5, pp. 731–761, 1984.
- [29] C. M. Fortuin and P. W. Kasteleyn, “On the random-cluster model: I. Introduction and relation to other models,” *Physica*, vol. 57, no. 4, pp. 536–564, 1972.

- [30] P. Fendley, “Loop models and their critical points,” *Journal of Physics A: Mathematical and General*, vol. 39, no. 50, pp. 15445–15475, 2006.
- [31] J. L. Jacobsen, “Conformal field theory applied to loop models,” in *Polygons, Polyominoes and Polycubes* (A. J. Guttmann, ed.), pp. 347–424, Dordrecht: Springer Netherlands, 2009.
- [32] P. Fendley and H. Saleur, “ $N = 2$ supersymmetry, Painlevé III and exact scaling functions in 2D polymers,” *Nuclear Physics B*, vol. 388, no. 3, pp. 609 – 626, 1992.
- [33] H. Saleur, “Polymers and percolation in two dimensions and twisted $n = 2$ supersymmetry,” *Nuclear Physics B*, vol. 382, no. 3, pp. 486 – 531, 1992.
- [34] P. Fendley and E. Fradkin, “Realizing non-Abelian statistics in time-reversal-invariant systems,” *Phys. Rev. B*, vol. 72, p. 024412, 2005.
- [35] H. E. Stanley, “Dependence of critical properties on dimensionality of spins,” *Phys. Rev. Lett.*, vol. 20, pp. 589–592, 1968.
- [36] P. G. de Gennes, “Scaling concepts in polymer physics,” *Cornell University Press*, 1979.
- [37] Y. Ikhlef, P. Fendley, and J. Cardy, “Integrable modification of the critical Chalker-Coddington network model,” *Phys. Rev. B*, vol. 84, p. 144201, 2011.
- [38] S. O. Warnaar, M. T. Batchelor, and B. Nienhuis, “Critical properties of the Izergin-Korepin and solvable $O(n)$ models and their related quantum spin chains,” *Journal of Physics A: Mathematical and General*, vol. 25, no. 11, pp. 3077–3095, 1992.
- [39] A. Bedini, A. L. Owczarek, and T. Prellberg, “Numerical simulation of a lattice polymer model at its integrable point,” *Journal of Physics A: Mathematical and Theoretical*, vol. 46, no. 26, p. 265003, 2013.
- [40] B. Duplantier and H. Saleur, “Stability of the polymer Θ point in two dimensions,” *Phys. Rev. Lett.*, vol. 62, pp. 1368–1371, 1989.
- [41] K. Osterwalder and R. Schrader, “Axioms for Euclidean Green’s functions,” *Comm. Math. Phys.*, vol. 31, no. 2, pp. 83–112, 1973.
- [42] H. N. V. Temperley and E. H. Lieb, “Relations between the ‘Percolation’ and ‘Colouring’ problem and other graph-theoretical problems associated with regular planar lattices: Some exact results for the ‘Percolation’ problem,” *Proceedings of the Royal Society of London. Series A, Mathematical and Physical Sciences*, vol. 322, no. 1549, pp. 251–280, 1971.
- [43] V. F. R. Jones, “Planar algebras, I,” arXiv:math/9909027.

- [44] H. W. J. Blöte, J. L. Cardy, and M. P. Nightingale, “Conformal invariance, the central charge, and universal finite-size amplitudes at criticality,” *Phys. Rev. Lett.*, vol. 56, pp. 742–745, 1986.
- [45] C. Itzykson, H. Saleur, and J.-B. Zuber, “Conformal invariance of nonunitary 2d-models,” *Europhysics Letters (EPL)*, vol. 2, no. 2, pp. 91–96, 1986.
- [46] L. Rozansky and H. Saleur, “Quantum field theory for the multi-variable Alexander-Conway polynomial,” *Nuclear Physics B*, vol. 376, no. 3, pp. 461 – 509, 1992.
- [47] V. Gurarie, “Logarithmic operators in conformal field theory,” *Nucl. Phys. B*, vol. 410, no. 3, pp. 535–549, 1993.
- [48] P. Pearce, J. Rasmussen, and J.-B. Zuber, “Logarithmic minimal models,” *J. Stat. Mech.*, p. P11017, 2006.
- [49] P. Mathieu and D. Ridout, “From percolation to logarithmic conformal field theory,” *Physics Letters B*, vol. 657, no. 1, pp. 120 – 129, 2007.
- [50] K. Kytola and D. Ridout, “On staggered indecomposable Virasoro modules,” *Journal of Mathematical Physics*, vol. 50, no. 12, p. 123503, 2009.
- [51] J. Germoni, “On the classification of admissible representations of the Virasoro algebra,” *Letters in Mathematical Physics*, vol. 55, no. 2, pp. 169–177, 2001.
- [52] V. Gurarie and A. W. W. Ludwig, “Conformal field theory at charge central $c = 0$ and two-dimensional critical systems with quenched disorder,” in *From Fields to Strings: Circumnavigating Theoretical Physics*, pp. 1384–1440.
- [53] A. M. Gainutdinov, J. L. Jacobsen, N. Read, H. Saleur, and R. Vasseur, “Logarithmic conformal field theory: a lattice approach,” *J. Phys. A: Math. Theor.*, vol. 46, p. 494012, 2013.
- [54] R. Vasseur, J. L. Jacobsen, and H. Saleur, “Indecomposability parameters in chiral logarithmic conformal field theory,” *Nucl. Phys. B*, vol. 851, pp. 314–345, 2011.
- [55] J. Cardy, “Logarithmic correlations in quenched random magnets and polymers,” 1999. arXiv: cond-mat/9911024.
- [56] J. Cardy, “Logarithmic conformal field theories as limits of ordinary CFTs and some physical applications,” *Journal of Physics A: Mathematical and Theoretical*, vol. 46, no. 49, p. 494001, 2013.
- [57] R. Vasseur, J. L. Jacobsen, and H. Saleur, “Logarithmic observables in critical percolation,” *J. Stat. Mech.: Theory Exp.*, vol. 2012, p. L07001, 2012.
- [58] R. Vasseur and J. L. Jacobsen, “Operator content of the critical Potts model in d dimensions and logarithmic correlations,” *Nucl. Phys. B*, vol. 880, pp. 435–475, 2014.

- [59] R. Vasseur, “Logarithmic correlations in quantum Hall plateau transitions,” *Phys. Rev. B*, vol. 92, p. 014205, 2015.
- [60] G. Moore and N. Seiberg, “Lectures on RCFT,” in *Physics, Geometry and Topology* (H. C. Lee, ed.), pp. 263–361, Boston, MA: Springer US, 1990.
- [61] M. R. Gaberdiel and H. G. Kausch, “A rational logarithmic conformal field theory,” *Physics Letters B*, vol. 386, no. 1, pp. 131 – 137, 1996.
- [62] G. Moore and N. Seiberg, “Naturality in conformal field theory,” *Nuclear Physics B*, vol. 313, no. 1, pp. 16 – 40, 1989.
- [63] C. Itzykson and J.-M. Drouffe, “Statistical field theory, volume 1: From Brownian motion to renormalization and lattice gauge theory,” *Cambridge University Press*.
- [64] J. L. Jacobsen, N. Read, and H. Saleur, “Dense loops, supersymmetry, and Goldstone phases in two dimensions,” *Phys. Rev. Lett.*, vol. 90, p. 090601, 2003.
- [65] Y. Ikhlef, J. Jacobsen, and H. Saleur, “A staggered six-vertex model with non-compact continuum limit,” *Nuclear Physics B*, vol. 789, no. 3, pp. 483 – 524, 2008.
- [66] É. Vernier, J. L. Jacobsen, and H. Saleur, “Non compact continuum limit of two coupled Potts models,” *Journal of Statistical Mechanics: Theory and Experiment*, vol. 2014, no. 10, p. P10003, 2014.
- [67] É. Vernier, J. L. Jacobsen, and H. Saleur, “Non compact conformal field theory and the $a_2^{(2)}$ (Izergin–Korepin) model in regime III,” *Journal of Physics A: Mathematical and Theoretical*, vol. 47, no. 28, p. 285202, 2014.
- [68] É. Vernier, J. L. Jacobsen, and H. Saleur, “The continuum limit of $a_{N-1}^{(2)}$ spin chains,” *Nuclear Physics B*, vol. 911, pp. 52 – 93, 2016.
- [69] É. Vernier, J. L. Jacobsen, and H. Saleur, “A new look at the collapse of two-dimensional polymers,” *Journal of Statistical Mechanics: Theory and Experiment*, vol. 2015, no. 9, p. P09001, 2015.
- [70] J. B. Marston and S.-W. Tsai, “Chalker-Coddington network model is quantum critical,” *Phys. Rev. Lett.*, vol. 82, pp. 4906–4909, 1999.
- [71] C. M. Bender, “Making sense of non-Hermitian Hamiltonians,” *Reports on Progress in Physics*, vol. 70, no. 6, pp. 947–1018, 2007.
- [72] A. Morin-Duchesne, J. Rasmussen, P. Ruelle, and Y. Saint-Aubin, “On the reality of spectra of $U_qsl(2)$ -invariant XXZ Hamiltonians,” *Journal of Statistical Mechanics: Theory and Experiment*, vol. 2016, no. 5, p. 053105, 2016.

- [73] C. Korff and R. Weston, “PT symmetry on the lattice: the quantum group invariant XXZ spin chain,” *Journal of Physics A: Mathematical and Theoretical*, vol. 40, no. 30, pp. 8845–8872, 2007.
- [74] A. B. Zamolodchikov, “Irreversibility of the flux of the renormalization group in a 2d field theory,” *JETP Lett.*, vol. 43, 1986.
- [75] O. A. Castro-Alvaredo, B. Doyon, and F. Ravanini, “Irreversibility of the renormalization group flow in non-unitary quantum field theory,” *Journal of Physics A: Mathematical and Theoretical*, vol. 50, no. 42, p. 424002, 2017.
- [76] R. Couvreur, J. L. Jacobsen, and H. Saleur, “Entanglement in nonunitary quantum critical spin chains,” *Phys. Rev. Lett.*, vol. 119, p. 040601, 2017.
- [77] R. Couvreur, E. Vernier, J. L. Jacobsen, and H. Saleur, “On truncations of the Chalker-Coddington model,” *Nuclear Physics B*, vol. 941, pp. 507 – 559, 2019.
- [78] R. Couvreur, J. L. Jacobsen, and R. Vasseur, “Non-scalar operators for the Potts model in arbitrary dimension,” *J. Phys. A: Math. Theor.*, vol. 50, no. 47, p. 474001, 2017.
- [79] X. Tan, R. Couvreur, Y. Deng, and J. L. Jacobsen, “Observation of nonscalar and logarithmic correlations in two- and three-dimensional percolation,” *Phys. Rev. E*, vol. 99, p. 050103, 2019.
- [80] J. I. Cirac and F. Verstraete, “Renormalization and tensor product states in spin chains and lattices,” *Journal of Physics A: Mathematical and Theoretical*, vol. 42, no. 50, p. 504004, 2009.
- [81] F. Verstraete, V. Murg, and J. Cirac, “Matrix product states, projected entangled pair states, and variational renormalization group methods for quantum spin systems,” *Advances in Physics*, vol. 57, no. 2, pp. 143–224, 2008.
- [82] M. Srednicki, “Entropy and area,” *Phys. Rev. Lett.*, vol. 71, pp. 666–669, 1993.
- [83] N. Laflorencie, “Quantum entanglement in condensed matter systems,” *Physics Reports*, vol. 646, 2016.
- [84] M. B. Plenio, J. Eisert, J. Dreißig, and M. Cramer, “Entropy, entanglement, and area: Analytical results for harmonic lattice systems,” *Phys. Rev. Lett.*, vol. 94, p. 060503, 2005.
- [85] J. Eisert, M. Cramer, and M. B. Plenio, “Colloquium: Area laws for the entanglement entropy,” *Rev. Mod. Phys.*, vol. 82, pp. 277–306, 2010.
- [86] G. Vidal, J. I. Latorre, E. Rico, and A. Kitaev, “Entanglement in quantum critical phenomena,” *Phys. Rev. Lett.*, vol. 90, p. 227902, 2003.

- [87] P. Calabrese and J. Cardy, “Entanglement entropy and quantum field theory,” *Journal of Statistical Mechanics: Theory and Experiment*, vol. 2004, no. 06, p. P06002, 2004.
- [88] C. Pasquale and C. John, “Entanglement entropy and quantum field theory: a non-technical introduction,” *International Journal of Quantum Information*, vol. 04, no. 03, pp. 429–438, 2006.
- [89] H. Ju, A. B. Kallin, P. Fendley, M. B. Hastings, and R. G. Melko, “Entanglement scaling in two-dimensional gapless systems,” *Phys. Rev. B*, vol. 85, p. 165121, 2012.
- [90] H. Casini and M. Huerta, “A finite entanglement entropy and the c-theorem,” *Physics Letters B*, vol. 600, no. 1, pp. 142 – 150, 2004.
- [91] D. Bianchini, O. Castro-Alvaredo, B. Doyon, E. Levi, and F. Ravanini, “Entanglement entropy of non-unitary conformal field theory,” *Journal of Physics A: Mathematical and Theoretical*, vol. 48, no. 4, p. 04FT01, 2014.
- [92] D. Bianchini, O. A. Castro-Alvaredo, and B. Doyon, “Entanglement entropy of non-unitary integrable quantum field theory,” *Nuclear Physics B*, vol. 896, pp. 835 – 880, 2015.
- [93] V. Pasquier and H. Saleur, “Common structures between finite systems and conformal field theories through quantum groups,” *Nuclear Physics B*, vol. 330, no. 2, pp. 523 – 556, 1990.
- [94] P. Calabrese and J. Cardy, “Entanglement entropy and conformal field theory,” *Journal of Physics A: Mathematical and Theoretical*, vol. 42, no. 50, p. 504005, 2009.
- [95] J. L. Cardy, O. A. Castro-Alvaredo, and B. Doyon, “Form factors of branch-point twist fields in quantum integrable models and entanglement entropy,” *Journal of Statistical Physics*, vol. 130, no. 1, pp. 129–168, 2008.
- [96] C. N. Yang and T. D. Lee, “Statistical theory of equations of state and phase transitions. I. Theory of condensation,” *Phys. Rev.*, vol. 87, pp. 404–409, 1952.
- [97] O. A. Castro-Alvaredo and A. Fring, “A spin chain model with non-Hermitian interaction: the Ising quantum spin chain in an imaginary field,” *Journal of Physics A: Mathematical and Theoretical*, vol. 42, no. 46, p. 465211, 2009.
- [98] D. Bianchini and F. Ravanini, “Entanglement entropy from corner transfer matrix in Forrester–Baxter non-unitary RSOS models,” *Journal of Physics A: Mathematical and Theoretical*, vol. 49, no. 15, p. 154005, 2016.
- [99] Y. Deng, T. M. Garoni, and A. D. Sokal, “Ferromagnetic phase transition for the spanning-forest model ($q \rightarrow 0$ limit of the Potts model) in three or more dimensions,” *Phys. Rev. Lett.*, vol. 98, p. 030602, 2007.

- [100] D. J. Amit, “Renormalization of the Potts model,” *J. Phys. A: Math. Gen.*, vol. **9**, p. 1441, 1976.
- [101] R. J. Baxter, S. B. Kelland, and F. Y. Wu, “Equivalence of the Potts model of Whitney polynomial with an ice-type model,” *J. Phys. A: Math. Gen.*, vol. **9**, p. 397, 1976.
- [102] R. J. Baxter, “Potts model at the critical temperature,” *J. Phys. C: Solid State Phys.*, vol. **6**, p. L445, 1973.
- [103] H. Saleur and J. B. Zuber, “Integrable lattice models and quantum groups,” 1990. http://inis.iaea.org/search/search.aspx?orig_q=RN:22052624.
- [104] V. Chari and A. Pressley, “A guide to quantum groups,” *Cambridge U. Press*, 1994.
- [105] P. di Francesco, H. Saleur, and J. B. Zuber, “Relations between the Coulomb gas picture and conformal invariance of two-dimensional critical models,” *Journal of Statistical Physics*, vol. 49, no. 1, pp. 57–79, 1987.
- [106] L. Dixon, D. Friedan, E. Martinec, and S. Shenker, “The conformal field theory of orbifolds,” *Nuclear Physics B*, vol. 282, pp. 13 – 73, 1987.
- [107] P. D. Francesco, H. Saleur, and J. Zuber, “Modular invariance in non-minimal two-dimensional conformal theories,” *Nuclear Physics B*, vol. 285, pp. 454 – 480, 1987.
- [108] V. Pasquier, “Two-dimensional critical systems labelled by Dynkin diagrams,” *Nuclear Physics B*, vol. 285, pp. 162 – 172, 1987.
- [109] V. Pasquier, “Operator content of the ADE lattice models,” *Journal of Physics A: Mathematical and General*, vol. 20, no. 16, pp. 5707–5717, 1987.
- [110] H. Saleur and M. Bauer, “On some relations between local height probabilities and conformal invariance,” *Nuclear Physics B*, vol. 320, no. 3, pp. 591 – 624, 1989.
- [111] S. Fredenhagen, M. R. Gaberdiel, and C. Schmidt-Colinet, “Bulk flows in Virasoro minimal models with boundaries,” *Journal of Physics A: Mathematical and Theoretical*, vol. 42, no. 49, p. 495403, 2009.
- [112] I. Affleck and A. W. W. Ludwig, “Universal noninteger “ground-state degeneracy” in critical quantum systems,” *Phys. Rev. Lett.*, vol. 67, pp. 161–164, 1991.
- [113] N. Read and H. Saleur, “Exact spectra of conformal supersymmetric nonlinear sigma models in two dimensions,” *Nuclear Physics B*, vol. 613, no. 3, pp. 409 – 444, 2001.
- [114] I. Runkel and G. M. Watts, “A non-rational CFT with $c = 1$ as a limit of minimal models,” *Journal of High Energy Physics*, vol. 2001, no. 09, pp. 006–006, 2001.
- [115] D. Bianchini and O. A. Castro-Alvaredo, “Branch point twist field correlators in the massive free boson theory,” *Nuclear Physics B*, vol. 913, pp. 879 – 911, 2016.

- [116] O. Blondeau-Fournier and B. Doyon, “Expectations values of twist fields and universal entanglement saturation of the free massive boson,” *Journal of Physics A: Mathematical and Theoretical*, vol. 50, no. 27, 2017.
- [117] T. Dupic, B. Estienne, and Y. Ikhlef, “Entanglement entropies of minimal models from null-vectors,” *SciPost Phys.*, vol. 4, 2018.
- [118] B. Kramer, T. Ohtsuki, and S. Kettemann, “Random network models and quantum phase transitions in two dimensions,” *Physics Reports*, vol. 417, no. 5, pp. 211 – 342, 2005.
- [119] A. Pruisken, “On localization in the theory of the quantized Hall effect: A two-dimensional realization of the θ -vacuum,” *Nuclear Physics B*, vol. 235, no. 2, pp. 277 – 298, 1984.
- [120] P. Fendley, “Critical points in two-dimensional replica sigma models,” in *New Theoretical Approaches to Strongly Correlated Systems* (A. M. Tsvelik, ed.), pp. 141–161, Dordrecht: Springer Netherlands, 2001.
- [121] M. Schreiber and H. Grussbach, “Multifractal wave functions at the Anderson transition,” *Phys. Rev. Lett.*, vol. 67, pp. 607–610, 1991.
- [122] M. Janssen, M. Metzler, and M. R. Zirnbauer, “Point-contact conductances at the quantum Hall transition,” *Phys. Rev. B*, vol. 59, pp. 15836–15853, 1999.
- [123] H. Obuse, S. Bera, A. W. W. Ludwig, I. A. Gruzberg, and F. Evers, “Statistics of conductances and subleading corrections to scaling near the integer quantum Hall plateau transition,” *EPL (Europhysics Letters)*, vol. 104, no. 2, p. 27014, 2013.
- [124] I. A. Gruzberg, A. W. W. Ludwig, A. D. Mirlin, and M. R. Zirnbauer, “Symmetries of multifractal spectra and field theories of Anderson localization,” *Phys. Rev. Lett.*, vol. 107, p. 086403, 2011.
- [125] I. A. Gruzberg, A. D. Mirlin, and M. R. Zirnbauer, “Classification and symmetry properties of scaling dimensions at Anderson transitions,” *Phys. Rev. B*, vol. 87, p. 125144, 2013.
- [126] R. Bondesan, D. Wieczorek, and M. Zirnbauer, “Gaussian free fields at the integer quantum Hall plateau transition,” *Nuclear Physics B*, vol. 918, pp. 52 – 90, 2017.
- [127] R. Bondesan, D. Wieczorek, and M. R. Zirnbauer, “Pure scaling operators at the integer quantum Hall plateau transition,” *Phys. Rev. Lett.*, vol. 112, p. 186803, 2014.
- [128] M. R. Zirnbauer, “The integer quantum Hall plateau transition is a current algebra after all,” *Nuclear Physics B*, vol. 941, pp. 458 – 506, 2019.

- [129] I. A. Gruzberg, A. Klümper, W. Nuding, and A. Sedrakyan, “Geometrically disordered network models, quenched quantum gravity, and critical behavior at quantum Hall plateau transitions,” *Phys. Rev. B*, vol. 95, p. 125414, 2017.
- [130] R. M. Gade, “Universal R-matrix and graded Hopf algebra structure of $U_qsl(2|2)$,” *Journal of Physics A: Mathematical and General*, vol. 31, no. 21, pp. 4909–4925, 1998.
- [131] E. Vernier, J. L. Jacobsen, and H. Saleur, “Dilute oriented loop models,” *Journal of Physics A: Mathematical and Theoretical*, vol. 49, no. 6, p. 064002, 2016.
- [132] I. Jensen and A. J. Guttmann, “Self-avoiding walks, neighbour-avoiding walks and trails on semiregular lattices,” *Journal of Physics A: Mathematical and General*, vol. 31, no. 40, pp. 8137–8145, 1998.
- [133] P. Fendley and J. L. Jacobsen, “Critical points in coupled Potts models and critical phases in coupled loop models,” *Journal of Physics A: Mathematical and Theoretical*, vol. 41, no. 21, p. 215001, 2008.
- [134] A. Nahum, “Universality class of the two-dimensional polymer collapse transition,” *Phys. Rev. E*, vol. 93, p. 052502, 2016.
- [135] B. Duplantier and H. Saleur, “Exact critical properties of two-dimensional dense self-avoiding walks,” *Nucl. Phys. B*, vol. 290, pp. 291–326, 1987.
- [136] B. Duplantier and F. David, “Exact partition functions and correlation functions of multiple Hamiltonian walks on the Manhattan lattice,” *Journal of Statistical Physics*, vol. 51, no. 3, pp. 327–434, 1988.
- [137] G. Parisi and N. Sourlas, “Self avoiding walk and supersymmetry,” *J. Physique Lettres*, vol. 41, 1980.
- [138] C. Domb, A. J. Barrett, and M. Lax, “Self-avoiding walks and real polymer chains,” *Journal of Physics A: Mathematical, Nuclear and General*, vol. 6, no. 7, pp. L82–L87, 1973.
- [139] F. Evers and A. D. Mirlin, “Anderson transitions,” *Rev. Mod. Phys.*, vol. 80, p. 1355, 2008.
- [140] A. Atland and M. R. Zirnbauer, “Nonstandard symmetry classes in mesoscopic normal-superconducting hybrid structures,” *Phys. Rev. B*, vol. 55, p. 1142, 1997.
- [141] I. A. Gruzberg, A. W. W. Ludwig, and N. Read, “Exact exponents for the spin quantum Hall transition,” *Phys. Rev. Lett.*, vol. 82, p. 4524, 1999.
- [142] J. Cardy, “Linking numbers for self-avoiding loops and percolation: Application to the spin quantum Hall transition,” *Phys. Rev. Lett.*, vol. 84, p. 3507, 2000.

- [143] A. R. Subramaniam, I. A. Gruzberg, and A. W. W. Ludwig, “Boundary criticality and multifractality at the two-dimensional spin quantum Hall transition,” *Phys. Rev. B*, vol. 78, p. 245105, 2008.
- [144] S. Bhardwaj, I. A. Gruzberg, and V. Kagalovsky, “Relevant perturbations at the spin quantum Hall transition,” *Phys. Rev. B*, vol. 91, p. 035435, 2015.
- [145] S.-W. Tsai, “DMRG of super spin chains,” *talk at Network Models in Quantum Physics in Bremen*, 2008.
- [146] H. W. J. Blote and B. Nienhuis, “Critical behaviour and conformal anomaly of the $O(n)$ model on the square lattice,” *Journal of Physics A: Mathematical and General*, vol. 22, no. 9, pp. 1415–1438, 1989.
- [147] G. Gotz, T. Quella, and V. Schomerus, “Representation theory of $sl(2|1)$,” *Journal of Algebra*, vol. 312, no. 2, pp. 829 – 848, 2007.
- [148] A. MacKinnon and B. Kramer, “One-parameter scaling of localization length and conductance in disordered systems,” *Phys. Rev. Lett.*, vol. 47, pp. 1546–1549, 1981.
- [149] J. Cardy, “Logarithmic correlations in quenched random magnets and polymers,” 1999. arXiv:cond-mat/9911024.
- [150] J. Cardy *J. Phys. A: Math. Theor.*, vol. 46, p. 494001, 2013.
- [151] R. Vasseur, J. L. Jacobsen, and H. Saleur, “Logarithmic observables in critical percolation,” *J. Stat. Mech.*, p. L07001, 2012.
- [152] J. L. Jacobsen, J. Salas, and A. D. Sokal, “Spanning forests and the q -state Potts model in the limit $q \rightarrow 0$,” *J. Stat. Phys.*, vol. 119, pp. 1153–1281, 2005.
- [153] S. Caracciolo, J. L. Jacobsen, H. Saleur, A. D. Sokal, and A. Sportiello, “Fermionic field theory for trees and forests,” *Phys. Rev. Lett.*, vol. 93, p. 080601, 2004.
- [154] J. L. Jacobsen and H. Saleur, “The arboreal gas and the supersphere sigma model,” *Nucl. Phys. B*, vol. 716, pp. 439–461, 2005.
- [155] S. Caracciolo, A. D. Sokal, and A. Sportiello, “Spanning forests and the $OSP(N|2M)$ -invariant σ -models,” *J. Phys. A: Math. Theor.*, vol. 50, p. 114001, 2017.
- [156] R. Vasseur and J. L. Jacobsen, “Operator content of the critical Potts model in d dimensions and logarithmic correlations,” *Nucl. Phys. B*, vol. 880, pp. 435–475, 2014.
- [157] M. Hogervorst, M. Paulos, and A. Vichi, “The ABC (in any D) of logarithmic CFT,” *Journal of High Energy Physics*, vol. 2017, no. 10, p. 201, 2017.
- [158] W.-K. Tung, *Group theory in physics*. World Scientific Publishing Company, 1985.

- [159] J. Stembridge, “On the eigenvalues of representations of reflection groups and wreath products,” *Pacific J. Math.*, vol. **140**, pp. 353–396, 1989.
- [160] A. M. Gainutdinov, N. Read, H. Saleur, and R. Vasseur, “The periodic $sl(2|1)$ alternating spin chain and its continuum limit as a bulk logarithmic conformal field theory at $c = 0$,” *J. High Energy Phys.*, vol. **5**, p. 114, 2015.
- [161] J. Cardy, “Conformal invariance and universality in finite-size scaling,” *J. Phys. A: Math. Gen.*, vol. **19**, 1984.
- [162] H. W. J. Blöte and M. P. Nightingale, “Critical behaviour of the two-dimensional Potts model with a continuous number of states: A finite size scaling analysis,” *Physica A*, vol. **112**, pp. 405–465, 1982.
- [163] J. Cardy, “Logarithmic corrections to finite-size scaling in strips,” *J. Phys. A: Math. Gen.*, vol. **19**, 1986.
- [164] H. Osborn and A. Petkos, “Implications of conformal invariance in field theories for general dimensions,” *Ann. Phys.*, vol. **231**, pp. 311–362, 1994.
- [165] M. S. Costa, J. Penedones, D. Poland, and V. S. Rychkov, “Spinning conformal correlators,” *JHEP*, vol. **1111**, p. 071, 2011.
- [166] Y. Deng and H. W. J. Blöte, “Red-bond exponents of the critical and the tricritical Ising model in three dimensions,” *Phys. Rev. E*, vol. 70, no. 5, p. 056132, 2004.
- [167] A. M. Ferrenberg, J. Xu, and D. P. Landau, “Pushing the limits of Monte Carlo simulations for the three-dimensional Ising model,” *Phys. Rev. E*, vol. 97, no. 4, p. 043301, 2018.
- [168] N. F. Robertson, J. L. Jacobsen, and H. Saleur, “Conformally invariant boundary conditions in the antiferromagnetic Potts model and $SL(2, \mathbb{R})/U(1)$ sigma model,” 2019. arXiv: 1906.07565.
- [169] Y.-Y. Shi, L.-M. Duan, and G. Vidal, “Classical simulation of quantum many-body systems with a tree tensor network,” *Phys. Rev. A*, vol. 74, p. 022320, 2006.
- [170] M. Hauru, C. Delcamp, and S. Mizera, “Renormalization of tensor networks using graph-independent local truncations,” *Phys. Rev. B*, vol. 97, p. 045111, 2018.